In vivo structure-mediated regulation of Ribonucleotide Reductase in *S. pombe*

Ann-Sofie Schreurs

A thesis submitted for the degree of Doctor of Philosophy at the University of Sussex

July 2012

Declaration:

I hereby declare that this thesis has not been and will not be submitted in whole or in part to another University for the award of any other degree.

Ann-Sofie Schreurs

Signature.....

Acknowledgements

To start with, I would like to thank Tony for the great opportunity of doing a PhD in his laboratory. During those 3 years I learned a lot from him, especially rigorous and clever science, but also a “savoir-vivre” of someone who extensively enjoys research as well as being an exceptional supervisor. *Thank you Tony.*

I would not have achieved so far in this project without my colleagues and collaborators in this project: Kostas, an amazingly science-driven researcher from whom I learned immensely, as well as at the bench as teamwork, *Ευχαριστώ*. Of course I have to thank Adam, his patience and ingeniousity never failed me, but his best tool in every situation was humor, *cheers Adam*.

I have to thank all my chemical physicist friends, Asma with whom I spend incredible time learning about various subjects, شكراً, and Remi who has been the best colleague possible for this duo biology-physics, *Merci*.

I am thankful to Mark Osborne for his help throughout the years with valuable discussions.

I have to thank all the people from the lab: Amal, ma complice éternelle شكراً; Stephi: the rock of the lab *Merci vielmal*; Yari: my favourite Casanova *Grazie*; Chris: a true sweet friend; Yasu: my very best enemy ありがと; Tom: young and innocent, Chieh-Ju: the funniest Taiwanese ever; Izumi: the smoking samurai; Takashi: my favorite Japanese teacher; Sujin: my protein buddy; Valerie: la patience incarnée; as well as all the students that came and brought even more diversity: Natalia, Laolu, Hannah…

Thank you to Jo for her support, discussions and corrections; as well as her whole team: Jennie, Ken, Gokhan and Saed.

I have to thank so many people from the Genome Centre: all the unique friends I made: Diana for her kindness and patience through this journey *Obrigado*, Carol for her sincerity and support *Go raibh maith agat*, Marcel for the hours of discussion covering music to space *Dank u*, Fernando for the fun moments Obrigado, Rasmus for the walks and talks *Tak*, Rita, Gill, Iga, Rolf, Phil, Claudia, Anoushka, Louise, Mariella, Jon W… and everybody in the GDSC; they are too many to mention, but every one and each of you made my stay there unique. I am thankful to the people from “LP’s” and Aidan’s lab, who gave me many advice on protein expression and purification.

Thank you for all the people that read my thesis and tried to help me become a better and more formal scientific writer.

Thank you to all the PIs with whom I had very insightful discussion: Alan, Eva, Tony O, Jon B, Penny, Helfrid, Mark O’ and many others.

Of course I have to thank Gee, our mother Gnome and the whole staff: Marie, Graham, Bernie, Jeannette, Sandhya and Philippa. I am also indebt to my exceptional Marie Curie grant, through which I made a bunch of new friends through science and travels, and which Hannah made work smoothly.

None of this would have been possible without my parents, Mia and Carlo to whom I owe everything in life from travelling through the world to unconditional support. *Dank u Mama en Papa, Ik hou van jullie*. Thank you to my whole family who always believed in me.

Finally, Thank you to *moje kochanie, mon amour*, my other half who has always been there when the end of this thesis seemed impossibly far; and has always accepted and appreciated me as I am, even during my mood swings. *Dziekuje bardzo, kocham cie.*

This thesis is dedicated to the all the dreamers out there: Never forget to dream. On that note, I would like to thank my new lab for bringing me one step closer to my dream.

Abstract

UNIVERSITY OF SUSSEX

Ann-Sofie Schreurs

A thesis submitted for the degree of Doctor of Philosophy

"In vivo structure-mediated regulation of Ribonucleotide Reductase in *S. pombe"*

Sufficient and balanced pools of deoxyribonucleotide triphophates (dNTPs) is crucial for high-fidelity DNA replication as well as correct DNA repair. The enzyme RiboNucleotide Reductase (RNR) catalyses NDP to dNDP and is therefore an essential enzyme by providing the "building blocks" to the cells. dNTPs production needs to be tightly regulated in order to minimize mutation frequencies and prevent genome instability.

RNR in *S. pombe* is composed of two proteins, $Cdc22^{R1}$ and $Suc22^{R2}$, and has been described as a heterotetramer with a dimer of each subunit: the big subunit $Cdc22^{R1}$ and the small subunit $Suc22^{R2}$. *S. pombe* also posseses an RNR inhibitor: Spd1, as well as a second RNR regulator Spd2 which has been newly discovered. Spd1 has been demonstrated to inhibit RNR and to regulate its activity throughout the cell cycle. The detailed mechanism of the RNR regulation during the cell cycle or after DNA damage is not entirely clear, as are the means of inhibition by Spd1. In order to shed some light on the RNR complex and its regulation, we used various microscopy-based methods to study RNR *in vivo* as well as *in vitro*.

The data of this thesis suggest there are different forms of active RNR heterocomplexes, found throughout the cell cycle in the cytoplasm as well as in the nucleus. We propose that the precise stoichiometry of subunits in the complexes may vary, or that the complex conformation may be modified in an Spd1-dependent manner. In addition, treatment of the cells with a UV mimetic agent, 4NQO, seems to promote RNR regulation in an Spd1-dependent manner. On the contrary, inhibition of RNR by HydroxyUrea (HU) affects the RNR in a possible structure-related manner, independently of Spd1 or Spd2. The *in vivo* observations correlate with structural and/or oligomerization modifications of the RNR, representing a novel RNR regulation in *S. pombe*.

Table of Contents

List of figures

List of abbreviations

4NQO	4-NitroQuinoline 1-Oxide
9-1-1 clamp	Protein complex composed of Rad9-Hus1-Rad1
Ade	Adenine
Amp R	Ampicillin resistance gene
AP site	Apurinic or Apyrimidinic site
AS	Ann-Sofie Schreurs strain
BER	Base excision repair
BP	Band Pass
bp	Base pairs
CFP	Cyan Fluorescent Protein
CLSM	Confocal Laser Scanning Microscopy
COP9	Signalosome complex
CSN	Catalytic subunit of the signalosome
DMSO	Dimethyl sulfoxide
DNA	Deoxyribonucleic acid
dNDPs	Deoxy nucleotide diphosphates
dNTPs	Deoxyribonucleotide triphosphates
DSB	Double Strand Breaks
Ec / *E. coli*	*Escherichia coli*
FACS	Fluorescence-activated cell sorting
FCS	Fluorescence Correlation Spectroscopy
FLIM	Fluorescence-lifetime imaging microscopy
FP	Fluorescent Protein
FRAP	Fluorescence recovery after photobleaching
FRET	Fluorescence Resonance Energy Transfer
G418	Geneticin
GFP	Green Fluorescent Protein
HJ	Holliday Junction
HR	Homologous recombination
HU	Hydroxyurea
IDP	Intrinsically disordered protein
kan	Kanamycin
kDA	KiloDaltons
MMR	Mismatch Repair
MRN complex	Protein complex composed of: Mre11-Rad50-Nbs1
NA	Numerical Aperture
NDP	Nucleotide diphospates
NER	Nucleotide Excision Repair
NHEJ	Non-Homologous End Joining
PAGE	Polyacrylamide gel electrophoresis
PALM	Photoactivated light/localization microscopy
PBS	Phosphate buffered saline
PCR	Polymerase chain reaction
PMT	Photomultiplier tube
RC	Replication Complex
RNR	Ribonucleotide reductase
ROI	Region of Interest
rpm	Revolutions per minute
Sc / *S. cerevisiae*	*Saccharomyces cerevisiae*

SDS	Sodium dodecyl sulphate
Sp / *S. pombe*	*Schizosaccharomyces pombe*
SSB	Single strand breaks
ssDNA	Single strand DNA
STORM	Stochastic optical reconstruction microscopy
TIRFM	Total Internal Reflection Microscope
Ura4	Uracil
UV	Ultra-violet
Wt	Wild type
YFP	Yellow Fluorescent Protein
Δ / -d	Gene deletion

CHAPTER I INTRODUCTION

Accurate genome duplication is dependent on several factors in order to achieve high fidelity replication of hereditary information. This information is supported in the genome of the organism, based in Deoxyribo Nucleic Acid (DNA). DNA is therefore an indispensable component of cells, and its maintenance is important. Different events in the cell can be source of instability to the genome during DNA replication in synthesis phase (S-phase), or after DNA damage from endogenous or exogenous sources. The aim of this project is to understand the role of an essential enzyme, Ribonucleotide Reductase (RNR) in genome maintenance and stability, due to its role of providing dNTPs to the cell. As dNTPs are the substrate for genome replication, RNR has an important role in genome stability.

I will introduce various important areas relevant to this work: genome stability during DNA replication and DNA repair, an overview of the Ribonucleotide Reductase (RNR) enzyme, followed by a summary of the advanced fluorescent microscopy methods used.

I. Genome Stability: Interplay between cell cycle checkpoints, DNA replication and DNA repair

1. Genome maintenance during cell division

A cell is duplicated in an orderly and sequential manner, in which the genetic material as well as the cell mass are copied and divided into two. This duplication step is part of the cell cycle, known as the S-phase or synthesis phase. Cells cycle through different phases that are fundamental for organism reproduction. Although the cell cycle varies from organism to organism, most mechanisms and components have been conserved throughout evolution.
I will focus on Eukaryotes, although the non-nucleated prokaryotes have a similar cell cycle mechanism.

1.1 Schizosaccharomyces pombe as a model organism:

Schizosaccharomyces pombe (*S. pombe*) (Figure I.1), also called fission yeast, was isolated from East African beer in 1893 by P. Lindner, who used the Swahili translation for beer: "pombe" to identify this yeast. It was further described by several more scientists (C. Eijkman in 1894 and M.W Beijerinck in 1897) but finally used as a model in the 1950's by Urs Leupold to study genetics (Leupold, 1949) and Murdoch Mitchison who worked on the cell cycle (Mitchison, 1957). Afterwards, Paul Nurse (1970's) used *S. pombe* extensively and helped towards *S. pombe* being accepted as a very good model for cell cycle analysis, DNA replication as well as DNA damage and repair (Nurse P, 1976).

This small unicellular eukaryote, 3-4 μm in diameter and 7-14 μm in length, is an ascomycete fungus with a unique rod-shaped cell growing in length and dividing by fission. In addition to the advantage of the cell shape and growth, *S. pombe* cells are usually haploid, and reside mostly in G2-phase. Finally, its genome consists of 3 chromosomes, making *S. pombe* a good eukaryotic model to study cell cycle, checkpoints and genetics (Nurse, 1992). Also worth mentioning is the fact that *S. pombe* was the sixth model organism to be fully sequenced (Wood et al, 2002) making it more approachable and interesting as a model organism. It is the organism used throughout this project.

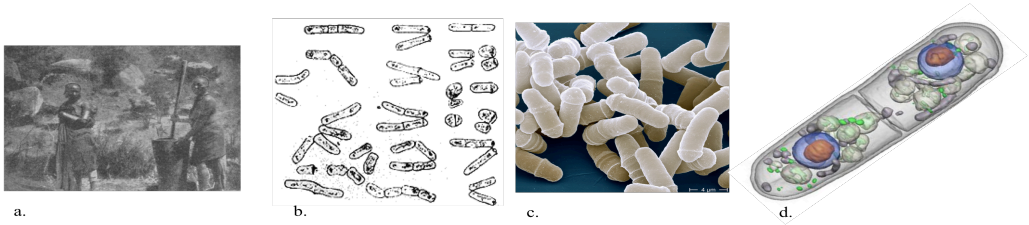

Figure I. 1 Schizosaccharomyces pombe, its origins and usages

Representative pictures of the origins and research evolution of the model yeast S. pombe. a. "Making Pombe in the hollowed-out stump of a tree" is from Swahili and other native tribes, Globusz publishing. Figure *b. represents drawings from the first description and publication of S. pombe, Lindner P. 1893. Schizosaccharomyces pombe, ein neuer Gärungserreger, Wochenschrift für Brauerei Third image c. is a scanning electron microscope image of dividing S. pombe cells from Jurgen Berger, Max Plank Institute. The image in d. is a soft X-ray tomography of rapidly frozen S. pombe from the National Centre for X-ray Tomography, Carolyn Larabelle. The key cell components are: nucleus in blue; nucleolus in orange; mitochondria in gray; vacuoles in white; and lipid-rich vesicles in green.*

1.2 Cell cycle and Checkpoints at a glance:

As mentioned above, the cell cycle is required for the division of one cell into two daughter cells, and the cell cannot divide unless its entire genome has been fully replicated. To achieve this, the cells undergo DNA synthesis followed by mitosis. The cell cycle happens in a chronological and sequential order of different phases (see Figure I.2), where the later phases are dependent on the completion of the earlier phases. The G1 phase stands for "GAP-1" and is required for cell growth and preparation of DNA synthesis. The S-phase stands for "synthesis" of DNA and replication of the entire genome. The G2 phase is "GAP-2" and is essential for cell growth and preparation for mitosis (Nurse P, 1976). Finally, the M phase stands for "Mitosis" and represents the chromosomes division generally segregating the newly duplicated DNA. In order to verify the correct progress of these, the cell has checkpoints at different stages of the cell cycle with various roles, but mainly to verify cell mass and assess DNA damage, as well as the correct chromosome alignment (Norbury & Nurse, 1992). These are detected by a sensor-signal-effector mechanism.

One checkpoint is at the start of S-phase, after completion of the G1 phase, and is called the G1, G1/S or Restriction checkpoint (Start Checkpoint in yeast) (Nurse & Thuriaux, 1980; Sveiczer et al, 1996). The G1-phase is characterized by an accumulation of proteins, which are required for progression through the cell cycle. At the end of the G1-phase, the decision is made whether the cell will continue to divide, arrest, or enter the G0 (quiescent) phase. The determination of entering S-phase is made on assessment of growth factors, cell mass, and undamaged DNA. Using a network of cyclin proteins (Hunt, 1991) (Evans et al, 1983), cyclin-dependent kinases (CDK) (Nurse & Thuriaux, 1980) and CDK inhibitors (Morgan, 1995); the cell will progress into S-phase (Langerak & Russell, 2011).

The next checkpoint is the intra-S phase checkpoint (Carr, 1998), as DNA replication is a complex process, with multiple and unsynchronized DNA origins firing, there are many possibilities for replication fork stalling and thus damage to the DNA. DNA replication and its inspection before cell cycle development will be explained more thoroughly later.

Before the start of Mitosis, the G2/M checkpoint, also called DNA damage checkpoint (Nurse, 1992) (Carr, 1998), ensures the cell size and morphogenesis are correct, but especially that the DNA replication happened faithfully thus establishing the absence of DNA damage (O'Connell et al, 2000). The Maturation/Mitosis Promoting Factor (MPF) will be activated, as it is necessary for entering mitosis. MPF will be activated by the phosphatase Cdc25, which removes the inhibiting phosphorylation on the MPF. However, when DNA damage occurred, the cell cycle will be arrested through the degradation of Cdc25 (Sveiczer et al, 1999) upon phosphorylation by the ATM kinase (Furuya & Carr, 2003) (Enoch et al, 1992).

The spindle checkpoint, also called metaphase or mitotic checkpoint ensures the correct alignment of the chromosomes on the spindle and will be the major decisive factor to proceed through the cell cycle in order to obtain an equal distribution of the genetic material (Norbury & Nurse, 1992).

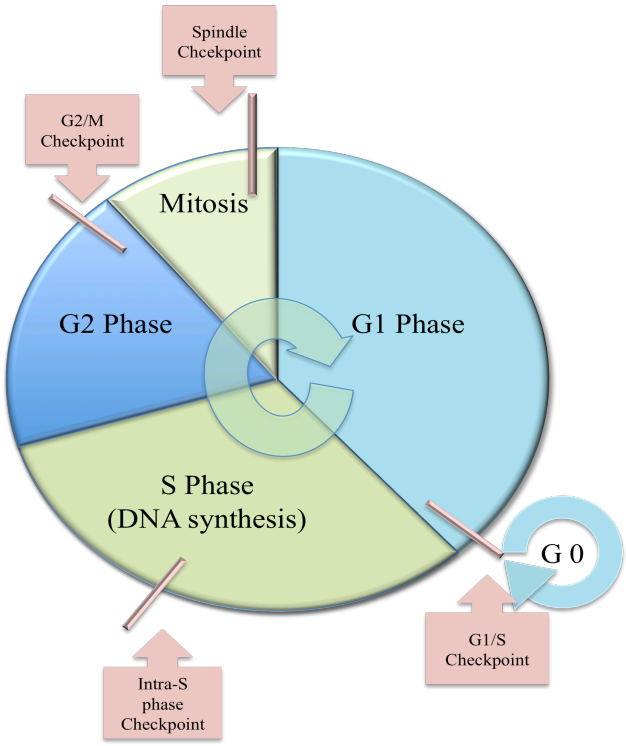

Figure I. 2 Simplified schematic of the general Eukaryotic cell cycle and the associated checkpoints

A cell progresses through a sequential cycle of phases: G1 (GAP-1), S (synthesis), G2 (GAP-2) and M (Mitosis). There are 4 checkpoints, the G1/S (Restriction or Start checkpoint) allowing the entry into S-phase, the intra-S phase in order to verify the correct DNA replication, followed by the G2/M checkpoint ensuring a correct cell mass and DNA duplication, and the spindle checkpoint in order to avoid missegregation of genomic material.

1.3 Cell cycle and checkpoints in S. pombe:

As mentioned before, the model yeast *S. pombe* has proven to be very useful, especially in the case of cell division studies to identify the implicated genes in the cell cycle: cell-division-control genes, or cdc genes (Nurse & Thuriaux, 1980) .

The cell cycle is mainly dependent on cyclin-dependent kinases (Cdk), resulting in cyclical phosphorylation of target proteins. In *S. pombe*, Cdc2 (Durkacz B, 1986) is the only Cdk, and in *S. cerevisae* $Cdc28^{Sc}$ is the Cdk, while mammalians have more than one (Langerak & Russell, 2011; Uranbileg et al, 2012).

During every cell cycle phase, specific Cdk-cyclin complexes are present in order to tightly regulate the Cdk proteins activity. The cyclin proteins will be

synthesized or degraded by the ubiquitin pathway in order to have them at precise levels at a specific cell cycle phase. In addition, another group of proteins are important for the regulation of the cell cycle progression: CKI (Cdk Inhibitor Proteins). They are small proteins that bind to Cdk. The CKI in *S. pombe* is Rum1 (Carr, 1994) (Sig^{Sc}), and inhibits Cdc2, ensuring a control of the Cdc2-cyclin complexes (Furuya & Carr, 2003).

The different steps of the cell cycle progression with the associated cell cycle "engines" (Nurse & Thuriaux, 1980) (Hunt, 1991) (Nurse, 1992) are as follow (see Figure I.3):

- The effector complex in G1 phase is Cdc2-Cig1 (Cdk-cyclin) which inhibits Rum1 (CKI) by phosphorylation. This process allows increased levels of the complex Cdc2-Cig2 in G1-S phase, triggering entry into S-phase (Labib et al, 1995) (Carr, 1994)
- Progressing through the cell cycle, the levels of the cyclin Cdc13 rise, resulting in an association with Cdc2 in S-phase. At this point, Cdc2-Cdc13 is regulated through inhibitory phosphorylation on Y15 of Cdc2: inhibited by the kinases $Wee1^{Sp}$ ($Wee1^{Hs}$ $Swee^{Sc}$) and Mik1 ($Myt1^{Hs}$) or activated by the phosphatase Cdc25 ($Cdc25^{Hs}$ $Mih1^{Sc}$) (Sveiczer et al, 1999) (Langerak & Russell, 2011)
- Ultimately, Cdc25 will fully regulate Cdc2, activating the Cdk and allowing the complex Cdc2-Cdc13 to reach its concentration peak required for entry in mitosis (Sveiczer et al, 1999)

One of many other mechanisms to regulate cell cycle progression is for example by control of gene transcription with DSC1. The DSC1 system regulates the transcription of genes containing a MCB sequence and are important for entry into S-phase. One target gene of DSC1 is *cdc22+* encoding the big subunit of the Ribonucleotide Reductase Cdc22 (Fantes, 1986) (Fernandez Sarabia MJ, 1993) (Maqbool et al, 2003).

I will now focus a bit more on the intra-S phase checkpoint (DNA replication checkpoint) as well as the G2/M checkpoint (DNA damage checkpoint).

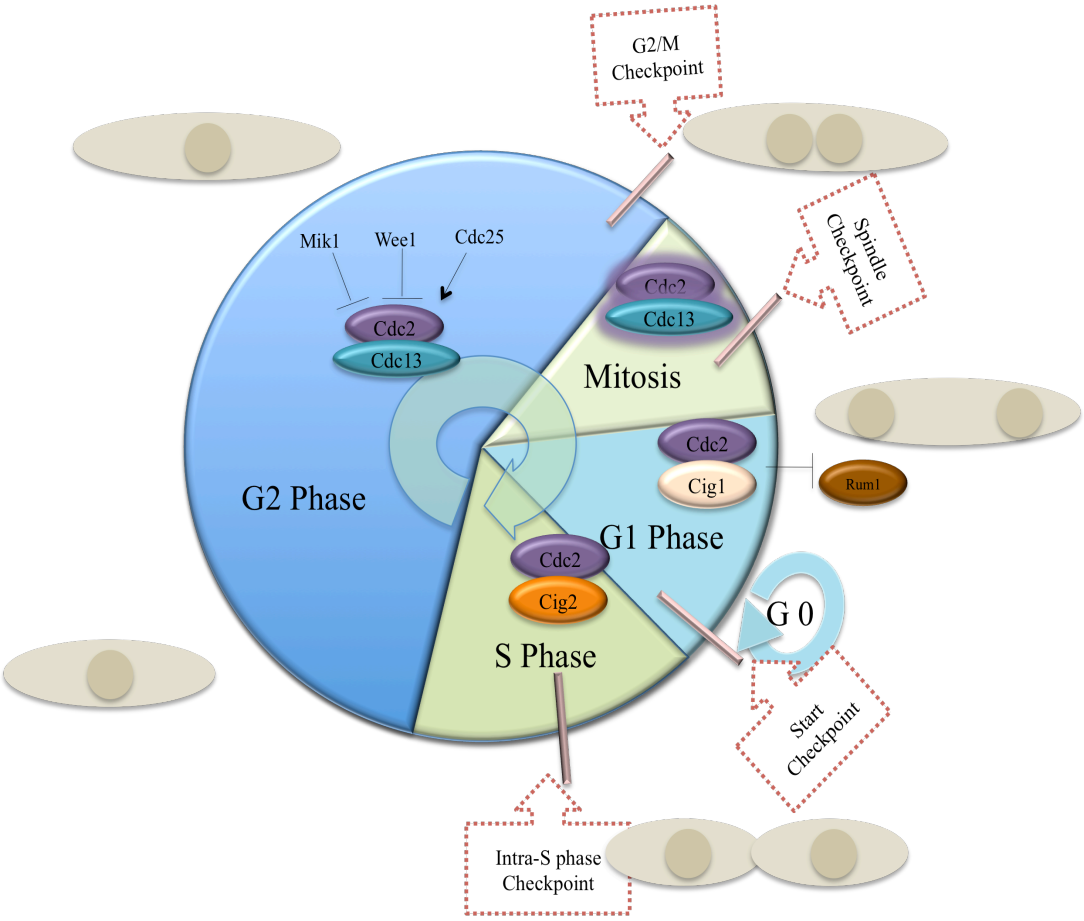

Figure I. 3 *Cell cycle of S. pombe*

Schematic of the cell cycle progression and checkpoints in S. pombe. The cell cycle is composed of sequential phases: G1, S G2 and Mitosis, but the length of the phases for S. pombe are different i.e. for the majority of the time, the fission yeast cell will be in G2. There are also 4 checkpoints, the G1/S (Start checkpoint), the intra-S phase followed by the G2/M checkpoint and the spindle checkpoint. Cdc2-Cig1 is the Cdk-cyclin complex present in G1 Phase, and by inhibition of Rum1, will allow the next complex to form: Cdc2-Cig2, thus promoting entry into S-phase. Cdc2-Cdc13 will increase during S-phase (regulated by balanced levels of kinases -Wee1 and Mik1- and phosphatase -Cdc25-) and at its peak will allow entry into mitosis. Also represented on the diagram are the distinctive cell shapes and nucleus formation drawn in accordance to the cell cycle phase stage.

1.4 DNA replication:

DNA replication is an essential process, and has complex assembly mechanisms as well as interplay with the cell cycle. As DNA replication needs dNTPs, RiboNucleotide Reductase (RNR) can therefore indirectly modulate the DNA replication, thus the cell cycle. I will give some insight into the DNA replication process.

a. Initiation of DNA replication

Although the replication of the genome happens during S-phase, it is a stepwise assembly requiring preparations completed beforehand: in G2-M the Origin Replicative Complex (ORC) binds to the DNA at sites of replications origins throughout the genome (Diffley, 1996). Subsequently, in G1 phase, the pre-Replicative Complex (pre-RC) is loaded on DNA, and is needed for the unwinding of the DNA strands during replication (Diffley, 2011) (Figure I.4):

- The pre-RC complex is composed of $Cdc18^{Sp}$ ($Cdc6^{Sc\ and\ Hs}$), Cdt1 and MCM (Mini Chromosome Maintenance). Cdc18 (with the help of Sap1) and Cdt1 are recruited to the site, allowing the loading of the MCM complex onto the DNA as part of the fully licensed pre-RC complex
- Next, the pre-RC complex has to be activated; therefore the pre-IC (pre-Initiation Complex) is formed in G1-S phase. The essential transition from the pre-RC (assembled complex) to pre-IC (active helicase) will involve two kinases: the Cdk $Cdc2^{Sp}$, and DDK which is composed of $Hsk1^{Sp}$ ($Cdc7^{Sc\ and\ Hs}$) and $Dfp1^{Sp}$ ($Dbf4^{Sc\ and\ Hs}$)
- Cdc2 and Hsk1 phosphorylate the heterohexamer MCM, followed by Cdc18 displacement whilst additional proteins are recruited: $Cdc45^{Sp}$, $Sld3^{Sp}$ and the GINS complex (Psf1-3, Sld5).
- The essential checkpoint and replication factor $Rad4^{Sp}$/$Cut5^{Sp}$ ($Dbp11^{Sc}$ $TopB1^{hs}$) is recruited. Subsequently, $Cdc23^{Sp}$ ($MCM10^{Sc}$) is loaded onto the origin and could be needed for loading of the polymerase. Polymerase ε (Pol ε) is loaded on the pre-RC, and in S phase the

replication can finally start, with the replisome complex complete upon recruitment of the replicative DNA polymerase Pol α.

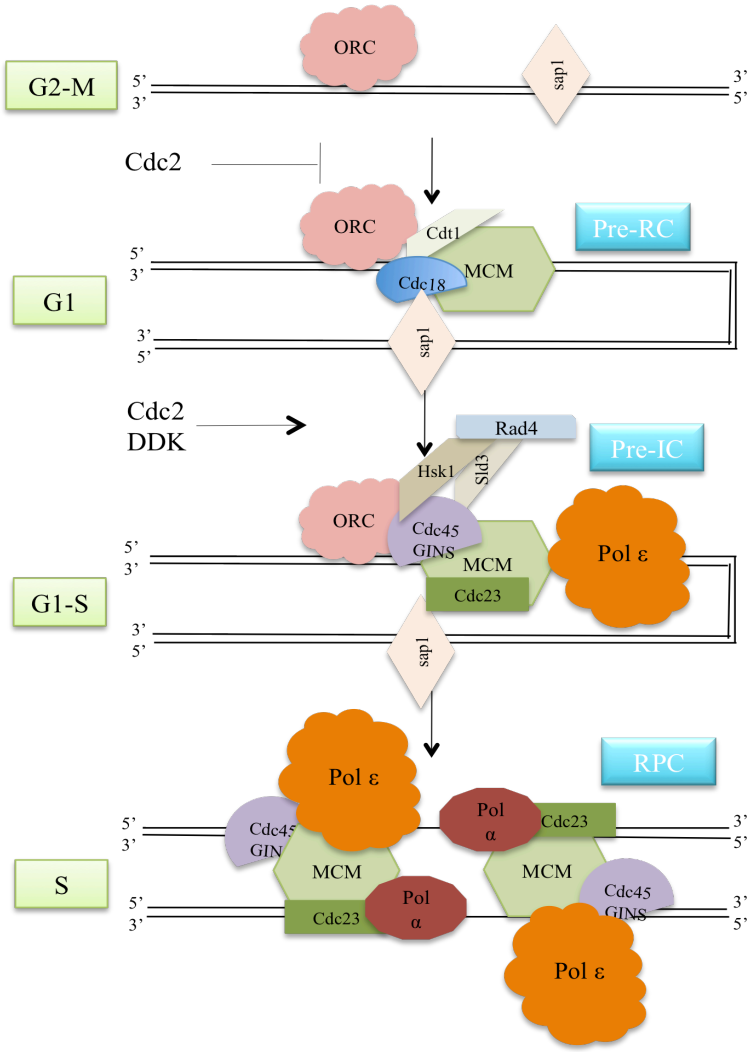

Figure I. 4 Simplified schematic of the initiation of DNA replication

Diagram of the stepwise complex assembly for the initation of DNA replication. Pre-RC: pre-Replication Complex; pre-IC: pre-initation Complex; RPC: Replisome Progression Complex. In first instance, ORC and Sap1 bind to the DNA replication origins during the cell cycle, then Cdt1 is loaded to the origin by ORC alone, but ORC and Sap1 are both required for loading of Cdc18 to the origins. Afterwards, Cdc18 and Cdt1 recruit MCM, and the pre-RC is assembled. Activation of the replication origins is partially accomplished by recruitment of Hsk1/Dfp1 followed by loading of Cdc45, Sld3, the GINS complex, Rad4, Cdc23 and polymerase ε (Pre-IC). Finally, polymerase α is recruited and the RPC is ready.

b. Fork Replication

The replication fork is an ingenious structure permitting the faithful and fast duplication of the double stranded DNA. Because of the particular anti-

parallel nature of the double helix, in addition to the fact that DNA polymerase does synthesize DNA in a 5' to 3' manner, the fork will have a leading strand and a lagging strand. The 3' to 5' DNA strand is used as template by Pol ε (to produce the nascent 5' to 3' leading strand), while the lagging strand uses a system of DNA primase and Okazaki fragments operated by Pol α to produce the 3' to 5' DNA. The DNA fork replication is composed of different sub-components with various roles (Stillman, 2008) as shown in figure I.5:

- Helicase proteins: MCM complex (with some of the above mentioned proteins i.e. Cdc45 and GINS). Other helicases have been described to play a role in replication i.e. $Dna2^{Sp}$, $Rqh1^{Sp}$
- Topoisomerases to relax the super-coiling of the DNA induced by the helicases
- DNA polymerases: Pol α and its associated primase to initiate the DNA replication, followed by Pol δ on the lagging strand and Pol ε on the leading strand. The clamp loader Replication Factor-C (RFC) and PCNA are important to load Pol δ and Pol ε while PCNA is also essential for the processivity of those DNA polymerases.
- Ligase is essential to ligate the Okazaki fragments
- The single-strand binding protein, RPA, is important to protect the single stranded DNA (ssDNA). RPA is essential for the recognition of ssDNA in order to signal the presence of ssDNA and therefore the necessity for DNA replication and especially DNA repair.

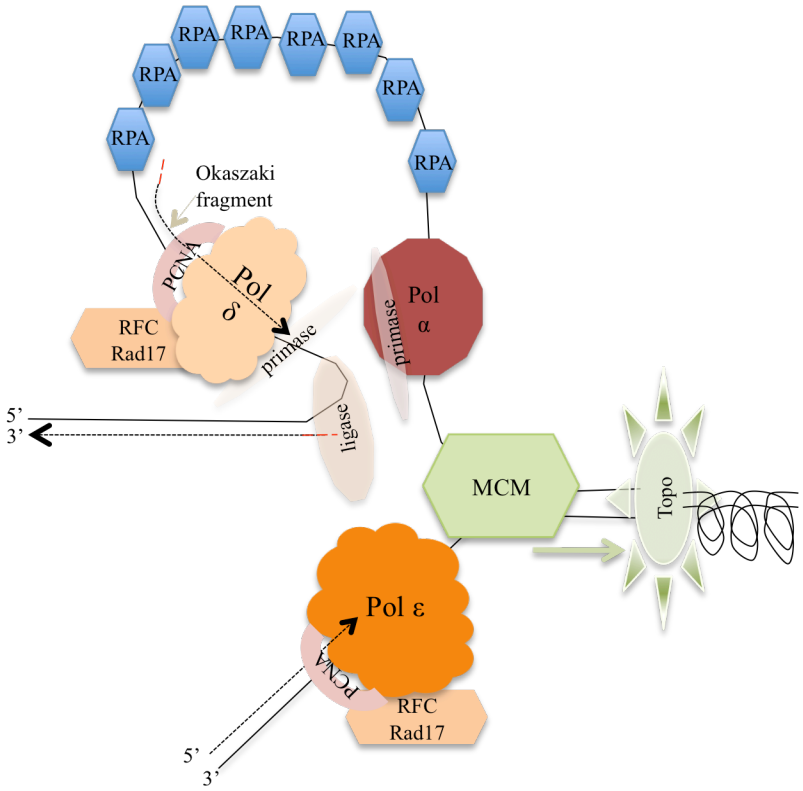

Figure I. 5 Simplified model of the Replisome Complex (RC)

Schematic of the proposed model based on the trombone model in Prokaryotes. The helicase will unwind the DNA, while the topoisomerase will allow the DNA to relax. Pol α, in association with the primase, initiaties the replication, and Pol δ and Pol ε will proceed on the lagging strand and the leading strand respectively. RFC and PCNA are present for the loading and processivity of the DNA polymerases. On the lagging strand, the replication is operated by Okazaki fragments, which will then be ligated. The single strand binding protein RPA is protecting the yet unreplicated single stranded DNA.

c. Fork stalling: stabilization and checkpoint activation

The replication fork is a multi-component complex (Fig I.5), with additional proteins associated with the replisome in order to maintain and stabilize it. DNA replication is tightly regulated, as each origin has to fire only once per cell cycle, and the replication has to be fully completed without any errors. In addition, different obstacles will destabilize the fork, a lack of dNTPS for the DNA polymerases, DNA damage, fork replication barriers or aberrant DNA structure.

If a fork stalls, in order to restart the fork once the obstacle is overcome, the cell cycle has to be paused, thus the checkpoint is activated. But the fork

will collapse if it is not maintained in a stable structure, leading to the loss of the fully functional replisome, which can lead to a broken fork.

The DNA replication checkpoint, or also called intra S-phase checkpoint, will come into play to arrest the cell cycle to permit the fork restart or recovery (Figure I.6) (Caspari, 1999) (Furuya & Carr, 2003):

- The Rad3-Rad26 kinase complex (ATR-ATRIP^{Hs} Mec1-Dcd2^{Sc}) is recruited to the stalled fork, together with the RFC-like (Rad17 and RFC2-5) and PCNA-like (Rad1-Hus1-Rad9 i.e. 9-1-1) complexes (Caspari et al, 2000) (Paciotti et al, 2001)
- Next, the essential step in the checkpoint activation is the phosphorylation of Cds1 (Chk2^{Hs} Rad53^{Sc}) by Rad3 (Lindsay et al, 1998)
- Mrc1 (Claspin^{Hs} Mrc1^{Sc}) is the mediator protein in the Cds1-dependent checkpoint activation
- This activation results in an accumulation of Mik1 (Myt1^{Hs} Swee1^{Sc}) leading to an inhibition of Cdc2 by phosphorylation of its residue Y15, therefore preventing entry in mitosis (Christensen et al, 2000)
- In addition, the Cds1-Mrc1 complex inhibits the firing of new origins of replication (through inhibition of Hsk1 which is part of the DDK essential to pass from pre-RC to pre-IC) and slowing down the progression of replication throughout the genome
- Finally, the Cds1-Mrc1 complex regulates the Mus81-Eme1 endonuclease complex required for fork restart

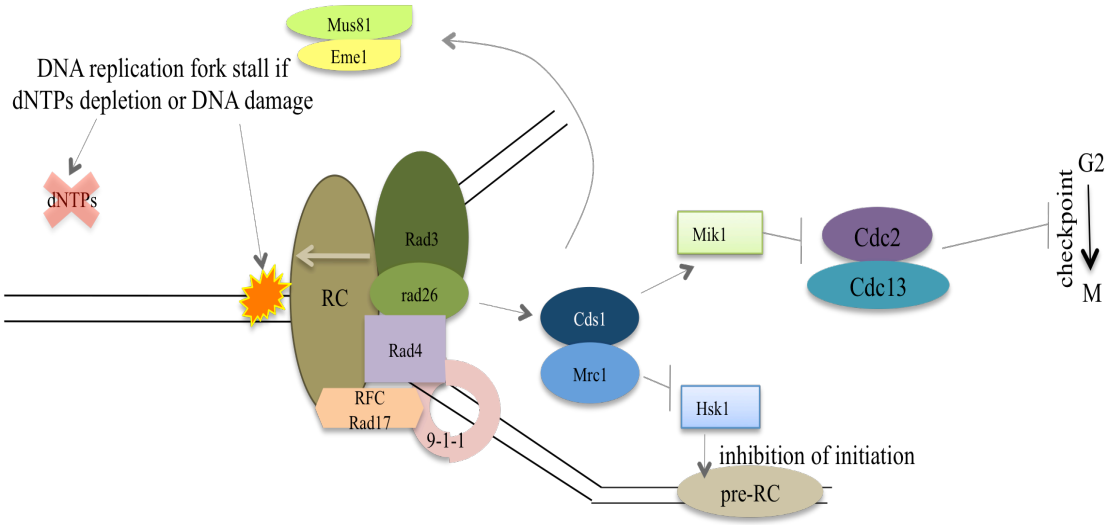

Figure I. 6 Simplified fork replication stabilization and checkpoint activation

When there is limited supply of dNTPS or DNA damage, the replication fork will stall, and after being stabilized will activate the checkpoint to arrest the cell in order to give time to overcome the obstacle. At the Replisome Complex (RC), the kinase complex Rad3-Rad26 is loaded, and the RFC-like complex as well as PCNA-like complex 9-1-1 might be linked for the recruitment of the mediator protein Mrc1. Mrc1 in turn, recruits the effector protein Cds1 which will inhibit entry in Mitosis (by accumulation of Mik1 which will increase the inactive Cdc2). At the same time, Cds1-Mrc1 will inhibit Hsk1, which is essential for origins firing; and the effector/mediator Cds1-Mrc1 module will also regulate Mus81-Eme1 and their role in fork restart.

In absence of this DNA replication checkpoint, the fork will collapse and ultimately create DNA strand breaks, possibility creating genomic instability (Lambert & Carr, 2005). Therefore the stabilization of the fork, as well as the preservation of the replisome, is important. After removal of the DNA lesion or increased supply of dNTPs, the replication will resume. Hydroxyurea (HU) is used to provoke fork stalling. HU is a Ribonucleotide Reductase inhibitor thus limits the dNTPS supply to the cell.

1.5 G2/M DNA damage checkpoint and comparison of the checkpoints

a. DNA Damage checkpoint

Damage to the DNA in cells occurs regularly, and can be due to different sources, resulting in various DNA damages. Corresponding DNA repair pathways repairs these DNA damages, once the DNA damage checkpoint is activated.

The G2/M checkpoint, also called the DNA damage checkpoint, and has the same cascade reaction as the previous checkpoint i.e. sensors, mediators and effectors. In *S. pombe*, considering that the longest phase is G2, this checkpoint is important (fig I.7) (Furuya & Carr, 2003; O'Connell et al, 2000) (Langerak & Russell, 2011).

- In first instance, the heterotrimer RPA binds to the single strand DNA, resulting from the DNA damage and is followed by recruitment of the kinase complex Rad3-Rad26
- It is thought that the PCNA-like complex 9-1-1 and Rad17 are recruited onto the damaged DNA enabling closer proximity between Rad3-Rad26 and the mediator proteins
- Rad4 is recruited by Rad9 (from the 9-1-1 complex)
- The mediator protein Crb2 ($53BP1^{Hs}$ $Rad9^{Sc}$) is loaded and activated by a Rad3-dependent phosphorylation, thus regulating the Chk1 effector protein
- Upon activation of Chk1, Mik1 and Wee1 accumulate (therefore inhibiting Cdc2) leading to non-entry into mitosis. It is thought that Chk1 may inactivate Cdc25 through the 14-3-3 complex, also resulting in a checkpoint inhibition.
- In addition, Rad3 phosphorylates H2A, hallmark of an active checkpoint and thus DNA damage nearby.

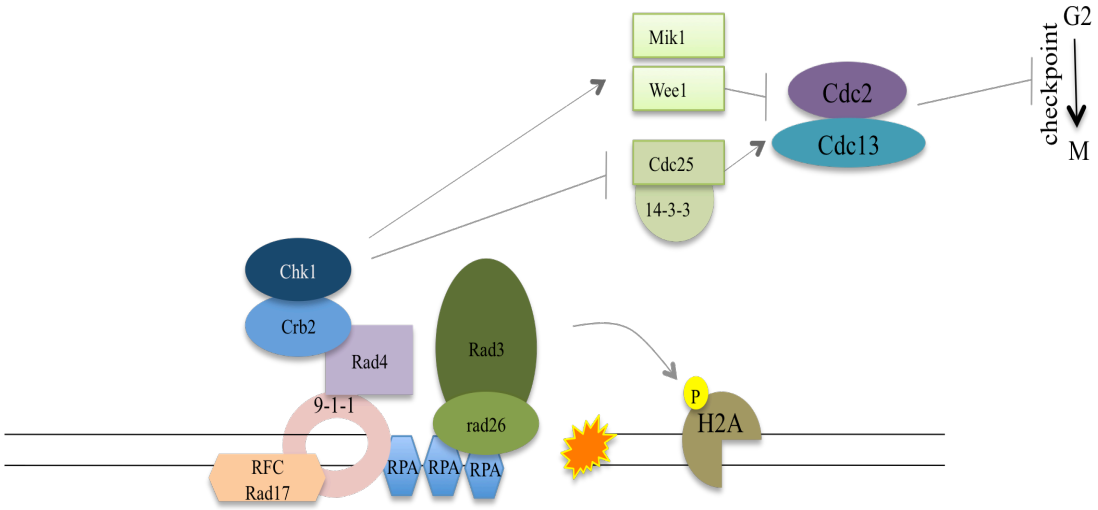

Figure I. 7 Simplified G2/M checkpoint activation

When DNA damage occurs, RPA will be the first present to protect single stranded DNA. Next the essential Rad3-Rad26 is recruited, followed by the loading of the 9-1-1 complex and Rad17. Rad4 is recruited and which in turn will bring the mediator protein Crb2 to the site, and the effector Chk1. Once activated, Chk1 will be able to prevent entry in mitosis through accumulation of the Cdc2 inhibitors Mik1 and Wee1. It might also inhibit the Cdc2 activator Cdc25 through the complex 14-3-3. In addition, Rad3 will phosphorylate H2A in order to flag DNA damage where an active checkpoint is already on site.

More recently, it has been described that Tel1^{Sp} (ATM^{Hs} Tel1^{Sc}) is also recruited to the DNA damage sites and interacts with Nbs1 from the MRN complex: Rad32 (Mre11^{Hs}) Rad50, and Nbs1 (Xrs2^{Sc}) (Langerak & Russell, 2011) (Mantiero et al, 2007).

b. Checkpoint signalling comparison

Below is a summary (Figure I.8) of the checkpoints (Furuya & Carr, 2003) , as well as the signaling cascade system in the cell to arrest the cell cycle in order to give time to restart a stalled/collapsed fork and repair DNA damage. Comparison is done with humans, *Homo sapiens*, and budding yeast, *S. cerevisae* (Longhese et al, 2003; Longhese, 1998) involving similar mechanisms although different denominations.

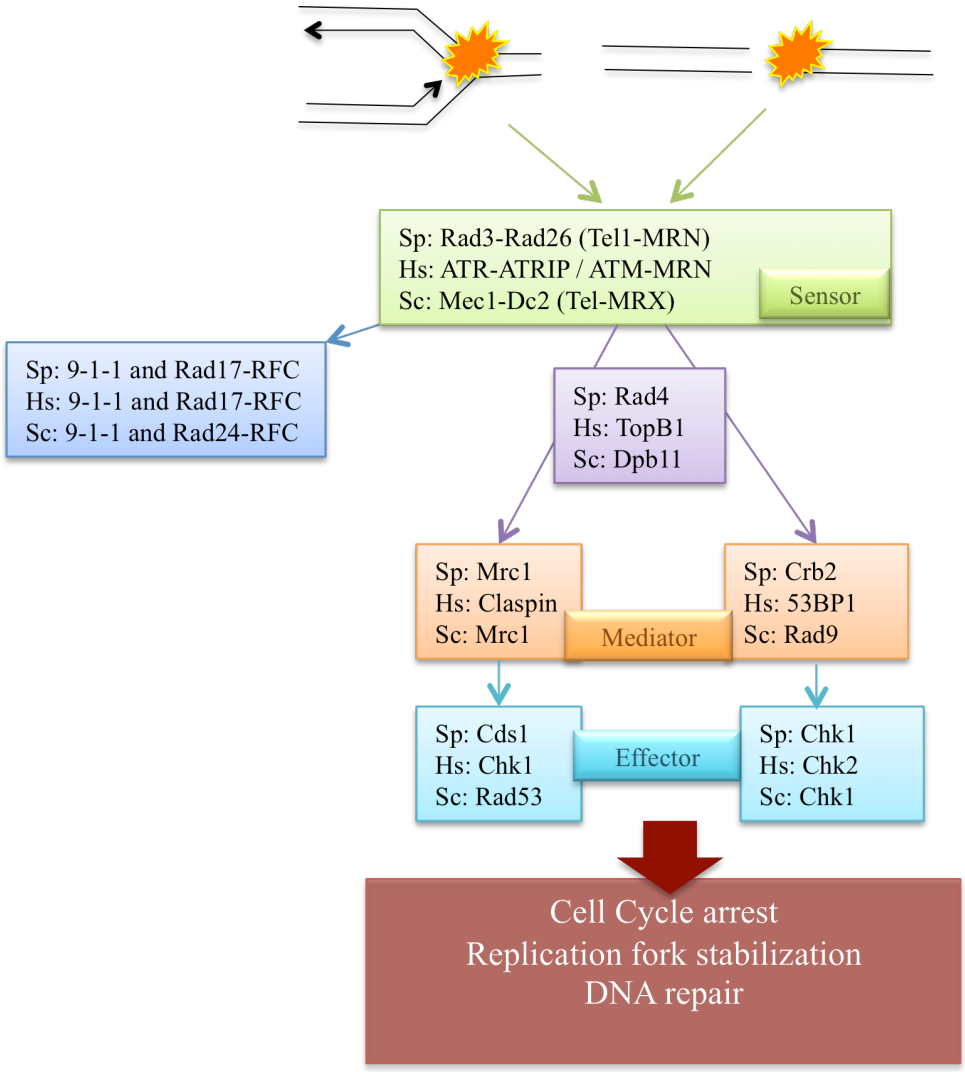

Figure I. 8 Simplified overview of the DNA checkpoints in Eukaryotes

When a replication fork is stalled, or when DNA damage occurs, cells use their DNA maintenance checkpoints to arrest the cell cycle and facilitate fork restart or DNA repair pathways. The signaling cascade is composed of sensors recruited to the damage, and whilst activating many proteins, they will mainly activate mediators needed to trigger the effectors. Those effectors will indirectly regulate the cell cycle arrest as well as assisting in the replication fork stabilization and/or the repair mechanisms.

Annotated are the proteins in each species: Sp.: Shizosaccaromyces pombe, Hs.: Homo sapiens, Sc. Saccharomyces cerevisae.

Now that we have an understandable view of the cell cycle and its checkpoints as well as the interplay of the proteins in DNA replication, I want to address how the enzyme Ribonucleotide Reductase (RNR) is involved in those pathways.

1.6 RNR involvement in the cell cycle and checkpoints

Cells are provided with a large supply of ribonucleotides, which serve as substrate for various important cellular functions including RNA synthesis, energy generation (ATP), as well as regulation of enzyme activities (GDP/GTP), post-translational modification of proteins (ATP), cell signaling (cAMP and cGMP) and others. Ribonucleotides also serve as precursor for deoxyribonucleotide tri-phosphates (dNTPs), which are essential for DNA synthesis (Nordlund & Reichard, 2006). The enzyme, which converts NucleoDiPhosphates (NDPs) to deoxyNucleoDiPhosphates (dNDPs) is Ribonucleotide Reductase (RNR). Therefore, as RNR is the main enzyme regulating the rate-limiting reaction of dNTPs supply to the cell, it has a key role in S-phase. RNR is tightly regulated to avoid an unbalanced or limited supply of dNTPs to the cell (Fernandez-Sarabia & Fantes, 1990). A limited amount of dNTPs can lead to fork stalling and collapse, possibly leading to rearrangements; and an unbalanced dNTPs pool can conduct to dNTPs misincorporations resulting in mutations and genomic instability (Chabes et al, 2003a; Chabes & Stillman, 2007).

I will describe the RNR complex and its regulation in more detail in Chapter I.2, but the following paragraph is to emphasize the interplay of RNR with the cell cycle.

In *S. pombe*, Cdc22 ($R1^{Hs}$ RNR1/$RNR3^{Sc}$) is the big subunit of the RNR complex, while Suc22 ($R2^{Hs}$ RNR2/$RNR4^{Sc}$) is the small RNR subunit. Both are targets of the DSC1-MCB system, thus transcriptionally induced during S-phase and after DNA damage (Fernandez Sarabia MJ, 1993). The RNR also has allosteric regulation, in addition to spatial regulation. $Suc22^{R2}$ and $Cdc22^{R1}$ are in different compartments during most of the cell cycle i.e. $Suc22^{R2}$ is nuclear while $Cdc22^{R1}$ is pan-cellular. There are also known inhibitors, or rather

regulators of the RNR: Spd1 and, the newly discovered, Spd2. In *S. cerevisae* the regulators are Sml1, Hug1, Dif1; and none so far have been found in humans (Lee et al, 2008) .

Spd1's degradation is induced upon activation of Chk1 (Liu et al, 2003) in G2 phase, and Spd1 is degraded in a ubiquitin-dependent manner. The COP9 SigNalosome (CSN) forms a complex with cullin4 and the E3 ubiquitin ligase to perform the ubiquitylation (Liu et al, 2003), which triggers the degradation of Spd1. This degradation is necessary to allow the relocalization of $Suc22^{R2}$ to the cytoplasm in S-phase to form complexes with $Cdc22^{R1}$, in order to have active RNR complexes to provide new dNTPs for the cell. If the signalsome is non-functional (for example in a Csn1 deletion) and Rad3 is deleted as well, it will result in lethality as Spd1 is not degraded anymore. If Spd1 is not degraded, it will constantly be present and inhibit the RNR therefore no dNTPs will be available for the cells (Liu et al, 2003). Over-expression of the small subunit $Suc22^{R2}$ or deletion of Spd1 will restore viability in the Csn1-deletion Rad3-deletion strain. I will go through more details later about that rescue, which can be used as an assay to measure the activity of RNR (Nestoras et al, 2010).

Despite the essential need for dNTPs during DNA replication and DNA repair, it must be remembered that the replication of mitochondrial genomes occurs independently of the cell cycle, through the process of D-loop replication. Therefore, dNTPs will be needed at those sites and at unsynchronized times with the genomic DNA replication cycle (Sazer & Sherwood, 1990) .

Also, some recent investigations suggest that the RNR is associated and involved with the replication machinery, providing the dNTPs locally. Through this, it could also co-ordinates initiation, elongation and termination of the DNA replication (Poli et al, 2012). It also has been proposed that the RNR is recruited to the sites of DNA damage (Niida et al, 2010a), therefore I will give an overview of the DNA damages occurring in cells and the repair mechanisms associated, in order to stress the importance and role of RNR in genome stability (Niida et al, 2010b).

2. DNA damage and repair: DNA repair pathways in Eukaryotes

DNA damages can arise from different sources, exogenous: UV (components of the sunlight) as well as other radiations (ionizing radiation: X-ray, γ), as well as numerous genotoxic chemicals can cause lesions. Also endogenous sources can damage DNA: DNA lesions, errors or gaps might occur during DNA replication, reactive oxidative species (ROS) resulting from cell processes, as well as spontaneous base losses. During DNA replication, translesion synthesis (TLS) will bypass such damages due to its DNA damage tolerance function. This happens by ubiquitylation of the PCNA, which then will recruit specialized DNA polymerases to get around the lesion or mismatch (Ulrich, 2011).

All these damages can result in gene mutations and general genomic instability leading to a variety of disorders. Fortunately, the cell has numerous mechanisms to repair them throughout the cell cycle (Nouspikel, 2009; Robertson et al, 2009).

I will describe those DNA repair mechanisms, which are grouped into categories with regards to the nature of the DNA damage.

2.1 Single Strand repair: Base Excision Repair (BER), Nucleotide Excision Repair (NER) and Mismatch repair (MMR)

There are several sources for damage to a single strand of the double helix: reactive oxygen species (ROS), radiations, and genotoxic chemicals, as well as topoisomerases that create single strand breaks to relax the DNA structure.

There are 3 main pathways to repair a defect on a single strand: BER, NER, MMR. In humans there is another single-strand repair pathway (Single-Strand Break Repair: SSBR (Caldecott, 2008) involving PARP, XRCC1 and DNA ligase III but homologous proteins or pathway has not been described in yeast yet.

a. Base Excision Repair (BER)

BER is used when bases have been affected by deamination, oxidation, and alkylation (Nouspikel, 2009; Robertson et al, 2009). It follows a classic DNA excision by endonuclease cut and filling of the gap by a polymerase system (fig. I.9).

DNA glycosylase recognizes the lesion and an AP (Apurinic/Apyrimidinic) endonuclease incises the single strand yielding a 3' OH (Hydroxyl) site as well as a 5'dRP (Deoxyribosephosphate). This reaction is followed by either the short patch way or the long patch repair pathway.

In the short patch, the 5'dRP gap is lysed by an AP lyase ($Nth1^{Sp}$ with $Apn1^{Sp}$ and $Apn2^{Sp}$) followed by filling with $Pol4^{Sp}$ (Pol β^{Hs}) and ligation with a DNA ligase (DNA ligase III^{Hs} and $XRCC1^{Hs}$).

The long patch can use Pol β^{Hs}, as well as Pol λ^{Hs} and Pol ε^{Hs}, and the polymerases will displace the 5' flap while filling the gap, thus creating a longer 5' flap, which can be processed by the flap endonuclease $FEN1^{Hs}$ ($Rad2^{Sp}$ $Rad27^{Sc}$). Finally the newly synthesized DNA is ligated by a DNA ligase.

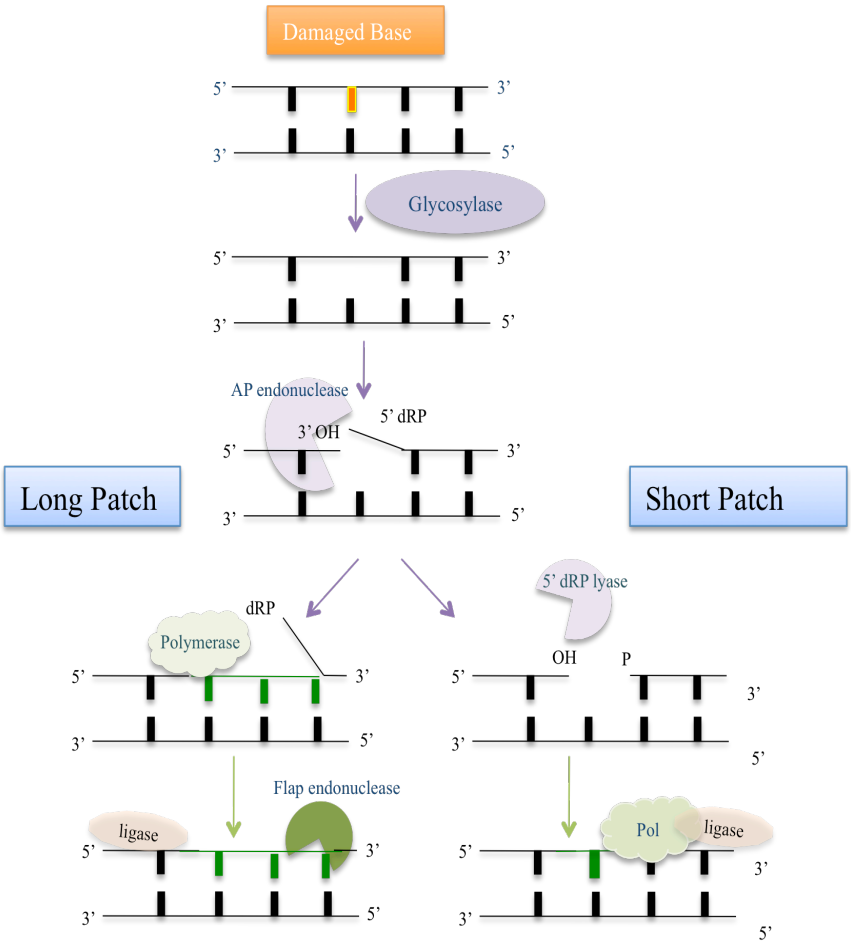

Figure I. 9 Diagram of the model for Base Excision Repair (BER)

A damaged base is repaired in different steps: first recognition of the damage by a glycosylase, followed by an AP endonuclease, which will provide a 5'dRP. The long patch will use displacing polymerases, ending the repair by a flap endonuclease and ligation. Whereas in the short patch, a lyase will remove the 5'dRP, followed by a single nucleotide filling by a polymerase, and ligation.

b. Nucleotide Excision Repair (NER)

NER is required to repair bulky DNA adducts that distort the double helix (Nouspikel, 2009). NER is divided in two groups, the Global Genome Repair (GGR or GC-NER) and the Transcription Coupled Repair (TCR or TC-NER) (Figure I.10). TC-NER occurs when the DNA is being transcribed, and the transcription machinery encounters the damage (Lehmann, 2011).

First, the damage is recognized by XPE^{Hs}, $HR23B^{Hs}$ ($Rhp23^{Sp}$) and XPC^{Hs} ($Rhp41^{Sp}$), in GC-NER. In TC-NER, it is recognized by CSA^{Hs} ($Ckn1?^{Sp}$) and CSB^{Hs} ($Rhp26^{Sp}$) where the RNA polymerase II is transcribing.

Next the transcription factor (TFIIH), along with XPB^{Hs} (Ercc3^{Sp}) and XPD^{Hs} (Rad15^{Sp}) unwinds the DNA, while XPG^{Hs} (Rad13^{Sp}) is recruited for its endonuclease activity. Subsequently, ERCC1^{Hs} (Rad16^{Sp}) (bound with XPF^{Hs}) will cut the damaged strand on the 5' end, completing the incision and the removal of the damage.

Finally, DNA polymerase Pol δ or Pol ε fill the gap with the help of RFC and PCNA, while a DNA ligase will complete the work.

NER is a good example of the importance of correct genome maintenance and efficient repair, as deficiency in NER is translated in various disorders: for example Xenoderma Pigmentosum (XP) and Cockayne syndrome (CS) (Lehmann, 2003).

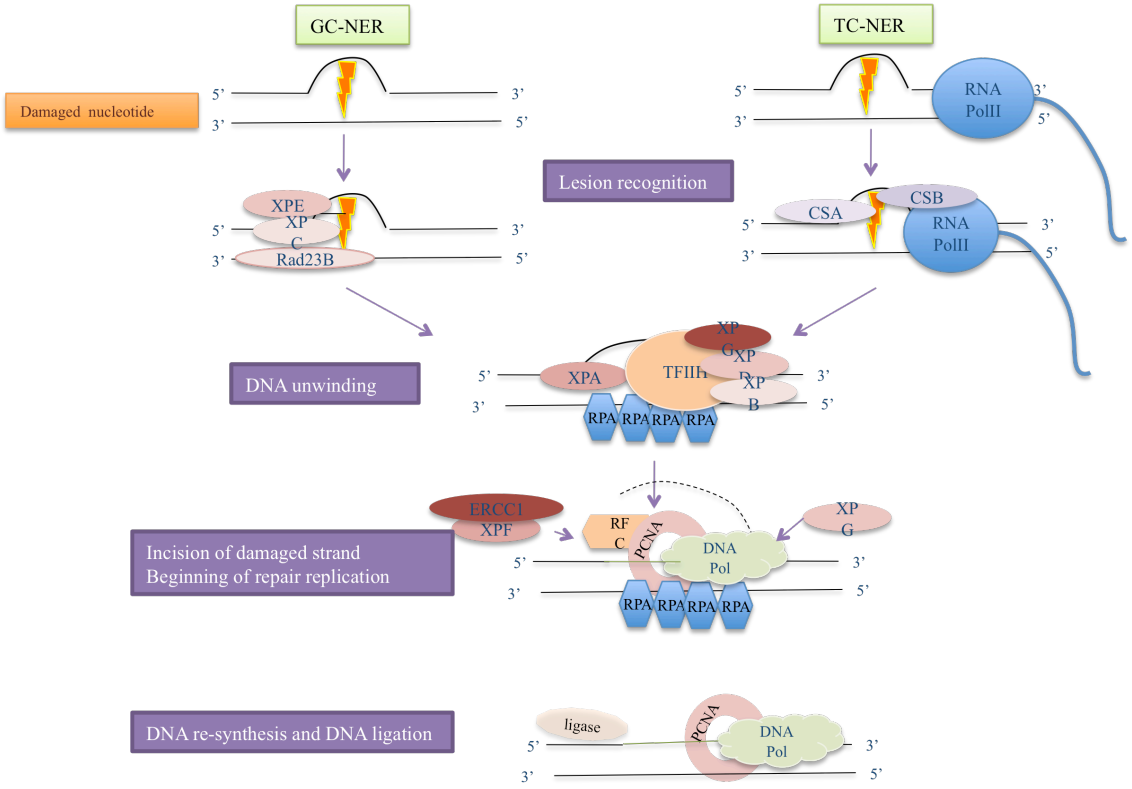

Figure I. 10 Diagram of generalized model for Nucleotide Excision Repair (NER)

Nucleotide excision repair is initiated by helical distortion. In first instance, DNA lesion is recognized by different proteins depending on the pathway: Global NER or Transcription coupled NER (RNA pol II collision). Helicase-proficient protein complexes unwind the DNA, allowing RPA to bind to the single stranded DNA. The damaged strand will be incised on both 5' and 3' in order to be removed. The gap will be filled by a DNA polymerase, and finally ligated.

c. MisMatch Repair (MMR)

Mismatch repair is very conserved from Prokaryotes to Eukaryotes, probably in part because MMR is actively involved in the fidelity of the DNA replication, thus limiting genome instability (Marti et al, 2002) (Jun et al, 2006). Many reasons can result in wrong nucleotide incorporation, but the most common is an unbalanced pool of dNTPs.

This repair mechanism has again a similar pathway as the above described system: recognition and removal of the damage followed by filling of the gap (Figure I.11).

The lesion recognition is done by:

- MutS: MutSα ($Msh2^{Hs}/Msh6^{Hs}$ $Msh2^{Sp}/Msh6^{Sp}$) or MutSβ ($Msh2^{Hs}/Msh3^{Hs}$ $Msh2^{Sp}/Swi4^{Sp}$)
- Together with MutL: MutLα ($Mlh1^{Hs}/Pms3^{Hs}$ $Mlh1^{Sp}$) or MutLγ ($Mlh1^{Hs}/Mlh3^{Hs}$)

The next step for the assembly of the repair complex involves PCNA and RFC, although their roles are not entirely clear yet. An exonuclease, $Exo1^{Hs\ Sp}$, digests the DNA strand resulting in ssDNA, which is protected by RPA. Pol δ fulfill the role of synthesizing new error-free DNA strand, ligated by DNA ligase I.

MMR is another example of the direct impact of a malfunction DNA repair system on human health, as there are disorders associated with MMR deficiency: mutation in the Mut genes will lead to microsatellites instability resulting in cancers, for example HNPCC (Hereditary Non-Polyposis Colorectal Cancer) (Hamelin et al, 2008).

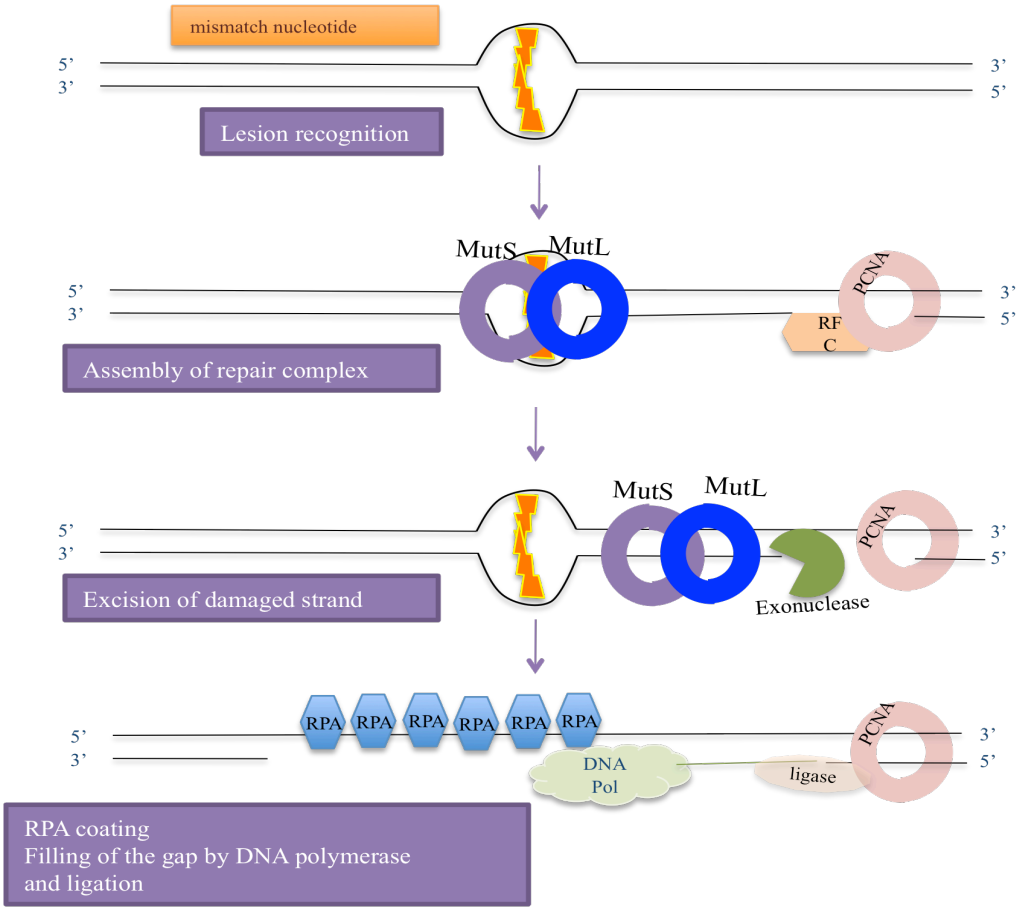

Figure I. 11 Diagram of a simplified model for MisMatch Repair (MMR)

The MutS and MutL clamps will be recruited to the mismatch, as well as PCNA and RFC. The clamps will diffuse to the PCNA complex, followed by excision of the damaged strand. Next, RPA will protect the single stranded DNA while the DNA polymerase resynthesises the DNA strand which is ligated by DNA ligase I.

2.2 Double Strand Breaks Repair: Homologous Recombination (HR), Non-Homologous End-Joining (NHEJ) and Single Strand Annealing (SSA)

When both strands of the DNA are broken, it is defined as a Double Strand Break (DSB) and can lead to cell death or worst: serious chromosomal aberrations. DSBs can occur in a programmed manner during meiosis (sexual replication), at replication forks (by topoisomerases) or for immunoglobins V (D) J variety, but can also arise from radiations (UV, X-ray, Gamma), genotoxic chemicals, free radicals and others.

There are mainly two mechanisms used by the cell to repair those damages: HR and NHEJ (Kass & Jasin, 2010; Langerak & Russell, 2011; Martín et al).

a. Homologous Recombination (HR)

HR is error-free as it uses the sister chromatid (available in G2, the prominent phase for *S. pombe*) or homologous chromosome as a template for DNA repair (Aylon & Kupiec, 2004). The steps of the early stages of DSB repair are (Figure I. 12):

- Recruitment and binding on either side of the MRN ($Rad32^{Sp}$ /$Mre11^{Hs, Sc}$ -$Rad50^{Sp, Hs, Sc}$ - $Nbs1^{Sp, Hs}$/$Xrs2^{Sc}$) complex (Williams et al, 2010)
- The MRN complex recruits and activates ATM ($Rad3^{Sp}$/$Tel1^{Sp}$) (Williams et al, 2010)
- ATM phosphorylates H2AX, $p53^{Hs}$, $53BP1^{Hs}$ as part of the checkpoint activation and allows DSB flagging (Martín et al, 2012)
- The MRN complex ($Rad32^{Sp}$-$Rad50^{Sp}$-$Nbs1^{Sp}$) resects both DNA ends in 5' to 3' with the help of other nucleases: the exonuclease $Ctp1^{Sp}$ and $Exo1^{Sp}$ (Sae^{Sc}) (Baroni et al, 2004; Clerici et al, 2006; Williams et al, 2010)
- RPA protects the ssDNA by binding to the 3' overhangs
- Recruitment of $Rad51^{Hs}$ ($Rhp51^{Sp}$) replace the RPA to form the Rad51 filament, facilitated by $Rad52^{Hs}$ ($Rad22^{Sp}$) (Caspari et al, 2002)
- Recruitment of $BRCA2^{Hs}$ (Holloman, 2011), $BRCA1^{Hs}$ (Ohta et al, 2011) by interaction to Rad51
- $Rad54^{Hs}$ ($Rhp54^{Sp}$) is recruited and has been shown to be important for pairing to the donor strand as well as the strand invasion (Krogh & Symington, 2004)

After the initial recognition and 5' to 3' resection, the Rad51 nucleoprotein will invade the template homologous DNA using its 3' overhang, thus forming a Displacement loop (D-loop). DNA synthesis by DNA polymerases will then occur, allowing strand extension.

Following the classical Szostak model (Szostak et al, 1983), the DNA strands will form a cross-shaped structure: the Holliday Junction (HJ). The Holliday Junction is a recombination intermediate with possibilities for two resolving methods, resulting in recombination with crossover or with non-

crossing over. Two RecQ helicases BLM^{Hs} and WRN^{Hs} ($Rqh1^{Sp}$ / $Sgs1^{Sc}$) are necessary for resolving the HJ, together with the endonuclease proteins $Mus81^{Sp}$ and $Eme1^{Sp}$ (Ho et al, 2010). Depending on the cutting sites, the resolving of the HJ will provide some genetic material exchange (cross-over) or keep the integrity of the genome (non crossing-over) (Wu & Hickson, 2006) (Longhese et al, 2006).

There are variants models for mechanism of homologous recombination as well as implication of HR in diverse pathways:

- Single-Displacement Strand annealing/ Synthesis-dependent Strand annealing (SDSA): this pathway involves strand displacement and branch migration without forming any HJ (Helleday et al, 2007)
- Single strand annealing (SSA): it occurs between repeated sequences, but is an error-prone mechanism (Raji & Hartsuiker, 2006)
- Break Induced Replication (BIR): although the mechanisms remains unclear, it seems to involve HR components at telomeres for example (McEachern et al, 2000)
- In addition, some components of HR are involved in the repair of Interstrand Cross Link (ICL) damage (Dronkert et al, 2000) (Hinz, 2010)
- Finally, HR also occurs during meiosis to provide meiotic chromosome crossover, and although the pathways are different, most mechanistic details remain (Youds & Boulton, 2011) (Phadnis et al, 2011)

Defects in the HR pathway can cause major genome instability (Gene conversion, Loss of Heterozygoty…) and disorders (for example Bloom and Werner syndrome, as well as breast cancer).

On a side note, HR has proven to be a great system for genetics and is used routinely for gene targeting in basic research but is also a hope for gene therapy.

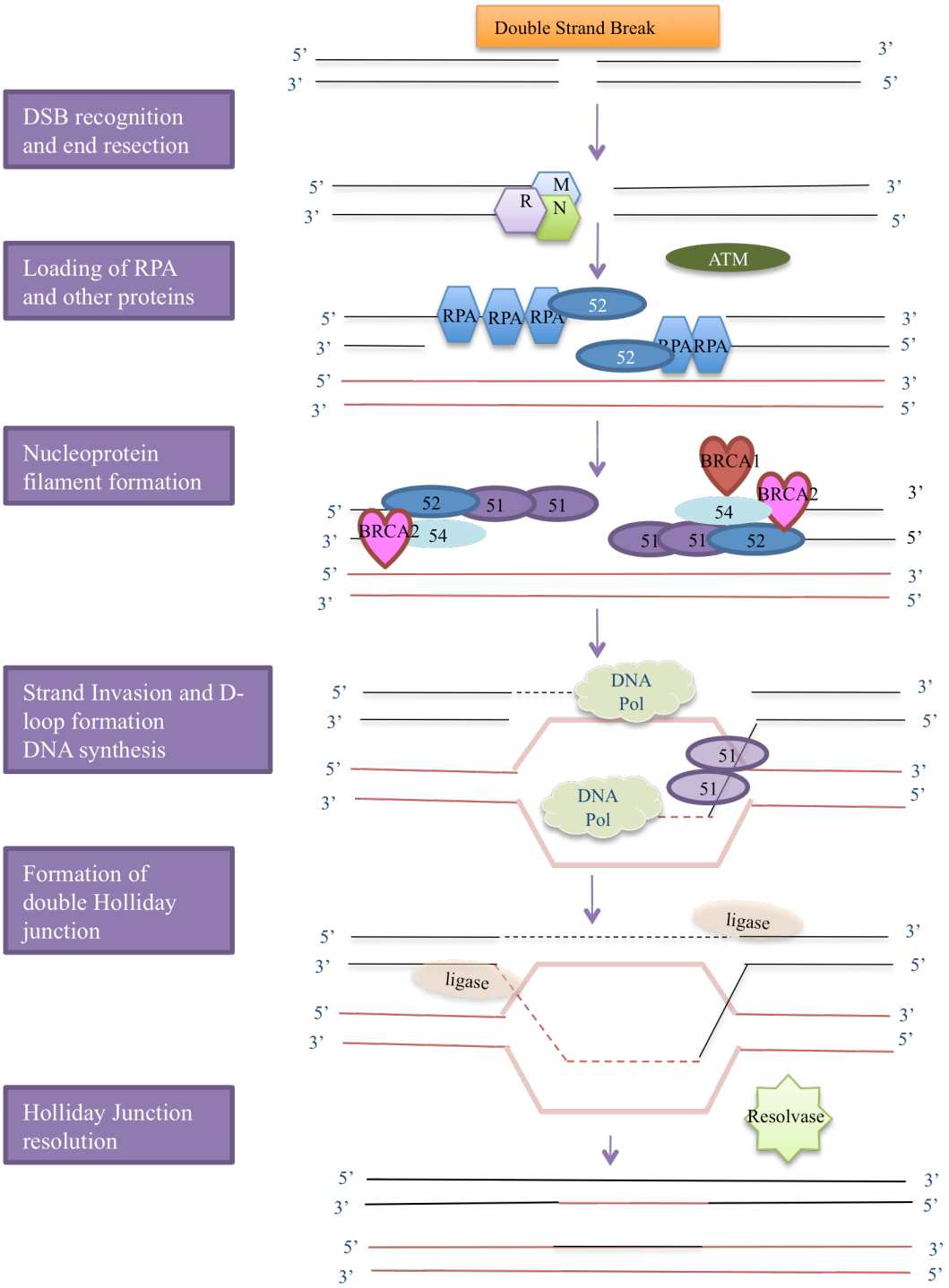

Figure I. 12 Simplified model of Homologous Recombination (HR)

Homologous recombination allows damaged DNA sequence to be repaired using an identical or nearly identical template (sister chromatid in G2 or homologous chromosome). The damage is first identified and signaled, ensuring the recruitment of the DSB repair machinery. Following resection of the DNA, a nucleoprotein filament will be formed and used to invade the homologous sequence in a D-loop formation. DNA synthesis and ligation will create a Holliday junction, which can be resolved in two manners, non-crossover or cross over.

b. Non-Homologous End-Joining (NHEJ)

The second main DSB repair pathway used in yeast is NHEJ, although in humans it is the most common pathway (Daley et al, 2005) (Lieber, 2010) (Langerak & Russell, 2011). NHEJ is error-prone due to the direct ligation of DNA strands. NHEJ can lead to chromosome translocation, rearrangements and telomere fusion if not controlled properly. It can be advantageous, for example in the case for the V (D) J system where new variants of antibodies can be made to help the immune system. The NHEJ mechanism is mainly prominent in humans, although some orthologues have been found in yeast.

- The heterodimer $Ku70^{Hs}$ and $Ku80^{Hs}$ ($Ku70^{Sp}$ and $Ku80^{Sp}$ $Yku70^{Sc}$ and $Yku80^{Sc}$) are recruited to the DSB, and in Humans, DNA PKcs seem to be important for the tethering of the ends (Clerici et al, 2008; Hammel et al, 2010)
- The MRN complex is loaded and may act at the resection of the DNA ends, while DNA Pol λ^{Hs} and Pol μ^{Hs} will process the ends (Lieber et al, 2003)
- Finally, the DNA ligase IV^{Hs} /$XRCC4^{Hs}$ complex will rejoin the ends (Wilson et al, 1997)

In *S. pombe*, $Ctp1^{Sp}$ has been described in the resections of the DNA ends along with $Exo1^{Sp}$, while $Pol4^{Sp}$ is the polymerase involved (Langerak & Russell, 2011).

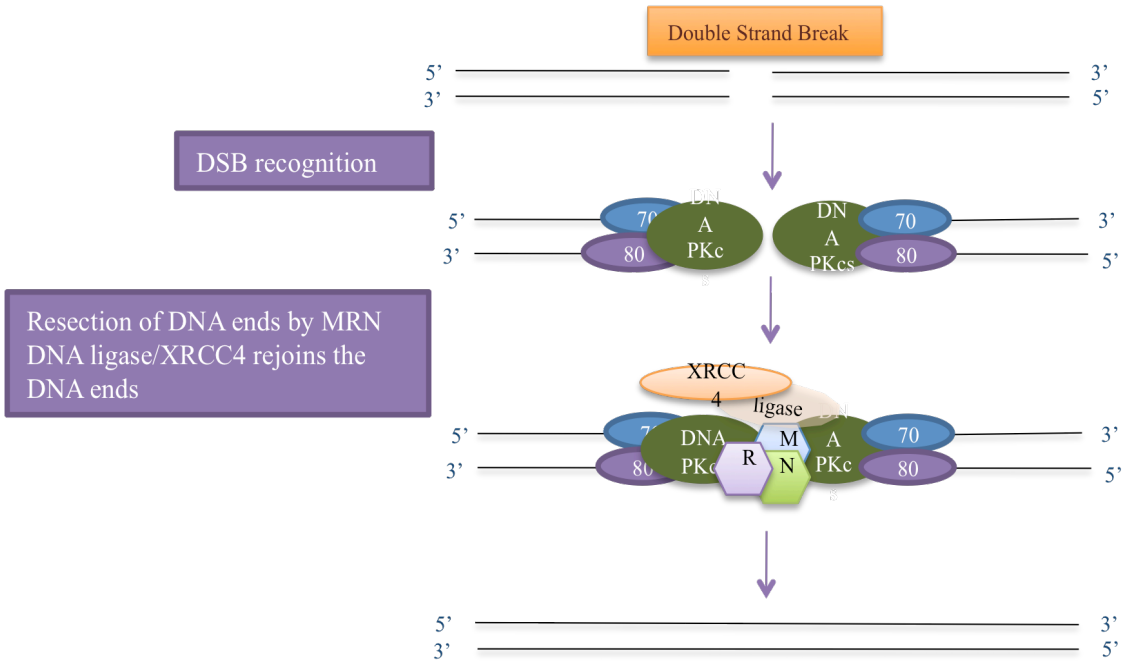

Figure I. 13 Simplified model of Non-Homologous End Joining (NHEJ)
Ku70/Ku80 will be recruited to the DSB allowing DNA PKCs recruitment and activation, followed by MRN complex loading. After resection, the DNA ends will be processed and then joined by XRCC4/ligase.

Defects in the NHEJ in humans can lead to various disorders ranging from radiosensivity to microcephaly-linked diseases.

c. RNR involvement in DNA damage and Meiosis

So far I have introduced the cell cycle and the implication of RNR in the cell cycle as well as the different DNA repair mechanisms in the cell, which involve DNA synthesis thus RNR. This sub-chapter will emphasize on the links between DNA repair and RNR in order to allow the appreciation of RNR's importance in genome stability.

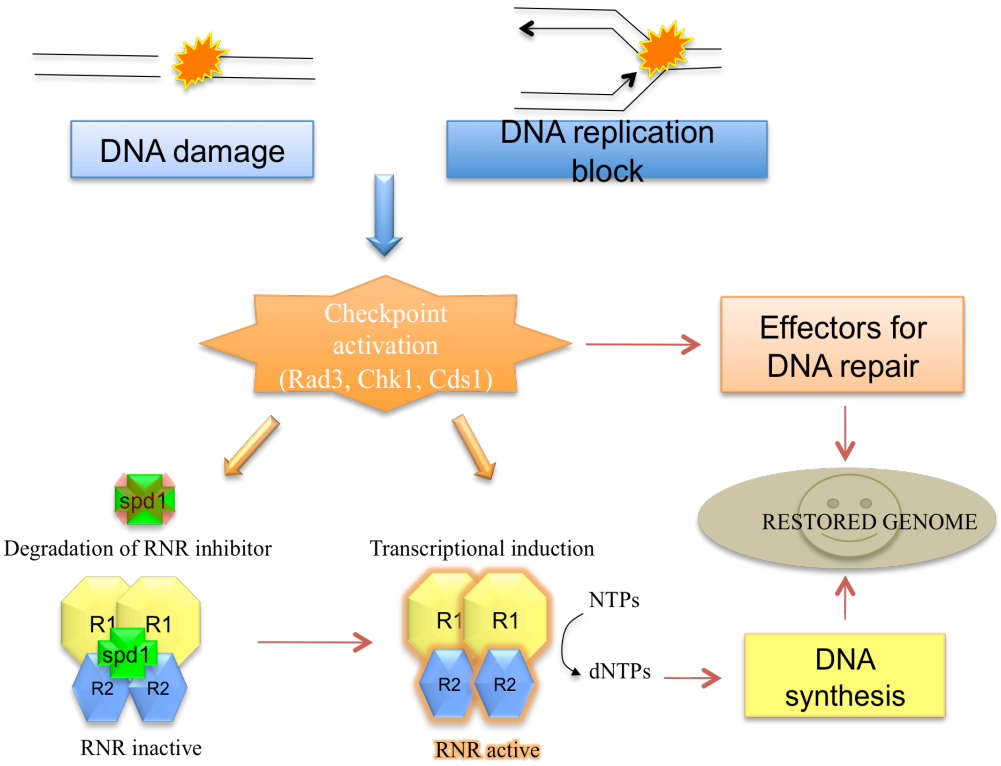

Figure I. 14 Basic current model for involvement of RNR in genome stability

Schematic of the implication of RNR in genome stability after DNA damage or DNA replication stalling. After activation of the checkpoint, there will be the degradation of the RNR regulator (Spd1^{Sp}), while the RNR subunits will be actively transcribed. This will lead to an active RNR enzyme providing dNTPs to the cell in order to allow DNA synthesis during repair.

Upon DNA damage, the RNR is actively transcribed and the RNR inhibitor Spd1 is degraded, leading to an increase in the pool of dNTPs. RNR has been demonstrated to be necessary for efficient HR (Moss et al, 2010) involving Rad3-dependent RNR activation as well as degradation of Spd1 by Ddb1^{Sp} (Holmberg et al, 2005) (Liu et al, 2005). Although providing more dNTPs to the cell will help to improve the pace and efficiency of the DNA repair, this could also lead to an increase in the mutation rate.

A recent study (Niida et al, 2010b) also allowed to link RNR activity and DNA repair, as the recruitment of RNR to the sites of damage in form of foci (colocalization with H2AX) was observed. In addition, they described R1 and R2 bound to the chromatin in a Tip60^{Hs} dependent manner, albeit in a small fraction.

This allows us to modify our view with regard to the localization of RNR, active RNR complexes and functions of RNR.

In humans there is an alternative small subunit R2: p53R2, which is induced after damage (Tanaka et al, 2000) (Guittet et al, 2001).This is also observed in *S. cerevisae* with RNR4 (Zhou & Elledge, 1992) (Huang & Elledge, 1997). I will later describe those subunits and their comparisons more thoroughly, as well as the RNR regulators.

Finally, meiosis is a specialized process to produce spores in yeast (i.e. “sexual reproduction”). During meiosis, DSB will be formed in a $Rec12^{Sp}$ dependent manner ($Spo11^{Sc}$) followed by DSB repair essential for chromosome cross-over with the aim of genetic material exchange (Youds & Boulton, 2011). Therefore, DSB repair is very important during meiosis, and indirectly so is RNR (Holmberg et al, 2005).

II. Ribonucleotide reductase

Ingenious *in vivo* experiments in the fifties (Reichard & Estborn, 1951) showed that ribonucleotides are the precursors of deoxyribonucleotides, and interestingly already observed a difference between different ribonucleotides precursors and their turnovers.

Very early on, it was understood how deoxyribonucleotides are formed by direct reduction i.e. oxygen removed from the compound (Reichard et al, 1961) (Brown et al, 1968). This is one of the first catalytic steps to provide the cells with those "building blocks" in order to supply the cell with a sufficient and balanced source of dNTPs. Another important observation made was that the Ribonucleotide Reductase subunits B1 and B2 (*E. coli*) were inactive on their own, but active when in complex and with iron as co-factor. Although a few important aspects of the function, regulation and structure were understood early on (Thelander & Reichard, 1979) (Reichard, 1987), until today we have not grasped the entire picture of the enzyme Ribonucleotide Reductase (RNR).

Since then, Ribonucleotide Reductase (or Ribonucleotide Diphosphate Reductase) has been described in many organisms, ranging from viruses, bacteria, sea urchin, yeasts, worms, mouse, mammalian etc… (Hofer et al, 2012).

In the next paragraph, I will review the RNR and the different classes, followed by some detailed description of both RNR subunits. Their regulation by many features as well as the structure will be finally depicted.

1. RNR classification and common characteristics

1.1 Variety of RNR enzymes

The RNRs have been classified in 3 classes, based on the nature of the thiyl radical, their essential metal cofactor and their interaction with oxygen as recently reviewed in (Cotruvo & Stubbe, 2011) (Hofer et al, 2012):

- Class I are aerobic heterocomplexes requiring oxygen in the iron centre. The subclass Ia has a diferric centre and a tyrosyl radical (Fe^{III}-O-Fe^{III}/Y•) while Ib uses manganese (Mn^{III}-O-Mn^{III}) instead of iron to provide and stabilize the tyrosyl radial Y•; and Ic lacks the tyrosyl radical whilst having an Mn^{IV}-O-Fe^{III} centre.
- Class II are oxygen independent homocomplexes (only one subunit of the complex) using adenosylcobalamin (AdoCbl) to generate the radical
- Class III are also homocomplexes using glycyl radical as cofactor

The RNRs from class I are found mostly in Eukaryotes but also in some bacteria, archea and viruses (Nordlund & Reichard, 2006), whereas class II and class III are found predominantly in bacteria, archea, viruses and a few Eukaryotes. Some species have multiple RNR enzymes from different classes, providing evolutionary advantage. The classes differ also in their structural composition, as class I has 2 subunits α and β, both essential for enzyme activity; whereas class II and II only have one subunit α. In addition, the RNR classes are different with regards to the substrates they use for producing de novo dNTPs: Class I using NDPs while class II and III use NTPs (Cotruvo & Stubbe, 2011).

Although the different RNR enzymes classes (and sub-classes) vary on oxygen dependency, free radical chemistry, subunit composition, substrates usage, as well as allosteric regulation; they do have a very striking common feature: the tertiary structure of the α subunit with a 10-stranded α/β barrel (Hofer et al, 2011).

I will now use mainly the RNR from class Ia as example, as it regroups bacteria, yeast and humans, allowing me to unravel in more detail the RNR whilst comparing through those few species.

1.2 Ribonucleotide Reduction mechanism

The RNR enzyme with its metallocofactor will catalyze the reduction of the –OH in position 2' of the ribose into –H through direct substitution, thus converting ribonucleosides diphosphate (NDP) into their deoxy forms (dNDP) (Figure I.15) (Reichard et al, 1961) (Stubbe, 1998) (Nordlund & Reichard, 2006).

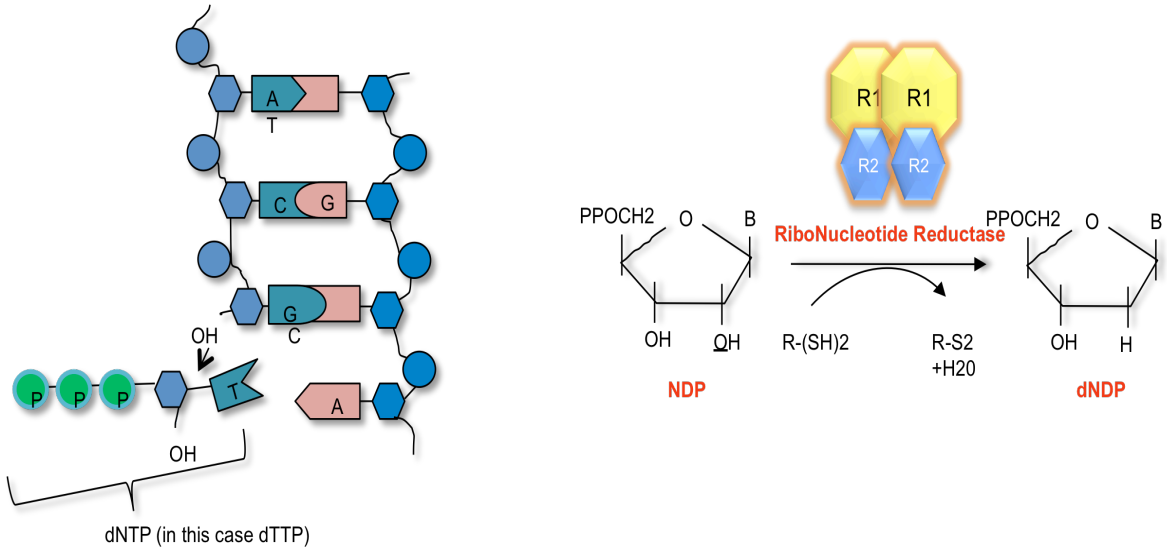

Figure I. 15 Representation of dNTPs in the DNA and the reduction done by RNR

DNA is composed of deoxyNucleotides TriPhosphates (dNTP), and in order to build the double helix necessary for the genome, a large and balanced supply of dNTPs are needed. RibNucleotide Reductase (RNR) catalyses the rate limiting step in the production of dNTPs. It will reduce Nucleotides DiPhosphates (NDP) into their deoxy form: deoxyNucleotides DiPhosphates.

The reduction reaction by RNR is a multicomponent oxidation-reduction reaction cascade (Figure I.16). Two different pathways are known for the *E. coli* RNR: the first one uses thioredoxin, and the second one glutathione and glutaredoxin are used. In both cases, NAPDH is the ultimate reductant (Eklund, 1994).

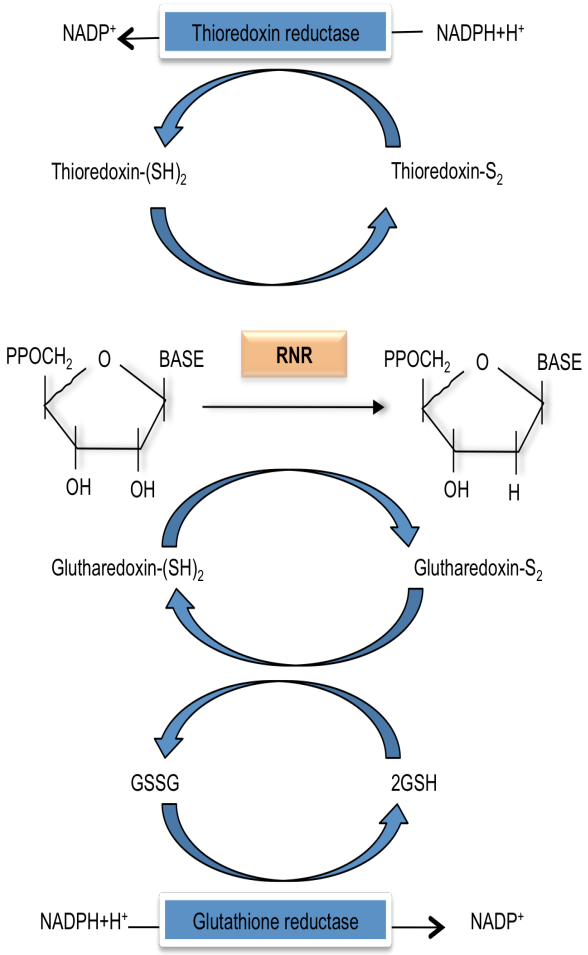

Figure I. 16 Reduction cascades of the E. coli RNR via Thioredoxin and glutaredoxin
Involvement of oxidation-reduction active disulfides in NDP reduction in E. Coli as part of a hydrogen transport system. $NADPH^+/NADP^+$ will use either a thioredoxin reductase/thioredoxin mode or a glutathione reductase + glutathione and glutaredoxin mode to allow NDP reduction by RNR.

1.3 General structure of RNR

Taking the *E. coli* RNR as example (but most RNR class Ia have similarities), RNRs were first described as heterotetramer. R1 is the big sub-unit, and is functional at least as a homodimer, as is the smaller sub-unit R2. The enzyme is in a $\alpha_2\beta_2$ conformation with R1: α and R2: β (Thelander & Reichard, 1979) (Nordlund & Reichard, 2006) (Hofer et al, 2011) (Figure I.17). R2 can be considered as the radical generator, while R1 as a reductant will need the radical. The stoichiometry of each subunit is modified depending on the state of the enzyme, and although the crystal structures of RNR subunits

have been resolved, some doubts remain about the quaternary structure configuration, especially *in vivo*. It has been modeled that the R1 dimer will fit on top of the R2 dimer (fig. I.17) (Eklund, 1994) (Hofer et al, 2011) (Cotruvo & Stubbe, 2011).

RNR is an allosteric enzyme, using the allosteric feedback by binding dNTPs in order to regulate the further production of dNTPs. The activity site on the big subunit R1 will bind activating-ATP and inhibitory-dATP. The specificity site at the dimer interface will bind ATP, dATP, dTTP and dGTP allowing a correct and balanced production of dNTPs. This allosteric feedback is part of a complex dNTPs regulatory production, which will be explained in the following sub-chapter. At the interface of the R1 dimer and R2 dimer, between the iron-generated tyrosyl radical of R2 and the active cysteines of R1, is the active site where the reduction of the NDPs will occur.

This model is mostly accepted for class Ia RNR although some differences between species are present as well as some unanswered questions, especially with regards to the stoichiometry and the mechanisms behind activation/inactivation of the RNR complex.

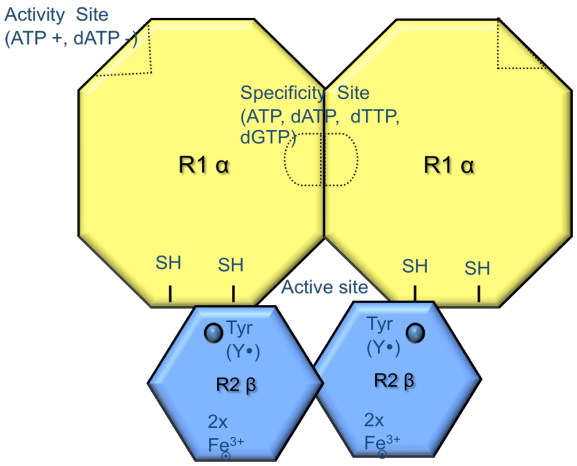

Figure I. 17 Schematic structure of E. coli RNR $\alpha_2\beta_2$

Diagram representing the RNR $\alpha_2\beta_2$ active form model in E. coli, R1 (α) corresponding to the big sub-unit and R2 (β) the small one. R1 has the 2 allosteric sites: activity site binding ATP and dATP, as well as the specificity site. R2 has the diferric centre and the tyrosyl radical, while the interface between the homodimers is the active site where the reduction reaction of NDPs will take place, using the free radical of R2 and the cysteines of R1.

2. The big subunit R1: gene, protein, structure and function

2.1 General

Each R1 subunit by itself is inactive, and needs to be dimerized in at least a one-to-one stoichiometry to be active. The binding is weak (easily dissociated during purification) and requires magnesium (Mg_{2+}). R1 has two allosteric binding sites (figure I.19) (Thelander & Reichard, 1979) (Stubbe, 1998) (Cotruvo & Stubbe, 2011):

- The overall activity site is also called “h-site” for high binding of dATP, also mentioned as the ATP-cone domain. The overall activity site binds Adenosine TriPhosphate (ATP) which will act as an activator, as well as deoxyAdenosine TriPhosphate (dATP) which by acting as an inhibitor will inform of the general levels of the dNTP pools thus inhibiting the RNR activity
- The specificity site is also called “l-site” for low binding of dATP. The specificity site binds ATP, dATP, as well as dTTP and dGTP. This will allow a balance of the 4 different dNTPs in the cell through a multifaceted feedback regulation. With ATP bound, the RNR will reduce CDP and UDP, while with dTTP bound it will reduce GDP, whereas with dGDP bound, ADP will be reduced

R1 also contains the catalytic site (Figure I.18) with the active dithiols (-SH), which are essential for the reduction process:

$$NDP + RNR\text{-}(SH_2) \rightarrow deoxyNDP + RNR\text{-}(S\text{-}S) + H_20$$

An intricate network of amino acids has been depicted as the active site using a radical-mediated reduction process: Cys^{439} is the initial thiyl radical carrier in the reaction (oxidized by the tyrosyl radical of R2), while two cysteins Cys^{225} and Cys^{462} are providing reducing equivalents, and are directly involved in the reaction (Cotruvo & Stubbe, 2011). Glu^{441} and Asn^{437} of R1 are also implicated in the catalytic mechanism, although to a lesser extent.

This multistep substrate turnover cycle will ultimately result in the 2’ ribose oxygen leaving as a water molecule using the two hydrogen molecules

from the cysteine pair, whom will subsequently form a disulfide bridge (see Figure I.18) (Cotruvo & Stubbe, 2011).

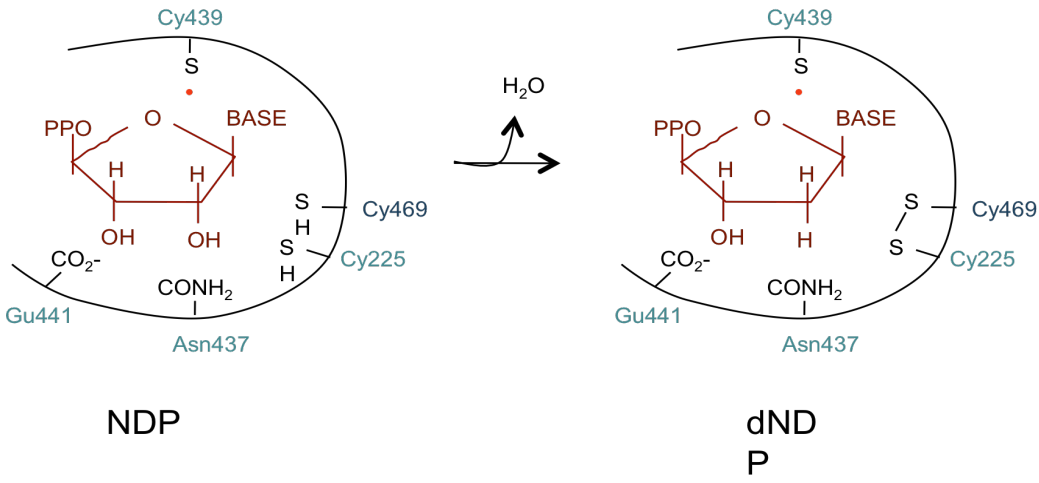

Figure I. 18 Schematic of the proposed mechanism of nucleotide reduction by RNR in E. coli
Simplified diagram representing the reaction mechanism of class I RNR. The network of amino acids given in E. coli numbering. The NDP substrate localizes in the active/catalytic site of reduced R1, followed by a reaction of substrates radical intermediates as well as R1 protein radical intermediate, dNDP will be produced.

R1 crystal's structure in *E. coli* (Figure I.19) has revealed a core domain of 10-stranded α/β-barrel conserved between species (Eklund et al, 2001). More precisely, R1 has an helical N-terminal domain of 220 residues; one ten-stranded α/β-barrel domain of 480 residues; and a small stretch of 70 residues with α helices and β strands domain. The α/β barrel is composed of two halves, where each half contains five parallel strands and four regularly arranged connecting helices (see I.19). The two halves are connected in an antiparallel fashion between strands. R1 has an approximate size of 11 nm long and 7.5 nm wide.

When in dimer, the two R1 have an "S" shaped structure. The important sites have been described in the crystal structure of R1 (Eriksson, 1997) (Eklund et al, 2001):

- The essential radical-carrier cysteine is on the central β-hairpin finger, and the other cysteines are localized on nearby β-strands (in the C-terminus); together this forms the active site, localized between the N-terminus and the barrel domains. This active site has been

shown to be flexible and by conformational change of the subunit make the active site more or less accessible as it is buried 2 nm deep (in *E. coli*)

- The specificity-binding site is found at the dimer interface, not far from the active site above-mentioned, linked by a loop (loop 2). The loop 2 (Figure I.19) is a major determinant for specificity regulation, as this loop will be induced into a distinct conformation depending on each effectors-substrate pair by direct bridging between the specificity site and the active site.
- The activity site (overall activity site, ATP cone) is positioned at the N-terminus in the form of a small α-helical bundle. Different experiments showed that the effectors on the ATP cone would stabilize R1 into an oligomer, and also steady the R1/R2 complexes (Xu et al, 2006).

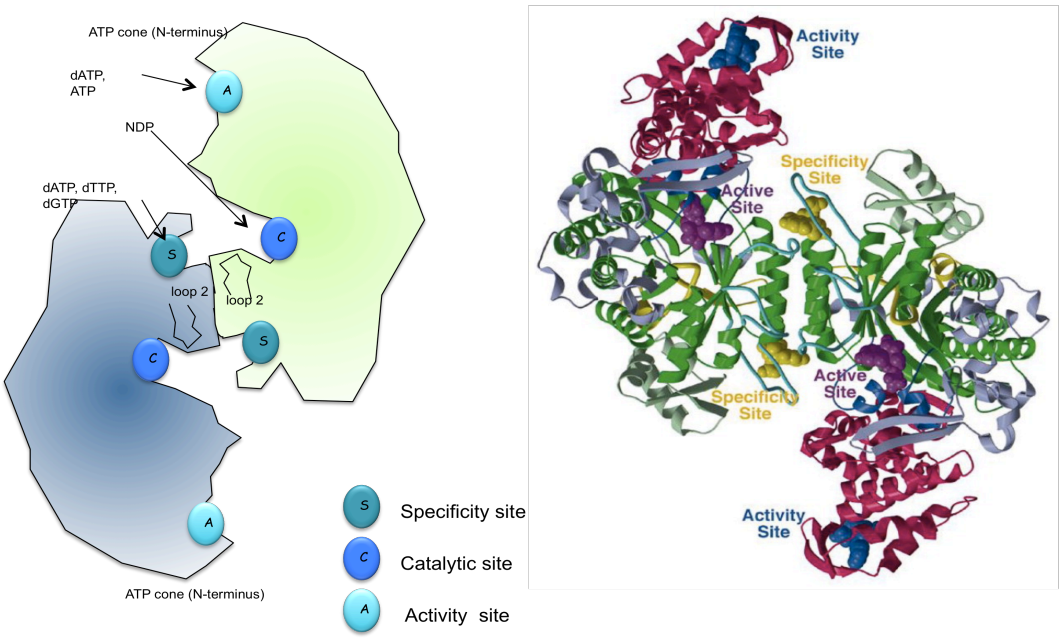

Figure I. 19 Schematic structure of R1 in E. coli along with tertiary structure model (Eriksson, 1997)

Schematic of the structure of the R1 dimer and the associated sites. The global activity is ruled by inhibitory dATP or activating ATP binding at the ATP cone domain situated at the N-terminal. The balanced production of dNTPs is governed by dNTPs binding to the specificity site. The reduction reaction will occur in the depth of the catalytic site, localized close to the dimer interface and to the just mentioned specificity site. The loop 2 is located nearby the catalytic site and will allow flexibility to the catalytic site necessary for the reduction of NDPs.

The second image is a tertiary structure borrowed from Eriksson et al., as it allows us to observe the important sites of R1 in relation to the secondary structure (α α-helices and β strands) as well as the model for the tertiary structure. (N-terminal: magenta; ten-stranded α/β-barrel domain: green; loop 2: yellow)

R1 has evolved into a sophisticated protein that properly supplies dNTPs by monitoring the ATP/dATP ratio thus modulating the overall activity. In addition, by means of the complex allosteric regulation, R1 will manage the right balance of dNTPs through the specificity site. Finally the catalytic site has a main role in the reduction of the NDP riboses 2' –OH. Also, an interesting observation is the flexibility of the C-terminus, and it has been proposed that the C-terminus of R1 can "swing out" of the surface to act as a reduction shuttle (Hofer et al, 2011).

S. cerevisae has a different version of R1, called R3 and seems to be induced after DNA damage (Zhou & Elledge, 1992) , and even though the null mutant has no phenotype, over-expression of this different version of the big subunit can rescue RNR1 null mutants.

2.2 R1 in S. pombe

S. pombe RNR is a class Ia, the same as *E. coli* described previously i.e. a heterocomplex with a big and small subunit in a $\alpha_2\beta_2$ complex.

The big subunit $Cdc22^{R1}$ (β) was first discovered in a collection of temperature-sensitive lethal mutants with a cell division cycle (cdc) phenotype of cell cycle arrest (Nurse P, 1976). $Cdc22^{R1}$ is required early in the cell cycle, and its transcripts fluctuate afterwards. In fact, transcription induction after DNA damage and during the cell cycle was really striking that it sparked some interest and was studied. Cdc22 was finally assigned as the big subunit of the RNR (69% amino acid identity with the mouse R1) (Fantes, 1986).

$Cdc22^{R1}$ achieves its expression peak during Mitosis - G1/ S-phase and is at its lowest during G2 phase. Indeed, $Cdc22^{R1}$ is needed for active RNR complexes during S-phase as well as after DNA damage (when it is also induced) and after HU treatment.

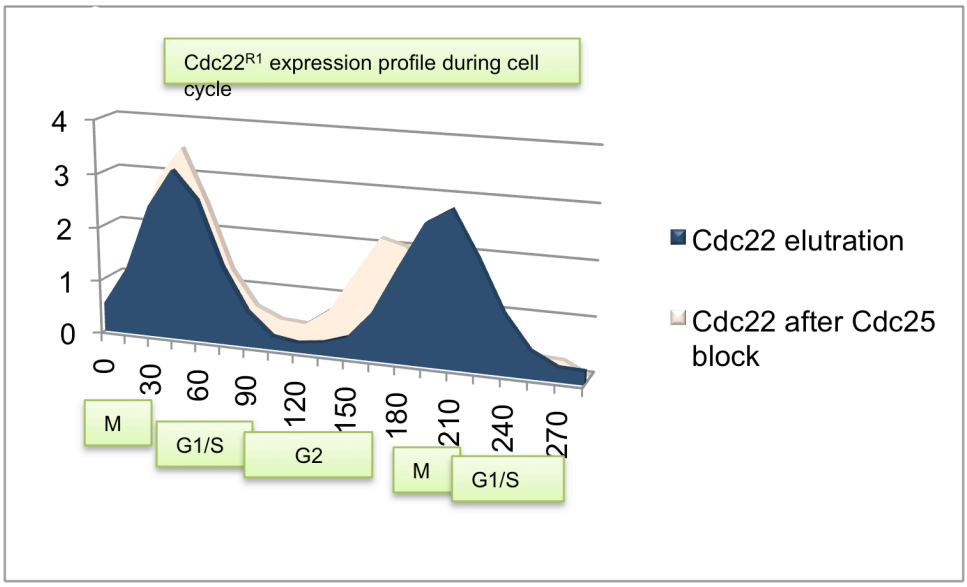

Figure I. 20 Cdc22^{R1} expression during the cell cycle in S. pombe (Bahler's laboratory data)
This represents the fluctuating levels of Cdc22^{R1} expression during the cell cycle after elutriation of the cells or after block-release with Cdc25 mutant. It clearly has a peak of protein expression during M/G1/S phase and is at lowest during G2 phase. This data is just indicative and has been borrowed from the Bahler's extensive online data. Same results were observed in the "CycleBase" data.

Cdc22^{R1} gene (SPAC1F7.05) is found on chromosome 1 (position 4226982-4229733) and is one of the targets DSC1-MCB system which acts on specific sequences upstream the coding sequence, in the gene's promoter (Fernandez Sarabia MJ, 1993).

Cdc22^{R1} has the relative unusual characteristic (in *S. pombe*) of having an intron in its 2752 bp sequence. The 811 amino acids protein (Figure I.21) shares the cystein network with *E. coli* described earlier. Thus the active site is present, and seems to be described as the amino acids at position 427 (proton acceptor), 218 and 444 (which will form the disulfide bond) as well as the cystein 429 (radical intermediate), 431 (proton acceptor) and others are still being investigated and assigned. While the previous amino acids described are situated at the C-terminus, the sites at positions 806 and 809 are suggested to interact with thioredoxin and glutaredoxin (Eriksson, 1997).

The allosteric activity site has also been situated by similarity at the position 11-17 in the ATP cone domain (1-92); and the sites 202 and 247 are for

binding of the NDP substrate, while the specificity site is composed of the sites 285-288.

This 2.7 kb gene results in a 91.6 kDa protein with a isoelectric point of 6.4, and slightly negatively charged (-0.5). $Cdc22^{R1}$ proteins are localized throughout the cell and are regulated by various methods, which I will portray later in more detail.

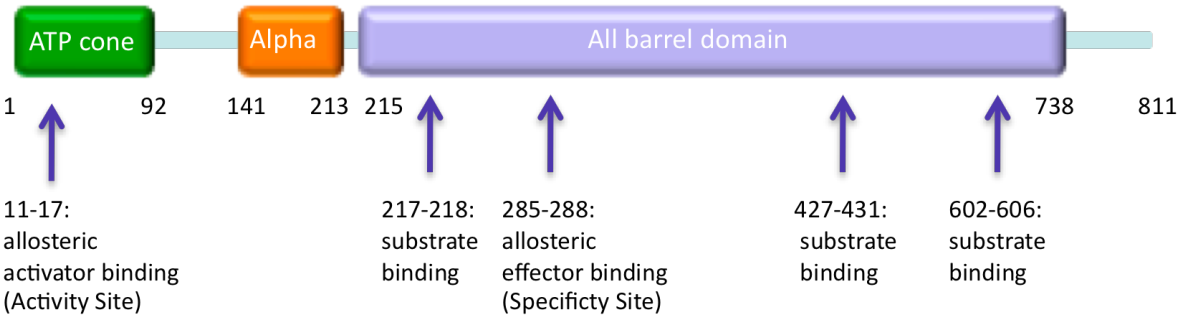

Figure I. 21 $Cdc22^{R1}$ protein domains and organization

This diagram represents schematically the $cdc22^{R1}$+ gene product at the protein level, with the different domains associated as well as the sites for $Cdc22^{R1}$ function. Data obtained from Uniprot with in silico similarity searches. The ATP cone domain is at the N-terminus (where the allosteric site is situated) followed by an all alpha α-helices domain and a all beta barrels domain where the specificity site can be found, as well as the amino acids necessary to constitute the active site.

3. The small subunit R2: gene, protein, structure and function

3.1 General

The small subunit R2 is also only active as a dimer, and each monomer contains a binuclear ferric (Fe^{III}) iron center. These metal cofactor are essential for activity as the apoprotein R2 (loss of iron center) is not functional.
This is due to the fact that the iron center generates and maintains the tyrosyl radical (Y•), via a process of oxidation through surrounding amino acids (Asp84, Glu115, His118, Glu204, Glu238 His241) represented in figure I.22 (Eklund et al, 2001) (Hofer et al, 2011).

R2 was one of the first proteins described to have a polypeptide serving as free radical (Reichard, 1987), and the tyrosine at position 122 of R2 was

described as the organic radical (in *E. coli*, (Larsson et al, 1988)). The Tyr^{122} is buried some 10 Å (1nm) inside a hydrophobic pocket in the structure and therefore cannot interact directly with R1, thus the cysteines network explained before (I.18). This free radical is essential for the activity of RNR, but its stability varies from species to species (4 days in *E. coli* vs. 25 min in humans) leading to speculate the *in vivo* stabilization and/or regeneration mechanisms (Hofer et al, 2011).

The loss of the free radical transforms the protein in a metR2, but still has the iron center intact (contrary to apoR2, where both the iron centre and free radical are lost). ApoR2 proteins can be obtained by iron-chelating agents, while metR2 occurs when radical scavengers are present such as hydroxyurea (HU) or ageing R2. HU is a small radical scavenger used in cancer treatments, but in our interest especially, it has been used since a long time (Elford, 1968) and extensively *in vivo* and *in vitro* to reduce the RNR's tyrosyl radical.

Structure analysis has shown that the iron center of each R2 monomer are 2.5 nm apart but in an metR2 it seems to have shifted further apart although it is not entirely clear how the metR2 is modified (Ormo et al, 1995) (Eklund et al, 2001). It seems that metR2 and apoR2 have a slightly different conformation as well as some denaturation leading to an array of results: unusual cluster of carboxyl-side chains instead of the iron center (Aberg et al, 1993) , differential allosteric binding, and upon iron intake R2 will have a conformational change which has been significantly studied by radical chemist (Logan DT, 1996) (Han & Noodleman, 2011) .

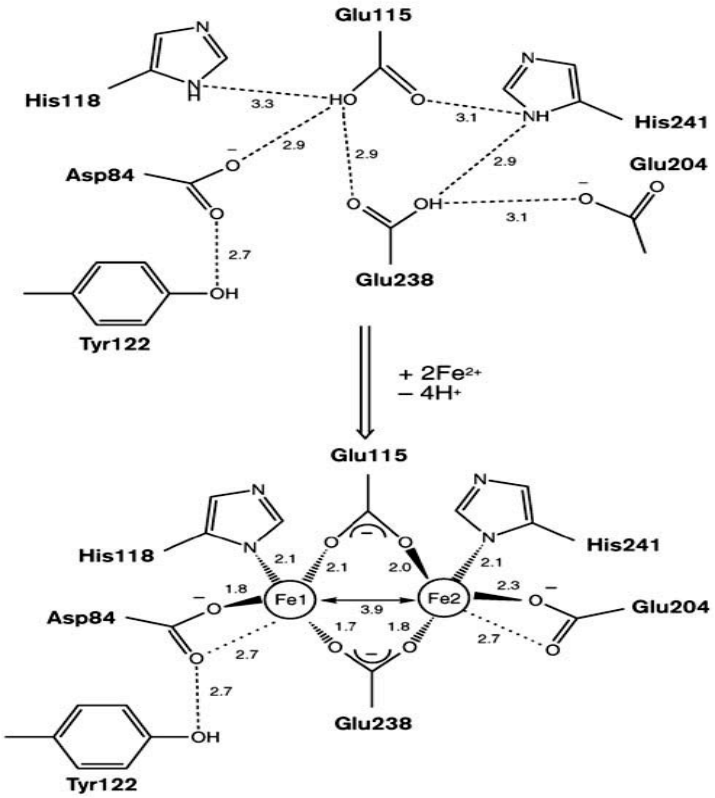

Figure I. 22 ApoR2 iron center and active R2 iron center organization (Logan DT, 1996)
This picture (Logan et al. 1996) shows a diagram of the iron center organization of R2 in apoR2 protein (without iron and without radical) to an active R2 Iron center. There are side chain shifts and deprotonation as part of the conformational changes in the formation of the active iron centre. Hydrogen bonds are in dashed lines and the interatomic distances are given in angstroms. NB: later studies have proven those specific distances to be different.

The *E. coli* R2 structure revealed a stable dimer of 2x43 kDa with the dimensions of 8x6x5 nm, composed mainly by α-helices, although with two β-sheet strands at the tip of the dimer (Figure I.23). The proteins are folded in 3 layers of α-helices, but with extensive dimer interaction. As mentioned just earlier, the iron centre and the free radical are located in the interior of the protein. The N-terminal of R2 is a random coil structure, with a lot of flexibility but does not seem important for enzyme activity (Eklund et al, 2001). Whereas the C-terminus tail of R2 is highly mobile and corresponds to the interaction domain with the C-terminus of R1.

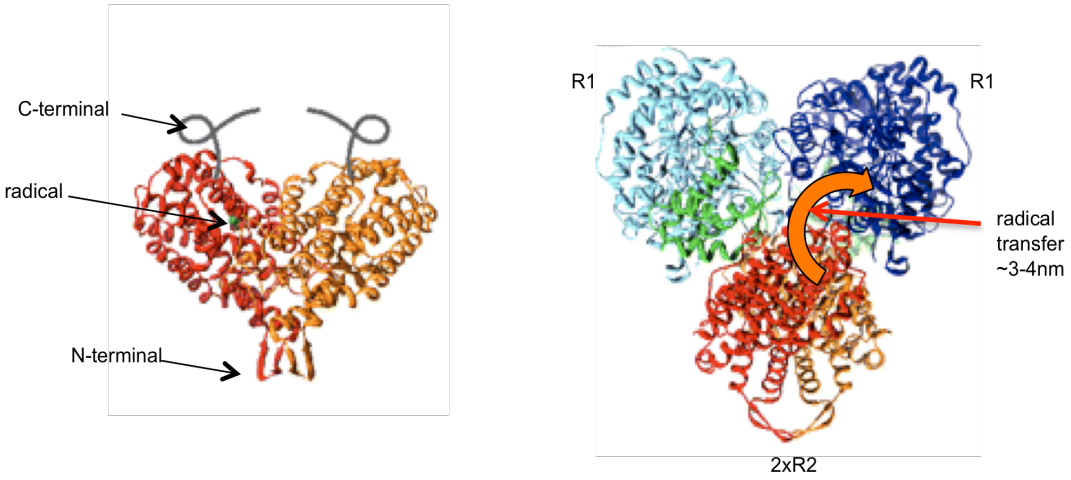

Figure I. 23 R2 protein structure and RNR model for $\alpha_2\beta_2$

These structures have been borrowed from (Ando et al, 2011). The first is the homodimer of R2 in order to represent the structure of the small subunit, mainly compose oh α-helices , and with a disorder C-terminal necessary for binding with R1. The free radical on Tyr122 is embedded inside the protein. The second picture represents the model for the docking between the 2 homodimers of R1 and R2, to form the complex $\alpha_2\beta_2$.

An important point to note is the distance between the tyrosyl radical (Y•) site of R2 and the thiyl radical site of R1 (~35 Å or 3.5 nm) as modeled by Eklund and Uhlin (Eklund, 1994) (Eklund et al, 2001). The detailed mechanism is not entirely clear, but the large distance between the proton coupled electron-transfer (PCET) sites implies some relatively large conformational rearrangements (Ando et al, 2011; Cotruvo & Stubbe, 2011). It seems that the PCET control is important to regulate the enzyme's activity as the PCET can be disrupted if the distances are too large (Reece et al, 2006) (Stubbe & Cotruvo Jr, 2011) (Ando et al, 2011). It has been proposed that the conversion between active RNR and inactive RNR through modification of the structure is the mechanism by which activity is controlled.

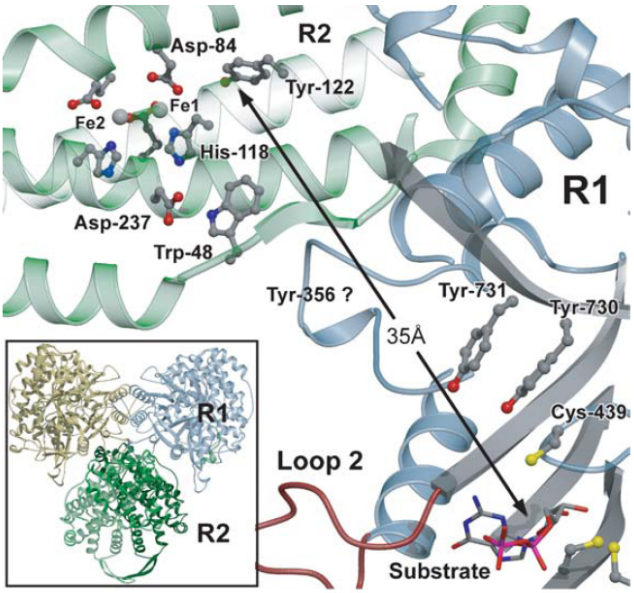

Figure I. 24 Radical transfer (Nordlund & Eklund, 1993)

This picture from Nordlund and Ekhlund 1993, shows the distance of the PCET and the relative position of the amino acids implicated as well as the position of the substrate and the loop 2. This is interesting as such a distance is quite remarkable and even with the network of amino acids for the transfer, the RNR complex must require flexibility to induce an optimal conformation.

Mammalian cells have another version of R2: p53R2 (Tanaka et al, 2000) (Smith et al, 2009) that has been showed to be involved in DNA repair, during which it seems to be induced and increase the concentration of active RNR complexes. More recently it has been proposed to have a role in mitochondrial dNTPs production (Wang et al, 2011). *S. cerevisae* also has a second version of R2 (RNR4 or β') that is required, and is slightly different than RNR2 (β). Together they form a heterodimer, and even though RNR4 is not able to form the radical, RNR4 is important to correctly fold RNR2 in order to generate its radical and correctly function in the $\alpha_2\beta\beta'$ complex (Elledge et al, 1992) (Huang & Elledge, 1997) (Zhang et al, 2011).

3.2 R2 in *S. pombe*

The smaller subunit $Suc22^{R2}$ was discovered as a suppressor of the $Cdc22^{R1}$ thermo-sensitivity lethality (Fernandez Sarabia MJ, 1993). $Suc22^{R2}$ (SPBC25D12.04) encodes for the small subunit of the RNR, and the 1176 bp

gene is localized on the chromosome 2 (position: 3721755-3722930). The protein is 391 amino acid long, and the 45.5 kDa protein has an isoelectric point of 14.6 and a charge of -20. The *suc22*^{R2}+ gene product has 62% amino acid identity with the mouse R2, and the similarity is particularly strong with the other species over the C-terminus (Kolberg et al, 2004).

The essential tyrosine for the free radical is in position 173, and the important amino acids involved in the iron centre are: D135, E166, H169, E229, E263, H266. The residues E360 and Y366 which are thought to be required for the interaction with the large subunit R1, are conserved (Nordlund & Eklund, 1993) (Eklund et al, 2001). (Figure I.25).

Suc22^{R2} has consistent protein expression levels throughout the cell cycle and is localized mainly in the nucleus, but during S phase is relocalized to the cytoplasm.

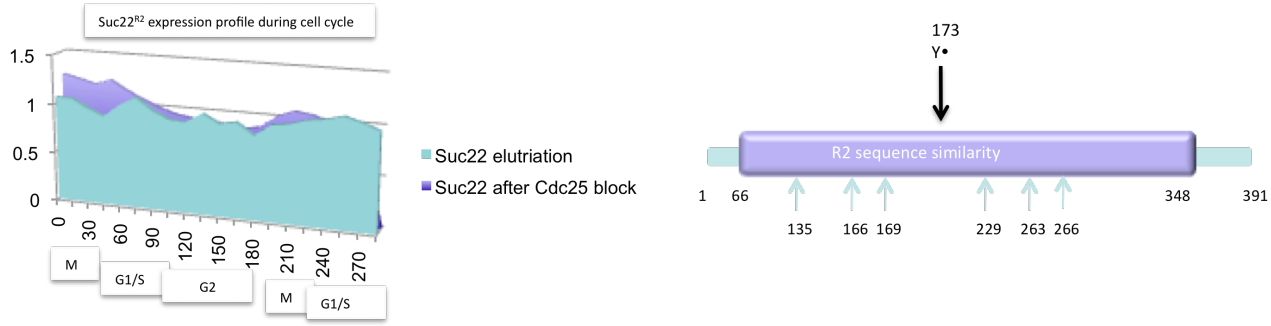

Figure I. 25 Suc22^{R2} protein expression during cell cycle and protein sequence

These diagrams represent schematically the suc22^{R2}+ gene expression during the cell cycle (Bahler's data and confirmed by "CycleBase"). It has a regular level during the cell cycle. Next image is a schematic representation of the protein sequence with associated domains and important amino acids (obtained from uniprot).

Interestingly, the *suc22^{R2}*+ gene has been described as having 2 transcripts, one of 1.5 kb, which is present throughout the normal cell cycle, and is the single transcript detected. But after HU treatment, DNA damage, or heat shock a second transcript of 1.9 kb appears (it is only present at low levels during S-phase). The larger transcript has a different initiation site (550 bp upstream) but both seem to have MCB elements upstream the initiations sites, and appear to code for the same protein (Fernandez Sarabia MJ, 1993) (Harris P, 1996).

4. Regulation of RNR

4.1 General

a. Cell-cycle specific gene regulation and protein localization

To overcome the enormous demand of dNTPs during the full genome replication (S-phase) RNR activity increases partly due to the induction of the RNR genes. The same process happens after DNA damage where dNTPs are needed for DNA repair.

It differs slightly from species to species, with *E. coli's* aerobic and anaerobic RNRs regulated differently but following the same general pattern earlier described.

In *S. cerevisae* all RNR genes are transcriptionally regulated during S-phase and after DNA stress (Zhou & Elledge, 1992) (Huang & Elledge, 1997). Also, RNR2 and RNR4 proteins are localized in the nucleus, but relocated to the cytoplasm to presumably form the active complex.

As for mammalian cells, the enzyme's activity increases greatly during S-phase too, but R1 and R2 have different regulation. Both R1 and R2 are in promoter-active regions, but in addition of transcription regulation; R2 seems to be degraded through a KEN box, for example during mitosis or after DNA damage (Chabes et al, 2003b). Also after DNA damage there is over-expression of p53R2 and R1, which will then form a different RNR complex that will provide the cell with dNTPs for DNA repair. All RNR proteins are found throughout the cytosol in the case of mammalian cells (Zhou et al, 2003).

b. dNTPs production by allosteric regulation

Providing adequate quantities of dNTPs to the cell is not the only role of RNR; there is an important need for a right balance between the four DNA building blocks (Chabes & Thelander, 2003). This is achieved by allosteric regulation of the RNR enzyme's activity. The active site will control the overall activity of the enzyme, while the specificity site will be part of a complex network in order to provide the right dNTPs. The active site can bind ATP (leading to the "switching on" of RNR) or dATP (turning off the overall activity). ATP has the

same affinity for both the activity site and the specificity site, whereas dATP has a much lower affinity for the activity site than the specificity site. Therefore, only at very high levels of dATP will this allosteric inhibitor bind to the activity site. An RNR mutant D57N is often used, as the mutation disables the activity site capacity to discern ATP or dATP (Chabes & Stillman, 2007).

The specificity site can bind ATP, dATP, dTTP and dGTP, but does not bind dCTP efficiently. There is a quite precise physiological level of each dNTPs in the cell, which seems optimized to limit the mutation rate.

ATP and dATP will stimulate the reduction of CDP and UDP, while dTTP will activate GDP reduction and dGTP will in turn encourage ATP reduction (Hofer et al, 2012).

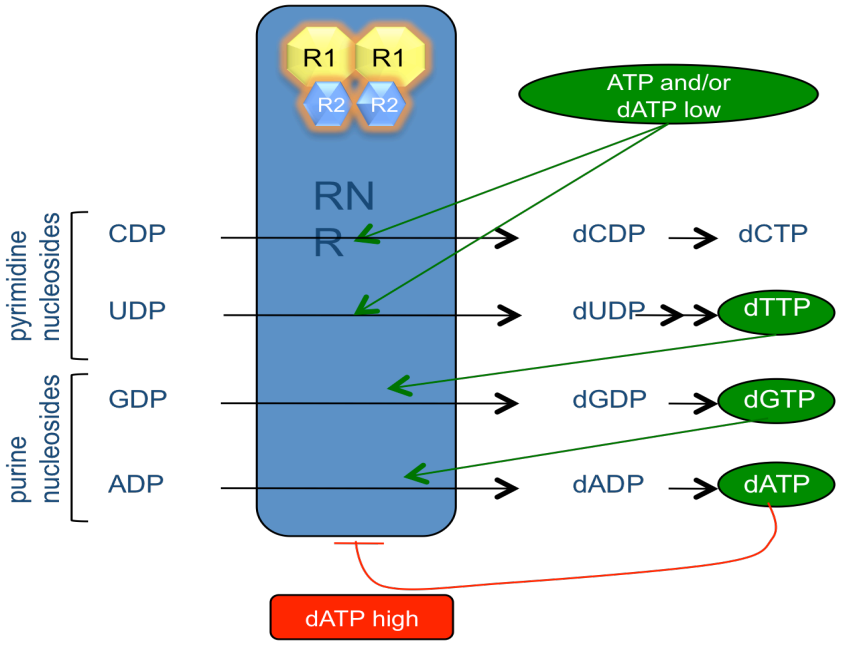

Figure I. 26 Simplified overview of the allosteric regulation of dNTPs production

Diagram of the allosteric effectors on RNR: through the specificity site, ATP and low dATP will activate dCDP and dUDP synthesis, while dTTP will activate dGDP reduction, and dGTP in turn will increase dADP production. But through the activity allosteric site, high concentration on dATP will inhibit the while RNR machinery, but ATP will activate RNR.

c. Inhibitors

Small proteins were found as RNR inhibitors, first *in S. cerevesiae*, and also in *S. pombe*. So far, in mammalian, nothing comparable as been described yet.

In *S. cerevisae* R1 is inhibited by interaction with Sml1, a small protein that is degraded once cells enter S phase or in response to DNA damage, due to the Mec1/Rad53 DNA damage checkpoint pathway (Zhang et al, 2007) (Andreson et al, 2010). A further method of negative regulation is obtained with Dif1, which in cooperation with the nuclear anchor Wtm1, promotes R2 nuclear import (Lee & Elledge, 2006) (Lee et al, 2008). This redistribution from the nucleus to the cytoplasm appears to be yet another layer of regulation, as it was proposed that the active form of the RNR complexes would be formed when both RNR subunits are in the cytoplasm, which corresponds to S-phase or after DNA damage. A last regulator, Hug1 has been proposed to regulate the RNR by preventing a correct feedback, but its role is still indistinct (Lee et al, 2008) (Benton et al, 2006) .

4.2 Regulation of RNR in *S. pombe*

The cell cycle based regulation has been described previously: $Cdc22^{R1}$ expression induced during S phase and after DNA damage, whereas $Suc22^{R2}$ has a second transcript also induced after DNA damage.

a. RNR Regulators: Spd1 and Spd2

During a screen for new *S. pombe* genes for cell cycle arrest (Woollard A, 1996), Spd1 (S-Phase delayed inhibitor) was found. When over-expressed (Borgne & Nurse, 2000), this small protein causes S Phase Delay (SPD). In normal circumstances, Spd1 is cell cycle regulated and degraded after DNA damage.

Spd1 (SPAC29B12.03) is a 375 bp long gene situated on chromosome 1 (position: 5412489-5412863) and encodes for a 14.2 kDa protein (124 amino acids) with 7.6 as isolectric point and a charge of 1.

Its expression is anti-correlated with the RNR's activity, as Spd1's expression is high in G2 and G1 but mostly degraded in S-phase. Spd1 is also degraded after DNA damage and DNA replication stress. This degradation is controlled by the Cop9-Pcu4-Ddb1 complex (i.e. Signalosome CSN) (Liu et al, 2003) (Liu et al, 2005) (Nestoras et al, 2010).

The signalosome is a complex of 6 subunits in *S. pombe* (Csn 1-5 and Csn 7) but 8 subunits are described in other species; moreover it is conserved as it has a variety of essential roles in the cell (Nielsen, 2003). One of these roles is with the cullin-dependent ubiquitin ligase (Pcu4), therefore the COP9/signalosome is involved in ubiquitin mediated protein degradation (Wei & Deng, 2003). In *S. pombe*, Ddb1 associates with Cop9-Pcu4 to promote Spd1 degradation and indirectly regulate RNR activity (Bondar et al, 2004). Two components of the CSN complex, Csn1 and Csn2 are essential for a correct regulation of RNR as during S-phase the ubiquitylation of Spd1 leading to its degradation happens in a Csn1- and Csn2-dependent manner. Whereas in G2, after DNA damage, Spd1 degradation requires both signalosome subunits Csn1 and Csn2, but also the Rad3- and Chk1-dependent DNA damage checkpoint. Therefore the Cop9-Pcu4-Ddb1 is involved in genome stability via regulation of RNR activity through Spd1 control. The mutant strain $Rad3^{ts}$ Csn1-deletion is lethal, but can be reverted by over expression of $Suc22^{R2}$ or Spd1 deletion (Liu et al, 2003) (Liu et al, 2005). Therefore, the reversion in the mutant strain $Rad3^{ts}$ Csn1-deletion is a good tool to measure Spd1 activity. Also, Ddb1 is needed for cells to progress through meiosis, as Spd1 degradation is essential at that time (Holmberg et al, 2005).

The small protein Spd1 is found throughout the cells: both in the cytoplasm and nucleus. Spd1 is involved in the localization of $Suc22^{R2}$: it was first described as a potential anchor (similarly to Wtm1 of *S. cerevisae*) but was later demonstrated to acts as a nuclear importer (Nestoras et al, 2010). Experiments with a nuclear export-blocking agent (leptomycin B) did not result in a $Suc22^{R2}$ nuclear accumulation, and in addition, when a nucleolus C-terminal signal was added to Spd1, it did not accumulate $Suc22^{R2}$ to the nucleolus. When Spd1 is degraded or the *spd1+* gene deleted, $Suc22^{R2}$ accumulates in the cytoplasm due to lack of nuclear import giving $Suc22^{R2}$ a clear pan-cellular phenotype. Similar observations are seen after treating the cells with HU (Nestoras et al, 2010) (Liu et al, 2005).

On the other hand, it has also been described to bind to $Cdc22^{R1}$ and through that binding acts as an inhibitor. But as the data in this thesis and the

publication Nestoras et al. shows, we should rather consider Spd1 as an RNR regulator instead of an inhibitor.

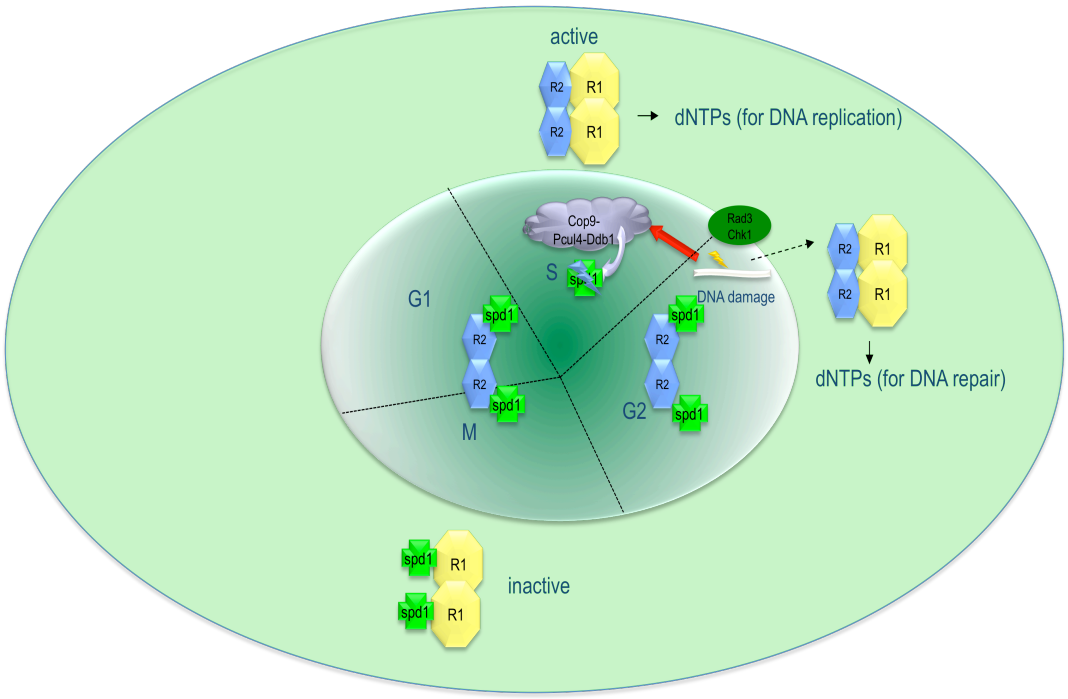

Figure I. 27 Schematic of the current model of RNR regulation during the cell cycle through Spd1

This diagram represents the cell with the nucleus (central) and the localization of each protein during the cell cycle. During M and G1 phase, Spd1 is present and regulates negatively the RNR by binding to $Cdc22^{R1}$ and importing $Suc22^{R2}$ to the nucleus. During S phase, the signalosome degrades Spd1 and the RNR can be complexed into an active form to provide dNTPs. In G2 Phase, if there is DNA damage, the signalsome will act again after Rad3-Chk1 checkpoint activation to degrade Spd1 and allow formation of active RNR for efficient DNA repair.

Spd1 is an Intrinsically Disordered Protein (IDP) (Nestoras et al, 2010), which means that Spd1 has no fixed tertiary structure and can be modulated into different conformations. This peculiar feature correlates well with the role of Spd1 as an RNR regulator, because even though it is missing a well-structured three-dimensional fold, it has the capability to adopt transient structure and fold into their protein partners with low affinity but high specificity (Sugase et al, 2007).

Very recently, Spd2 was found by sequence homology and is now being described in more details with regards to its functions. Spd2 (SPAC3F10.19) is also found on chromosome 1 (position 2830517-2831209) and after splicing

(the Spd2 gene contains 2 introns) it is a small transcript of 309 bp. Spd2 is an even smaller protein than Spd1 with 102 amino acids, resulting into a 11.6 kDa protein (isolectric point: pH 4.9, charge: -4).

b. Comparison between the regulators *S. pombe* and *S. cerevisae*

Spd1 and Spd2 have some proposed domains, found in the sequence-conserved *S. cerevisae* orthologues: Sml1, Dif1, Hug1. The HUG domain (a.a 30 to 62) as in Hug1 and Dif1; and an R1 domain (a.a 83 to 97) which is a part of *S. Cerevisae* Sml1's protein R1 binding domain.

Work in *S. cerevisae* has shown that Dif1 and Wtm1 act as nuclear import and nuclear anchor respectively; and that Dif1 binds R2 by the HUG domain (Lee & Elledge, 2006) so the HUG domain can be considered as the R2 binding domain.

Spd1 also binds to Cdc22^{R1} (Hankansson et al, 2006a) (Nestoras et al, 2010) and seems to inhibit it, by which means is yet unclear, but in *S. cerevisae* Sml1 inhibits R1 by binding to the C-terminal part of the large RNR subunit (Zhang et al, 2007) and would therefore interfere not only with the R1 dimerization, RNR structure formation but also the R1 reduction capacities (Cotruvo & Stubbe, 2011).

```
Spd1            ---MHSSKRVMTTKTHVEQPESSM---RPQLPESIQGSLMDVGMRVRKSISTGYKSKQTT 54
Spd2            ----------MSETFKLPDHD--------ELPQLVQTTLFDVGARVRKAVQTGYKFDQQL 42
Hug1            ----------MTMDQGLNPKQ------FFLDDVVLQDTLCSMSNRVNKSVKTGY-----L 39
Dif1            MDAQLEWASSLVPKRQLQQQQQQQEQQQQQQQDFHKDQLMTVGMRIRQRVDQGYASRTPS 60
Sml1            ---MQNSQDYFYAQNRCQQQQ---------APSTLRTVTMAEFRRVPLPPMAEVPMLSTQ 48
                            :         :              :        *:

Spd1            FPAYNPPLYNTVSENIALKNTAFSYEPNGTKRPFEQAIPNYNWANPPQD-FEEPEWLKP- 112
Spd2            FPSYHKDQTDRNELPQQKHDPNLRLDDLKQELAADSIFWDTASTQEIADSFAKPDFLKS- 101
Hug1            FPKDHVPSAN--IIAVERRG---GLSDIGKNTSN--------------------------- 68
Dif1            TSDASLQPGVIRDYSSVIVP-QFTRSPLPTANSLPPMLINQRTMSTEASSLEKWDVAEPA 119
Sml1            NSMGSSASASASSLEMWEKDLEERLNSIDHDMNNNKFGSGELKSMFNQGKVEEMDF---- 104
                 .                          .

Spd1            --FDVVMEGTNERL 124
Spd2            --H----------- 102
Hug1            -------------
Dif1            AEHETMVNGSKRRL 133
Sml1            --------------
```

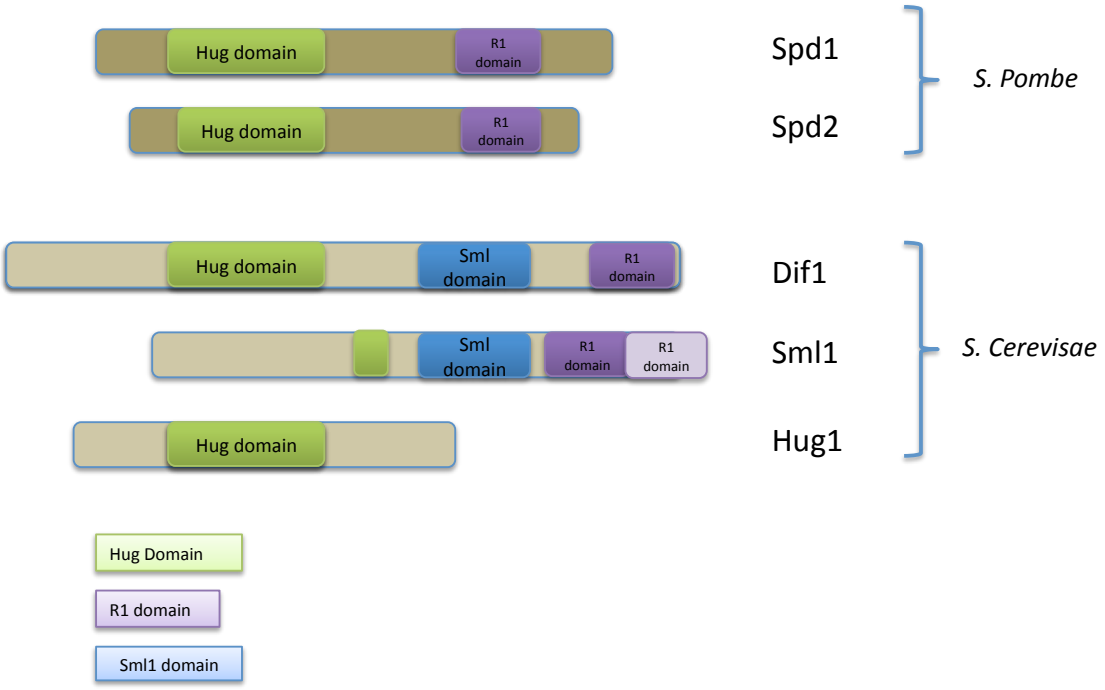

Figure I. 28 Comparison of the RNR regulators in S. cerevisae and S. pombe

The alignment of the amino acid sequence of Spd1, Spd2, Hug1, Dif1 and Sml1 represented in the first image shows close sequence identity. The second picture is a diagram of the regulators with the different domains described. Again, there is a strong sharing of domains.

4.3 RNR complex oligomerization and structural modification

Many *in vivo* studies have informed us about the importance of RNR for genome stability, and *in vitro* studies have helped us understand how the RNR complex is structured and functions. But as RNR is very tightly regulated *in vivo*, it is hard to have a direct view of the RNR regulation *in vivo* in the cell. *In vitro* studies are very helpful, but do not reflect the exact reality, as in the cell there are some precise physiological levels of the proteins, inhibitors and especially allosteric effectors. In addition, the activity site and the specificity site are often occupied and there might be other unknown partners.

R1 (α) has been described early on to be oligomerized (Brown et al, 1968) and to sediment into a tetramer. The dynamics of the R1(α)/R2(β) aggregation status seems to be controlled in part by the ATP/dATP effectors. The ability to differentiate between the activator ATP and the inhibitor dATP at the ATP cone domain is one of the keys for better understanding of the RNR regulation. The discrimination between ATP and dATP seems to be due to the

structure of the effectors, as dATP can bind deeper. Thus specific conformational changes of the ATP cone domain recognizing one or the other effector will allow distinction between activation and inhibition. Interestingly, these conformational changes also involve the loops described in the dimerizaton of R1 (Cotruvo & Stubbe, 2011) (Hofer et al, 2012).
The specificity site also influences the overall structural regulation, as it has been shown that the specificity site and the activity site have a long-range communication (Ando et al, 2011).

The model is that the allosteric effectors would first promote R1(α) dimerization, which would in turn facilitate binding to the R2 dimer, forming the heterocomplex $\alpha_2\beta_2$. The $\alpha_2\beta_2$ was for long considered to be the active form, but the last few years publications have demonstrated that the stoichiometry of the RNR subunits can vary a lot: for eukaryotes $\alpha_2\beta_{2\text{-}6}$ (Kashlan et al, 2001) (Rofougaran et al, 2006) (Xu et al, 2006) and in *E. coli* $\alpha_{2\text{-}4}\beta_{2\text{-}4}$ (Rofougaran et al, 2008a).

Even more recently the picture became a lot clearer with structural studies of dATP-induced inactive RNR forms. In human and *S. cerevisae*, the dATP induced RNR is indeed a $\alpha_2\beta_6$ form with 3 dimers of R1(α) in a ring and the R2(β) dimer inside the α_6 ring (Fairman, 2011). This protein architecture is proposed to abolish the electron transport (PCET) thus inhibiting the activity of RNR (Ando et al, 2011; Xu et al, 2006). Other data also demonstrated that the ATP induced active form in eukaryotes could be in a $\alpha_6\beta_{2\text{-}6}$ form with a different α_6 variant. The active and inactive forms could be structurally very different, as a mutation (D16R) at the interface between the dimer area would not allow dATP α_6 formation anymore (Hofer et al, 2011), whereas with ATP the hexamers α_6 could still be formed (Hofer et al, 2011). Some data suggest the big subunit α would also be in an hexameric ring while the stoichiometry of the small subunit is not clear yet, although some studies (Wang et al, 2009) with gemcitabine (substrate analogue) demonstrated that up to 3 β dimers can bind to the ATP induced α_6, forming a $\alpha_6\beta_6$ complex.

In *E. coli*, the $\alpha_2\beta_2$ form was the accepted model for the active RNR complex, but recently (Ando et al, 2011) the inactive form of RNR has been structurally solved and is also a ring structure although a quite different ring.

The $\alpha_2\beta_2$ complex opens and a second $\alpha_2\beta_2$ complex binds creating a ring of sequential $\alpha_2\beta_2$ $\alpha_2\beta_2$.

It has been proposed and modeled that this quaternary structure modification would disrupt the radical pathway thus inactivating the RNR protein. The conversion between one form to the other could be quite dynamic and although the regulation between one form to the other is barely understood, it proves to be an ingenious system to control the dNTPs levels in the cell (Ando et al, 2011; Fairman, 2011; Hofer et al, 2011).

This clearly deserves further investigation in order to understand the tight regulation of the RNR using higher order complexes and structural modification.

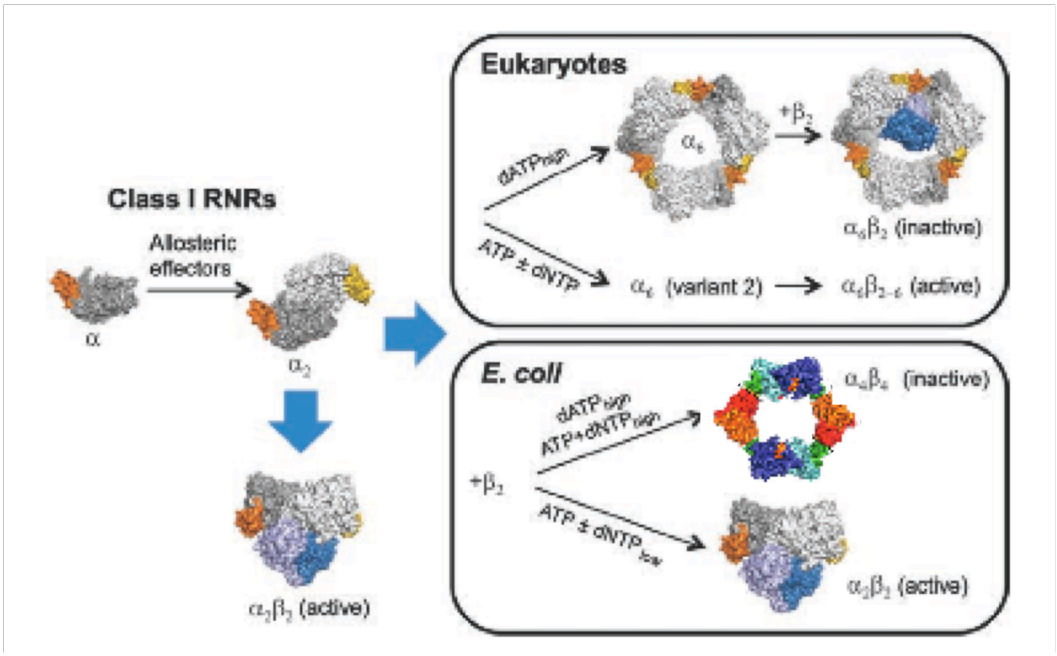

Figure I. 29 Activity regulation in Class I RNR (Hofer et al, 2011)

Diagram showing the quaternary structure related regulation of the RNR complexes. The dimer α2 will bind to the dimer β2 and form $\alpha_2\beta_2$. In Eukaryotes, the dATP induced RNR $\alpha_6\beta_2$ will be inactive and in a ring shaped of hexameric α with the β2 dimer in the centre. The ATP induced active RNR has been described to be composed of also a hexameric α, although structurally different, and the smaller subunit β could be in a dimer, tetramer or hexamer. In E. coli, the inactive RNR form is also a ring, although different as it is composed of 2 times $\alpha_2\beta_2$ with sequential $\alpha_2\beta_2$ $\alpha_2\beta_2$. The active form is so far still described as a $\alpha_2\beta_2$.

4.4 Aims of this project

Albeit a good amount of qualitative work has been done on the RNR throughout different species, some questions remains.

On the structural side, more details are needed in order to understand the structural regulation of the enzyme, especially *in vivo*. In addition, the regulation of Spd1 and Spd2 are undefined but represent a good setting to study RNR regulation in the cell.

It is clear that the RNR complex has flexibility in its structure, not only to achieve oligomerization but also conformational changes. But how exactly does this affect the activity of the RNR? Does it only influence the overall activity and thus dNTP pool? Are some complexes more active than others? How important are these oligomeric states, and how do they proceed?

What about the roles of Spd1 and Spd2? How do they affect the RNR general structure? In what ways does Spd1 regulate the RNR, indeed it does interact with both subunits, controls $Suc22^{R2}$ localization and RNR activity, but how does this relate to the general architecture of the complex enzyme?

As some questions remain unanswered, in general but also in *S. pombe*, this project has for aim to uncover some of the RNR regulation, in particular the regulation by Spd1 and Spd2 and structural/architectural related regulation.

III. Advanced Fluorescence Microscopy methods

Various microscopy methods were used to investigate the regulation of RNR i*n vivo* and *in vitro*, thus I will introduce fluorescence microscopy and methods used in this project.

1. Fluorescence, origins and applications

1.1 Fluorescence origins

Sharing the 2008 Nobel Prize in chemistry, Tsien R., Chalfie M. and Shimomuru O. allowed huge steps in biology research by discovering, cloning and enhancing the Green Fluorescent Protein (GFP).

The discovery and the isolation of GFP was done successfully by Osamu Shimomura in 1962 from *Aequorea Victoria* (Osamu et al, 1962). In the nineties, Douglas Prasher (Prasher et al, 1992) cloned the GFP gene (wtGFP), which was then used by the laboratories of Martin Shalfie and Frederik Tjusi, who successfully integrated and expressed GFP in *E. coli* and *C. elegans* (Chalfie et al, 1994). Other laboratories then provided the structure of GFP (Cody, 1993) (Ormo et al, 1996) thus also allowing the engineering of enhanced stable variants (Tsien, 1998).

Since then, the GFP sequence has been manipulated extensively to provide improved proteins as well as a wide range of colors. Blue (BFP), Cyan (CFP), Yellow (YFP) just to name a few; and the additional fluorescent protein, providing the color red (RFP) has been added to the collection after being discovered in corals (Seward & Bagshaw, 2009).

The use of fluorescent proteins is wide and varied, ranging from following proteins *in vivo*, staining cellular components, and more recently using fluorescence methods to study protein interaction, or protein dynamics for example. Additionally, cloning of these fluorescent proteins have been done successfully in many organisms and in most cases, without having a significant impact on the function of the labeled protein (Giepmans et al, 2006) (Nowotschin et al, 2009).

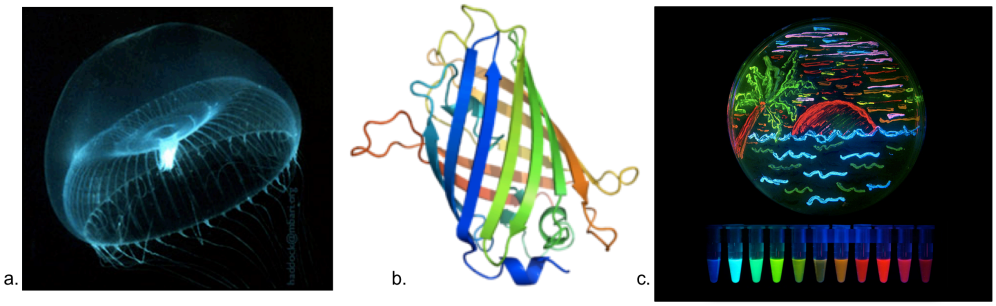

Figure I. 30 Origins and evolution of GFP

GFP was isolated from the jellyfish Aequorea Victoria (a.: Picture from Steve Haddock, bioluminescence web page). Picture b. represents the GFP protein structure (source Protein Database Bank). And finally the extensive GFP improvements and GFP variants engineered (c.: R. Tsien Lab website)

1.2 GFP and derivatives characteristics

GFP is a small gene encoding for a 238 amino acids long protein, with actually only four amino acids directly producing the fluorescence effect. The protein is 27 kDa and is 4,2 nm long and 2,4 nm width (Cody, 1993) (Ormo et al, 1996) .

The fluorescent protein GFP and its derivatives have a unique barrel shape structure. eleven β-strands make up the barrel, and a α-helix runs through the middle. The covalently bonded chromophore is located in the center of the barrel, as it needs to be protected by the fully correct folded protein. Mutations modifying the hydrogen-bonding network of GFP leads to a variety of color, intensity and stability (Hadjantonakis & Nagy, 2001) (Giepmans et al, 2006).

All those fluorophores are excited by a certain wavelength (for wtGFP the excitation peak centered is at 395 nm), and will emit in another wavelength (emission peak centered at 509 nm). Fluorescent proteins are characterized by their excitation and emission spectrum, as well as their relative brightness (depending with the quantum yield and the extinction coefficient of the protein).

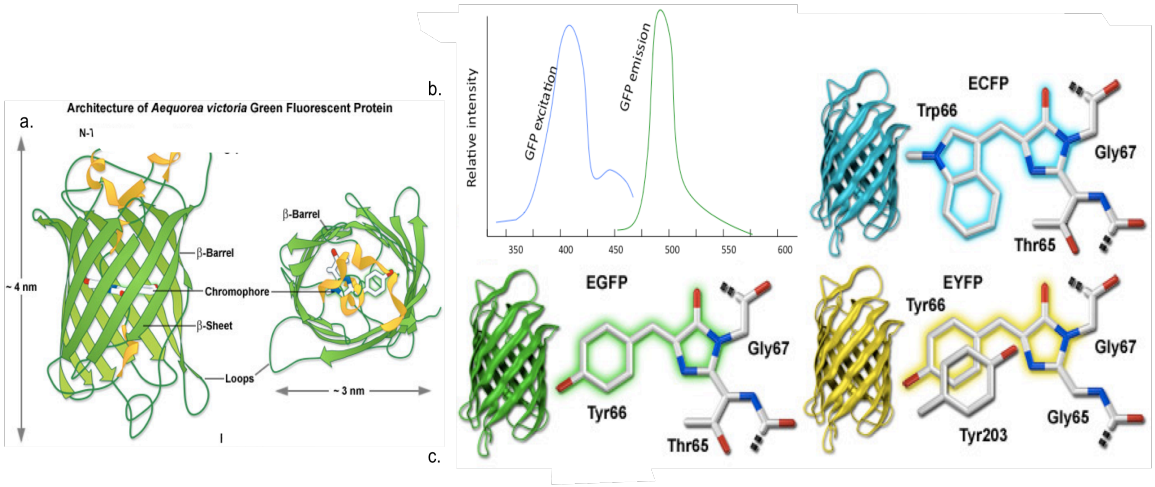

Figure I. 31 GFP characteristics and GFP variants

Picture representing the GFP structure in a barrel with approximate sizes of 4nm on 2 nm (a.: source Zeiss campus website) In b. is an example of a fluorescent protein spectra, with its excitation and emission, for example here wtGFP has an excitation peak at 395 nm and emission peak around 509 nm.

Picture c. represents the chromophore structural motif in GFP and two variants CFP (tryptophan residue instead of Tyr66) and YFP (stacking of a second tyrosine (Tyr203) on Tyr66 along with substitution of Ser65 for glycine), and how mutations change the spectra of these proteins. (Source: Olympus confocal website)

1.3 Applications

GFP and its derivatives have been extensively used in all fields of biology, biochemistry and chemistry. Other fluorophores (i.e. FITC) can be toxic to living cell, therefore GFP has improved the field of live cell imaging as it allows to follow proteins during the cell cycle, after damage, in presence of drugs; but also in whole organisms development. This brings a fourth dimension to microscopy, after x,y, and z, the time factor (t) allows to study in more depth biological processes (Giepmans et al, 2006).

In addition, due to its non-invasive and versatile qualities, it has the capacity to be cloned into many organisms, ranging from virus to cat, which is also a novelty.

One of the many ingenious usages of GFP is symbolized by the brainbow, which is very representative of the engineering and creative possibilities with genes encoding fluorescent proteins. Combining several GFP and RFP

variants, nervous cell will express a different combination resulting in different colors: the brainbow (Livet, 2007) (Figure I.32).

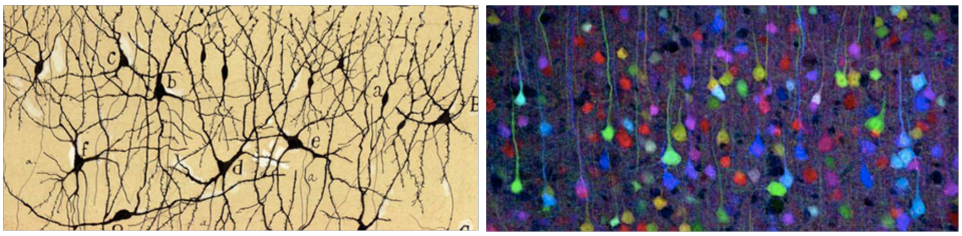

a. b.

Figure I. 32 Brainbow

This figure *shows the striking similarity between an old drawing from Cajal (a.: Santiago Ramón y Cajal. 1901. from "Herederos de Ramón y Cajal") next to the brainbow (b.: Livet et al, 2007, from the Harvard brain centre)*

Although the brainbow is a success with regards to creativity, it does not allow studying particular molecular mechanisms. Thus, in order to study more precise protein interaction, dynamics structure, modifications, and localization; a few methods have emerged lately (Schmolze et al, 2011). Just to name a few: FRAP (Fluorescence Recovery After Photobleaching) will allow measuring the dynamics of proteins, FLIM (Fluorescence Lifetime IMaging) is a very precise methods to measure the lifetime of the emitted fluorescence, FCS (Fluorescence Correlation Spectroscopy) is rather for *in vitro* studies, for example to study protein binding. Another one of these is FRET (Fluorescence Resonance Energy transfer), which I will now explain in detail.

2. FRET: Fluorescence Resonance Energy Transfer

2.1 FRET principle

A powerful tool to investigate inter- and intra-molecular modifications is Fluorescence (or Förster) Resonance Energy Transfer (Truong & Ikura, 2001) (Pollok & Heim, 1999) (Pietraszewska-Bogiel & Gadella, 2011). An initially excited donor fluorophore can transfer non-radiative energy to another fluorophore, which will act as acceptor. In order to have this energy transfer between chromophores, a few requirements have to be met: a distance between 1-10 nm (10-100 Å), the right dipole-dipole conformation of both

chromophores, and a minimum of overlay of the donor emission spectra with the acceptor excitation spectra (Pietraszewska-Bogiel & Gadella, 2011) (Marc et al, 2006).

This FRET phenomenon has been studied by physical chemistry laboratories, but has gradually made its way into biophysics, molecular biology and biochemistry as a technique to study protein folding (Truong & Ikura, 2001) (Heyduk, 2002), protein interaction (Truong & Ikura, 2001), DNA-protein interactions (Hillisch et al, 2001) and protein dynamics (Tadross et al, 2009).

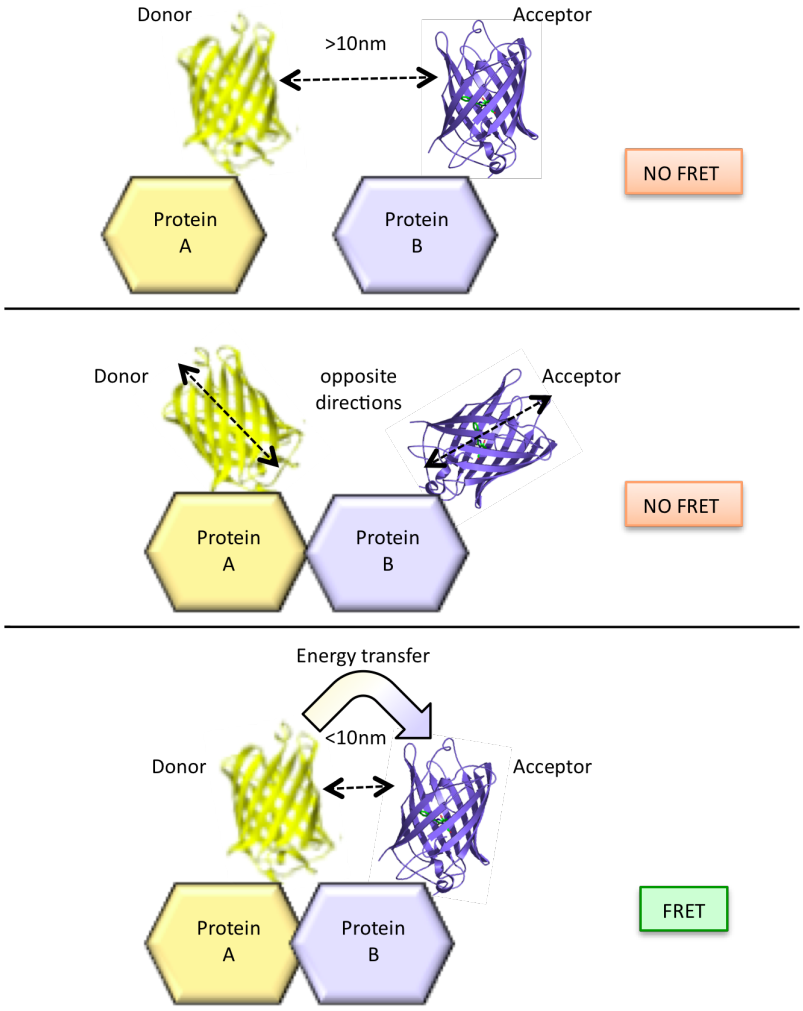

Figure I. 33 Fluorescence Resonance Energy Transfer

Simplified illustration explaining the FRET requirements: the donor fluorophore and the acceptor fluorophore have to be less than 10 nm distance; the chromophores need the right dipole conformaton i.e. orientation of the fluorophores. If all these standards are met, energy transfer will occur between the donor and the acceptor. This can be used on two different proteins, but as well as to observe dimerization, or even conformation change of a unique protein with the donor and the acceptor are tagged at the opposite ends of the protein.

One of the most popular FRET pair used is cyan fluorescent protein (CFP) and yellow fluorescent protein (YFP) (Tadross et al, 2009). Both are color variants of GFP, and more color variants are available enabling different combinations of pairs (Marc et al, 2006). As CFP/YFP is a good FRET pair partly due to its ideal spectras (Figure III.5), it was the one used throughout this project.

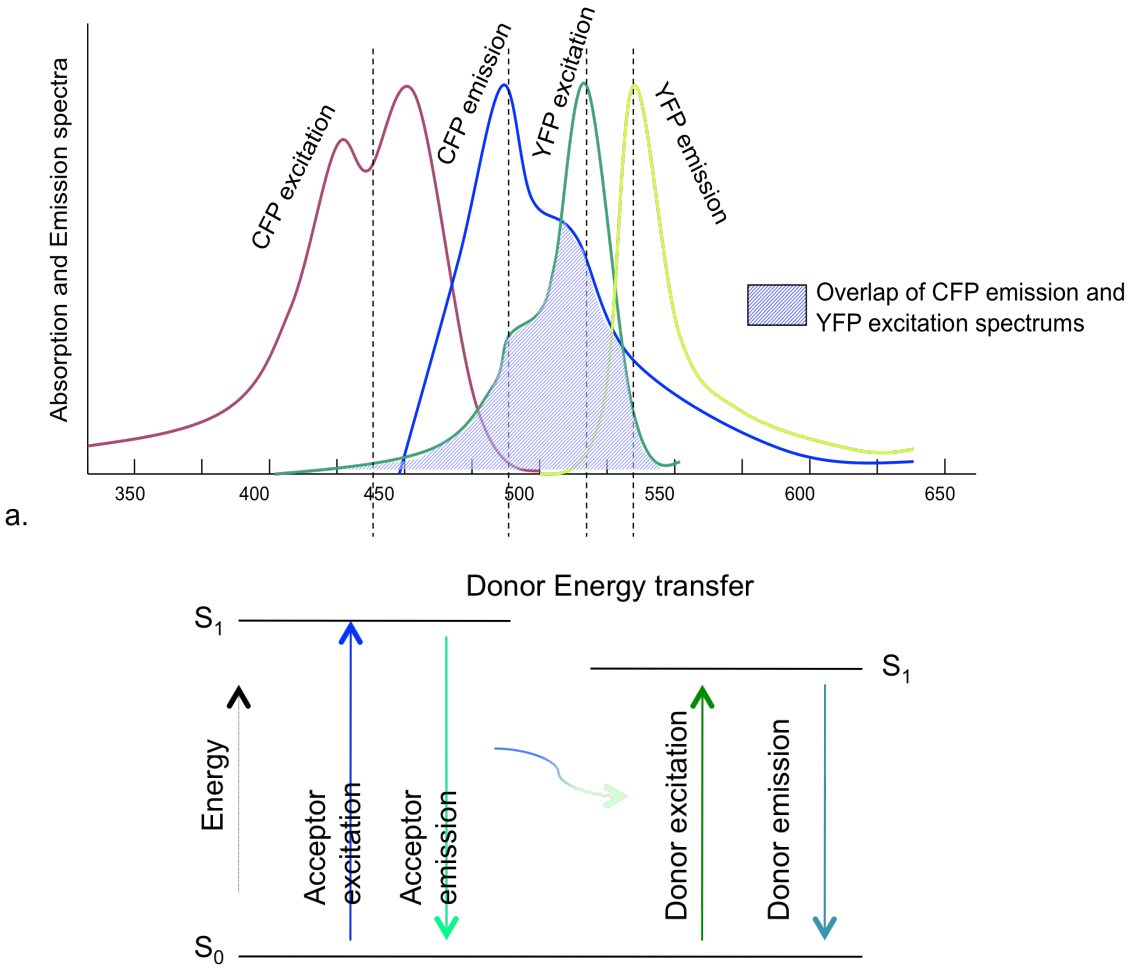

Figure I. 34 CFP/YFP FRET pair

Image a. represents the excitations and emissions spectra of CFP and YFP and the overlap between the donor CFP's emission and the acceptor YFP's excitation. Image b. is a simplified Jablonski diagram illustrating the processes of FRET: the excited donor will transfer non-radiative energy to the donor, resulting in emission of the donor fluorescence.

The FRET efficiency (*E)* is determined by the characteristic Förster distance R_0 at which 50% energy transfer occurs, and by the donor-acceptor distance r. The distance r is limited between 1-10 nm, because the efficiency of energy transfer is linked with the inverse of the sixth power of the distance over which FRET can occur (Periasamy & Day, 1998) (Pietraszewska-Bogiel & Gadella, 2011) (Figure I.35).

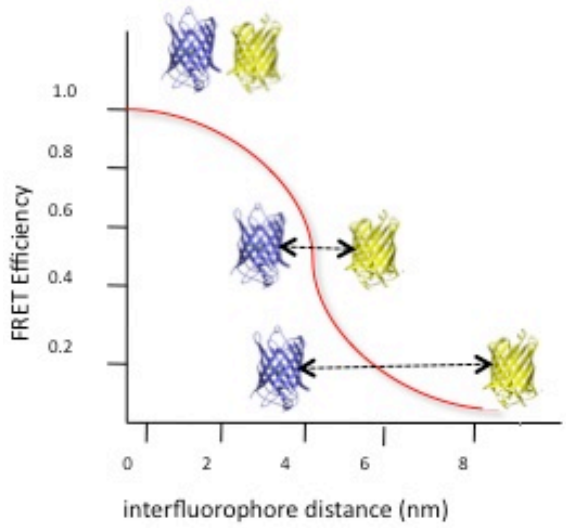

$$E = \frac{1}{1 + (r/R_0)^6}$$

Figure I. 35 FRET efficiency

The FRET energy efficiency (E) is dependent on the Förster distance R_0 and the distance r between the acceptor and the donor.

FRET can be measured directly using FLIM (Wallrabe & Periasamy, 2005) to quantify the acceptor's emission variation, and other methods have been established to measure FRET. FLIM could not be used in our case, as a special microscope is required to measure the lifetime of the fluorescence. But we decided to use another method, which could be done using the confocal microscope, called the acceptor photobleaching FRET method (Wang et al, 2010) .

2.2 Acceptor Photobleaching FRET

For FRET detection of the RNR in *S. pombe* a variant of the FRET method was applied. When quenching the acceptor (YFP), the acceptor energy transfer will not occur, and therefore will come back to the donor fluorophore

(CFP). By measuring the donor's signal, we are then able to determine if the fluorophore pair undergoes FRET. Confocal imaging microscopy was used, which allowed to photo-bleach the acceptor at a wavelength of 514 nm, and detect the effect on the donor emission intensity (Nestoras et al, 2010). The following calculation process was applied to measure FRET efficiency:

- Normalization of the images (subtraction of the background, normalization of the CFP/YFP intensities)
- Measurement of the intensities of the bleached area in the pre-bleached images of the acceptor and donor, and the same area in the post-bleached cell
- Intensity of the donor pre-bleach = IDA, Intensity of the donor post-bleach = ID, and I Autofluorescence of the cells

And finally:

% FRET Efficiency = 1 – {(IDA – I Auto.) / (ID – I Auto.)} x 100

These measurements were verified by various controls (see chapter II), and compared with a plug-in of ImageJ.

3. Single molecule methods: FCS and TIRFM

In chapter 6, I will be using single molecule methods *in vitro*, which might require some brief introduction.

3.1 Fluorescence Correlation Spectroscopy (FCS)

Confocal microscopy can be used for cell imaging as we have just seen, but the confocal volume also brings an advantage to measure fluorescence in a very small volume.

Fluorescence Correlation Spectroscopy (FCS) is a method to measure the fluctuation of fluorescence in a confocal volume. The analysis will provide information with regards to the parameters of the observed molecules. The molecules are moving due to Brownian motions, and the measurements of

these fluctuations over time will gather information of thousands of molecules (Kolin & Wiseman, 2007) (Al-Soufi et al, 2008).

This data can then be correlated and supply us with the information of average number of molecules and average diffusion time. Eventually the size of the molecule can be determined. FCS is very sensitive due to the detection of very low concentrated molecules and in a small volume. It can also be used *in vivo* (Fitzpatrick & Lillemeier, 2011).

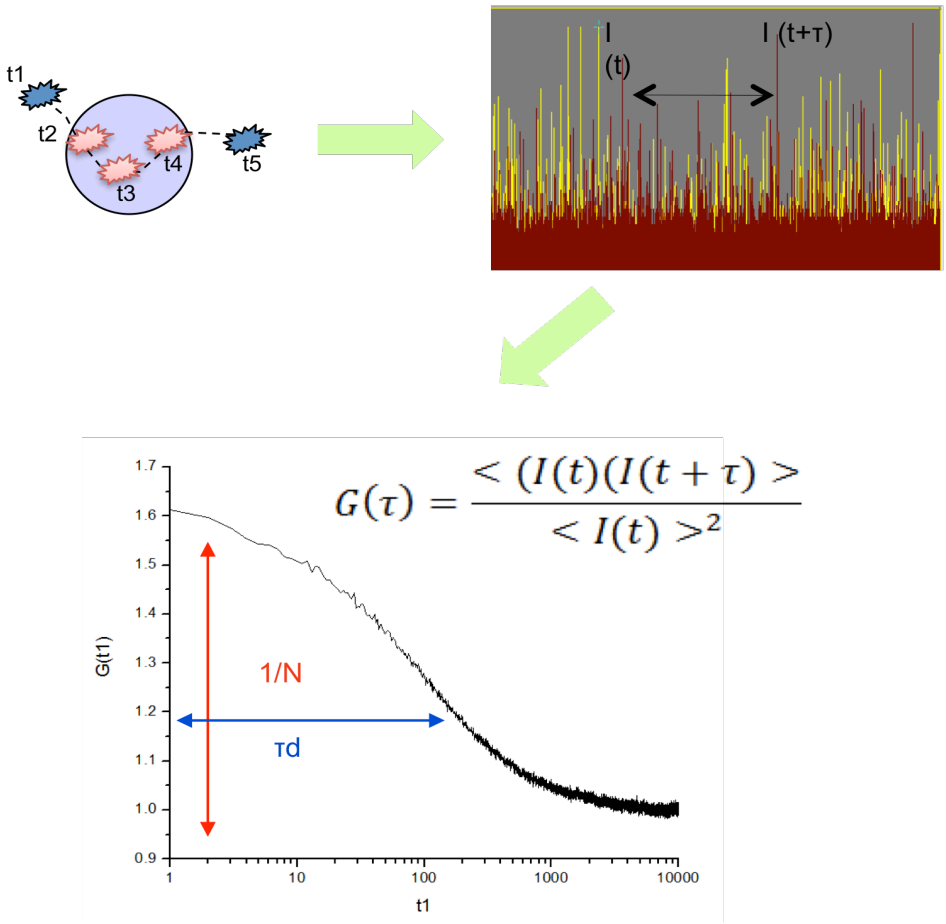

Figure I. 36 Fluorescence Correlation Spectroscopy (FCS)

Schematic of FCS: Fluorescence signal is acquired when molecules move through the confocal detection volume. A correlation process is then applied, providing a diffusion time τ d, while N represents the number of molecules.

We used FCS as we wanted to observe the binding process of both RNR proteins, but also the binding with the regulators Spd1 and Spd2. In addition, if the conformational modifications are large enough or a clear population of oligomers is present, we could observe it. This opens a door to a lot of sensitive

in vitro experiments to understand protein complexes and interactions. Ultimately, FRET experiments could be repeated in a more controlled *in vitro* set-up, confirming the *in vivo* data with the advantage of obtaining the exact stoichiometry of the subunits present (Price et al, 2011).

3.2 Total Internal Reflection Microscope (TIRFM)

Another method I would like to mention briefly is the Total Internal Reflection Microscope, as I will be using it for investigation of the RNR *in vitro*. In TIRFM, the excitation laser is not perpendicular to the observation plane but in an angle thus the laser will be entirely reflected (Axelrod, 2001) (Reck-Peterson et al, 2010). This produces an evanescent wave, due to the water-glass interface (high different refractive index) and will illuminate the sample to a depth of 100-200 nm. It is used to observe cell membranes, or regions close to it; but can also be used for single molecules studies. TIRFM and the derived Near-TIRFM (which allows to modify the laser angle) are methods to achieve high contrast, lower background, high frame-rate and simultaneous dual-channel imaging, ultimately for long-term live cell studies.

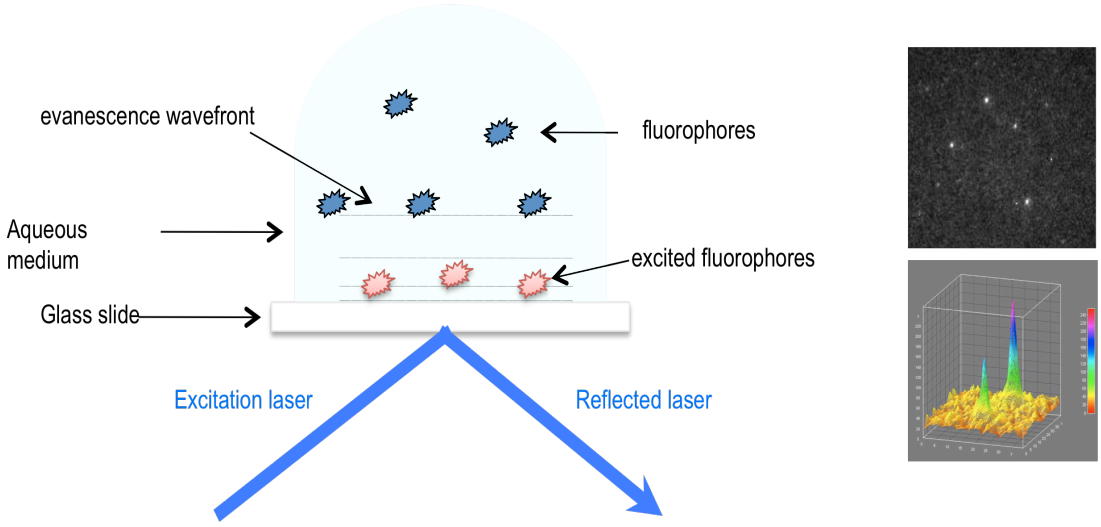

Figure I. 37 Total Internal Reflection Microscope (TIRFM)

Schematic of the TIRFM: the excitation laser will reflect on the glass slide due to its coming angle, and because of the glass/water interface refraction index, evanescence wavefront will be produced illuminating the plane to a depth of 100-200 nm. Images on the right represent examples of fluorophores observed on the TIRFM and their point spread function (PSF) reproduced in ImageJ.

3.3 Other advanced imaging techniques

Microscopy is by it-self a whole field with constant new and updated methods to improve resolution, intensity, quality, quantification etc… Also, there seems to be a consensus for giving them interesting acronyms. There are too many of them to be listed but I wanted to mention at least a few which are relevant for the future of this project.

To improve the resolution during imaging, a few methods have been developed (Wang et al, 2008) (Patterson et al, 2010). One of them is STED (StimulaTed Emission Depletion), which de-excite the surrounding fluorophores thus reducing the PSF (Point Spread Function); while SIM (Structured Illumination Microscopy) uses a combination of patterns during illumation therefore incasing the resolution after treatment due to the Moiré pattern characteristics.

Another method with a lot of future is PALM (Photo Activable Light Microscopy) / STORM (Stochastic optical reconstruction microscopy) which uses photoactivable fluorophores (i.e. paGFP) to improve the localization. They can also be photoconvertible fluorophores (i.e. mEOS2) or photoswitchable fluorophores. This localization-enhanced technique allows super-resolution by reducing the background and activating sequentially and specifically some fluorophores at a time. In addition a lot of possibilities are conceivable, linking PALM (and even 3D PALM) with live cell imaging for some super-resolution protein tracking, FRAP, FRET ect…

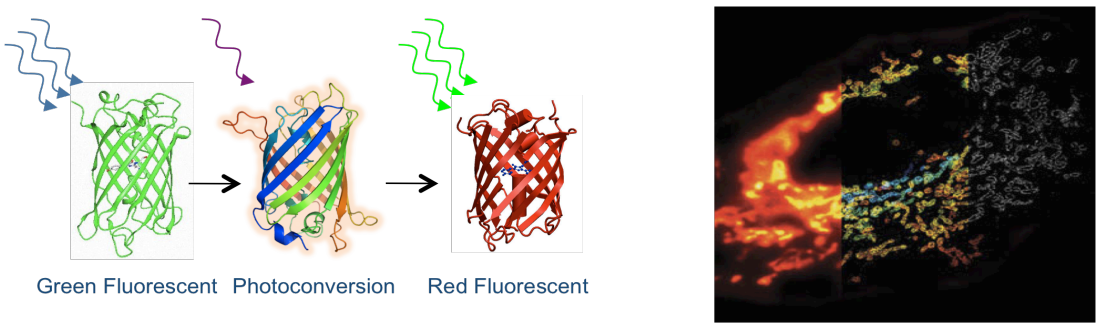

a. b.

Figure I. 38 PALM/ STORM (PhotoActivable Light Microscopy /Stochastic optical reconstruction microscopy)

Schematic of the photoconvertible mEOS2 (a.): the excitation laser will excite mEOS2 as a normal GFP, but upon conversion by UV light, the fluorophores will be a RFP thus excite and emit as a RFP.

In b. (picture from Xiaowei Zhuang, HHMI Harvard) Visualization of a Mitochondrial network in a mammalian cell in 3D STORM. Conventional fluorescence image (left), 3D STORM image with colors denoting z location (middle) and single xy cross-section from the 3D STORM image (right).

Finally, other methods in post-acquisition are worth mentioning: treating your images with softwares for denoising, deconvolution, or others like SOFI (Super-resolution Optical Fluctuation Imaging) can yield improved quality images.

CHAPTER II MATERIAL AND METHODS

I. General media and reagents

1. Media used for the *S. pombe* cultures

The protocols used for preparing the necessary culture media for *S. pombe* during this project are listed below. For the use of the media in plates, as a solid form, agar (DIFCO) was added to a final concentration of 1.5% if not stated otherwise. Most components are from Sigma-Aldrich or specified.

YE: Yeast Extract (for normal *S. pombe* cell growth)

Yeast extract 5g/l (0.5% w/v)
Glucose 30g/l (3% w/v)

EMM: Edinburgh Minimal media (for increased sensitivity to select of *S. pombe* strains)

Na_2HPO_4: 25 ml/l of 0.4M Na_2HPO_4 (final: 10 mM)
NH_4Cl: 25 ml/l of 20% of NH_4Cl (final: 0.5%)
Glucose: 12,5 ml of 40% glucose (final: 0.5%)
EMM Salts*: 50 ml of 20x EMM2 salts (final: 1x)
Vitamins**: 1 ml of 1000x vitamins (final: 1x)
Minerals***: 100 μl of 10000x trace elements (final: 1x)

*** 20X EMM2 Salts stock (filter sterilize):**

Potassium hydrogen phthalate: 61.2 g/l
KCL: 20 g/l
$Mgcl_2$: $6H_20$: 21.4 g/l
Na_2S0_4: 0,2 g/l

$CaCl_2$ $2H_20$: 0.26 g/l

****1000X Vitamins stock (keep in the dark at 4°C):**

Pantotenic Acid calcium salt: 1g/l
Nicotinic acid: 10g/l
Inositol: 10g/l
Biotin: 10 mg/l

*****10,000X Mineral stock (trace elements)**

Boric acid 5g/l
$MnSO_4$ 4g/l
$ZnSO_4.7H_2O$ 4g/l
$FeCl_2.6H_2O$ 2g/l
Molybdic acid 0.4 g/l
KI 1g/l
$CuSO_4.5H_2O$ 0.4 g/l
Citric acid 10g/l

YNB: Yeast Nitrogen base (minimum media for *S. pombe* culture; sterilization required)

YNB: 1,7 g/l (*Formendium)*
Ammonium sulfate: 5 g/l
Dextrose 20 g/**l**

ELN: Extremely Low nitrogen (media for *S. pombe* crosses)

EMM broth without nitrogen: 27.3 g/l (Formendium)
Ammonium chloride: 0.05 g/l
Uracil: 0.1 g/l
Leucine: 0.1 g/l
Histidine: 0.1 g/l
Arginine: 0.1 g/l
Adenine: 0.2 g/l

2. Amino Acid mixes for the minimal media (sterilization required)

In order to select for specific markers in *S. pombe* stains, various amino acids can be added to the minimal medias.

Leucine 100X: 7.5 g/l
Adenine 100X: 7.5 g/l
Histidine 100X: 7.5 g/l
Uracile 50X: 3.75 g/l

3. Medias used for *E. coli* culture (sterilization required for all)

This project also required some extensive work with *E. Coli* and diverse medias.

LB: Luria Broth

Tryptone: 10 g/l
Yeast extract: 5 g/l
NaCl: 10 g/l

TB: Terrific Broth

Tryptone: 12 g/l
Yeast extract: 24 g/l
Glycerol: 4ml/l
0.17M KH_2P0_4, 0.72M K_2HP0_4: 100 ml/l (autoclaved separately then added to the previous components after they have been autoclaved)

SOC: Super Optimal broth with Catabolite repression

Tryptone: 20 g/l
Yeast extract: 5 g/l
NaCl: 0.5 g/l
250 mM KCL: 10 ml/l

Adjust pH to 7.0 with 5 N of NaOH: ~0.2ml/l and autoclave
2 M $Mgcl_2$: 5 ml/l (autoclaved)
1 M glucose: 20 ml/l (filtered)

4. Some of the general buffers used

10 mM Tris-HCL: 1,2 g/l

1 M Tris-HCL: 121,1 g/l

0.2 M Citric acid: 42 g/l (filter)

2,4 M Sorbitol: 437 g/l

5 M KAC: 490 g/l

1 M EDTA pH 8: 372 g/l

250 mM KCL: 18,6 g/l

2 M $Mgcl_2$: 190 g/l

1 M glucose: 180 g/l

3M Sodium Acetate: 408,3 g/l

CSE: Citric Sorbitol (Filter sterilize)

0.4 M $Na_2H_2PO_4$: 70 ml/l (final: 28 mM)
0.2 M Citric acid: 44 ml/l (final: 8.8 mM)
EDTA: 14.9g/l $Na_2EDTA.\ 2H_20$ (final 40 mM)
Sobritol: 218.6 g/l (final 1.2 M)

Tris-EDTA (TE)

10 mM Tris-HCL: 10 ml/l
1 mM EDTA: 2 ml/l

5X TBE

Tris-Base: 54 g/l
Boric acid: 27.5 g/l
EDTA: 3.72 g/l $Na_2EDTA.\ 2H_20$

PBS (Phosphate buffered saline)

137mM NaCl
2.7mM KCl
10mM Na_2HPO_4
1.76mM KH_2PO_4

PBS-T: same as above but with 0.1 % Tween 20

0.17M KH_2P0_4, 0.72M K_2HP0_4:

2.31 g of KH_2P0_4 and 12.54 g of K_2HP0_4 in 100 ml of H_20

4X Sample buffer (100ml):

250mM Tris pH 6.8
8% SDS
20% glycerol
20% b-mercaptoethanol
Bromophenol blue: final concentration 0.4%

5. Reagents

Ampicillin (Sigma): 50 mg/ml

Carbenicillin (Sigma): 50 mg/ml

Chloramphenicol (Sigma): 34 mg/ml in Ethanol

G-418 (Melford): 100 mg/ml in H_2O

1 M HU (Sigma): 0.7605 g in 10 ml of H_20

1 mM 4NQO (Sigma): 0.0019 g in 10 ml DMSO

II. *S. pombe* protocols

1. Gene targeting protocols

1.1 Gene targeting methodology

The methodologies for PCR-based gene targeting in *S. pombe* have been described before(Bähler et al, 1998) (Werler PJ, 2003), however I will describe them briefly. To modify the sequence of a gene of interest, in order to tag a gene of interest for example with the tags CFP or YFP; at least 80 bp of homology to the endogenous genomic site is cloned to the tag in 5' and in 3'. By homologous recombination, the tag is inserted at the genomic sequence. If more homology is needed, fusion PCR will allow to reach up to 600 bp of homology, increasing the probability to insert the tag of interested to the endogenous target gene site. In case of gene disruption, the same method of homology is used but instead of inserting a gene in 5' or 3' of the target gene, it will be cloned in order to exchange the entire target gene with another exogenous marker gene.

1.2 General cloning method

Restriction with NEB enzymes and ligation with T4 DNA ligase (NEB), of plasmids and DNA fragments, were done following the manufacturer's conditions (New England Biolabs: NEB). Fusion PCR was done with KOD hot start DNA polymerase (Novagen). The reaction mixture is:

DNA: 50-100 ng
dNTPs: 0.2 mM of each
Primers: 0.3 μM of each
KOD reaction buffer: 1x
MgSo4: 1-6 mM
KOD polymerase enzyme: 0.02 U/μl

The PCR program is 98°C for 3 minutes, 5x 98°C for 30 seconds, 50°C for 1 minute, 68°C for 1 minute, 24x 98°C 30 seconds, Tm°C for 30 seconds, ended

by 68°C during the extension time. The various primers used can be found later in the annexe in the primer list.
The digested fragments as well as the amplified fragments were purified by gel extraction kit (Qiagen) or PCR clean-up (Machery-Nagel).

1.3 *S. pombe* transformation

S. pombe cells are grown overnight to $1x10^7$ cells/ml, from which 10 ml of cells are centrifuged at 3000 rpm for 5 min. The cells are washed with H_20 and with LiAc-TE (0.1 M LiAc, 0.01 M Tris-HCl, 0.001 M EDTA pH7.5) and resuspended with 100 µl LiAc-TE. Single stranded sperm DNA (Invitrogen Salmon Sperm DNA) and 1 µg of plasmid DNA or PCR fragment (up to 10 µg) are added and incubated for 10 mins at room temperature. 260 µl of 40% PEG-LiAc-TE were added and incubated 30-60 mins at 30°C. Followed by addition of 43 µl of DMSO and incubation at 42°C for 5 mins. Finally the samples are washed with 1 ml of H_2O and resuspended in 500 µl YE. 300 µl and 200 µl were plated onto selective plates.

1.4 Genomic DNA extraction

Cells were grown overnight in 10 ml YE at 30°C followed by centrifugation at 3000 rpm for 5 mins. Pellets were resuspended in 1 ml of CSE containing zymolyase 100T (final 1 mg/ml) and incubated for 15 minutes at 37°C. Correct cell lysis was checked under microscope. Cells were centrifuged at 3000 rpm for 5 minutes followed by pellet resuspension in 450 µl of 5X TE + 50 µl of 10% SDS, then incubated for 5 mins at room temperature. 150 µl of 5 M KAC was added and the samples were incubated 10 mins on ice. Centrifugation (13 000 rpm for 10 min at 4°C) allowed recuperation of the supernatant. 1 volume of isopropanol was added to precipitate the DNA, and subsequently the samples were centrifuged (13 000 rpm for 10 mins at 4°C). The pellets were washed with 500 µl of 70% ethanol followed by centrifugation (13 000 rpm for 10 mins at 4°C). The supernatant was discarded and the pellet was resuspended in 200 µl of H_20 containing RNAse A (10 µg/ml).

1.5 Verification by PCR

In case of absence of a selection marker, PCR has to be conducted to verify the correct insertion of the tag adjacent to the gene of interest. PCR was used routinely with the enzyme Taq polymerase, in a PCR reaction mixture:

DNA: 50-100 ng
dNTPs: 0.2 mM of each
Primers: 0.3 μM of each
Taq reaction buffer: 1x
$MgS0_4$: 2-4 mM
Taq polymerase enzyme: 0.02 U/μl

The PCR program was: 94°C for 3 minutes, 29x (94°C for 15 seconds, Tm°C for 30 seconds, 72°C for 1 minute) and a final extension at 72°C.

1.6 Strain crosses, random spore analysis and tetrad dissection

To obtain crossed strains, fresh strains with opposite mating type were streaked on ELN plates and mixed together with sterile water. The ELN plates were incubated for 2-3 days at 25°C. For random spore analysis, the spore's asci were resuspended and incubated overnight in 1 ml sterile water containing helicase (helix pomatia juice) at 1:100 dilution. After washing with 1 ml of sterile water, 100 and 1000 spores were plated on YEA plates and incubated at 30°C until colonies reached a satisfactory size. Colonies were then replicated on selective plates and grown at 30°C. In addition, the selected cells were streaked again to form new single colonies.
Tetrads were dissected by a micromanipulator on YEA plates, after incubation at 30°C for 3-5 days, as this allowed to select more carefully for spores scored on their genetic background.

1.7 Diploids strains

In order to obtain stable diploids, crossing of an ade6-M210 strain with ade6-M216 strain is required. After 2-3 days of incubation at 25°C, a small loophole of cells were plated onto a minimal plate (YNBA) without any adenine.

Only the *ade+* intra-complementing diploid cells will then grow. The growing colonies were restreaked on minimal medium without adenine for single colonies, and verified for sporulation on an ELN plate. The diploids strains were cultured in YE media without extra adenine, and maintained on YEA plates without extra adenine to ensure stabilization.

1.8 *S. pombe* strains used during this project

Nearly all strains made and used have the genetic background: *ade6-704 leu1-32 ura4D-18*. The strains with this background were often used as wild type strain, and they need media complemented with adenine, uracil and leucine for normal growth. The RNR single tagged strains (YFP-Suc22^{R2}, CFP-Suc22^{R2}, Cdc22^{R1}-CFP:KanMX and Cdc22^{R1}-YFP:KanMX) as well as the double-tagged strains (YFP-Suc22^{R2} Cdc22^{R1}-CFP:KanMX, CFP-Suc22^{R2} Cdc22^{R1}-YFP:KanMX) were made previously by Dr Adam Watson. I used the available Spd1::ura4+ strain, which will be referred as the Spd1 deleted strain for crossing to obtain a various set of single tagged RNR strains, double tagged, with *spd1* deleted.

The *spd1* mutants constructs were created by independent alanine mutagenesis PCR by Dr Marius Poitela and Dr Konstantinos Nestoras and integrated by homology to the genomic *spd1* sequence.

Finally, to make the strains needed for the microscopy and FRET experiments, I crossed the *spd1* mutants to the double-tagged strains (YFP-Suc22^{R2} Cdc22^{R1}-CFP:KanMX Spd1::ura4, CFP-Suc22^{R2} Cdc22^{R1}-YFP:KanMX Spd1::ura4) and selected for the different markers:

- G418 resistance validating the presence of Cdc22^{R1}-CFP/YFP:KanMX construct
- Loss of uracile resistance proving the correct integration of the Spd1 mutant
- PCR to confirm the CFP/YFP-Suc22^{R2} construct

All the Spd1 mutants were incorporated in the YFP-Suc22^{R2}Cdc22-CFP^{R1} strains, and most of them also in the “swapped” tagged strain i.e. CFP-Suc22^{R2} YFP-Cdc22^{R1} strain (see Table 1). After verification by sequencing of all the correct mutants inserted, the strains were ready for FRET experiments as well as other microscopy and biochemical studies. The same methods were used for

the *spd2* deletion strains, although more PCR verifications were needed due to the redundancy of marker genes.

The *cdc25-22 Ts* strains (Table 1) have been used in the laboratory before, and as they are thermo-sensitive, they arrest in G2 phase when maintained 3 hours at 36°C. The *Cdc25-22 Ts* strain was used to cross with both double RNR-tagged strains with *spd1* wt and *spd1* deletion. Therefore, a collection of single tagged RNR and double-tagged RNR strains is available.
The diploids strains were made by adenine complementation as described previously, and allowed to obtain a collection of RNR tagged diploids strains, with *spd1* wt and *spd1* deleted. All the strains used in this study are in Table 1. They have been stored in 50% glycerol stocks and are maintained at -80°C.

	Genotype	**Mating type**
Base strains ("Wild types")		
AS501	ade6-704 *leu*1-32 *ura*D18	h-
AS503	ade6-704 *leu*1-32 *ura*D18	h+
***spd1* and *spd2* deleted**		
AS128	*Spd*1::*ura*4 ade6-704 *ura*4-D18 *leu*1-32	h-
AS129	*Spd*1::*ura*4 ade6-704 *ura*4-D18 *leu*1-32	h+
AS130	*Spd*2::*ura*4 ade6-704 *ura*4-D18 *leu*1-32	
AS140	*Spd*2:KanMX	
Mutants *spd*1 no tags		
AS01	*Spd*1::mutant 1 ade6-704 *ura*4-D18 *leu*1-32	h+
AS02	*Spd*1::mutant 2 ade6-704 *ura*4-D18 *leu*1-32	h-
AS03	*Spd*1::mutant 3 ade6-704 *ura*4-D18 *leu*1-32	h+
AS04	*Spd*1::mutant 4 ade6-704 *ura*4-D18 *leu*1-32	h+
AS05	*Spd*1::mutant 5 ade6-704 *ura*4-D18 *leu*1-32	h+
AS06	*Spd*1::mutant 6 ade6-704 *ura*4-D18 *leu*1-32	h-
AS07	*Spd*1::mutant 7 ade6-704 *ura*4-D18 *leu*1-32	h+
AS08	*Spd*1::mutant 8 ade6-704 *ura*4-D18 *leu*1-32	h-
AS09	*Spd*1::mutant 9 ade6-704 *ura*4-D18 *leu*1-32	h+
AS10	*Spd*1::mutant 10 ade6-704 ura4-D18 leu1-32	h+
AS11	*Spd*1::mutant 11 *ade*6-704 *ura*4-D18 *leu*1-32	h+
AS12	*Spd*1::mutant 12 *ade*6-704 *ura*4-D18 *leu*1-32	h+
AS13	*Spd*1::mutant 13 *ade*6-704 *ura*4-D18 *leu*1-32	h-
AS14	*Spd*1::mutant 14 *ade*6-704 *ura*4-D18 *leu*1-32	h+
AS15	*Spd*1::mutant 15 *ade*6-704 *ura*4-D18 *leu*1-32	h-
AS16	*Spd*1::mutant 16 *ade*6-704 *ura*4-D18 *leu*1-32	h+

AS17	*Spd*1::mutant 17 *ade*6-704 *ura*4-D18 *leu*1-32	h-
AS18	*Spd*1::mutant 18 *ade*6-704 *ura*4-D18 *leu*1-32	h-
AS19	*Spd*1::mutant 19 *ade*6-704 *ura*4-D18 *leu*1-32	h+
AS20	*Spd*1::mutant 20 *ade*6-704 *ura*4-D18 *leu*1-32	h-
AS21	*Spd*1::mutant 21 *ade*6-704 *ura*4-D18 *leu*1-32	h+
AS22	*Spd*1::mutant 22 *ade*6-704 *ura*4-D18 *leu*1-32	h+
AS23	*Spd*1::mutant 23 *ade*6-704 *ura*4-D18 *leu*1-32	h+
AS24	*Spd*1::mutant 24 *ade*6-704 *ura*4-D18 *leu*1-32	h+
AS25	*Spd*1::mutant 25 *ade*6-704 *ura*4-D18 *leu*1-32	h-
AS26	*Spd*1::mutant 26 *ade*6-704 *ura*4-D18 *leu*1-32	h+
AS27	*Spd*1::mutant 27 *ade*6-704 *ura*4-D18 *leu*1-32	h+
AS28	*Spd*1::mutant 28 *ade*6-704 *ura*4-D18 *leu*1-32	h-
AS29	*Spd*1::mutant 29 *ade*6-704 *ura*4-D18 *leu*1-32	h+
AS30	*Spd*1::mutant 30 *ade*6-704 *ura*4-D18 *leu*1-32	h-
AS31	*Spd*1::mutant 31 *ade*6-704 *ura*4-D18 *leu*1-32	h+
AS32	*Spd*1::mutant 32 *ade*6-704 *ura*4-D18 *leu*1-32	h+
AS33	*Spd*1::mutant 33 *ade*6-704 *ura*4-D18 *leu*1-32	h+
AS34	*Spd*1::mutant 34 *ade*6-704 *ura*4-D18 *leu*1-32	h+
AS35	*Spd*1::mutant 35 *ade*6-704 *ura*4-D18 *leu*1-32	h+
AS36	*Spd*1::mutant 36 *ade*6-704 *ura*4-D18 *leu*1-32	h+
AS37	*Spd*1::mutant 37 *ade*6-704 *ura*4-D18 *leu*1-32	h-
AS38	*Spd*1::mutant 38 *ade*6-704 *ura*4-D18 *leu*1-32	h+
AS39	*Spd*1::mutant 39 *ade*6-704 *ura*4-D18 *leu*1-32	h-
AS40	*Spd*1::mutant 40 *ade*6-704 *ura*4-D18 *leu*1-32	h+
AS41	*Spd*1::mutant 41 *ade*6-704 *ura*4-D18 *leu*1-32	h+

Mutants *spd1* CFP-Suc22 Cdc22-YFP (CY)

AS-CY2	CFP-Suc22 Cdc22-YFP:KanMX *spd*1-m2 *ade*6-704 *ura*4-D18 *leu*1-32
AS-CY4	CFP-Suc22 Cdc22-YFP:KanMX *spd*1-m4 *ade*6-704 *ura*4-D18 *leu*1-32
AS-CY7	CFP-Suc22 Cdc22-YFP:KanMX *spd*1-m7 *ade*6-704 *ura*4-D18 *leu*1-32
AS-CY10	CFP-Suc22 Cdc22-YFP:KanMX *spd*1-m10 *ade*6-704 *ura*4-D18 *leu*1-32
AS-CY11	CFP-Suc22 Cdc22-YFP:KanMX *spd*1-m11 *ade*6-704 *ura*4-D18 *leu*1-32
AS-CY12	CFP-Suc22 Cdc22-YFP:KanMX *spd*1-m12 *ade*6-704 *ura*4-D18 *leu*1-32
AS-CY13	CFP-Suc22 Cdc22-YFP:KanMX *spd*1-m13 *ade*6-704 *ura*4-D18 *leu*1-32
AS-CY14	CFP-Suc22 Cdc22-YFP:KanMX *spd*1-m14 *ade*6-704 *ura*4-D18 *leu*1-32
AS-CY19	CFP-Suc22 Cdc22-YFP:KanMX *spd*1-m19 *ade*6-704 *ura*4-D18 *leu*1-32
AS-CY21	CFP-Suc22 Cdc22-YFP:KanMX *spd*1-m21 *ade*6-704 *ura*4-D18 *leu*1-32

AS-CY22	CFP-Suc22 Cdc22-YFP:KanMX *spd*1-m22 *ade*6-704 *ura*4-D18 *leu*1-32
AS-CY23	CFP-Suc22 Cdc22-YFP:KanMX *spd*1-m23 *ade*6-704 *ura*4-D18 *leu*1-32
AS-CY24	CFP-Suc22 Cdc22-YFP:KanMX *spd*1-m24 *ade*6-704 *ura*4-D18 *leu*1-32
AS-CY26	CFP-Suc22 Cdc22-YFP:KanMX *spd*1-m26 *ade*6-704 *ura*4-D18 *leu*1-32
AS-CY27	CFP-Suc22 Cdc22-YFP:KanMX *spd*1-m27 *ade*6-704 *ura*4-D18 *leu*1-32
AS-CY29	CFP-Suc22 Cdc22-YFP:KanMX *spd*1-m29 *ade*6-704 *ura*4-D18 *leu*1-32
AS-CY33	CFP-Suc22 Cdc22-YFP:KanMX *spd*1-m33 *ade*6-704 *ura*4-D18 *leu*1-32
AS-CY34	CFP-Suc22 Cdc22-YFP:KanMX *spd*1-m34 *ade*6-704 *ura*4-D18 *leu*1-32
AS-CY36	CFP-Suc22 Cdc22-YFP:KanMX *spd*1-m36 *ade*6-704 *ura*4-D18 *leu*1-32
AS-CY37	CFP-Suc22 Cdc22-YFP:KanMX *spd*1-m37 *ade*6-704 *ura*4-D18 *leu*1-32
AS-CY38	CFP-Suc22 Cdc22-YFP:KanMX *spd*1-m38 *ade*6-704 *ura*4-D18 *leu*1-32
AS-CY41	CFP-Suc22 Cdc22-YFP:KanMX *spd*1-m41 *ade*6-704 *ura*4-D18 *leu*1-32

Mutants *spd1* YFP-Suc22 Cdc22-CFP (YC)

AS-YC1	YFP-Suc22 Cdc22-CFP:KanMX *spd*1-m1 *ade*6-704 *ura*4-D18 *leu*1-32
AS-YC2	YFP-Suc22 Cdc22-CFP:KanMX *spd*1-m2 *ade*6-704 *ura*4-D18 *leu*1-32
AS-YC4	YFP-Suc22 Cdc22-CFP:KanMX *spd*1-m4 *ade*6-704 *ura*4-D18 *leu*1-32
AS-YC5	YFP-Suc22 Cdc22-CFP:KanMX *spd*1-m5 *ade*6-704 *ura*4-D18 *leu*1-32
AS-YC9	YFP-Suc22 Cdc22-CFP:KanMX *spd*1-m9 *ade*6-704 *ura*4-D18 *leu*1-32
AS-YC12	YFP-Suc22 Cdc22-CFP:KanMX *spd*1-m12 *ade*6-704 *ura*4-D18 *leu*1-32
AS-YC13	YFP-Suc22 Cdc22-CFP:KanMX *spd*1-m13 *ade*6-704 *ura*4-D18 *leu*1-32
AS-YC14	YFP-Suc22 Cdc22-CFP:KanMX *spd*1-m14 *ade*6-704 *ura*4-D18 *leu*1-32
AS-YC15	YFP-Suc22 Cdc22-CFP:KanMX *spd*1-m15 *ade*6-704 *ura*4-D18 *leu*1-32
AS-YC16	YFP-Suc22 Cdc22-CFP:KanMX *spd*1-m16 *ade*6-704 *ura*4-D18 *leu*1-32
AS-YC17	YFP-Suc22 Cdc22-CFP:KanMX *spd*1-m17 *ade*6-704 *ura*4-D18 *leu*1-32

AS-YC18	YFP-Suc22 Cdc22-CFP:KanMX *spd*1-m18 *ade*6-704 *ura*4-D18 *leu*1-32
AS-YC21	YFP-Suc22 Cdc22-CFP:KanMX *spd*1-m21 *ade*6-704 *ura*4-D18 *leu*1-32
AS-YC22	YFP-Suc22 Cdc22-CFP:KanMX *spd*1-m22 *ade*6-704 *ura*4-D18 *leu*1-32
AS-YC23	YFP-Suc22 Cdc22-CFP:KanMX *spd*1-m23 *ade*6-704 *ura*4-D18 *leu*1-32
AS-YC24	YFP-Suc22 Cdc22-CFP:KanMX *spd*1-m24 *ade*6-704 *ura*4-D18 *leu*1-32
AS-YC25	YFP-Suc22 Cdc22-CFP:KanMX *spd*1-m25 *ade*6-704 *ura*4-D18 *leu*1-32
AS-YC26	YFP-Suc22 Cdc22-CFP:KanMX *spd*1-m26 *ade*6-704 *ura*4-D18 *leu*1-32
AS-YC27	YFP-Suc22 Cdc22-CFP:KanMX *spd*1-m27 *ade*6-704 *ura*4-D18 *leu*1-32
AS-YC28	YFP-Suc22 Cdc22-CFP:KanMX *spd*1-m28 *ade*6-704 *ura*4-D18 *leu*1-32
AS-YC29	YFP-Suc22 Cdc22-CFP:KanMX *spd*1-m29 *ade*6-704 *ura*4-D18 *leu*1-32
AS-YC30	YFP-Suc22 Cdc22-CFP:KanMX *spd*1-m30 *ade*6-704 *ura*4-D18 *leu*1-32
AS-YC31	YFP-Suc22 Cdc22-CFP:KanMX *spd*1-m31 *ade*6-704 *ura*4-D18 *leu*1-32
AS-YC32	YFP-Suc22 Cdc22-CFP:KanMX *spd*1-m32 *ade*6-704 *ura*4-D18 *leu*1-32
AS-YC34	YFP-Suc22 Cdc22-CFP:KanMX *spd*1-m34 *ade*6-704 *ura*4-D18 *leu*1-32
AS-YC35	YFP-Suc22 Cdc22-CFP:KanMX *spd*1-m35 *ade*6-704 *ura*4-D18 *leu*1-32
AS-YC36	YFP-Suc22 Cdc22-CFP:KanMX *spd*1-m36 *ade*6-704 *ura*4-D18 *leu*1-32
AS-YC38	YFP-Suc22 Cdc22-CFP:KanMX *spd*1-m38 *ade*6-704 *ura*4-D18 *leu*1-32
AS-YC39	YFP-Suc22 Cdc22-CFP:KanMX *spd*1-m39 *ade*6-704 *ura*4-D18 *leu*1-32
AS-YC40	YFP-Suc22 Cdc22-CFP:KanMX *spd*1-m40 *ade*6-704 *ura*4-D18 *leu*1-32

Double tags

AS108	CFP-Suc22 Cdc22-YFP:KanMX *spd*1 wt *ade*6-704 *ura*4-D18 *leu*1-32	h-
AS120	YFP-Suc22 Cdc22-CFP:KanMX *spd*1 wt *ade*6-704 *ura*4-D18 *leu*1-32	
AS122	CFP-Suc22 Cdc22-YFP:KanMX *spd*1::*ura*4+ *ade*6-704 *ura*4-D18 *leu*1-32	h-
AS123	CFP-Suc22 Cdc22-YFP:KanMX *spd*1::*ura*4+ *ade*6-704 *ura*4-D18 *leu*1-32	h+

AS154	YFP-Suc22 Cdc22-CFP:KanMX *spd*1::*ura*4+ *ade*6-704 *ura*4-D18 *leu*1-32	h+
AS155	YFP-Suc22 Cdc22-CFP:KanMX *spd*1::*ura*4+ *ade*6-704 *ura*4-D18 *leu*1-32	h-
AS131	YFP-Suc22 Cdc22-CFP:KanMX *spd*1 wt *Spd*2::*ura*4+ *ade*6-704 *ura*4-D18 *leu*1-32	
AS132	YFP-Suc22 Cdc22-CFP:KanMX *spd*1::*ura*4+ *Spd*2::*ura*4+ *ade*6-704 *ura*4-D18 *leu*1-32	
AS141	CFP-Suc22 Cdc22-YFP:KanMX *spd*1 wt *Spd*2:KanMX *ade*6-704 *ura*4-D18 *leu*1-32	
AS142	CFP-Suc22 Cdc22-YFP:KanMX *spd*1::*ura*4+ *Spd*2:KanMX *ade*6-704 *ura*4-D18 *leu*1-32 -1	
AS143	CFP-Suc22 Cdc22-YFP:KanMX *spd*1::*ura*4+ *Spd*2:KanMX *ade*6-704 *ura*4-D18 *leu*1-32 -2	
AS144	CFP-Suc22 Cdc22-YFP:KanMX *spd*1::*ura*4+ *Spd*2:KanMX *ade*6-704 *ura*4-D18 *leu*1-32 -3	
AS145	CFP-Suc22 Cdc22-YFP:KanMX *spd*1::*ura*4+ *Spd*2:KanMX *ade*6-704 *ura*4-D18 *leu*1-32 -4	

Single tags

AS101	YFP-Suc22 *ade*6-704 *ura*4-D18 *leu*1-32
AS102	Cdc22-YFP:KanMX *ade*6-704 *ura*4-D18 *leu*1-32
AS103	CFP-Suc22 *ade*6-704 *ura*4-D18 *leu*1-32
AS104	Cdc22-CFP:KanMX *ade*6-704 *ura*4-D18 *leu*1-32

***Cdc25-22* TS strains**

AS441	cdc25-22 TS *ura* deleted	h -
AS442	cdc25-22 TS *ura* deleted	h +
AS443	cdc25-22 TS *ura*4-D18	
AS444	cdc25-22 TS *ura*4-D18	
AS 450	YFP-Suc22 *spd*1 wt *ade*6-704 *ura*4-D18 *leu*1-32 Cdc25TS	
AS 451	YFP-Suc22 *spd*1::*ura*+ *ade*6-704 *ura*4-D18 *leu*1-32 Cdc25TS	
AS 452	Cdc22-CFP:KanMX *spd*1 wt *ade*6-704 *ura*4-D18 *leu*1-32 Cdc25TS	
AS 453	Cdc22-CFP:KanMX *spd*1::*ura*4+ *ade*6-704 *ura*4-D18 *leu*1-32 Cdc25TS	
AS 454	YFP-Suc22 Cdc22-CFP:KanMX *spd*1 wt *ade*6-704 *ura*4-D18 *leu*1-32 Cdc25TS	
AS 455	YFP-Suc22 Cdc22-CFP:KanMX *spd*1::*ura*+ *ade*6-704 *ura*4-D18 *leu*1-32 Cdc25TS	
AS 456	CFP-Suc22 *spd*1 wt *ade*6-704 *ura*4-D18 *leu*1-32 Cdc25TS	
AS 457	CFP-Suc22 *spd*1::*ura*4+ *ade*6-704 *ura*4-D18 *leu*1-32 Cdc25TS	
AS 458	Cdc22-YFP:KanMX *spd*1 wt *ade*6-704 *ura*4-D18 *leu*1-32 Cdc25TS	
AS 459	Cdc22-YFP:KanMX *spd*1::*ura*4+ *ade*6-704 *ura*4-D18 *leu*1-32 Cdc25TS	

AS 461	CFP-Suc22 Cdc22-YFP:KanMX *spd*1 wt *ade*6-704 *ura*4-D18 *leu*1-32 Cdc25TS
AS 462	CFP-Suc22 Cdc22-YFP:KanMX *spd*1::*ura*4+ *ade*6-704 *ura*4-D18 *leu*1-32 Cdc25TS

Diploids

AS 200	972 all wt h-	h-
AS 201	975 all wt h+	h+
AS 202	CFP-Suc22 *spd*1 wt - all wt	
AS 203	YFP-Suc22 *spd*1 wt - all wt	
AS 204	YFP-Suc22 *spd*1 wt *ade*216	
AS 205	CFP-Suc22 *spd*1 wt *ade*216	
AS 206	CFP-Suc22 *spd*1 wt *ade*210	
AS 207	YFP-Suc22 *spd*1 wt *ade*210	
AS 208	Cdc22-YFP:KanMX *spd*1 wt - all wt	
AS 209	Cdc22-CFP:KanMX *spd*1 wt - all wt	
AS 210	Cdc22-YFP:KanMX *spd*1 wt *ade*216	
AS 211	Cdc22-CFP:KanMX *spd*1 wt *ade*216	
AS 212	Cdc22-CFP:KanMX *spd*1 wt *ade*210	
AS 213	Cdc22-YFP:KanMX *ade*216 Cdc22-CFP:KanMX *ade*210 I	
AS 214	Cdc22-YFP:KanMX *ade*216 Cdc22-CFP:KanMX *ade*210 II	
AS 215	YFP-Suc22 *ade*216 CFP-Suc22 *ade*210 I	
AS 216	YFP-Suc22 *ade*216 CFP-Suc22 *ade*210 II	
AS 217	YFP-Suc22 *ade*210 CFP-Suc22 *ade*216 I	
AS 218	YFP-Suc22 *ade*210 CFP-Suc22 *ade*216 II	
AS 219	Cdc22-YFP:KanMX *ade*210 Cdc22-CFP:KanMX *ade*216 I	
AS 220	Cdc22-YFP:KanMX *ade*210 Cdc22-CFP:KanMX *ade*216 II	
AS 221	Cdc22-YFP:KanMX *ade*210 Cdc22-CFP:KanMX *ade*216 *Spd*1::*ura*4+ -1	
AS 222	Cdc22-YFP:KanMX *ade*210 Cdc22-CFP:KanMX *ade*216 *Spd*1::*ura*4+ -2	
AS 223	Cdc22-YFP:KanMX *ade*210 Cdc22-CFP:KanMX *ade*216 *Spd*1::*ura*4+ -3	
AS 224	Cdc22-YFP:KanMX *ade*210 Cdc22-CFP:KanMX *ade*216 *Spd*1::*ura*4+ -4	
AS 225	YFP-Suc22 *ade*216 CFP-Suc22 *ade*210 *Spd*1::*ura*4+ -1	
AS 226	YFP-Suc22 *ade*216 CFP-Suc22 *ade*210 *Spd*1::*ura*4+ -2	
AS 227	YFP-Suc22 *ade*216 CFP-Suc22 *ade*210 *Spd*1::*ura*4+ -3	
AS 228	YFP-Suc22 *ade*216 CFP-Suc22 *ade*210 *Spd*1::*ura*4+ -4	

AS250	*ade*6-210	h+
AS251	*ade*6-216	h-
AS252	*ade*6-216	h+

Table1: List of strains used in this project

2. Other *S. pombe* protocols

2.1 Cdc25-22 TS synchronization

The *S. pombe* mutant strain *cdc25-22* ThermoSensitive (TS) allows us to block the cells in G2 and after release, the cell population will be synchronized. First a pre-culture of 20 ml at 25°C of the strain is measured for the cell density, and a 100 ml culture is set at 25°C in order to obtain $3x10^6$ cell/ml the next morning. The cultures are then put in a 36°C waterbath for 3.5 hours for the blocking of the cells. To release the cells into the cell cycle, the cultures are cooled down in a sink with ice for rapid decrease of the temperature, followed by culture in a 25°C shaking waterbath. The time point started at that moment, and sample were taken before the release, as well as after, every with 20 min intervals. The samples were prepared for FACS and microscopy.

2.2 FACS (Fluorescence activating cell sorting)

Exponential cell cultures were used in order to have healthy cells for FACS analysis. 1 ml of the culture was centrifuged (3000 rpm) and the pellet was washed and resuspended with 500 µl of 50 mM sodium citrate. Next, addition of 50 µl of 10 mg/ml RNaseA was done and the samples incubated at 37°C for 2-3 hours. In FACS tube, 200 µl of the sample was mixed with 10 µl of 500 mg/ml of propidium iodide (PI) and 1 ml of sodium citrate buffer. After a throughout vortexing of the samples, they were used on the FACS machine (FACS canto) following the manufacturer's protocol, and previously established calibrations for *S. pombe* cells.

2.3 Chromosomal DNA and septum staining

1 ml of exponentially growing cells were pelleted at 3000 rpm, washed in 1ml PBS and resuspended in methanol. Cells were spread onto a glass slide and stained with DAPI (1 µg/ml) and Calcofluor (50 µg/ml) in 50% Glycerol 50 % H_20 for analysis.

2.4 *S. pombe* protein extraction

Cells were grown in 10 ml of culture overnight. About 5 ODs of cells were harvested (3000 rpm 5 minutes) and washed with PBS. The pellets were resuspended in 200 µl 20% TCA (Trichloroacetic Acid) and transferred to ribolyser tubes. Cells were ribolysed by using glass beads (Sigma) for at least 2 cycles (30 sec each) at speed 6.5, or until lysis of approximately 90% of the cells was accomplished. The contents of the ribolyser tubes were filtered and centrifuged at 3000 rpm for 2 minutes at 4°C into fresh centrifuge tubes. These were then centrifuged again at 14000 rpm for 5 minutes at 4°C. The supernatants were discarded and the pellet resuspended in 200 µl 1X sample buffer, and boiled at 95°C for 10 mins.
Those samples were later visualized by SDS-PAGE gel and Western blot.

2.5 *S. pombe* protein purification

Another method for protein extraction was “popcorn” making of the *S. pombe* cells and grinding with liquid nitrogen, allowing larger volumes of cells to be processed. The cells were pelleted at 6000 rpm for 5 mins, resuspended in 1 ml of lysis buffer B (50 mM tris pH7.5, 250 mM NaCl, 50 mM NaF, 5mM EDTA, 0.1% NP40) added with 1 tablet/50 ml Complete protease inhibitors EDTA-free (Roche) + 1mM AEBSF (Sigma). The samples were centrifuged again (3000 rpm, 5 mins) and the pellets were thoroughly resuspended in buffer B with protease inhibitors, before being solidified drop by drop in liquid nitrogen. The “popcorn” samples were then grinded for 3 cycles of 2 mins at full power in tubes with a magnet, kept in liquid nitrogen. The supernatant was recuperated after centrifugation at 4000 rpm for 15 mins at 4°C.

Firstly, Co-immunoprecipitation was used with antibody-coated Dynabeads (Protein G, Invitrogen) to pull-down the CFP and YFP tagged endogenous proteins with the anti-GFP antibody (the cross-talk of the anti-GFP antibody allows to target CFP and YFP). The protocol provided by the manufacturers was followed. Cell extracts were incubated for 2 h with the anti-GFP dynabeads, washed 3 times with lysis buffer B, followed by elution in boiling sample buffer.

But as the yield was not enough, as well as the options for native elution was limited, the anti-GFP trap system (Chromotek) was used. The specificity of

the GFP-trap is extremely high, allowing purifying the endogenous protein from *S. pombe*. Both GFP-trap bound to agarose beads and magnetic beads were tried, but the following protocol is based on the agarose beads.

The cells pellets were treated with lysis buffer (10 mM Tris-HCL pH7.5, 150 mM NaCl, 0.1% SDS, 1% Triton X-100, 5 mM EDTA, 1mM AEBSF and Complete protease inhibitors) centrifuged at 20 000 g for 10 mins at 4°C, and the supernatants were transferred to a pre-cooled tube followed by addition of 1 ml of dilution buffer (10 mM Tris-HCL pH7.5, 150 mM NaCl, 0.5 mM EDTA, 1mM AEBSF and Complete protease inhibitors). The beads were washed twice and resupended in dilution buffer, followed by addition of the cell lysate. Incubation of the GFP-Trap and cell lysates was done for 2 hours on a rotor at 4°C. The beads were then washed twice with ice-cold wash buffer (10 mM Tris-HCl pH7.5, 300 mM NaCl, 1mM AEBSF and Complete protease inhibitors) and native elution was done by adding 50 μl of 0.2 M glycine pH 2.4, incubated for 30 seconds, and neutralized by 5 μl of 1 M Tris-base (pH 10.4). The purification was verified by SDS-PAGE gel, where the input, non-bound, washes, elution and native elution were loaded and observed by coomassie stain and western blot. The eluted native proteins were kept in aliquots at -20°C.

III. *E. coli* protocols and *E. coli* protein Expression/Purification

1. Preparation of competent *E. coli* cells (DH5α, BL21(DE3), BL21-CodonPlus(DE3))

A single colony is grown to saturation overnight at 37°C in 5 ml of LB (BL21 strains require 34 μg/ml of chloramphenicol). The preculture is used to inoculate a pre-warmed 1 L culture of LB, and grown with shaking until the $O.D_{550nm}$ is approximately 0.6. The cells were chilled on ice and in the cold room for 1 hour followed by centrifugation at 5000 rpm for 5 mins at 4°C. The cell pellet was resuspended in 25 ml of cold TRNS1 solution.

After a short incubation of 5 mins, the tubes are centrifuged at 3000 rpm for 5

mins at 4°C, and the pellet resuspended again in 25 ml of cold TRNS1 solution. An incubation of the tubes on ice in the cold room for 1-2 h is then followed by centrifugation at 3000 rpm for 5 mins at 4°C, and the cells resuspended in 8 ml of cold TRNS2. The samples were incubated for 10 mins, followed by aliquoting in 100-300 μl and snap-frozen by liquid nitrogen in order to be stored at -80°C.

TRNS1 (adjusted to pH 5.8 with acetic acid and filter sterilized)

RbCl: 12.1 g/l
$MnCl_2$: 9.6 g/l
$CaCl_2$: 1.48 g/l
CH_3COONa: 2.88 g/l
Glycerol: 66 ml/l

TRNS2 (adjusted to pH 6.8 with acetic acid and filter sterilized)

RbCl: 1.2 g/l
$CaCl_2$: 11 g/l
MOPS: 2.1 g/l
Glycerol: 66 ml/l

2. *E. coli* transformation

Competent *E. coli* cells were thawed on ice, DNA was added and incubated for 10-30 mins on ice before bacteria were heat-shocked at 42°C for 60-90 seconds. Cells were incubated on ice further for 5 mins, followed by addition of 1ml of pre-warmed LB (or SOC) and the reactions were incubated at 37°C for 1 h. 100μl and 900μl were plated onto LBA plates with the appropriate selective antibiotic and grown over night at 37°C.

3. Plasmid DNA preparation

Minipreparations of plasmid DNA were based on the Qiagen protocol. 2-5 ml of *E. coli* cultures were grown overnight at 37°C in LB supplemented with the appropriate selective antibiotic. The cells were then pelleted (1 min, 13 000 rpm, room temperature) and resuspended in 200 μl P1 (50 mM Tris-HCl pH8.0, 10

mM EDTA, 100 µg/ml RNaseA), followed by addition of 300µl of P2 (200 mM NaOH, 1% w/v SDS). The samples were incubated at room temperature for 5 mins. Next, 300 µl of P3 (3M KAC pH5.5) were added, and the samples were incubated on ice for 10 mins. The tubes were centrifuged (10 mins, 13000rpm, 4°C) and the supernatants were transferred to a new tube and mixed with an equal volume of isopropanol. The samples were then incubated for 5 mins at room temperature and centrifuged for 10 minutes at 13 000 rpm at 4°C. The pellets were washed with 500µl of 70% Ethanol, centrifuged as before and resuspended in 20 µl of H_2O added with 1 µg/ml of RNaseA.
In addition Qiagen miniprep kits were used, as well as Machery-Nagel miniprep kits. Also, for Midipreps, the Qiagen Midiprep Kit was used and carried out according to the manufacturers instructions.

4. Cloning for protein purification

4.1 PCR amplification of DNA

In general, the KOD enzyme (Agilent Technologies) was used for DNA amplification by PCR, as it is an error-free enzyme. The PCR mixture was:

DNA: 50-100 ng
dNTPs: 0.2 mM of each
Primers: 0.3 µM of each
KOD reaction buffer: 1x
MgSo4: 1-6 mM
KOD polymerase enzyme: 0.02 U/µl

And the PCR program:

1: Initial denaturation for 2 min at 94°C
2: Denaturation for 20 seconds at 94°C
3: Annealing of the primers for 30 seconds at the TM
4: Extension for of the DNA synthesis for 1 min- 3 mins at 68°C
Return to step 2 for cycles of 20-35

5: Final extension for 3 mins at 68°C

4.2 Site directed mutagenesis by PCR

PCR site directed mutagenesis was done by using primers with complementary sequence and containing the mutation of interest in the middle of the ~30 nucleotides long primers. The PCR was done with Pfu (Agilent Technologies) and the reaction mixture contains:

DNA: 50 ng for 50 μl reaction
dNTPs: 0.2 mM of each
Primers: 1 μM of each
Pfu reaction buffer: 1x
Pfu Turbo polymerase enzyme: 2.5U/μl

The program used was:

1: 94°C for 3 mins
2: 94°C for 30 sec
3: Tm for 1 min
4: 68°C for 120 seconds/kb of the plasmid length

The PCR product was digested with 20 Units of Dpn1 (NEB) for 2 hours at 37°C, which digest the parental methylated plasmid. The newly amplified plasmid containing the mutation was then transformed into *E. Coli* to provide larger stocks by midi-preparation of plasmid DNA.

4.3 Digestion and ligation

Following NEB's guidelines, 1 μg of plasmid DNA was digested in a total volume of 30 μl, with 1 μl of restriction enzyme and 3 μl of the appropriate 10x

buffer. Digestions were conducted for at least 1 h at 37°C, and verified by electrophoresis gel, followed by gel extraction and DNA purification by kits (Qiagen, MN). Ligations were done by T4 DNA ligase (NEB) overnight at 16°C according to the manufacturer's guidelines. The vector and insert were ligated in a 1:2 – 1:3 ratio, in a mixture of 20 μl total reaction, the vector DNA and insert DNA were added (minimum 50-100 ng), along with 2 μl of 10X T4 DNA ligase buffer and 1 μl of the enzyme T4 DNA ligase.

4.4 Classical cloning

The classical cloning method involves studying the plasmids maps, and using the multiple cloning sites to find appropriate enzymes for potential cloning of the gene of interest in the plasmid. Those restriction enzyme sites are then added by PCR on the gene, and upon digestion and ligation the gene of interested is inserted in the plasmid. A list of primers used is available in the appendix. The expression vectors used were pET3a (Stratagene), pET21a (Stratagene), and pET28a (Stratagene). As some problems were encountered to clone in the recombinant genes (amplifications, introns, lack of restriction enzyme sites…), another method was used, the InFusion cloning (Clonetech).
For XFP-Suc22^{R2} cloning, the steps were: first amplification using the primers suc22XFP_PET_F (gggaagcttcatatgtctaaaggtgaagaattattcactggt) and suc22_PET-R (ggggggatccctaaaatcctcatcgattgtaaatgtatgatc), and cloned into pUC19 in order to mutate out the NdeI site in CFP and YFP. Finally it was subcloned into the pET3a vector as an NdeI/BamHI fragment.

4.5 InFusion cloning

The In-Fusion HD kit (Clonetech) was also used, following the manufacturer's guidelines. The in-fusion reaction was: 50-200 ng of linearized vector, with 10-100 ng of purified PCR fragment with 15 bp overhang homology (the ratios plasmid/insert are 1:2 -1:3), 1X of In-Fusion HD Enzyme premix in a total of 10 μl. The samples were incubated at 50°C for 15 minutes, followed by cooling on ice. Transformaed *E. coli* cells with the newly in-fused DNA are finally plated.

4.6 Sequencing

Most of the DNA samples, plasmids or genomic-amplified DNA, were sequenced by sending the samples to GATC (GATC-biotech). 30-100 ng/μl of the DNA along with 30 pmol/μl of the corresponding primer were sent. Available programs were used to study the output files.

5. Protein expression and solubility

Protein expression was done using expression vectors, which are under the control of the T7 promoter, activated by the T7 polymerase. The bacterial strains BL21(DE3) and BL21-CodonPlus(DE3) (optimized for eukaryotic codon expression) were originally from stratagene. Both strains have a copy of the T7 polymerase gene, under control of the *lacZ* promoter. The addition of IPTG will induce the expression of the T7 polymerase, thus also induce the expression of the gene of interest. Expression of the RNR tagged proteins were done in *E. coli* BL21-CodonPlus(DE3) competent cells, and pET3a was used for $Suc22^{R2}$ while pET21a was used for $Cdc22^{R1}$. Determining the protein expression and solubility was done by testing different conditions (temperature, incubation times…), medias (LB, TB) and protocols.

Generally, a single colony (BL21-CodonPlus(DE3) was used to inoculate a 50-100 ml pre-culture of TB with with 100 μg/ml of carbenicillin and 34 μg/ml of chloramphenicol, and left to grow overnight at 30°C. Next morning, a 1-2 L culture of pre-warmed TB added with 100 μg/ml of carbenicellin was inoculated with the pre-culture, and left to growth at adequate temperature and incubation times (see results) to reach an O.D of 0.9-1.2. At that moment, IPTG was added at concentrations varying from 0.2 mM to 0.8 mM, and left from 3 h to overnight (see results). Cells were centrifuged at 4000 rpm for 10 mins at 4°C and resuspended in lysis buffer (50 mM Tris, 250 mM Nacl, 10% glycerol, 20% Triton X-100, 1mM DTT, 1mM Orthovonate, 1mM AEBSF, 1 tablet/50 ml protease inhibitor cocktail and 50 mM NaF), and sonicated 4 times for 20 seconds at 40%. The supernatant was obtained after centrifugation for 10 min at 14000 rpm at 4°C. To verify the expression as well as the solubility, the pellet (soluble) and supernatant (insoluble) were boiled in 4x or 6x Sample buffer and

loaded on a SDS-PAGE gel diverging from 6% to 12%.

6. Protein purification

6.1 Classical method

A classical protein purification method was first tested, following described protocols:

- The supernatant was treated by streptomycin sulfate to precipitate the unwanted DNA. 30% w/v of streptomycin sulfate was added slowly, and left stirring overnight at 4°C, followed by 30 min centrifugation at 12 000 rpm, and the supernatant was again treated as the previous step for 24 h
- 12%, 50%, and 68% ammonium sulfate precipitation was done on the supernatant in order to precipitate the protein of interest. The ammonium sulfate powder was added slowly while stirring the samples at 4°C, and left to incubate 1 h. A sample of each step was loaded on a SDS-PAGE gel to assess the different purification steps.
- Next step was to dialyse the proteins to obtain them in a suitable buffer for size exclusion chromatography. The samples were dialyzed (Slyde-a-lyzer dialysis cassettes, Pierce) against PBS or Tris-HCL pH7 in the cold room for 3 h, and overnight in a dialysis buffer volume 500 times larger than the sample.
- Size exclusion chromatography was performed on an AKTA purifier, where the column was equilibrated with 10 mM potassium phosphate. Once the proteins were loaded on the column, the elution was done by linear gradient of 0-500 mM NaCl or 0-500 mM KCL.

But this method showed to give variable results, with low yield and especially precipitation problems at the dialysis step.

6.2 Co-Immunoprecipitation (Co-IP)

Firstly, anti-GFP bound dynabead (protein G, Invitrogen) were used. The beads were washed in PBS-T followed by antibody coating in PBS-T containing 5µg of anti-GFP antibody for 10 mins at room temperature. Two anti-GFP antibodies were tried (monoclonal and polyclonal from Roche) for immunoprecipitation with the cell lysates. The Co-IP was done following the manufacturer's protocol. Cell extracts were incubated for 2 h with the anti-GFP dynabeads, washed 3 times with lysis buffer, followed by co-immunprecipitation done by boiling the beads in 4x sample buffer.

As there seemed to be a weak coating of the beads with the antibody and a generally low yield, a kit using already bound anti-GFP magnetic beads was used (µMACS epitope tag protein isolation kit). The cell pellets were treated with the µMACS lysis buffer (150 mM NaCl, 1% Triton X-100, 50 mM Tris-HCL pH8) implemented with 1mM DTT, 1mM orthovanadate, 1mM AEBSF and complete proteinase inhbitors. Sonication of the cells by 4 times for 20 seconds at 40% was followed by centrifugation for 14 000 rpm at 4°C for 10 mins. The supernatant was mixed to the magnetic microbeads, and left for incubation for 1 h in the cold room. The entire procedure was done in the cold room, where the µMACS columns were washed with the lysis buffer. The cell lysate incubated with the magnetic anti-GFP beads are then run though the columns, which will retain the magnetic beads. The columns were rinsed 4 times with the wash buffer 1 (150 mM NaCl, 1% NP-40, 0.5% sodium deoxycholate, 0.1% SDS, 50 mM Tris-HCL pH8), followed by a rinse with wash buffer 2 (20 mM Tris-HCL pH7.5). The native elution consists of applying 20 µl of 0.1 M triethylamine pH 11.8, 0.1% Triton X-100 to the column and leave to incubate at room temperature for 5 mins. 50 µl of 0.1 M triethylamine pH11.8, 0.1% Triton X-100 was added to the column, and the eluate was collected in a tube with 3 µl of MES pH 3 for neutralization.

Samples for the input, washes, normal elution and native elution were loaded on SDS-PAGE gel and revealed by coomassie staining and immuno-staining.

7. SDS-PAGE and Immunostaining

7.1 SDS- PolyAcrylamide Gel Electrophoresis

The gels for SDS-PAGE were prepared with ProtoGel (30%, 37.5:1 Acrylamide to Bisacrylamide stabilized solution optimized for SDS-PAGE of proteins, National Diagnostics), TEMED: N, N, N', N'-Tetramethylethylenediamine, APS: Ammonium persulfate, SDS and Tris. Depending on the percentage of the separating gel, the composition for a total of 10 ml varied:

Reagents to add in ml	6%	8%	10%	12%
H_20	5.3	4.6	4	3.3
30% acrylamide mix	2	2.7	3.3	4
1.5 M Tris pH8.8	2.5	2.5	2.5	2.5
10% SDS	0.1	0.1	0.1	0.1
10% APS	0.1	0.1	0.1	0.1
TEMED	0.008	0.006	0.004	0.004

The gel solution was poured between glass plates with a separator and once polymerized, the gel was washed with water and the stacking gel was poured on top. The stacking gel composition for 5 ml is 3.4 ml of H_20, 0.83 ml of 30% acrylamide mix, 0.63 ml of 1 M Tris pH6.8, 50 μl of 10 % SDS, 50 μl of 10% APS and 5 μl of TEMED.

The gel was left to fully polymerize, mounted on the running apparatus (BIORAD) and was loaded with prestained protein markers (NEB), as well as the samples of interest. The gels were then run in 1x running buffer (0.025 M Tris-HCL, 0.19 M Glycine, 0.1% SDS pH8.6) at 80-120 V for 1-2 hours.

To stain for total protein, coomassie brilliant blue staining (0.1% w/v Coomassie Brilliant blue, 20% Methanol and 10% acetic acid) was used. The gel was placed into a tray and stained by heating for 20 seconds in the microwave, followed by 15 mins of incubation on a shaker. Destaining was done with multiples washes using a solution of 50% methanol 10% acetic acid in water.

7.2 Immunostaining (Western Blot)

In order to proceed to immunostaining, the SDS-PAGE gels had to be transferred onto a nitrocelullose membrane (GE Healthcare) for ~2 h at room temperature at 300mM or overnight at 4°C at 10 V in transfer buffer (25mM Tris-HCL, 20% Methanol, 192mM Glycine pH 8.3). The membrane was blocked with shaking incubation in 3% milk powder in PBS-T for at least 1 hour at room temperature or overnight at 4°C. The primary antibody was added at a specific dilution factor (mouse anti-GFP 1:4000, Roche) in PBS-T including 3% milk and the membrane was incubated for 1 hour at room temperature. The membrane was washed trice in PBS-T for 10 minutes. The secondary antibody was added (anti-mouse HRP 1:5000) in PBS-T including 3% milk and the membrane was incubated for 1 hour at room temperature with agitation. The membrane was washed trice in PBS-T for 10 minutes and the bound antibody was detected by chemiluminescence (ECL Plus Western Blotting Detection Reagents, GE Healthcare). The reaction was detected with a film (GE Healthcare Hyperfilm ECL), and was developed with a Xograph Imaging Systems.

IV. Microscopy methods

1. Cell Sample preparation

1.1 Cell Sample preparation for imaging on the Zeiss, DV, Confocal microscopes

Cells were grown in culture at 30°C in YE media (unless otherwise specified), with or without drug as specified. HydroxyUrea (HU) was added to a final concentration of 20mM, and 4 NitroQuinoline 1-Oxide (4NQO) was added to a final of 5 μM, and both were used for 4 hours in the cultures. In case of time points (during Cdc25-22 TS synchronization) or heat shock cultures, samples at every time point were taken from the cultures. 1 ml of the culture was centrifuged to pellet the cells, washed with PBS, and the final cell pellet was fixed with 500 μl cold methanol. Cells were spread on glass slides and left to dry, upon which the glass slides were rinsed with PBS and dried again. Finally,

the mounting agent was added, 50% glycerol 50% water for FRET experiments but vectashield-mounting agent (Vector Laboratories) containing DAPI was used for other applications.

The Zeiss Axioplan and CoreDV were used following the guidelines and imaged for the present fluorescence: CFP, YFP, GFP, and DAPI using the sets of excitation and emission filters available. For FRET analysis, the fluorescent proteins were visualized using a laser scanning confocal microscope (LSM 510, Zeiss). More details of the LSM confocal microscope settings will be given.

1.2 Cells sample preparation for other fluorescence methods

In case of imaging cells on the Total Internal Reflection Microscope (TIRFM), the cells were grown in EMM media, harvested and washed with PBS. This allowed reduction of the auto-fluorescence and performing FRET on live cells.

Cells were sampled the same way for measuring the fluorescence of the CFP and YFP tagged proteins in the cells by FACS and fluorometer.

2. Fluorescence Resonance Energy Transfer (FRET)

2.1 Confocal microscope settings

A laser-scanning microscope (LSM 510, Zeiss) was used to image and perform FRET experiments. The argon ion gas laser is switchable via a long pass dichroic beam splitter (in our case either mainly 458 nm or 514 nm were used). The excitation laser is directed through a tube lens and objective lens (C-Apochromat NA 1.2 x63, Zeiss) to the sample. Due to its confocal capacities, emission emerging from above and below the plane of focus will be rejected at the pinhole and only fluorescence from the focal plane will pass to the photomultiplier (PMT) detector. The emissions wavelengths are separated at a dichroic beam splitter (545 nm) and filtered through band pass filters: 475-525 nm for CFP and 530-600 nm for YFP. Photobleaching of the acceptor (YFP) was performed by scanning with the 514 nm argon ion laser across a specific region of interest (ROI) within a cell (cytoplasm or nucleus) for 1000-3000 iterations. At satisfactory photobleaching of the YFP (>70%), images were

collected in a set of pre-bleach and post-bleach in both the CFP and YFP emission spectrum channels.

2.2 Controls

Although FRET is a good tool, various controls have to be done to ensure the presence of genuine FRET signal:

- Verification of the natural autofluorescence in non-tagged strains, measuring the intensities as well as positive photo-bleaching in both the CFP and YFP channels
- No FRET in the single tagged strains, when the acceptor or donor only is present
- Also, having a positive and negative FRET control for every new day of experiment, as there can be unwanted modifications due to the confocal microscope

2.3 FRET imaging and calculation

After that, those images were collected and processed in Image-J (NIH). Different measurements are done on each image in each channel:

- Measurement of the background (outside the cell)
- Measurement of a non-bleached cell area before and after photobleaching (provides general photobleaching of the sample, and will allow to normalize the images)
- Measurement of the photobleached ROI, providing the fluorescence intensity of the donor pre- and post-bleach (will provide the FRET efficiency), as well as the acceptor pre- and post- bleach (will provide the % of photobleaching)

The FRET efficiency can then be calculated and expressed as a percentage:

$$\text{FRET efficiency \%} = 1-[(IDA - IAuto)/(ID - IAuto)] \times 100$$

With the parameters being

IDA = Intensity of the donor in the presence of acceptor (pre-bleach)

ID = Intensity of the donor in the absence of acceptor (post-bleach)
IAuto = background intensity

We also verified the FRET efficiencies using a dedicated Image-J macro, for which they corresponded.

3. Live cell imaging

The pDV, a wide field microscope, was used with a 100x magnification and 1.40 oil objective. Three channels were used: DIC, CFP and YFP with the appropriate filter. The microscope was housed in a climate control chamber with the temperature set to 30˚C. The transmission and exposure times were tailored to each channel to achieve the best signal without damaging the cells. Various systems were used for immobilizing live *S. pombe* cells: agar pads, ConcanavallinA (ConA, Sigma) coated chambers (Lab-tek), and microfluidics chambers (CellAsic).

The CellAsic (Imsol) microfluidic chambers were chosen as they allow performing long imaging with the possibility of constant fresh media flowing as well as addition of drugs at different times points. The preparation of the microfluidic chambers were used following the manufacturer's guidelines, with many washes using sterile water as well as YE medium. The strains of interest were grown overnight in 100 ml at 30˚C to obtain the required cell concentration ($1x10^6$ - $2x10^7$ cells per ml) for loading on the microfluidic plates.

The software was programmed as indicated by the manufacturer's guidelines with a constant flow of media for 2-10 h. Imaging required some initial calibration to ensure no photo-damage was done to the cells, but still aiming to obtain reasonable quality images. At least 4 points per cell chamber were imaged through 20 z-stacks every 10 or 30 mins. Post-imaging process were done, including Z-stacking, deconvolution, and denoising softwares were applied.

4. Proteins preparation

The purified proteins were prepared for the various single molecule

methods used. The protocols were experimental and I will only present the most optimal ones.

4.1 Fluorescence Correlation Spectroscopy (FCS)

The native purified recombinant proteins were thawed on ice and diluted with filtered PBS to the single molecule concentration established previously. In the case of proteinase K addition, 50% v/v was added to the protein and left to incubate at 37˚C for 1 h. The corresponding control of the same reaction but without the proteinase K was done to prove the direct effect of the proteinase K on the purified proteins. Denaturation of the proteins was done by heating at 95˚C for 1 h and snap-freeze on ice. Hydroxyurea, Salts ($MgCl_2$, NaCl) and other reagents were tried.

For the antibody binding experiments, increasing concentrations of antibody were added to a constant concentration of purified proteins. The total volume remained the same, and they were all incubated for at least one hour. The interpretation columns show the sample and the theoretical bound population of anti-GFP to the purified CFP- or YFP-tagged proteins. The mock purification (the empty vector) was also mixed to the antibody to ensure the specificity of the binding; as well as unrelated antibodies to the purified proteins were tested as additional negative control.

Sample	Protein at 0.4 mg/ml in μl	Anti-GFP at 0.4 mg/ml (Ab) in μl	PBS in μl	Interpretation
1	0	20	20	Ab alone
2	10	0	30	Protein alone
3	10	2	28	9% bound
4	10	4	26	20% bound
5	10	7	23	32% bound
6	10	9	21	42% bound
7	10	11	19	51% bound
8	10	13	17	60% bound
9	10	15	15	70% bound
10	10	17	13	80% bound
11	10	20	10	93% bound
12	10	22	8	100% bound

13	10	30	0	Saturation
14	10	10 + 10 of 2nd antibody	10	Secondary

The FCS microscope is a custom-built confocal microscope, using 532 nm for the excitation and 593 ± 40 nm as emission filter for YFP fluorescence. The detector is a photon counting TSPC.

4.2 Total Internal Reflection Fluorescence Microscope (TIRFM)

The preparation of the purified proteins for the TIRFM was mainly done for the photobleaching step assay. Pre-cleaned cover slips for single molecule studies were used. First, a drop of 500 μl of 0.01 mg/ml of antibody is incubated for 15 mins, followed by two washes with filtered PBS with 5% of BSA (NEB) and a further 15 mins of incubation. The cover slip was washed with filtered PBS, and the purified protein was left to incubate for 30 mins on the coverslip. Alterations can be done to the protocol without affecting the assay.

The controls effectuated here were the antibodies alone, the BSA alone, as well as the PBS 5% BSA solution. The mock protein purification also allowed assessing the background, and imaging the protein in various channels provided the specificity of the signal.

The near TIRFM is a custom-built microscope inverted microscope coupled to a mixed gas ion tunable laser. Using the adequate microscope setting (ex.458 nm, filters 457 nm and 514 nm) the images were taken by an I-CCD camera.

CHAPTER III Ribonucleotide Reductase (RNR): Dynamic regulation and architecture

I. Introduction: The architecture and dynamics of RNR

Although discovered and described in the fifties (Reichard & Estborn, 1951) (Reichard et al, 1961), many questions remain with regards to the accurate stoichiometry ratio, conformation and general architecture of the enzyme RiboNucleotide Reductase (RNR). In *S. pombe*, while the regulation of RNR through transcription control (induced during S-phase, and after DNA damage) (Liu et al, 2003) (Liu et al, 2005) (Hankansson et al, 2006b) and cell cycle checkpoint control through the RNR regulator Spd1 (Liu et al, 2005) (Nestoras et al, 2010) is well described, the regulation of RNR by architectural modification has yet to be fully understood.

Originally RNR was described as a heterotetramer: 2x R1 and 2x R2 ($\alpha_2\beta_2$), but recently many reports of higher order oligomers formed upon activation, and inhibition have been published (Kashlan et al, 2001) (Rofougaran et al, 2008a) (Fairman, 2011). Higher order oligomerization is one of the keys for a better understanding of this essential enzyme's activity and regulation.

The big RNR subunit R1 (α) needs to be at least in a dimeric conformation. Diverse allosteric regulation sites are present on R1. The overall activity site (ATP cone domain) which binds ATP (activator) or dATP (inhibitor) regulating general RNR activity. This activity site is positioned at the N-terminus (Cotruvo & Stubbe, 2011).

The C-terminal part of R1 is structurally flexible and contains the other important features of R1, the specificity site and the catalytic site. The specificity site binds

dNTPs to allow a balanced supply of dNTPs to the cell of dNTPs and is found near the dimerisation domain. The catalytic site with the active dithiols (-SH) is important for the NDP reduction (Hofer et al, 2011). Finally, “loop 2”, a major determinant for specificity regulation by conformational flexibility, is also found near the dimer interface.

The small subunit R2 is also active as a dimer, and each monomer contains a binuclear ferric iron centre that generates and maintains the tyrosyl radical (Y•) essential for the enzyme’s activity (Hofer et al, 2011). Tyr^{122} is buried some 10 Å (1nm) inside the structure and therefore cannot interact directly with R1, thus the need for the active cysteines network of R1 to transfer the electron from the tyrosyl radical on R2. The distance between the tyrosyl radical (Y•) site of R2 and the thiyl radical site of R1 is ~35 Å or 3.5 nm (Zhang et al, 2011).

The free radical is essential to have an active enzyme, and its loss transforms the protein in a “metR2”, leaving the iron center intact, whereas an “apoR2” has lost both the iron centre and the free radical (Stubbe & Cotruvo Jr, 2011).

In addition to the unclear conformational status, there are uncertainties about the stoichiometry of RNR. Different heterocomplexes have been described between species with a wide range differences for the active and inactive states of the enzyme. The classical proposed model is $\alpha_2\beta_2$ (Thelander & Reichard, 1979), but recent studies have modified this model. In mice (Rofougaran et al, 2006), the $\alpha_6\beta_2$ complex has been described as being the primarily active enzyme form. In addition, a $\alpha_6\beta_6$ form has also been portrayed in mouse after addition of gemcitabine (Wang et al, 2009). In humans $\alpha_6\beta_2$ is the major form present, especially after inactivation. Similarly in *S. cerevisae*, $\alpha_2\beta_2$ is the inactive form described *in vitro,* but the active form in yeast has not been fully described yet (Ando et al, 2011). In contrast, studies have demonstrated that in *E. coli*, RNR forms $\alpha_4\beta_4$ complexes (Rofougaran et al, 2008a) representing the inactive form.

The architecture of RNR clearly deserves further investigation in order to understand its tight regulation. In *S. pombe*, RNR is part of the class Ia of the RNR classification (as most eukaryotes) and the big subunit is called $Cdc22^{R1}$ (β) while the smaller subunit is $Suc22^{R2}$ (α).

II. Ribonucleotide Reductase subunits labelled with fluorophores: Characterization and Quantification

In order to study the RNR subunits, the genes *suc22*^{R2} and *cdc22*^{R1} were tagged with CFP and YFP fluorophores (Nestoras et al, 2010). Suc22^{R2} is labeled at the N-terminus, as the C-terminal tagging causes lethality to the strain, which is not surprising, as it is known that the C-terminus of Suc22^{R2} is most probably necessary for interaction with Cdc22^{R1}. Cdc22^{R1} is tagged at the C-terminus, which should not disrupt the ATP cone domain at the N-terminus, which is important for different functions (Lee et al, 2008).

In both cases, a linker is present between the protein and the fluorescent tag, which confers flexibility to the structure between the proteins and the fluorescent tags. The strains used in this study are shown in Figure III.1. The parameters used to image the cells with the use of the confocal Zeiss LSM throughout the experiments are described in the figure legend.

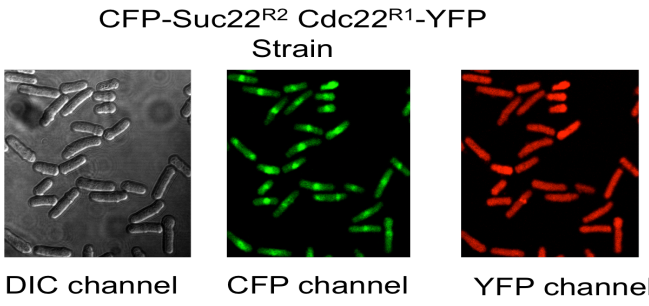

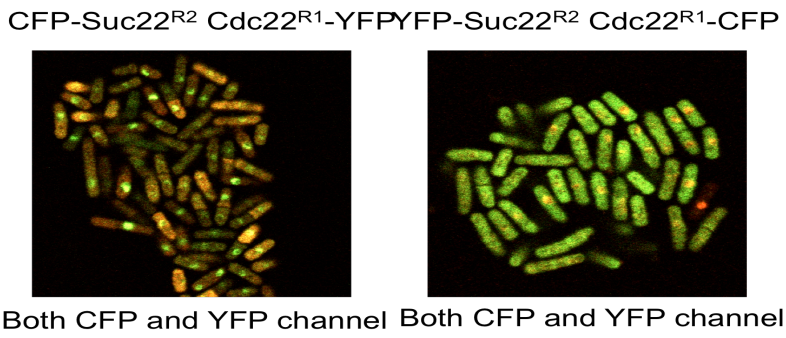

Figure III. 1 Images of CFP-Suc22^{R2} Cdc22-YFP^{R1} strain and YFP-Suc22^{R2} Cdc22-CFP^{R1} strain
Example of images of both S. pombe strains used throughout the experiments: both subunits of the RNR tagged with the fluorophores CFP or YFP. Images were collected with a 63x objective lens (N.A 1.2) on a confocal microscope (LSM500, Zeiss) in bright field DIC, CFP channel (band pass filer 475-524 nm) and YFP channel (band pass filter 550-650 nm), after excitation with a 458 or 514 nm Argon laser. Images were processed in Image-J as well as the provided program of the confocal (Zeiss LSM).

The relative intensities of both subunits were measured (Figure III.2), and compared between S-phase cells and G2 phase cells in the different sub-cellular compartments. Cdc22^{R1} showed little difference in intensity throughout the cell and cell cycle phases (around 100 to 170 arbitrary units).
On the other hand, Suc22^{R2} has quite dynamic and fluctuating protein intensities. In S-phase cells, the levels of Suc22^{R2} in the cytoplasm are comparable with the levels in the nucleus. Also, Suc22^{R2} has about half the fluorescence intensity of Cdc22^{R1}. Suc22^{R2} protein concentration in G2-phase cells is quite distinctive, with only a fraction of the Suc22^{R2} proteins in the cytoplasm, and the rest of the Suc22^{R2} being nuclear. All these measurements are similar to semi-quantitative measurements done by SDS-PAGE gel with the double-tagged strain. Indeed the small RNR subunit Suc22^{R2} is about half as concentrated than Cdc22^{R1} when detected by immunostaining after SDS-PAGE Gel.
Taking into account that *S. pombe* cells are mostly in G2 phase, Suc22^{R2} can be considered typically nuclear.

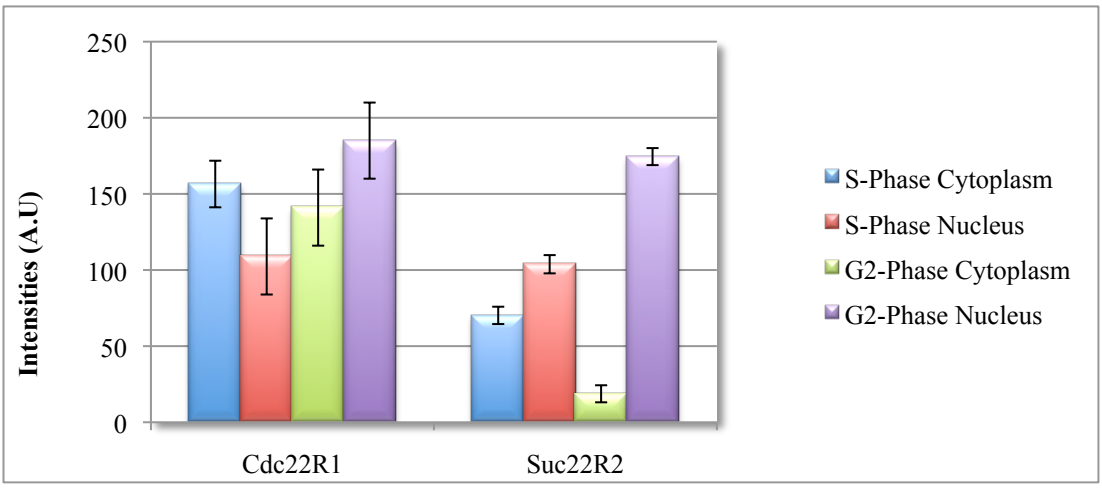

a.

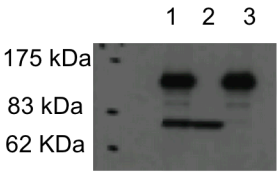

Lane 1: CFP-Suc22^{R2} Cdc22^{R1}-YFP

Lane 2: CFP-Suc22^{R2}

Lane 3: Cdc22^{R1}-YFP

b.

Figure III. 2 Comparison of the RNR subunits intensities in S-phase cells and G2-phase cells in both compartments

a. Measurements of the intensities are in arbitrary units (a.u) done in specific ROI (regions of interest) followed by average and standard deviation calculation. Cells were visually distinguished and categorized, and measurements done in the different strains of single tagged RNR subunits i.e.. RNR subunits tagged with either CFP or YFP.

Cdc22^{R1} is localized throughout the cell, without significant difference about the localization in the nucleus versus cytoplasm during the cell cycle.

Suc22^{R2} is localized in the whole cell but is predominately present in the nucleus in G2 phase.

b. Immunostaining of the RNR tagged proteins: TCA extract followed by loading of the samples on SDS-PAGE gel. The protein extract of RNR double-tagged strain CFP-Suc22^{R2} Cdc22^{R1}-YFP, and single tagged strains CFP-Suc22^{R2} and Cdc22^{R1}-YFP are then immunostained by anti-GFP (recognizes CFP and YFP) indicating the endogenous levels of the RNR tagged proteins. Indeed, the smaller subunit Suc22^{R2} (expected around 75 kDa) is approximately half the level of the big subunit Cdc22^{R1} (expected around 119 KDa). Immunostaining done in collaboration with Dr. Adam Watson.

III. Fluorescence Energy Transfer (FRET) assay between the RNR subunits

The FRET experimental set up is illustrated Figure III.3. CFP-Suc22^{R2} is present throughout the cell but mostly in the nucleus, whereas Cdc22^{R1}-YFP is pan-cellular. Each fluorophore, thus protein, is imaged in a specific channel as mentioned before.

As explained in the introduction, due to an overlap in the emission of the donor and the excitation of the acceptor, an energy transfer will be possible between the donor and acceptor fluorophores. But a few conditions need to be met: if the fluorophores are at a larger distance than 10 nm, or are not in an aligned dipole conformation, there will not be an energy transfer from the donor to the acceptor. Our chosen method is the Acceptor Photobleaching Fluorescence Resonance Energy Transfer. Once the acceptor is photobleached, there will be a decrease in the acceptor's channel (in our case YFP). In addition, there will be a slight decrease in the donor channel (CFP) due to overlap of spectrums and bleed-through between the channels. This inter-fluorophore bleed-through has been previously characterized (Wang et al, 2010). As a result, in case of no FRET there will be a decrease in the fluorescent intensity in both channels.

On the contrary, if the fluorophores are closer than 10 nm and in the correct alignment, there will be an energy transfer between the donor (CFP) and acceptor (YFP). This time, after photobleaching of the acceptor (YFP), there will be a decrease in the acceptor channel (YFP) but an increase in the donor channel (CFP), as the donor's emission will increase (Wang et al, 2010).

The lack of FRET signal does not necessarily mean that proteins do not interact, but only demonstrates that all the required conditions for energy transfer are not present. Specifically, in our RNR analysis, we know that the two RNR subunits are able to interact and that they do, as this is required for cell survival.

In order to include another level of controls in the experiments, we also swapped the fluorophores i.e. the donor CFP on the Cdc22^{R1} and the acceptor

YFP on Suc22^{R2}. This strain has then been used in every experiment to verify the results.

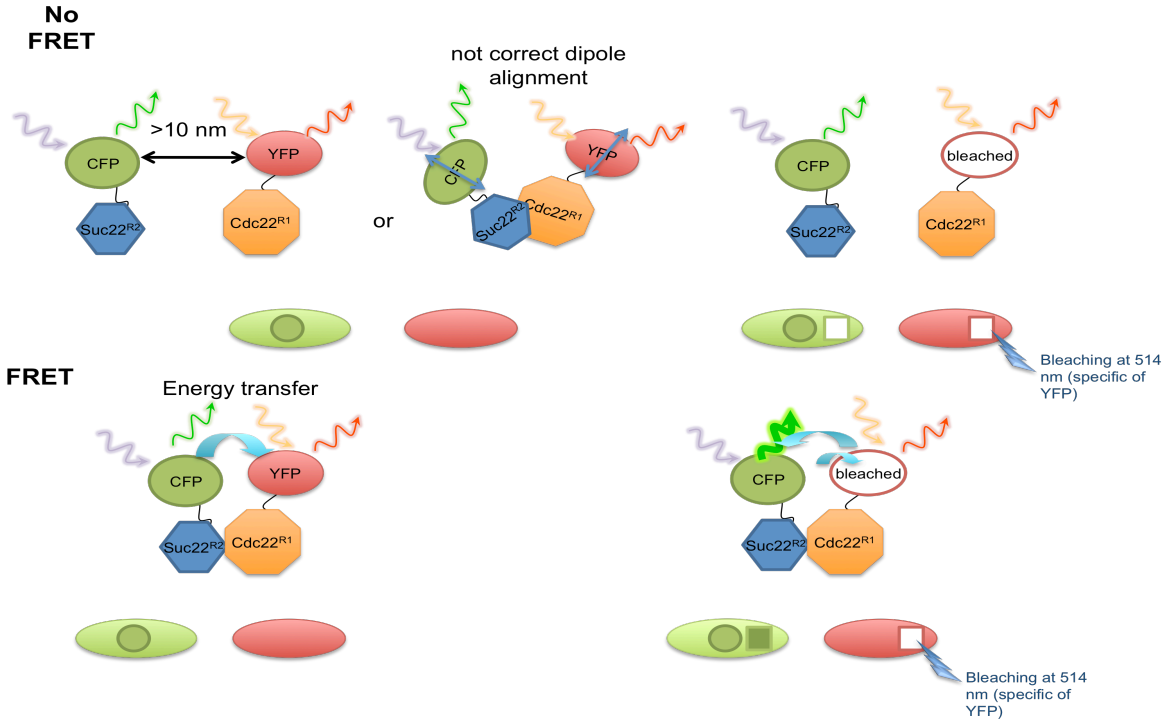

Figure III.3 Acceptor Photobleaching Fluorescence Resonance Energy Transfer (FRET) assay set up between the RNR subunits Suc22^{R2} and Cdc22^{R1} in S. pombe.

Suc22^{R2} tagged at the N-terminus with CFP is localized throughout the whole cell but predominately in the nucleus. In the case of CFP, an excitation source of 458 nm will give an emission with a peak at 500 nm. Cdc22^{R1} is tagged with YFP and localized throughout the cell. The fluorophore YFP has an excitation peak at 515 nm and will emit at ~ 530 nm.

If Suc22^{R2} and Cdc22^{R1} are in close proximity and therefore their respective fluorophores are within 10 nm, an energy transfer can occur (providing the right dipole conformation of the donor/acceptor pair) due to the overlap of the CFP/donor emission spectra and the YFP/acceptor excitation spectra.

If the YFP/acceptor is photobleached with a 514 nm laser, the energy transfer will not occur due to inactivation of the acceptor, and the result will be an increase in the donor's emission fluorescence.

In the case where there is no FRET, the photobleaching will decrease the YFP/acceptor fluorescence as well as slightly decrease the CFP fluorescence due to the overlap of spectra (bleed-through).

Next Figure (fig. III.4) is an example of images of the acceptor photobleaching FRET assay, in a set of images taken in each channel before and after bleaching. In this example, the strain is CFP-Suc22^{R2} Cdc22^{R1}-YFP,

and the FRET between both RNR subunits is positive. As shown in the previous diagram, after photobleaching of the YFP/acceptor, there is a decrease in the YFP channel. Whereas in the CFP channel, those bleached regions have now an increased intensity in the CFP channel. Arrows mark the regions of interest (ROI).

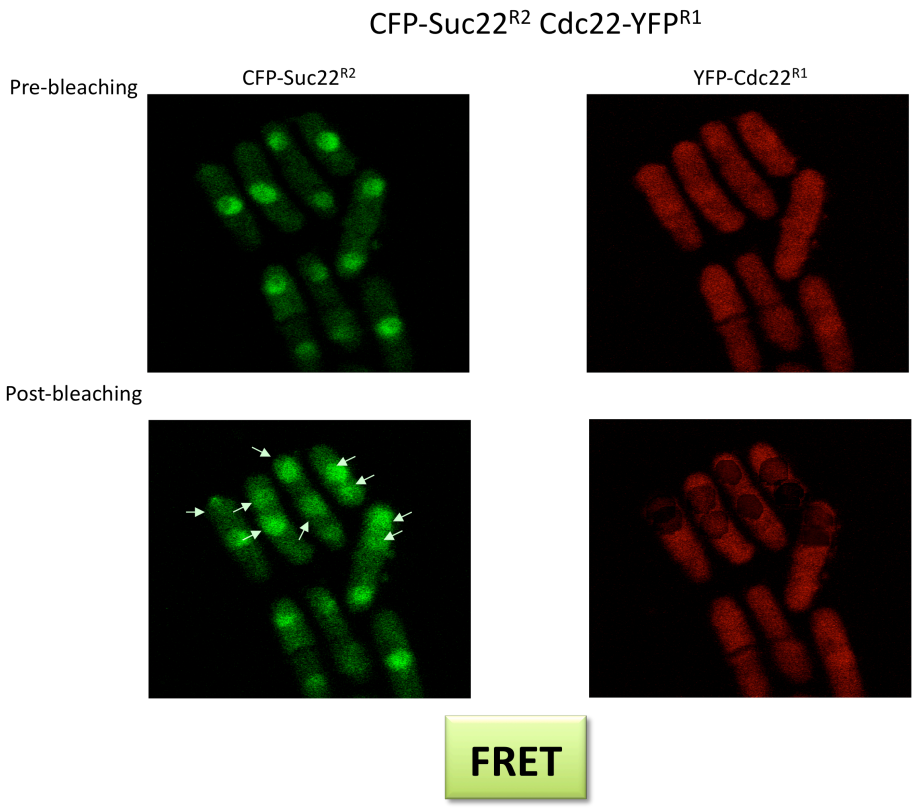

Figure III.4 Image of the donor photobleaching FRET experiment in the CFP-Suc22^{R2} Cdc22-YFP^{R1} strain

Images were taken on a confocal microscope (LSM500, Zeiss): A set of images consists of pre-bleach images in the CFP channel (band pass filer 475-524 nm) and YFP channel (Band pass filter 550-650 nm), as well as images after bleaching, again in each channel. The bleaching is done in a ROI (region of Interest) at 514 nm for 2000-6000 iterations.

In this case, the increase of fluorescence in the CFP channel is very clear, as shown by arrows, and corresponds with the photobleached zones in the YFP channel. Measurements of the CFP fluorescence pre- and post- bleach are then used to calculate the FRET efficiency.

IV. Ribonucleotide Reductase complex formation measured by $Suc22^{R2}$ and $Cdc22^{R1}$ FRET throughout the cell cycle in distinct cell compartments

Sets of images such as those previously shown (fig. III.4) were used to calculate the FRET efficiency by measuring the intensity in both channels before and after bleaching in the regions of interests. General photobleaching of the cells as well as background autofluorescence are taken into account in the calculations, as described in material and methods. Also, this method of FRET calculation cannot be considered quantitative *per se*; but considering the numbers of repeat and the consistency of the FRET efficiencies, they can be used as semi-quantitative estimates. The FRET efficiency between $Suc22^{R2}$ and $Cdc22^{R1}$ were measured specifically in the cytoplasm and the nucleus. In addition, distinction was made between S-phase cells and G2-phase cells (Figure III.5).

We aimed to use the FRET experiment to observe the fluctuation of the RNR activity throughout the cell cycle and therefore we expected to have positive FRET between the RNR subunits in the cytoplasm, specifically of S-phase cells. During the S-phase, the RNR complexes are thought to be assembled and activated in the cytoplasm (due to R2 re-localization to the cytoplasm) in order to provide dNTPs to the cell during DNA replication. We were surprised to observe a positive FRET between the RNR tagged subunits, in the cytoplasm as well as in the nucleus. In addition, the FRET signal was also positive during the whole cell cycle.

In general, the FRET efficiency was around 35% in the cytoplasm of both S-phase cells and G2-phase cells. In contrast, we had not expected to detect a positive FRET signal between the RNR subunits in the nucleus, where it was not thought that they would interact. Although it has to be considered that the upper layer of the ROI can be composed of cytoplasm, the observation of positive nuclear FRET signal in G2 cells and S-phase cells, when $Suc22^{R2}$ is largely relocated to the cytoplasm, is interesting.

Considering the levels of each subunit as described before (Figure III.2), there is some discrepancy between Suc22^{R2} levels and the FRET efficiency, as there is relatively little Suc22^{R2} present in the cytoplasm in G2-phase cells, but still a high FRET signal is observed. On the contrary, there is much more Suc22^{R2} present in the nucleus, while the FRET efficiency is then lower. This FRET efficiency increases in the nucleus during S-phase when Suc22^{R2} re-localizes to the cytoplasm.

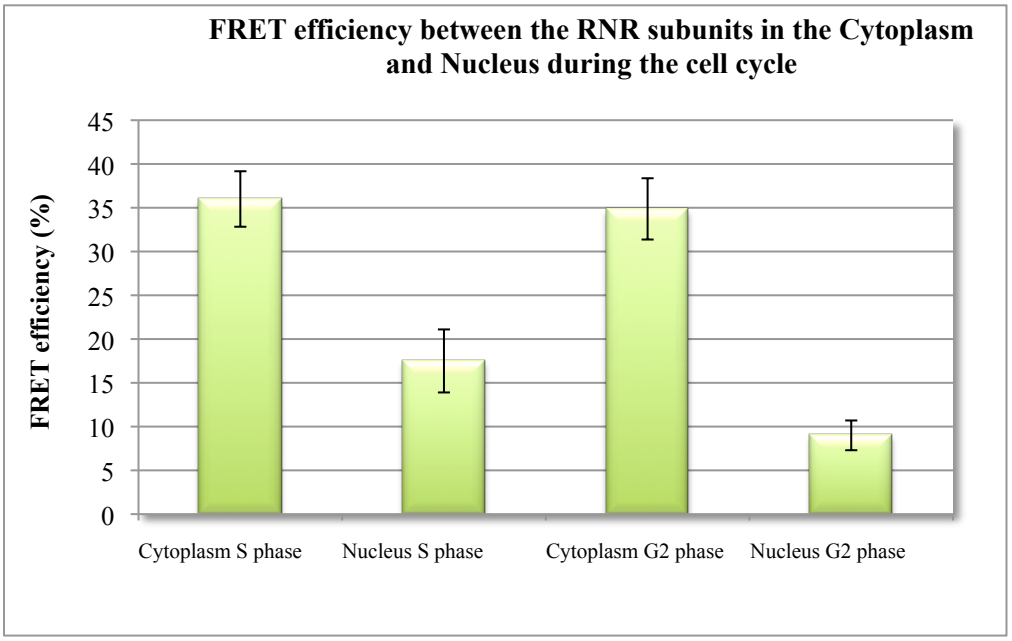

Figure III. 5 FRET efficiencies between CFP-Suc22^{R2} and Cdc22^{R1}-YFP in different cell compartments during the cell cycle

The FRET efficiencies have been calculated by keeping the measurements separate for cells in S-phase or in G2-phase (as distinguished by the stage of cell division and nucleus). In addition, the measurements in the nucleus and the cytoplasm have also been separated.

The FRET efficiency is positive in all cases, thus demonstrating an interaction (formed complex) between Suc22^{R2} and Cdc22^{R1} at all times, both in the cytoplasm and the nucleus.

Thus, it can be said that there is an interaction and potential complex formation between Suc22^{R2} and Cdc22^{R1} at all times, in both compartments of the cell, contrary to what was thought: i.e. active RNR complex in the cytoplasm only during DNA replication (S-phase); and after DNA damage of G2 phase cells. These results provide a novel insight of the complexity of the formation and regulation of the Ribonucleotide Reductase enzyme.

The positive FRET signal in both cell compartments during the cell cycle was also verified in collaboration with Dr Asma Mohammed on live cells using

another microscope (TIRFM) with similar levels of FRET efficiencies. (Figure III.6)

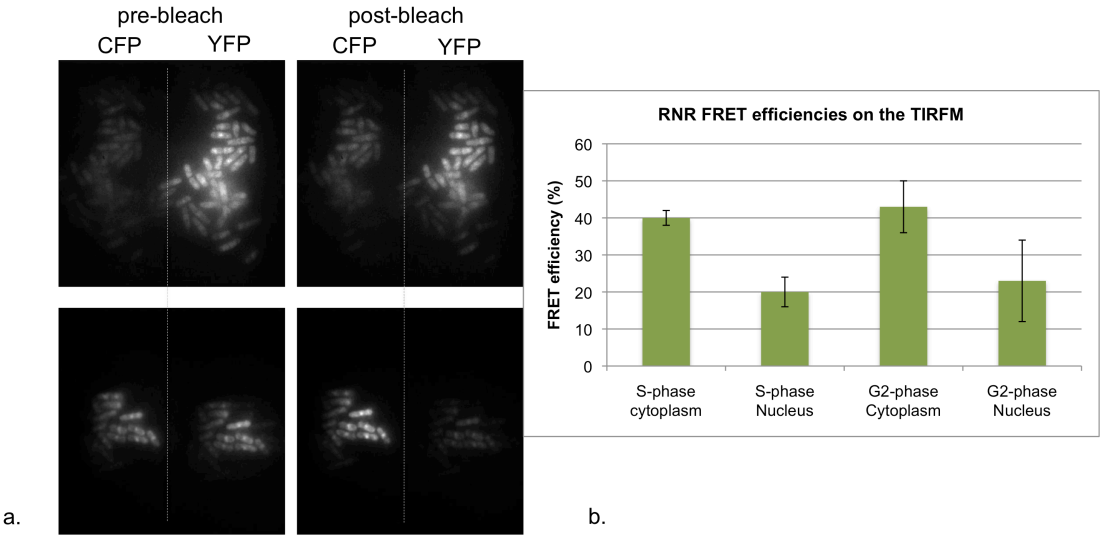

Figure III. 6 FRET efficiencies between CFP-Suc22^{R2} and Cdc22^{R1}-YFP in live cells on the near TIRFM

The FRET efficiencies have been calculated as mentioned above, but these cells have not been fixed therefore these FRET signal are from live cells. The near Total Internal Reflection Microscope (TIRFM) has been used. Although less precise photobleaching is possible, the imaging is done by dual channel at very fast acquisition. Two examples are presented in a. with the cells in CFP and YFP, before and after bleaching. b. The FRET efficiencies are again positive in all cases and to very similar levels to the ones obtained on the confocal microscope in fixed cells, thus demonstrating an interaction between Suc22^{R2} and Cdc22^{R1} at all times, both in the cytoplasm and the nucleus. This has been done in collaboration with Dr. Asma Mohammed.

V. Ribonucleotide Reductase activity after drug treatment

Two very distinct drugs were used to observe the effects on the RNR complexes measured by FRET. Hydroxyurea (HU), which is a radical scavenger and thus inactivates the activity of Suc22^{R2} required for functional RNR. HU has been used extensively to inhibit the RNR, resulting in depletion of dNTPs, and subsequent stalling of replication forks, thus blocking cells in S-phase. Some of the visual characteristics when using HU are a clear re-localization of Suc22^{R2} from the nucleus to the cytoplasm as well as an elongation of the cells due to the cell cycle arrest (see Figure III.7).

The second drug used is 4-Nitroquinoline 1-oxide (4NQO): a DNA damaging agent that causes DNA adducts. It is considered to be a UV mimetic leading to the damaged DNA being repaired by the nucleotide excision repair (NER) pathway .

When treating the strain CFP-Suc22^{R2} Cdc22^{R1}-YFP with 4NQO, a noticeable elongation of the cells length is observed, however in contrast to HU, the RNR small subunit Suc22^{R2} remains clearly nuclear. This is an important observation, as it demonstrates that the hypothesis of Suc22^{R2} re-localization to the cytoplasm after DNA damage is not applicable in these circumstances.

From the images presented in Figure III.6, we can observe that after HU treatment there is no FRET (clear decrease in the CFP channel). Whereas after treatment with 4NQO, there is a clear FRET signal, indicated by an increase in the CFP channel.

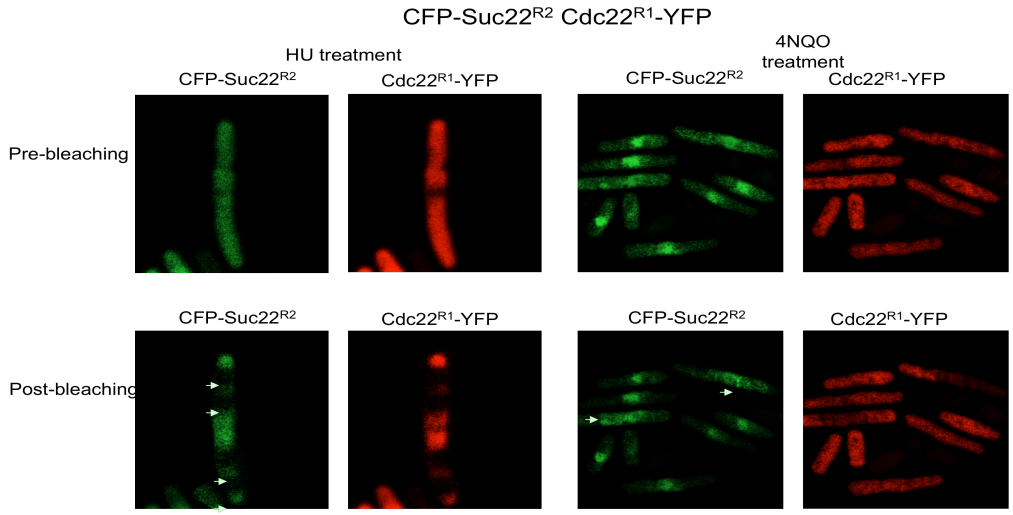

Figure III. 7 Images set of the FRET experiment in the CFP-Suc22^{R2} Cdc22-YFP^{R1} strain after treatment with hydroxyurea (HU) and 4NQO

Images were taken on a confocal microscope (LSM500, Zeiss) as described in Figure *III.4, and the FRET analyzed by Acceptor Photobleaching. The cells treated with hydroxyurea (radical scavenger) for 4 hours at 20 mM have a decrease in fluorescence intensities in both channels in the ROI, indicating no FRET. Cells treated with 4 Nitroquinoline 1-oxide (a UV mimetic inducing DNA lesions) for 4 hours at 5 μM, maintain the Suc22^{R2} nuclear (in opposition with the HU). The cells also show an increase in the CFP fluorescence (donor) after bleaching of the YFP (acceptor) indicating the occurrence of FRET.*

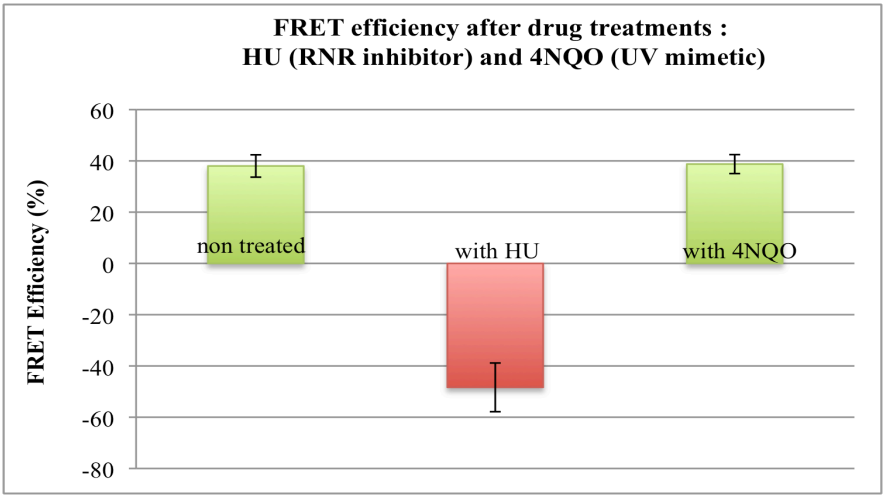

Figure III. 8 FRET efficiencies between CFP-Suc22^{R2} and Cdc22^{R1}-YFP after treatments with HU and 4NQO

As shown before, the CFP-Suc22^{R2} and Cdc22^{R1}-YFP strain displays positive FRET signal (around 38% FRET efficiency). This FRET is lost after treatment with hydroxyurea (a radical scavenger) for 4 hours at 20 mM. Whereas after treatment of the cells with 4 Nitroquinoline 1-oxide (a UV mimetic inducing DNA lesions) for 4 hours at 5 μM, the FRET signal is maintained.

These experiments have been repeated in the YFP-Suc22^{R2} Cdc22-CFP^{R1} strain, where the fluorophores tags have been swapped.

The graph shown in figure III.8 is the comparison of the FRET efficiencies of the subunits Suc22^{R2} and Cdc22^{R1} after treatment with the indicated drugs. Consistent with previous data, in case no treatment, the FRET efficiency is approximately 40%, which is lost upon treatment with HU (treatment of 4 hours at 20 mM). The negative FRET efficiency value represents the decrease in CFP fluorescence due to the bleed-through of the channels.
This negative FRET signal could be explained by the scavenging activity of HU, and thus inactivation of Suc22^{R2}. How precisely HU affects the FRET is not entirely clear: it could be that the loss of the tyrosyl radical in the Suc22^{R2} affects the structure of the subunit, and induce a change in conformation, which will therefore affect the energy transfer. It has been described that the apoR2 and metR2 have a different structure of the iron centre. An alternative explanation could be a change in oligomerization where the stoichiometry of dimer Suc22^{R2} is modified.

After treatment with 4NQO (4 hours at 5 μM), the FRET efficiency is positive and the FRET efficiency is comparable to the efficiency before treatment. This is consistent with the DNA damaging activity of 4NQO, and the need for dNTPs for repair.

VI. Verification of the effect of HU in G2 arrested cells

In order to investigate further the effect of HU on the FRET assay, cells were arrested in G2 phase using a temperature sensitive mutant Cdc25-22.
The cells are kept at 36°C for 3 hours resulting in a population of cells synchronically blocked in G2. This was verified by FACS profile in addition to septation index monitoring. Cells were blocked in G2 and while a control culture was not treated with HU, the other culture was treated with HU in the same conditions as described before. Samples for the FRET assay were taken every 30 mins, as well as for FACS analysis.
In the control experiment, it is clear that there is FRET between the two RNR subunits, during the whole experiment (Figure III.9).

Whereas in the cells treated with HU at time 3h, the FRET signal is lost, and becomes negative. This effect is independent of S-phase and could represent a direct effect of HU inhibiting RNR consequently modifying the energy transfer from YFP-Suc22^{R2} to Cdc22^{R1}-CFP fluorophores.

Also, there is a clear nuclear localization of Suc22^{R2} even after HU treatment, whereas Suc22^{R2} is usually relocated to the cytoplasm upon HU treatment after checkpoint activation and degradation of Spd1. In this case, cells are in G2 phase thus Suc22^{R2} is nuclear.

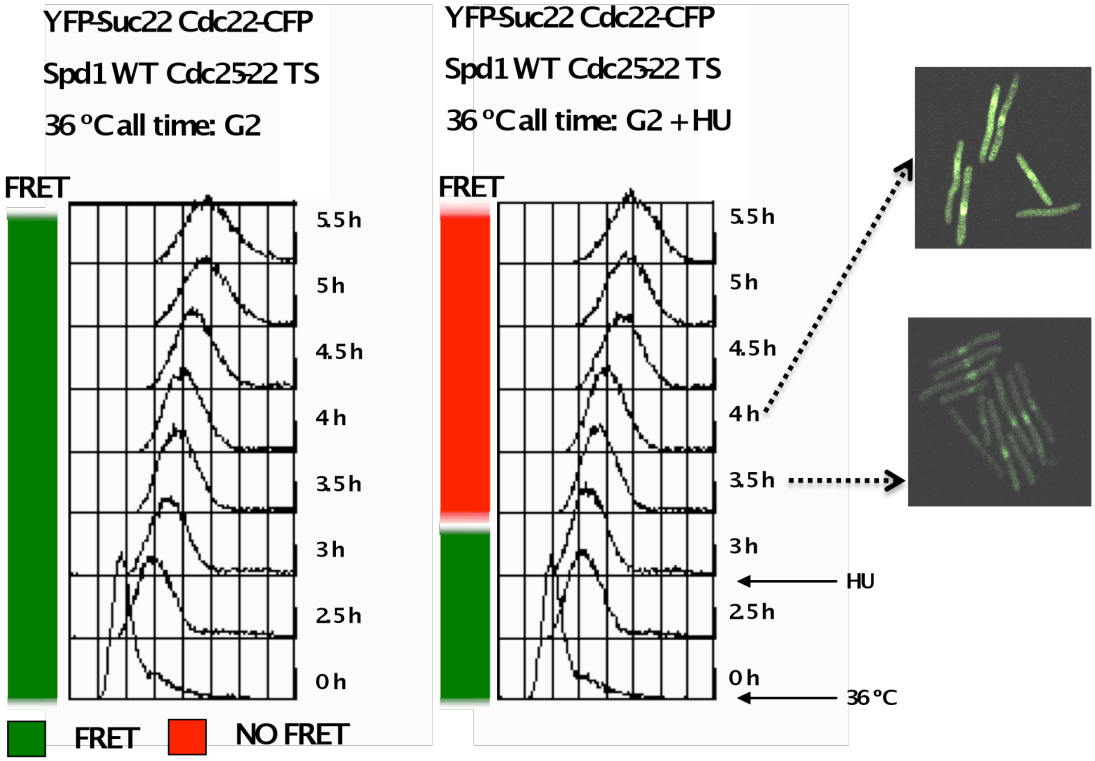

Figure III. 9 FRET measurements of synchronized cells arrested in G2 treated with HU

The YFP-Suc22^{R2} and Cdc22^{R1}-CFP strain has been crossed with the cdc25-22^{ts} mutant, allowing G2 arrest of the cells at 36°C. FACS profile shows the correct G2 arrest of the cells (samples taken every 30 mins from the shift to 36°C), and the color-coded FRET on the side is the result of the FRET experiment using the same sample (green: positive FRET, red: negative FRET). HU was added to the cells arrested in G2 (at time 3 hours) and almost instantly the FRET signal was lost. This experiment shows that the loss of FRET signal is most probably due to the action of the HU directly on the Suc22^{R2}, and S-phase independent. In parallel non-arrested cells were assayed to verify the correct cell cycle of these cells.

VII. FRET assay of the RNR homo-complexes of subunits Suc22^{R2} and of Cdc22^{R1} in diploids strains

To have a clearer view of the RNR complex as well as the stoichiometry ratio of each of the subunits and their modifications, diploids strains were made to perform FRET. The diploid strains have each Suc22^{R2} subunit tagged, one with the FRET donor and the other with the acceptor. Another diploid strain was constructed to achieve Cdc22^{R1} homo-FRET. Using *ade6* intragenic complementation (as explained in chapter II), CFP-Suc22^{R2} YFP-Suc22^{R2} diploid strains were made as well as Cdc22^{R1}-CFP Cdc22^{R1}-YFP strains.

In Figure III.10, part a., images show the cells of both diploids strains, and below (part b.) the results of the FRET: Suc22^{R2} subunits do interact closely enough for FRET to occur between the donor (CFP) on one monomer of Suc22^{R2} and the acceptor (YFP) on the monomer copy of Suc22^{R2}. This indicates that the complexes of Suc22^{R2} seem to be a close dimer. However, the Cdc22^{R1} diploids strains do not FRET. We do know that Cdc22^{R1} subunit does form a multimer, but it is possible that due to its large size and unknown stoichiometry (2, 4 or 6 subunits) the FRET pair fluorophores are too far apart for FRET to occur.

Once quantified (Figure III.10 part b.), it is clear that the FRET observed in the Suc22^{R2} homo-dimer complex is reasonably high efficiency (around 30%) and is observed in the nucleus as well as in the cytoplasm.

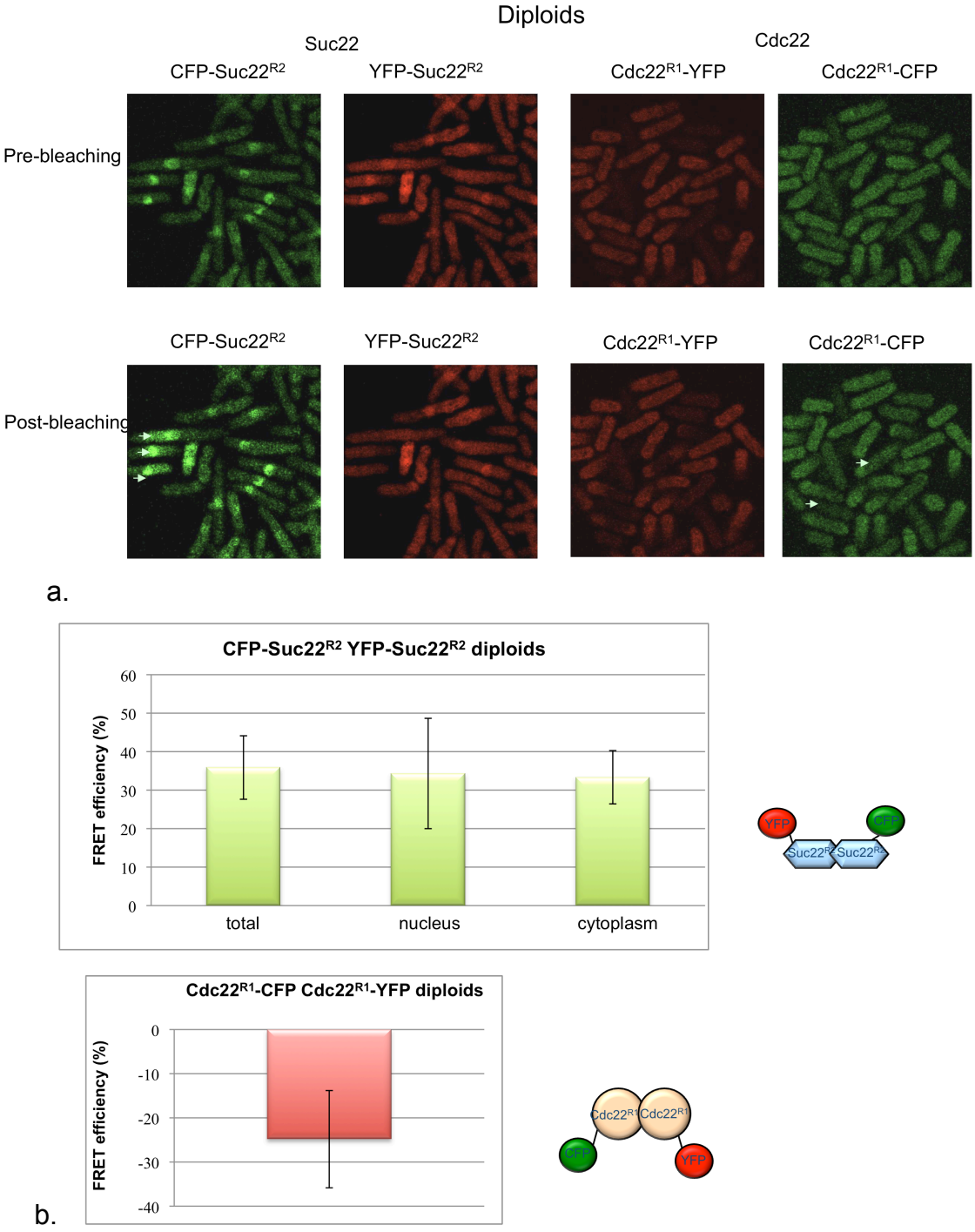

Figure III. 10 FRET measurements in Suc22^{R2} and Cdc22^{R1} diploids: images and FRET efficiency

Diploids strains have been made (using the ade6 intragenic complementation) in order to have CFP-Suc22^{R2} YFP-Suc22^{R2} and Cdc22^{R1}-YFP Cdc22^{R1}-CFP, which are potential tools to observe the FRET between the subunits in the formation of homocomplexes. Above (a.), an image set of FRET conducted on the diploids strains. In the case of the Suc22^{R2} tagged with the donor CFP on one copy and the acceptor YFP on another protein, there is FRET (quantified in b.). Whereas in the Cdc22^{R1} diploid strain, there is clearly no FRET, allowing us to speculate that the distance between the fluorophores is too great or the dipole conformation is incorrect.

VIII. FRET assay between the RNR subunits homo-complexes after drug treatment

In order to obtain a better understanding of the effect of the drugs used previously on RNR, HU and 4NQO were used on the diploid strains.
In the case of the Suc22^{R2} homo-dimer FRET, the FRET signal was positive with approximately 30% of FRET efficiency (Figure III.10). After HU treatment, this FRET was lost. We can speculate again that the effect of HU on Suc22^{R2} could be important, modifying its structure or conformation. As the free tyrosyl radical is embedded inside the small RNR subunit's structure, it could be that during the scavenging process, the structure is relaxed and/or the general conformation of Suc22^{R2} is modified. Another possibility is the modification of stoichiometry of Suc22^{R2}.

In contrast, after treatment with 4NQO, a UV mimetic that will create DNA damage thus activate (or hyper-activate) RNR, the positive FRET signal is maintained. Suc22^{R2} might maintain its dimeric form, allowing the energy transfer.

The same drugs have been applied to the diploids Cdc22^{R1}-CFP Cdc22^{R1}-YFP (data not showed), but as in the non-treated strain, no FRET is observed.

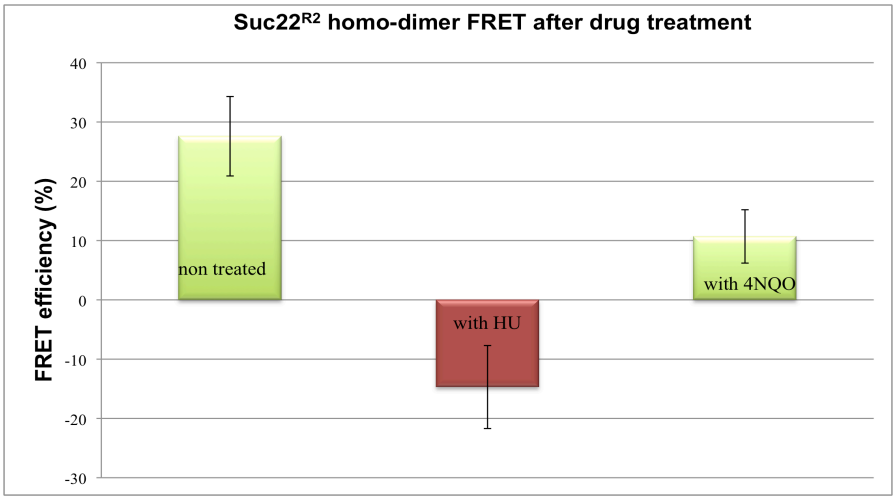

Figure III. 11 FRET efficiencies measurements in Suc22^{R2} diploids strains
The diploid strain CFP-Suc22^{R2} YFP-Suc22^{R2} was used to observe the FRET of the subunits in the formation of Suc22^{R2} homocomplexes. The FRET is positive (28%), translating a close

interaction of the small RNR subunits thus possibly form a dimer in vivo. This FRET is lost after treatment with hydroxyurea (a radical scavenger) for 4 hours at 20 mM. But, after treatment of the cells with 4 Nitroquinoline 1-oxide (a UV mimetic inducing DNA lesions) for 4 hours at 5 μM, the FRET signal is maintained.

IX. Ribonucleotide Reductase after heat shock

The transcriptional response to heat shock is conserved in eukaryotes organisms, and is controlled by Heat Shock Factors (HSF). In *S. pombe*, this transcription factor is essential for growth (Gallo et al, 1991).

It has been described that a *suc22*^{R2}+ larger transcript (Harris P, 1996) is highly induced after heat shock (42°C), while *cdc22*^{R1}+ transcripts are reduced. This strong induction of *suc22*^{R2}+ has been demonstrated to be part of a separate pathway from the DNA damage pathway. We wanted to investigate how the heat shock might affect the FRET experiments.

Using the RNR double-tagged strain CFP-Suc22^{R2} Cdc22^{R1}-YFP, the FRET efficiencies between Suc22^{R2} and Cdc22^{R1} were compared in cells from cultures at 30°C and 42°C (heat shock temperature). Samples were taken every 20 mins, and the FRET efficiencies were measured in both compartments of cells in S-phase or G2-phase (Figure III.12).

In general, the cells at 30°C show FRET efficiencies consistent with the ones measured before: around 40% in the cytoplasm at any cell stage, and around 15-20% in the nucleus of cells in S-phase, and 5-10% for nuclei in G2 cells.

After approximately 100 mins of heat shock, the cells exhibit a higher FRET efficiency, in particular in cells with septa (S-phase cells). Interestingly after shifting the heat shock cultures back to 30°C (at time 145 mins), this FRET efficiency is reduced back to the control's FRET efficiency level.

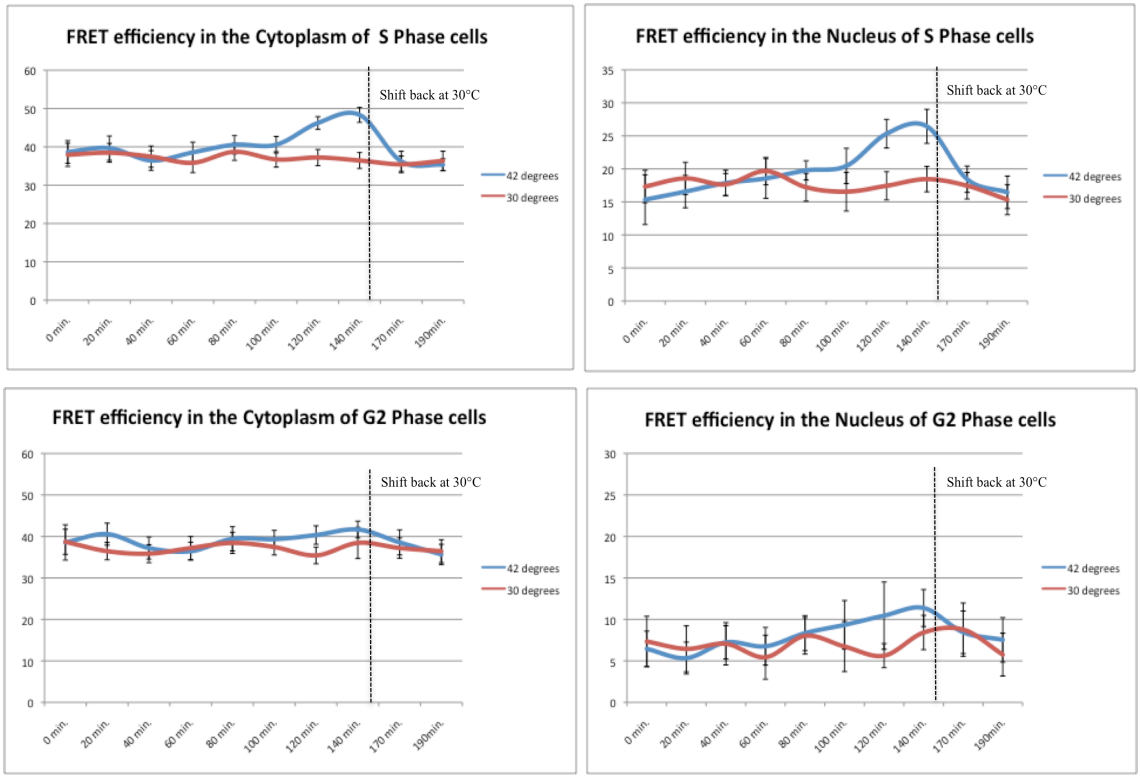

Figure III. 12 FRET efficiencies between Suc22^{R2} and Cdc22^{R1} in cell after heat shock at 42 degrees Celsius

The different FRET efficiencies have been calculated as described before, and compared in parallel with cells maintained at 30°C and cells in heat shocked cultures (42°C.) Samples were taken every 20 minutes and prepared for FRET. At 145 min, the heat shock cultures were shifted back to 30°C. Interestingly, there is an increase in FRET efficiencies after about 100 min, which was most apparent in S-phase cells. Furthermore, after the shift to normal temperature, the FRET efficiencies revert back to normal levels.

X. Ribonucleotide Reductase dynamics during live cell imaging

These experiments aim to visualize the dynamics of the RNR enzyme during unperturbed cell cycle but also after addition of various drugs. As there were some technical issues with the stability of the focus of the microscopy system, only movies of a couple hours were possible, thus not ideal for drug treatment yet (over 5 hours necessary).

In Figure III.13 part a., although we expected to see Suc22^{R2} release to the cytoplasm during S-phase, we instead observed the constant nuclear localization of Suc22^{R2} throughout the cell cycle.

We also observed (Figure III.13 part b.) formation of foci-like or aggregations of both Suc22^{R2} and Cdc22^{R1}. We hypothesize that these aggregations could be degradation vesicles for the RNR subunits perhaps reflecting some photo-damage induced aggregation as those foci seemed to be correlated with the laser power, strength and frequency of exposure. They are mainly nuclear and very dynamic, although they can become cytoplasmic.

Other hypotheses to explain these observed foci are for example replisome/replication factory aggregation. It could be a possibility, and there are some reports that the RNR is required near the replication sites. The same can be said for DNA repair, as RNR could be recruited to the DNA to facilitate the repair by providing dNTPs locally .

In humans, PML bodies have been described as “nuclear dots” and are thought to be a vesicle-like formation for recruitment of proteins involved in a range of roles including DNA damage response, gene regulation, apoptosis (Carracedo et al, 2011) . Although not described in yeast, maybe some similar formation could be present.

Although the foci-like formation are interesting to investigate further, we must first verify if there is a correlation between photo-damage and foci formation, as it could be a secondary effect of live cell imaging. Then, the study could lead to colocalization with the above-mentioned proteins and foci, including the DNA repair machinery and the DNA replication proteins.

a.

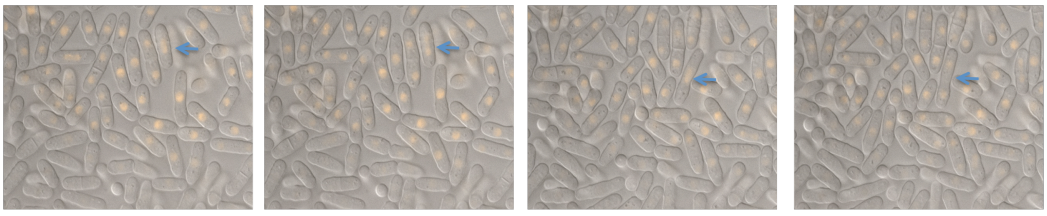

b.

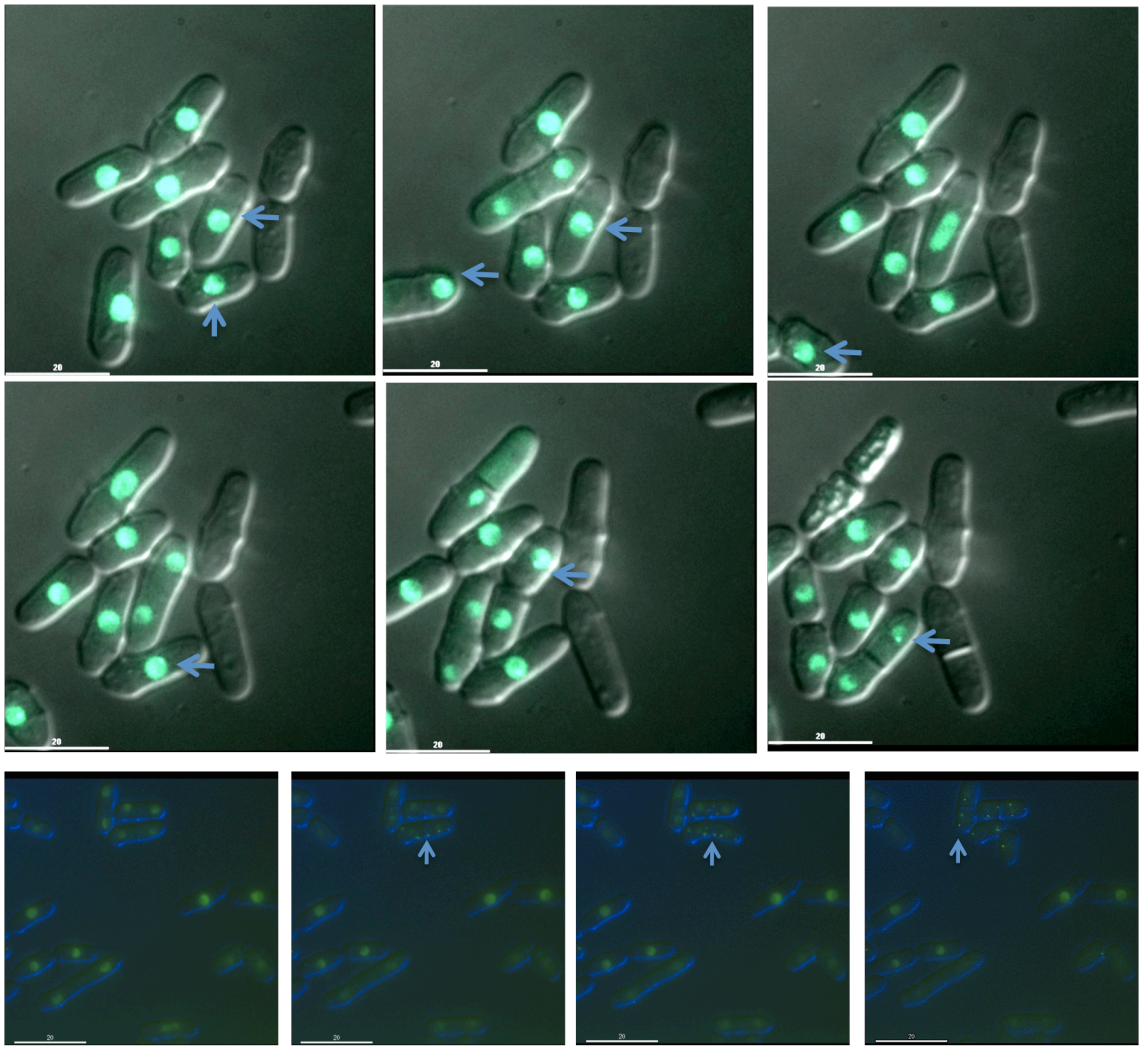

Figure III. 13 Ribonucleotide Reductase subunits dynamics using live cell imaging

Movies were acquired on the personal DeltaVision (pDV) with a 100x magnification, 1.40 oil objective. Three channels were used: DIC, CFP and YFP with the appropriate filter provided. Pictures were taken in different Z-levels and stacked afterwards as well as deconvolved. The microscope was in a climate control chamber and set to 30˚C and the cells were imaged using microfluidics chambers (CellAsic) with a continuous flow of medium, enabling the cells to be theoretically immobilized and focused for over 16 hours. The transmission and exposure times were tailored to each channel to achieve the best signal whilst minimizing the damage to the cells. Images were taken every 2-10 mins for total times of 2 – 16 hours.

Presented are snapshots of some movies. The two main observations are: Suc22^{R2} does remain nuclear, even during what approximates for S-phase (a.). Secondly, aggregates of both RNR subunits are visualized (b.) in shapes of "foci" or "spots". Those are at first nuclear and very dynamic, but at later times are spread to the rest of the cell. They could be linked to photodamage, thus being assembled in degradation vesicles.

CHAPTER IV RNR regulation by Spd1: a multiple level regulator

I. Introduction: Multiples roles of Spd1 as regulator of the RNR

Spd1 (S-Phase Delayed 1) is a small intrinsically disordered protein (IDP) with no fixed tertiary structure (Figure IV.1). Using various predications tools to assess the structure of Spd1, the results strongly suggest that Spd1 has no regular secondary structure and indeed no fixed tertiary structure. Spd1 is mainly unfolded and is an Intrinsically Disorder protein (IDP). This has been demonstrated in (Nestoras et al, 2010).

Other *in silico* tools provided some predictions about the small protein Spd1: estimation of a possible size (~5 nm on ~3 nm) and a high flexibility of the structure (Figure IV.2). IDP have been described to have a low affinity but high specificity in order to bind to enzymes in a coupled folding and binding manner. The high flexibility of IDP allows conformational changes that could be required for enzyme activities.

Spd1 is degraded during S-phase, after DNA damage and DNA replication stress by the Cop9-Pcu4-Ddb1 complex (Liu et al, 2003). The degradation occurring in S-phase is done through ubiquitylation of Spd1 in a Csn1- and Csn2-dependent manner. Whereas in G2 Phase, after DNA damage or DNA replication stress, Spd1 degradation requires both the signalosome subunits (Csn1 and Csn2), as well as the rad3- and chk1- dependent DNA damage checkpoint (Liu et al, 2003) (Liu et al, 2005).
Spd1 regulates $Suc22^{R2}$ nuclear import and also binds to $Cdc22^{R1}$ in order to inhibit it (Hankansson et al, 2006a).

a.

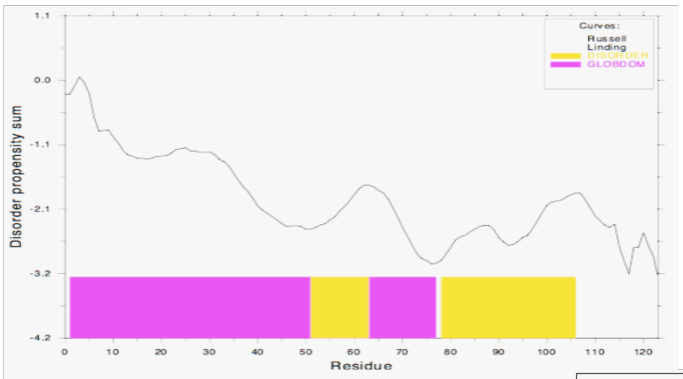

b.

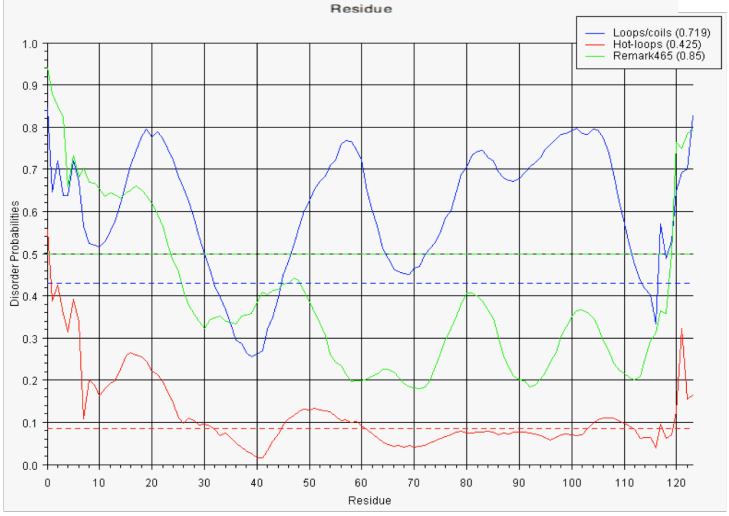

c.

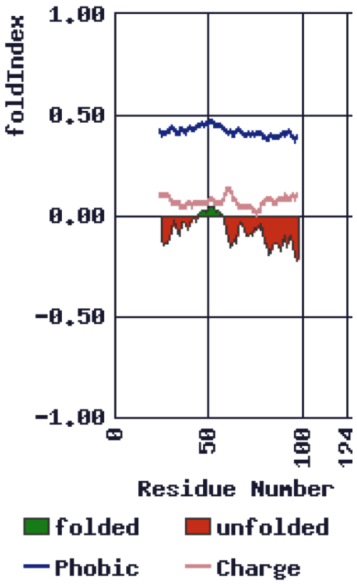

Figure IV. 1 Spd1 is an Intrinsically Disordered Protein (IDP) protein

Using some in silico softwares, Spd1 is indeed a typical IDP with 2 main globular regions linked by disorder regions (a), has many regions without fixed secondary structure (b) and is mainly unfolded (c).

a. GlobPlot: exploring protein sequences for globularity and disorder. Regions with high propensity for globularity on the Russell/Linding scale

b. DisEMBL: LOOPS (regions devoid of regular secondary structure); HOT LOOPS (highly mobile loops); REMARK465 (regions lacking electron density in crystal structure)

c. Foldindex: Regions that have a low hydrophobicity and high charge (either loops or unstructured regions) based on Charge/hydropath analyse

a.

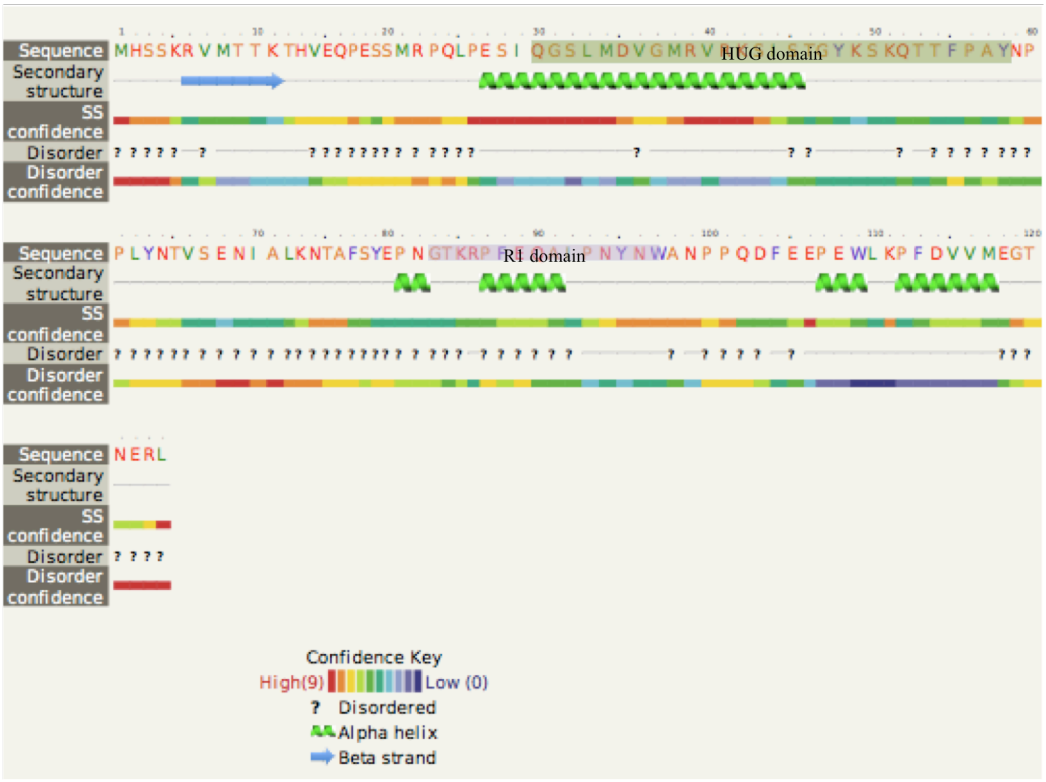

b.

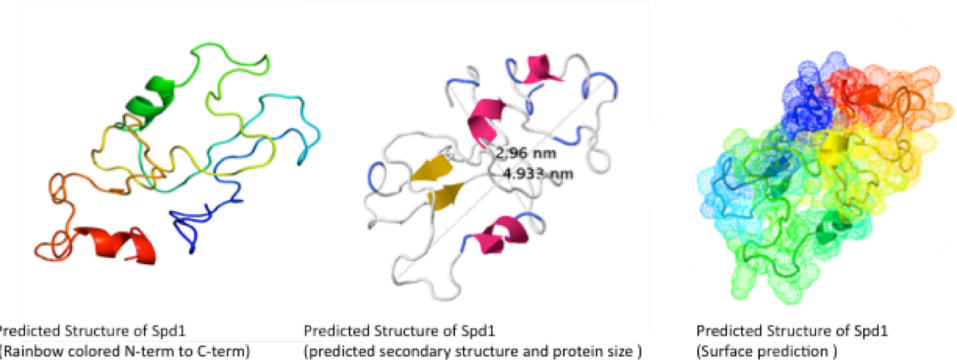

c.

Figure IV. 2 Predicted structure of Spd1

Using Phyre2 software, as well as I-TASSER, this figure shows a predicted structure of Spd1. Due to its highly disorder nature, the structure cannot be meaningful predicted, but it is however interesting to compare the predicted secondary structure with the Spd1 domains.

In a. the secondary structure is indicated on the amino acid sequence of Spd1, as well as the disordered structure. Using this predicted structure, it was possible to visualize Spd1, estimate its size and surface. Finally, the known domains of Spd1 are reminded in c.

spd1 was deleted using an *ura4+* marker, and a few characteristics were observable: complete loss of $Suc22^{R2}$ nuclear localization as well as a normal cell cycle, although slightly faster (Figure IV.3).

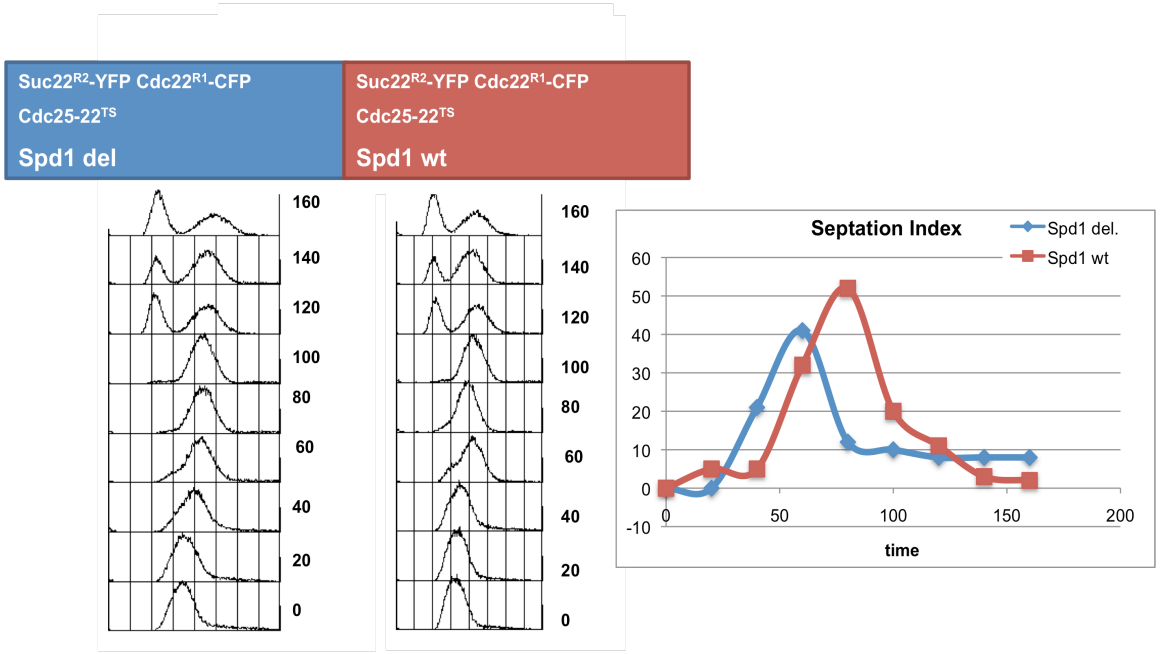

Figure IV. 3 spd1 deleted strain simple characterization

Spd1 was deleted with an ura4+ gene marker (Nestoras et al. 2010), and was characterized by 2 features mainly: slightly faster growth, as seen on the FACS profile and septation index. $Suc22^{-R2}$ is not localized in the nucleus anymore but spread throughout the cell (fig. IV.4). spd1 Δ was crossed with the both FRET strains: CFP-$Suc22^{R2}$ Cdc22-YFP^{R1} and YFP-$Suc22^{R2}$ Cdc22-CFP^{R1}, as explained in material and methods.

II. Spd1 is required for FRET of the RNR subunits

When Spd1 is absent, the small RNR subunit Suc22^{R2} localization is pan-cellular due to the loss of nuclear import activity of Spd1 (Figure IV.4). The FRET experiment was conducted with the expectation to observe an increase of interaction between Suc22^{R2} and Cdc22^{R1}, as the "inhibitor" Spd1 is deleted. Although no FRET was observed this cannot mean that there is no interaction *per se* between the different subunits, as the cells would not survive. Instead it can be interpreted as a large distance between the acceptor/donor fluorophore pair, or not the right dipole alignment resulting most probably from a conformational change or modification in the stoichiometry ratio.

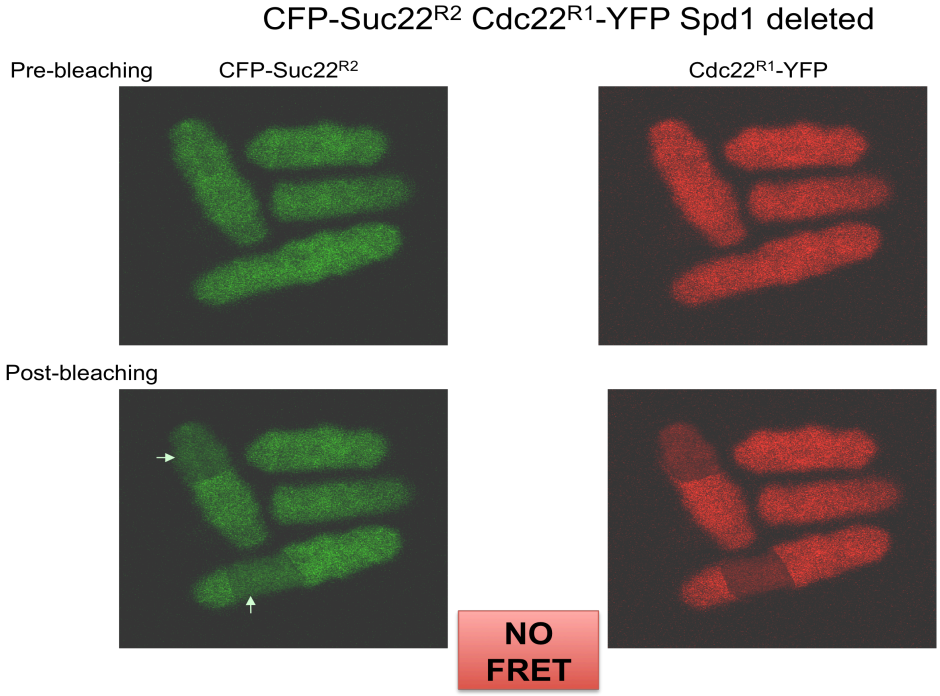

Figure IV. 4 Images the FRET experiment in the CFP-Suc22^{R2} Cdc22-YFP^{R1} Spd1 deleted strain

In the spd1 deleted strain, Suc22^{R2} is now throughout the whole cell as is Cdc22^{R1}.

The decrease of fluorescence in the CFP channel is very clear, as shown by arrows, and verified by the photobleached zones in the YFP channel. The bleach in the CFP channel is due to the overlap in spectrums of the fluorophores, therefore the FRET efficiency will be negative.

III. RNR FRET experiments in Spd1 Δ after HU and 4NQO treatment

The negative FRET is quantifiable although its "FRET efficiency" is not interpretable. In Figure IV.5, the deletion of Spd1 (Spd1 Δ strain) abolishes the FRET signal observed in presence of Spd1. Furthermore; none of the treatments with the drugs used previously (HU and 4NQO) change this negative FRET result. Clearly, Spd1 is required for some specific architecture of the RNR complex allowing it to perform FRET between the fluorophores pairs.

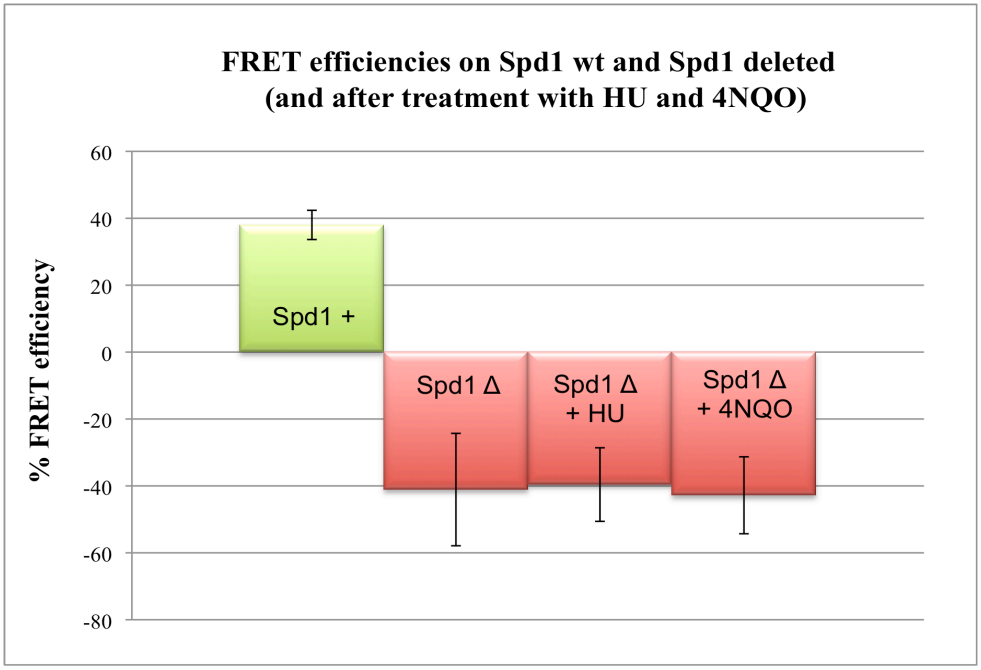

Figure IV. 5 FRET efficiencies between CFP-Suc22^{R2} and Cdc22^{R1}-YFP in spd1+ wildtype (wt) versus spd1 deleted (Spd1 Δ) strains, and after treatment with HU (RNR inhibitor) and 4NQO (UV mimetic)

The FRET efficiencies have been calculated as described before, the FRET efficiency is positive only in the spd1+ wt strain. In the spd1 deleted strain the FRET signal is lost, and even negative due to the overlap of spectrums. But we know that Suc22^{R2} and Cdc22^{R1} do bind and form complexes, if not the cells would not survive. Thus, the loss of FRET can be explained in a few ways: the fluorophores are further apart than 10 nm and/or they are not in the right dipole conformation. After addition of the drugs: HU (a radical scavenger) for 4 hours at 20 mM and 4NQO (a UV mimetic inducing DNA lesions) for 4 hours at 5 μM, the FRET signal is still negative. These results have been confirmed with swapped fluorophores tagged on the RNR proteins: YFP-Suc22^{R2} and Cdc22^{R1}-CFP.

IV. RNR subunits homo-dimers and homo-complexes after *spd1* deletion

In the *spd1* Δ background, diploids strains were made using *ade6* intragenic complementation in order to observe the formation of the homo-complexes CFP-Suc22^{R2} YFP-Suc22^{R2}, and Cdc22^{R1}-CFP Cdc22^{R1}-YFP.

Previously, in the presence of Spd1, the small subunit Suc22^{R2} probably was in a homo-dimer conformation (as observable by the positive FRET signal), whereas after deletion of *spd1*, there has been some alteration, as the FRET is no longer positive. Most probably a change in conformation or maybe change in stoichiometry ratio modified the fluorophores inter-distance. Considering the intrinsically disordered protein Spd1 could act in some ways as a scaffold for the RNR complex, the loss of Spd1 could modify the complex of the homo-dimers of Suc22^{R2} subunits.

While with the Cdc22^{R1} homo-dimer FRET experiments, the result was negative FRET in presence of Spd1, it is the same result without Spd1. Not much conclusion can be drawn from that observation, apart from the fact that the FRET pair is not in a correct condition to perform FRET.

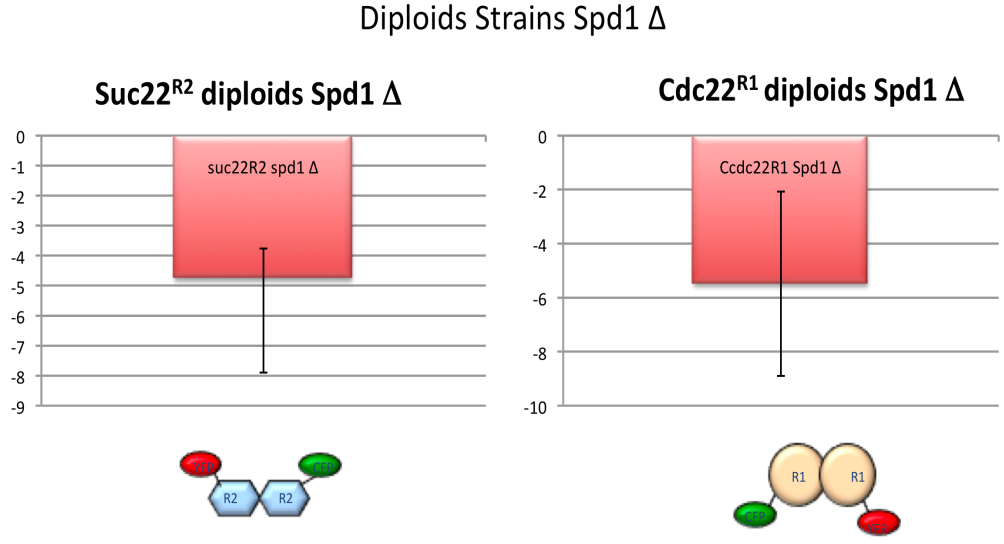

Figure IV. 6 FRET measurements in Suc22^{R2} Spd1 deleted diploid and in Cdc22^{R1} spd1 deleted diploids

Diploids strains have been made in order to have CFP-Suc22^{R2} YFP-Suc22^{R2} and Cdc22^{R1}-YFP Cdc22^{R1}-CFP in addition of Spd1 deletion. This enables us to observe the FRET between the subunits in the formation of homo-complexes after deletion of Spd1.

In the case of Cdc22^{R1}, there is still no FRET after deletion of Spd1 whereas Suc22^{R2} subunits, which had the capacity to FRET in presence of Spd1, have lost that capacity after deletion of Spd1.

V. Spd1 mutants

Using alanine scanning mutagenesis, 41 mutant were made scanning the entire *spd1* gene . The mutations were made in a group of 3 amino acids (see Figure IV.7). The aim was to distinguish domains and functions already described, by using those set of mutants in different assays. The inhibition capacity of RNR has been measured in the 41 Spd1 mutants, as well as the nuclear import function of Suc22^{R2}. In addition the stability of the Spd1 mutants were monitored. Later, I will go through those findings and compare them with my FRET data.

I used these mutants and crossed them in an *spd1* Δ background with both RNR subunits tagged for the FRET assay as described in Chapter II Material and Methods. After final verification of the strain, the 41 mutants were sequenced to ensure the correct assignments of the mutants.

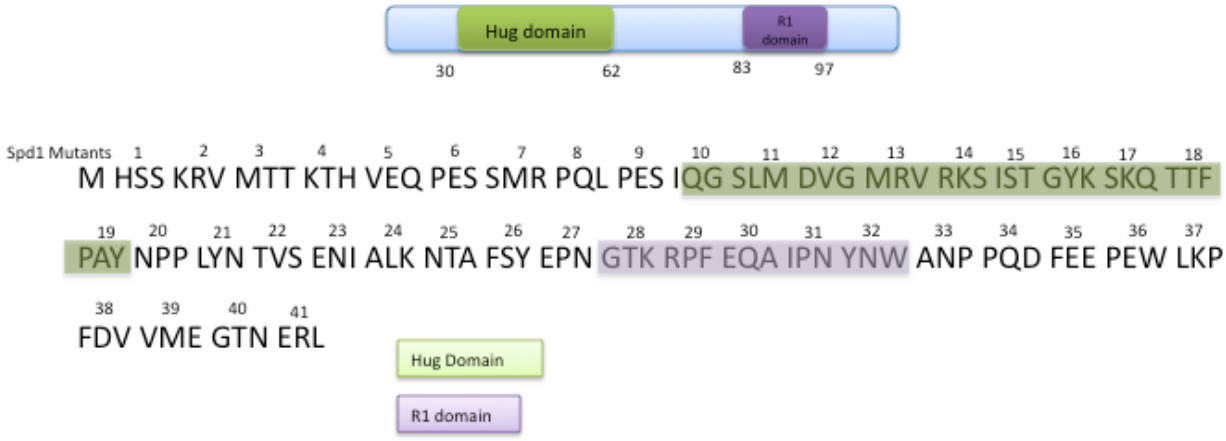

Figure IV. 7 spd1 mutants 1-41 made by alanine scanning mutagenesis per group of 3 amino acids

This diagram illustrates the 41 spd1 mutants made previously in the laboratory. The 2 identified domains (by sequence homology with orthologues) are colored: the HUG domain (green) and the R1 domain (purple). These 41 strains have then been crossed with the CFP-Suc22^{R2} Cdc22-YFP^{R1} spd1 Δ as well as the swapped fluorophores FRET strain YFP-Suc22^{R2} Cdc22-

CFP^{R1} Spd1 Δ. These strains have then all been verified and the Spd1 mutants have been sequenced.

The FRET experiments have been quantified and are shown in Figure IV.8. Of a total of 41 spd1 mutants, 12 did have a positive FRET between Suc22^{R2} and Cdc22^{R1}, whereas the others did not. The positive FRET efficiencies of the spd1 mutants are comparable with the spd1 wt strain, although Spd1 mutant 8 and mutant 36 have a notably lower FRET efficiency. Even though this FRET method is semi-quantitative, this information can still be taken into account allowing us to speculate that there might be less complexes where FRET occurs or different complexes conformations.

The spd1 mutants with a positive FRET result are dispersedly covering the gene, except maybe for two groups of mutants that are clustered (mutants 2-4 and mutants 33-36). The other FRET positive strains are the *spd1* mutants 8, 12, 23, 25 and 41.

It is important to remember that even though two mutants can have the same FRET result, they might not have the same conformation or architecture to achieve this positive FRET read-out. Thus the FRET does not distinguish between different FRET positive conformations.

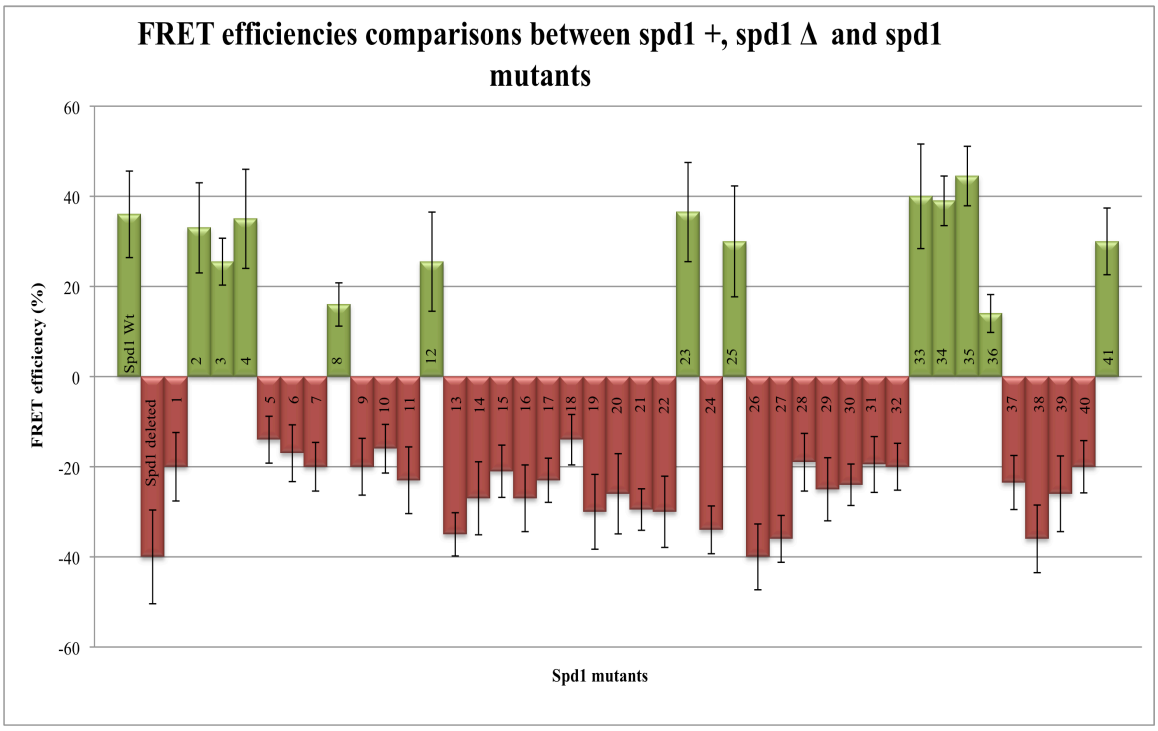

Figure IV. 8 FRET efficiencies between CFP-Suc22^{R2} and Cdc22^{R1}-YFP in spd1 mutant strains

The different FRET efficiencies have been calculated as described before; the FRET signal is positive in 12 mutants: mutant 2,3,4,8,12,23,25,33,34,35,36 and 41. All of these have FRET efficiencies above 25% apart from mutant 8 and 36 who seem to have consistently lower FRET efficiencies.

The other mutants have a negative FRET, meaning that the fluorophores are too far apart or in a different conformation, therefore not allowing energy transfer. Most of them were confirmed with swapped tags YFP-Suc22^{R2} and Cdc22^{R1}-CFP (see Figure *IV.14)*

Most of the spd1 mutants have been crossed in both RNR double-tagged strains (CFP-Suc22^{R2} Cdc22^{R1}-YFP and YFP-Suc22^{R2} Cdc22^{R1}-CFP) allowing us to control our results in a different strain, which were all consistent.

The images below (Figure IV.9) are examples of some of the *spd1* mutants: *spd1* mutant 2 has no Suc22^{R2} localization but a clear FRET signal. Mutants 12 and 25 also have a FRET positive signal observed by CFP fluorescence increase in the ROI after photobleaching, whilst the mutant 31 has no FRET.

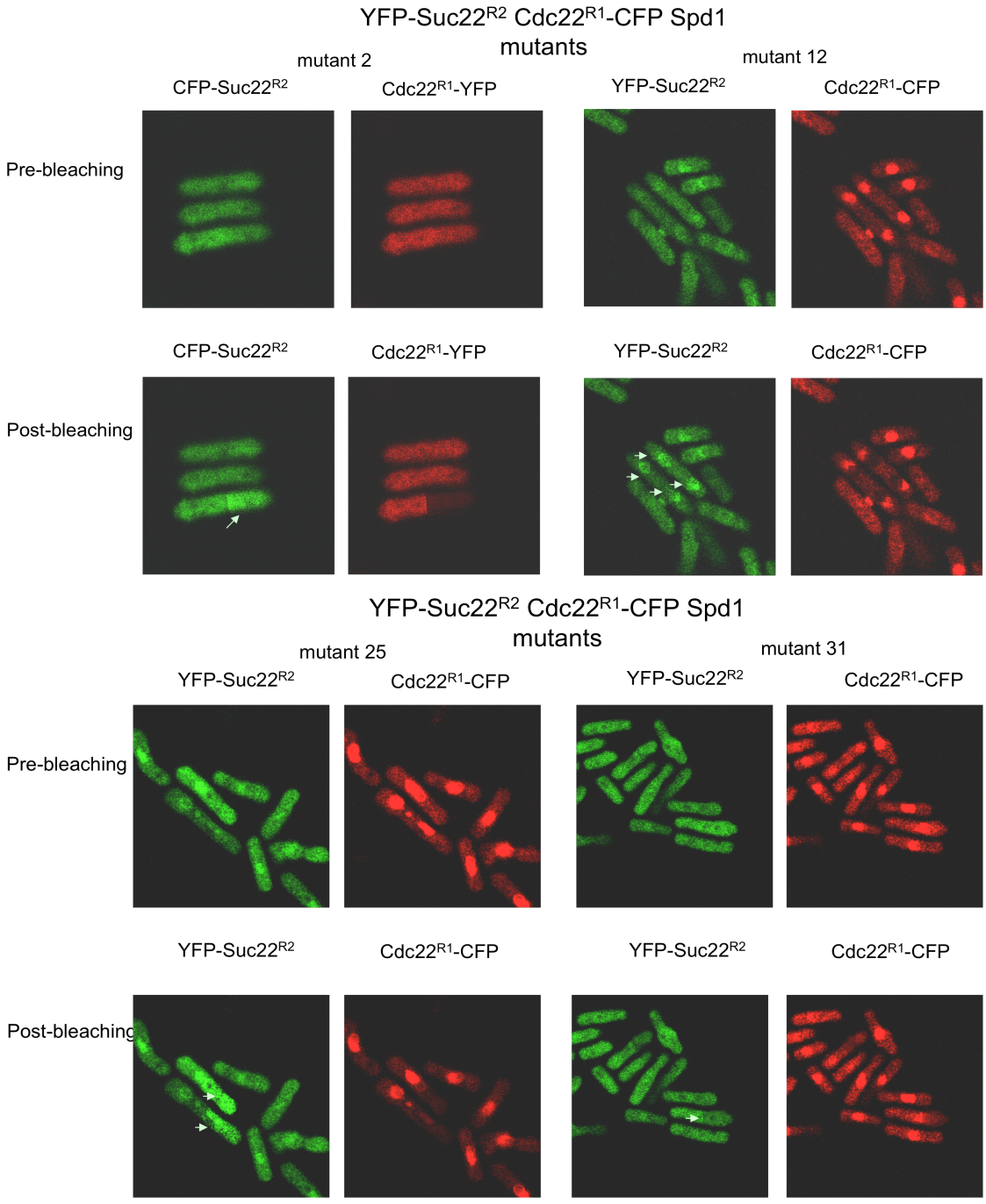

Figure IV. 9 Example of the FRET experiment in some spd1 mutant strains

Images were taken on a confocal microscope (LSM500, Zeiss) as described before, and the FRET experiment also as described previously. Here is an example of 4 mutants: spd1 mutant 2, 12 and 25 that all have positive FRET. spd1 mutant 31 does not have FRET occurring between CFP and YFP.

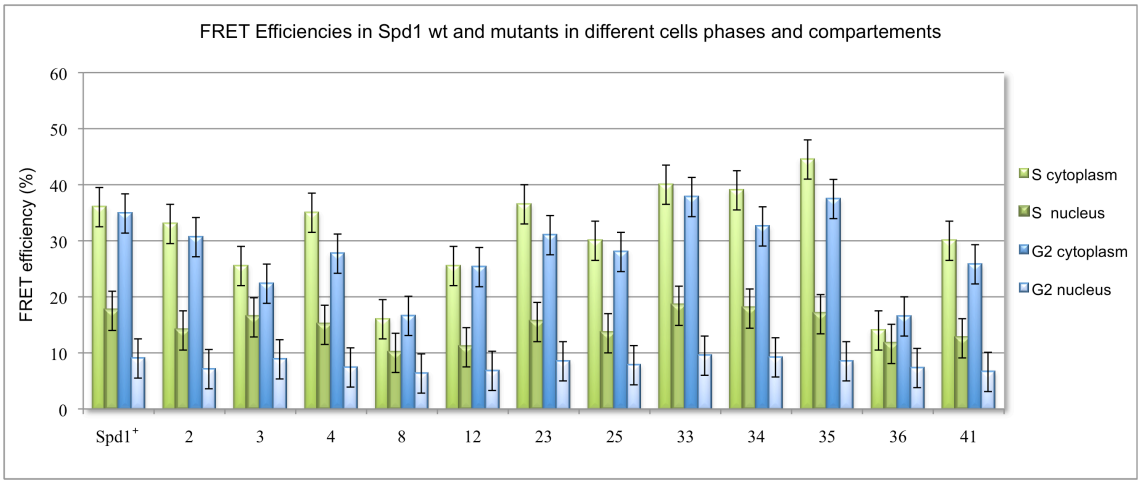

Figure IV. 10 FRET efficiencies comparison in both cellular compartments during the cell cycle in spd1 mutant strains

The different FRET efficiencies have been calculated as described before, discriminating the nucleus from the cytoplasm and the approximate cell cycle phase. The FRET efficiency of the 12 FRET positive mutants has been measured (Spd1 mutants 2,3,4,8,12,23,25,33,34,35,36 and 41). The different FRET efficiencies are similar, as are the ratios S-phase Nucleus/ S-phase Cytoplasm and G2-phase Nucleus/ G2-phase Cytoplasm. Again, there are noticeable differences for the Spd1 mutants 8 and 36 as reported earlier, as their FRET efficiencies are quite low in each category.

In the same manner than *spd1+* wt, the FRET positive *spd1* mutants exhibit a FRET occurring during all phases in both compartments of the cell. As described earlier, it most probably reflects that there are already RNR complexes formed and present. The RNR is tightly regulated, but there might be some basal activity or some immature complexes present to allow a quick response and supply of dNTPs.

Also, the FRET efficiencies measured of the *spd1* mutants are comparable to the *spd1+* wt.

VI. *spd1* mutants after treatments

The same drugs used previously on the *spd1* wt strain and *spd1* deleted strains, were also used on the 41 *spd1* mutants in order to investigate the effect of each *spd1* mutant and RNR regulation after the addition of the drugs. HU

(RNR inhibitor) and 4NQO (UV mimetic) were used as described before, followed by FRET assay and quantification.

After addition of HU, none of the *spd1* mutants has FRET occurring between the RNR subunits (Figure IV.11). Even the 12 *spd1* mutants that did undergo FRET before treatment lost their ability to transfer the energy between the FRET pair (CFP/YFP).

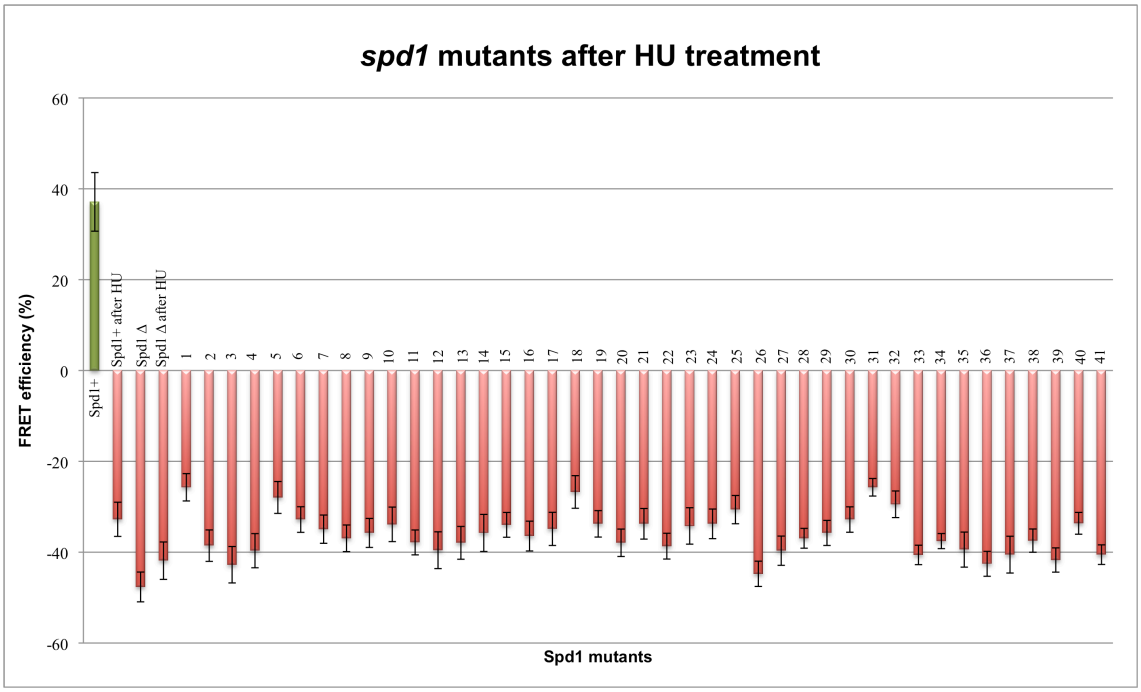

Figure IV. 11 FRET signal negative of all spd1 mutants after treatment with HU

After addition of HU to the spd1 mutant strains, the FRET signal is negative for all of them. This is the same result as the spd1 wt strain and the spd1 deleted strain. Knowing that HU is a radical scavenger and inhibits the RNR activity, it might affect the structure or the stoichiometry of the RNR.

In Figure IV.12 the FRET efficiencies after treatment with 4NQO are shown. These have been calculated in S-phase and G2-phase cells, comparing the FRET values in the nucleus and the cytoplasm. Also, the positive controls of the spd1 wt strain and the negative control of the spd1 Δ strain were used in parallel during the FRET experiment as well as for the calculations.

When DNA damage is induced after 4NQO treatment, all *spd1* mutants strains do FRET, even the *spd1* mutants strains that without any treatment were FRET negative. Those have now the ability to perform FRET between the

fluorophores. The FRET efficiencies are variable but following the general trend of the *spd1+* wt FRET efficiencies i.e. higher FRET efficiencies in the cytoplasm compared to the nucleus.

This result could be explained by the fact that after DNA damage the RNR complex is more active as the dNTPs levels are increased (Chabes & Stillman, 2007). Therefore the RNR complex could be modified into a mature/active complex in which the conformation allows FRET between the fluorophores.

Also observable are the different levels of FRET efficiency, some *spd1* mutants (11, 14, 16, 26 especially) have very low FRET efficiency, which could reflect a low population of FRET positive RNR complexes.

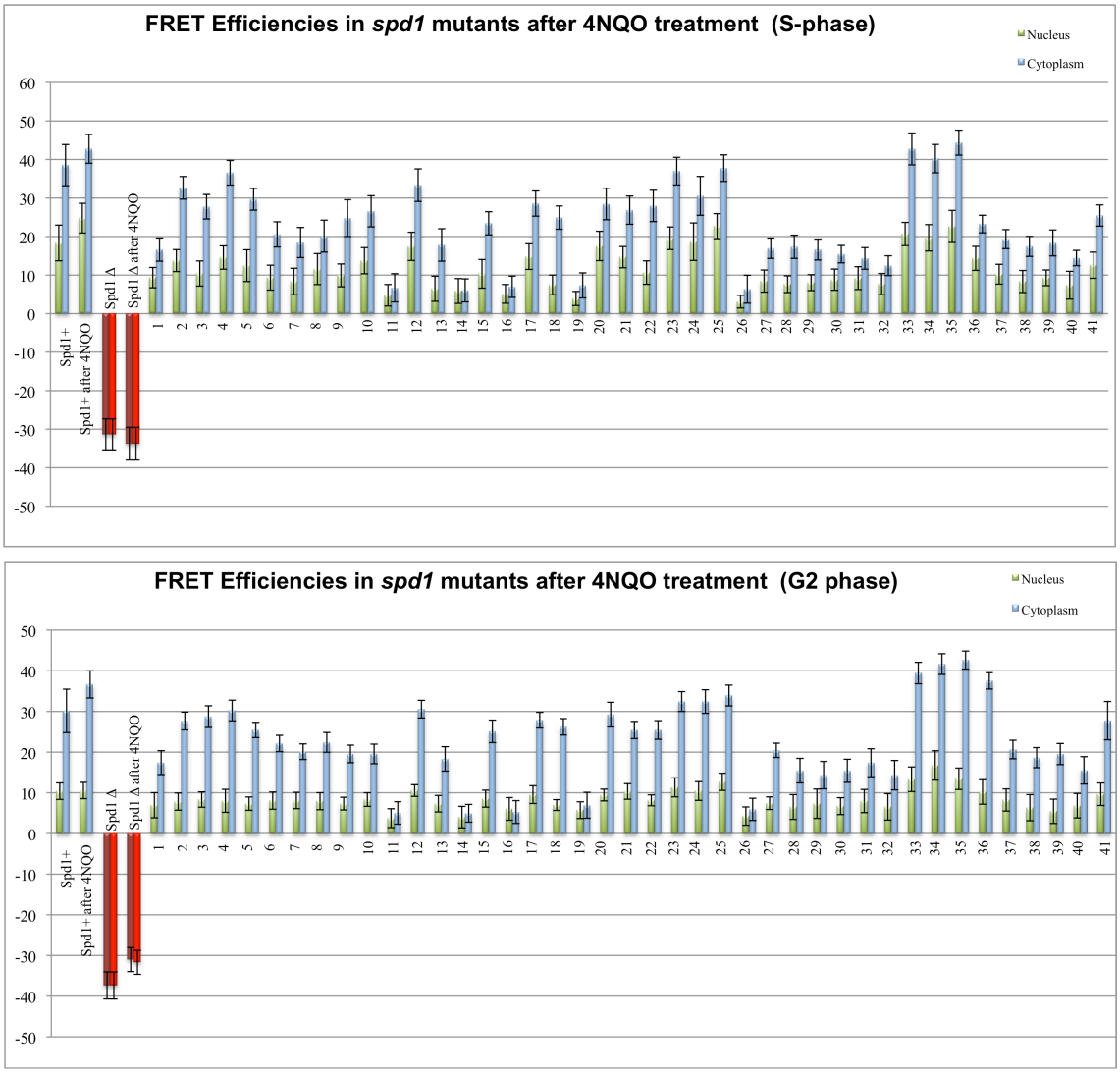

Figure IV. 12 FRET signal positive for all spd1 mutants after treatment with 4NQO

All the 41 spd1 mutants were treated with a UV mimetic (4NQO) for 4 hours at 5 μM in order to induce DNA damage. There is a positive FRET signal in all the spd1 mutant strains; even the ones that did not have FRET occurring between the RNR subunits without any treatment.

The FRET efficiencies were measured and compared in S-phase cell and G2 phase cells, in both cellular compartments as described before. In general, the FRET efficiencies of the spd1 mutants are at similar levels as the spd1+ wt apart from mutants 11, 14, 16, 19, and 26 that are very low. Noticeably, the FRET is always more efficient in the cytoplasm.

VII. Suc22^{R2} nuclear localization in the *spd1* mutants

In order to investigate the correlation between RNR regulation, represented in part by the Suc22^{R2} nuclear delocalization, with the FRET results, all the *spd1* mutants strains were scored for the small RNR subunit Suc22^{R2} nuclear localization in non-treated and drug treated conditions.

The same drugs were used i.e. HU (RNR inhibitor) and 4NQO (UV mimetic) and 100 cells were scored for clear nuclear accumulation of Suc22^{R2}. In an *spd1* wt strain Suc22^{R2} is mainly nuclear (~90%) but after HU treatment for 4 hours, this localization is lost and most cells have Suc22^{R2} localized throughout the cell. After HU treatment, Spd1 is degraded leading to Suc22^{R2} being relocalized from the nucleus to the cytoplasm. Interestingly, after 4NQO treatment, Suc22^{R2} is nuclear, with similar nuclear localization levels as without treatment.

In the *spd1* deleted strain, Suc22^{R2} is never localized in the nucleus, which has been described before (Liu et al, 2003) and is due to the nuclear import function of Spd1. None of the treatments modify these observations.

Finally, the *spd1* mutants strains have a vast array of different phenotypes: most *spd1* mutants behave like the *spd1* wt, except mutants 2, 14 and 26 which have no nuclear localization of Suc22^{R2}. Other mutants for example *spd1* mutants 10, 11 and 12 have lower Suc22^{R2} nuclear localization, which is quickly lost upon HU treatment. On the contrary, some *spd1* mutants, for example *spd1* mutants 21, 31, 38 – 41 have a stronger Suc22^{R2} nuclear localization after HU treatment than the *spd1* wt.

With the 4NQO treatment, the small subunit Suc22^{R2} localization is similar to the cell without treatment. If Suc22^{R2} is ~80% nuclear in an *spd1* mutant strain, it will be the same level after treatment with 4NQO.

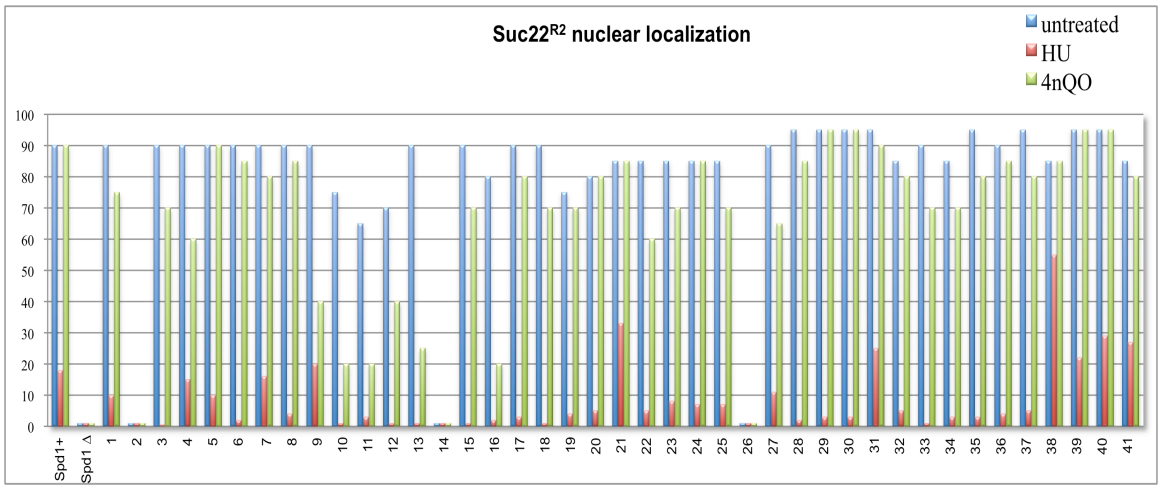

Figure IV. 13 Suc22^{R2} nuclear localization in the spd1 mutant strains after drug treatment

Around 100 cells were scored for Suc22^{R2} nuclear localization in the spd1+ wt strain, spd1 deleted and all the 41 mutants. spd1+ wt strain retains Suc22^{R2} nuclear localization in most cells (up to 90%) but is mostly lost after addition of HU (around 18%) but still nuclear localized after addition of 4NQO. In the spd1 deleted strain, the localization of the small RNR subunit in the nucleus is completely abolished. Neither drug treatments change anything to this phenotype.

The 41 spd1 mutants have a different display of Suc22^{R2} nuclear localization. Some mutants, for example mutant 2, 14, 26 have the same phenotype as the spd1 deleted strain. But on the opposite, some mutants, i.e. spd1 mutant 38 has a strong Suc22^{R2} nuclear localization even after HU treatment. Also spd1+ wt and most mutants have a clear Suc22^{R2} nuclear localization after 4NQO treatment.

VIII. Discussion of the role of Spd1 in the RNR architectural regulation

This is an intermediate discussion about the results from this chapter, in order to understand the role of Spd1 in the regulation of RNR through conformational modification.

Figure IV.14 is a summary of the FRET results of this chapter. What is striking is that Spd1 is necessary for FRET to occur, as the *spd1* deleted strain never has a FRET positive result. The deletion of *spd1* even abolishes the positive FRET between the $Suc22^{R2}$ dimers. The regions of the Spd1 protein necessary for FRET are diverse: mutant 1, mutants 5-32 (apart from mutant 8, 12, 23 and 25) as well as mutants 37-40. The other *spd1* mutants do not affect the positive FRET signal. Interestingly, after treatment with HU the FRET signal is lost for all the strains (*spd1* wt and 41 mutants) as well as for the homo-dimer $Suc22^{R2}$ strain.

The complete opposite 4NQO results are interesting giving us insight into the *in vivo* RNR complex upon DNA damage. We can even assume that the structure of the RNR complex after 4NQO is an active one as dNTPs are necessary for the DNA repair machinery. In this case, all the *spd1* mutants exhibit a positive FRET signal, even the ones that did not have the capacity to provide FRET in non-treated conditions.

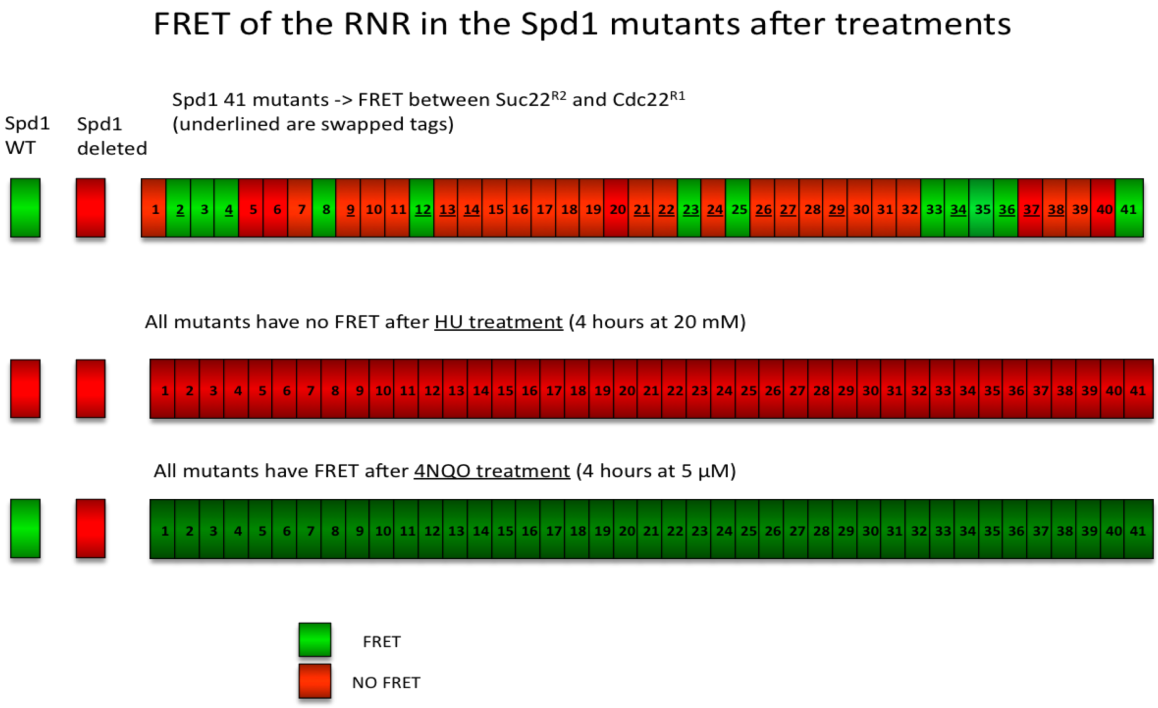

Figure IV. 14 Summary of FRET with the spd1 wt, spd1 deleted and spd1 mutants strains
The Figure *is a simplified summary of the FRET experiments on the spd1+ wt, spd1 deleted and spd1 mutant strains, in normal conditions or after addition of drugs: HU and 4NQO.*

Subsequently, comparing the results with Spd1's structure and domains is done in figure IV.15. It seems like the few structured domains are necessary for FRET occurrence: *spd1* mutants 8-11 are probably part of an α-helix, and they are needed for positive FRET. The same applies to the *spd1* mutants 13-14 and 38-40 which are probably β-strands and do not FRET when mutated. On the contrary, there does not seem to be any correlation with solvent accessibility (Figure IV.15 part a.).

Other *in silico* data provides the predicted protein binding sites of Spd1 (Figure IV.15 part b.), while no DNA binding sites were predicted, 33 amino acids were assigned as possible binding sites with proteins. Unfortunately, this does not seem to correlate with the FRET results. Regions of no FRET (i.e. mutants 5-7) can be regions of predicted protein binding but as are regions that do FRET (i.e. mutants 33-36).

The assigned domain regions of Spd1 (by homology to other RNR regulators) are annotated as well: the HUG region (*spd1* mutants ~10-19) and the R1 region (*spd1* mutants ~28-31). Although with one exception (mutant 12)

when those two regions are affected, Spd1 looses the ability to provide FRET between the RNR subunits.

Different assays have been done in parallel with the *spd1* mutants to assess the degradation of Spd1 and other roles. The nuclear importer role as well as the inhibition of RNR was studied. I will incorporate those results in the final discussion.

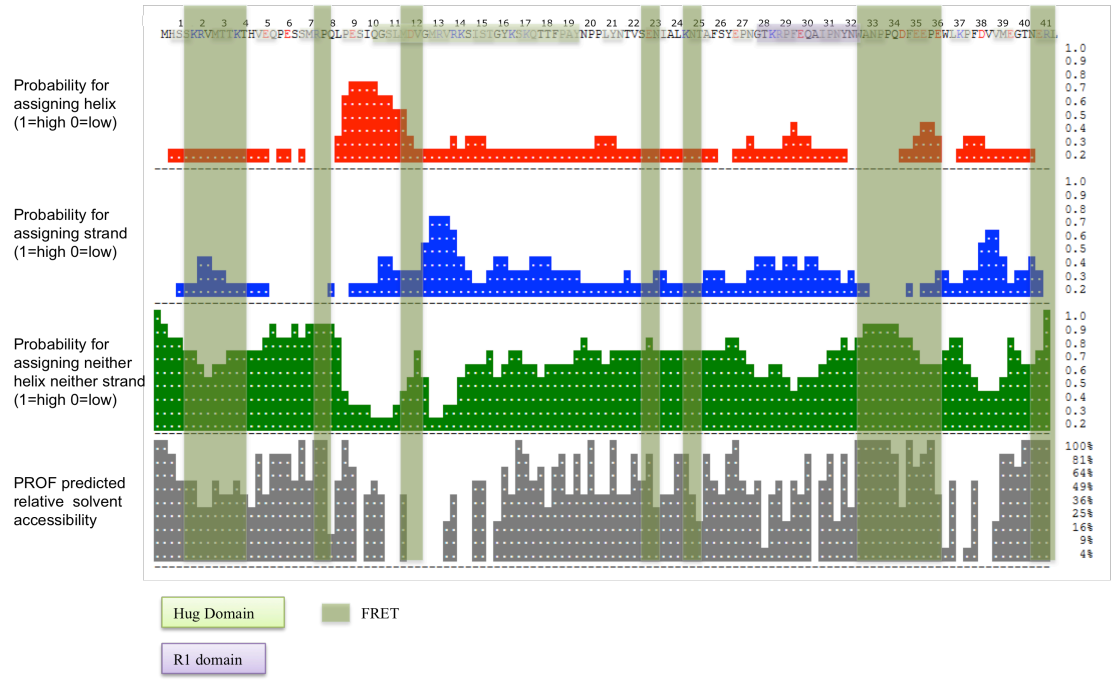

a.

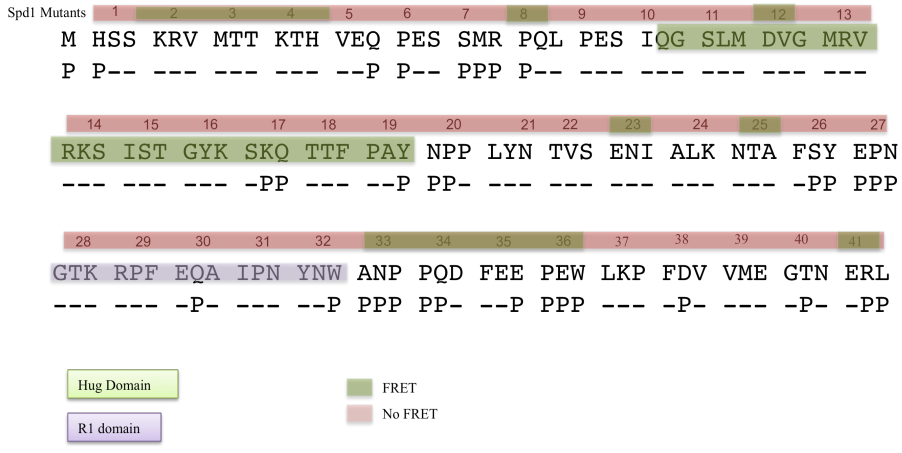

b.

Figure IV. 15 Comparison of the FRET experiments with in silico data

In silico research on Spd1 has been done to have more precise information of the secondary structure as well as predicted protein interaction domains. The images shown here are from the online software "PredictProtein" which uses a suite of structure prediction programs in order to give an output file of compiled data with detailed predictions. In picture a. the PROF prediction is given with the relevant information (pH_sec: probability for assigning an α-helix; pE_sec: probability for assigning a strand, pL-sec: probability for assigning neither an α-helix nor a strand, PROF_acc: predicted solvent accessibility). And the data in part b. is provided also by the "ProteinPredict" software, through the PROFisis program to predict protein-protein binding. These data are then compared with the predicted domains HUG and R1, as well as with the FRET results.

CHAPTER V Ribonucleotide Reductase regulation by Spd2, a novel RNR regulator

I. Spd2 description

Spd1 was first thought to be the sole *S. pombe* ortholog to *S. cerevisae*'s Dif1, Sml1, and Hug1. During this project, a new gene has been found by sequence alignment with Spd1, and named Spd2 for its very high sequence identity with Spd1.

Spd2 is a small protein of 11.8 kDa, and some early investigation demonstrates it is very similar to Spd1. Spd2 is also an Intrinsically Disordered Protein (IDP) and has a role in RNR inhibition. One of the main differences is that Spd2 is not involved in $Suc22^{R2}$ nuclear localization. In the *spd2* deleted strain, $Suc22^{R2}$ is nuclear.

While collaborators are further characterizing the Spd2 role in RNR inhibition and the Spd2 protein cycle and degradation (data not published), I investigated whether Spd2 has also a role in the RNR complex architecture.

spd2+ has a high similarity DNA sequence to *spd1+* (Figure V.1 part a.), with mainly the ~20 first bases missing, as well as the ~10 last ones. Thus Spd2 is shorter resulting in an even smaller protein than Spd1. In Figure V.1 part b., the amino acid alignment of Spd1 and Spd2 enables to compare the conservation of the domains. Notably, the HUG and R1 domains are highly conserved between the two proteins. In addition, the *spd1* mutants are noted allowing comparison of the conserved amino acids between Spd1 and Spd2.

```
Spd1            ATGCACAGCAGCAAGCGAGTTATGACCACAAAGACTCATGTTGAGCAGCCTGAGTCTTCA 60
Spd2            --------------------ATGTCTGAAACG-TTCAAG-----CTTCCCGA----TCA 29
                                     ***:* ..**.*  ***:*     *: ** **    ***

Spd1            ATGCGTCCTCAGCTTCCCGAAAGCATTCAAGGCTCCTTAATGGACGTGGGAATGCGGGTT 120
Spd2            TGACG-----AACTTCCCCAGCTAGTTCAAACTACTCTTTTTGATGTTGGAGCCAGAGTT 84
                : .**     *.****** *.. ..*****.  :*  *::* ** ** ***.  .*.***

Spd1            CGTAAATCAATTTCCACCGGATACAAGTCGAAACAAACCACGTTTCCTGCCTATAACCCA 180
Spd2            CGCAAAGCTGTTCAAACTGGTTACAAATT-TGACCAACAACTTTTCC--CTTCTTACCAC 141
                ** *** *:.** ..** **:*****.*  :.**.***.** *****  * *.*:***..

Spd1            CCGCTTTACAACACTGTTTCTGAAAACATTGCTTTAAAAAATACCGCATTTTCTTATGAG 240
Spd2            AAGG---ATCAAACTGATAGAAATGAGCTTCCTCAGCAAAAACATG---ATCCTAATCTT 195
                ..*    * .*.****:*: :.*:.* .** ** :..****:.. *   :* **:** :

Spd1            CCTAACGGTACTAAGCGTCCATTCGAGCAAGCAATTCCTAATTATAACTGGGCCAATCCT 300
Spd2            CGTCTCGATGATTTGAAGCAAGAATTGGCTGCTGATTCTATTTT---CTGGG--ATACCG 250
                * *.:**.*..*::*.. *.* :. :* .:**:.:* ***:**:   *****  *::**

Spd1            CCTCAAGACTTTGAAGAACCGGAATGGTTG--AAGCCGTTTGACGTTGTCATGGAGGGTA 358
Spd2            CCTCCACTCAAGAAATCGCCGATTCTTTTGCCAAGCC---TGATTTTCTCAAG-----TC 302
                ****.* :*:: .** ..***.::   ***  *****   ***  ** ***:*     *.

Spd1            CCAATGAGAGATTATAA 375
Spd2            TCATTAA---------- 309
                 **:*.*
```

a.

b.

Figure V. 1 Spd1 and Spd2 sequence alignment

Spd1 and Spd2 DNA sequences have been aligned using the EBI tool ClustalW2, and show a high sequence identity (a. alignment using coding DNA sequences). Comparison of the amino acid sequence of Spd1 and Spd2 (b.) also reveals high domain similarity and conservation (Hug domain in green and R1 domain in purple). The spd1 mutants have also been annotated above the sequences for comparison.

Using a prediction tool to assess the secondary structure of Spd1 and Spd2, it seems that Spd2 is also an IDP with very little structure and most probably no fixed tertiary structure. Even if Spd2 seems to have slightly more α-helices predicted when compared to Spd1.

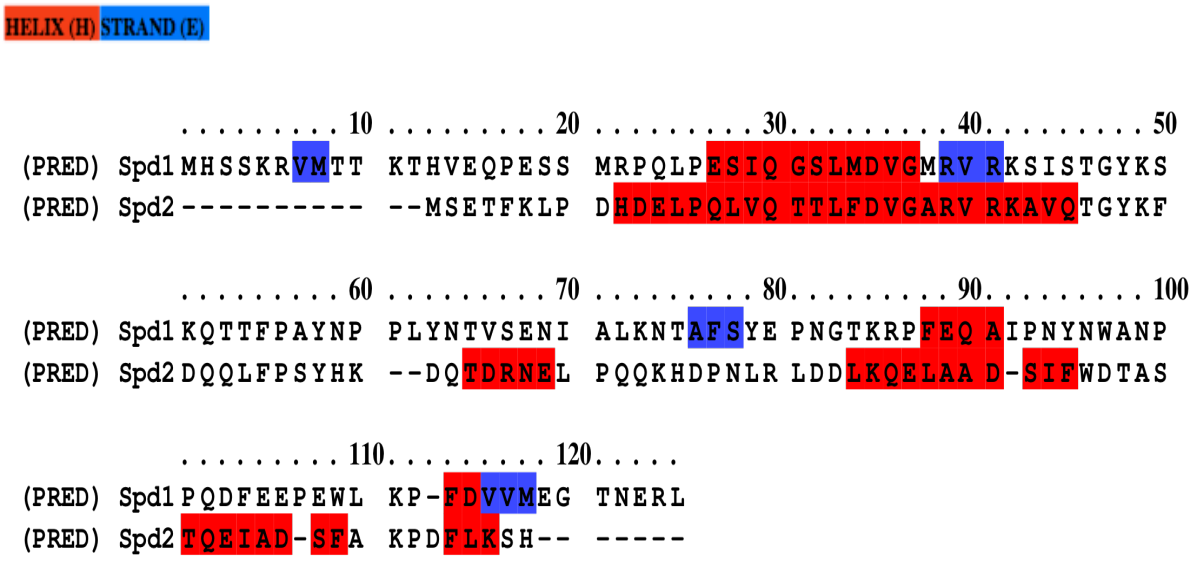

Figure V. 2 Comparison between Spd1 and Spd2 secondary structure predictions

This structure prediction is the alignment for secondary structure type. The 3-state (H: Helix, E: Strand, C: Coil) secondary structure for each sequence is represented by a color: red for α-helix and blue for β-strand. It is clear that Spd2 has similar predicted structure to Spd1, mostly being unstructured with some possible α-helices. Therefore it is probable that Spd2 is also an IDP (Intrinsically Disordered Protein). This secondary structure prediction was done using PSIPRED (Jones, 1999).

II. Spd2 has also a role in RNR architecture

spd2+ was deleted with *ura4*+ and kanamycin cassettes (by Dr K. Netsoras and Dr R. Vesjstrup). This allowed me to cross them in the FRET strains CFP-Suc22^{R2} Cdc22 ^{R1}-YFP and YFP-Suc22^{R2} Cdc22 ^{R1}-CFP. The first observation was the nuclear localization of Suc22^{R2} in the *spd2* deleted strain (Figure V.3). Spd2 is not necessary for the nuclear localization of the small RNR subunit. Next, FRET experiments were done as described before and the images are shown in Figure V.3. There is a decrease in both the donor and the acceptor

channels, thus no energy transfer has occurred. Therefore, the RNR subunits $Cdc22^{R1}$ and $Suc22^{R2}$ are too far apart or not in the right conformation for FRET.

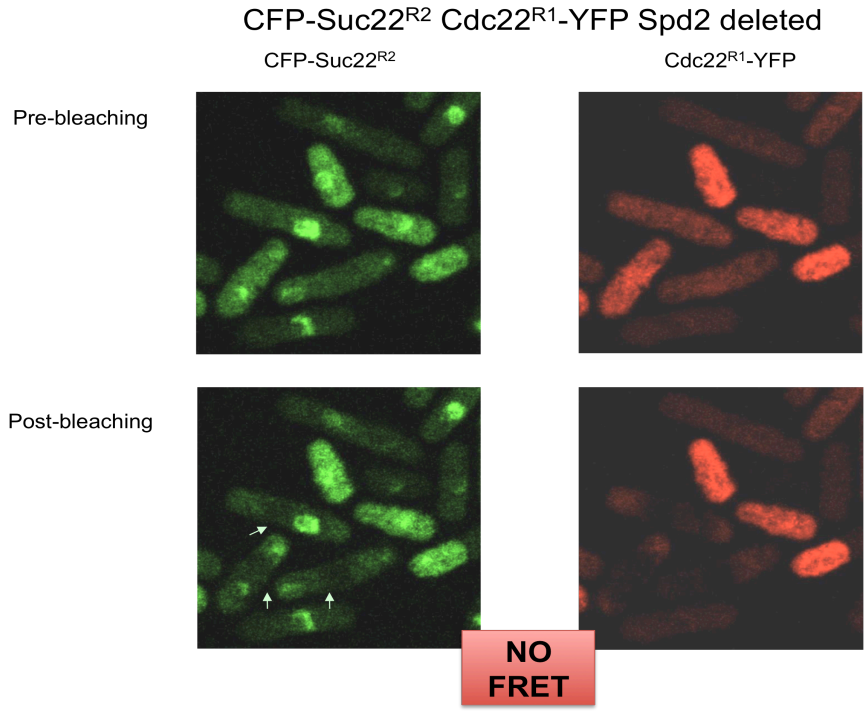

Figure V. 3 FRET experiment images in the CFP-$Suc22^{R2}$ $Cdc22^{R1}$-YFP spd2 deleted strain
Images taken as described earlier. The decrease of fluorescence in the CFP channel is very clear, as shown by arrows, and verified as well as by the photobleached regions in the YFP channel. Measurements of the CFP fluorescence in pre- and post- bleach ROI (Region Of Interest) will then be used to calculate the FRET efficiency.

The negative FRET efficiency is shown in figure V.4, and compared with the *spd1*+ wt and the *spd1* deleted strain. In addition, the FRET signal is negative in both cellular compartments. (Figure V.4 b.)

a. b.

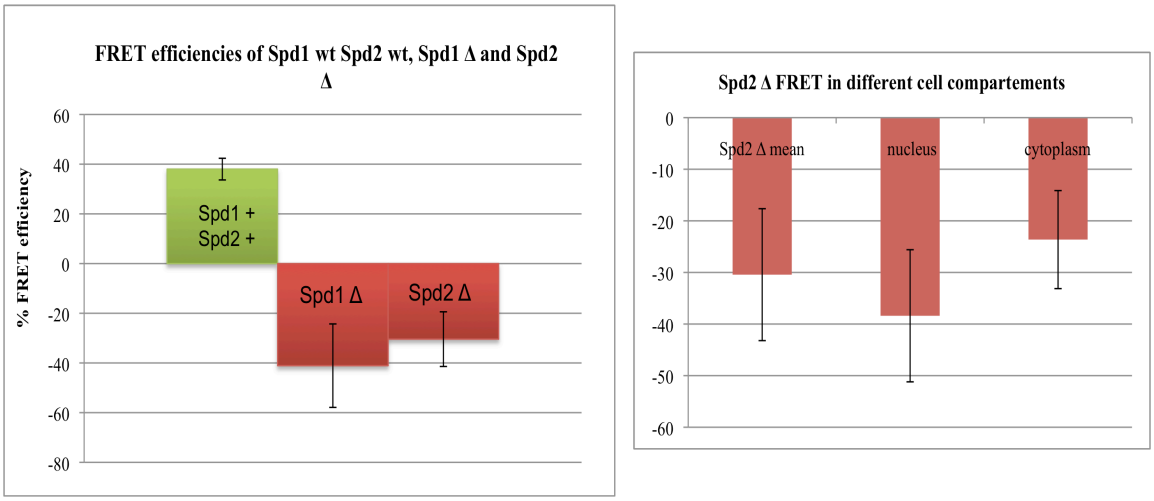

Figure V. 4 FRET efficiencies between CFP-Suc22^{R2} and Cdc22^{R1}-YFP in Spd2 deleted strain
Spd2 may have a role in regulating the RNR structure (a.). Using the RNR FRET strain (CFP-Suc22^{R2} Cdc22^{R1}-YFP) in addition of the deletion of Spd2, it was clear that no FRET occurs between Cdc22^{R1} and Suc22^{R2}, both in the nucleus and in the cytoplasm (b.).

Therefore, we can speculate that Spd2 is also needed for an optimal RNR structure, allowing FRET between the two subunits.

III. FRET in the *spd2* deletion strain after drug treatment

To assess further the role of Spd2 in the structure-related RNR regulation, the drugs HU and 4NQO were used. This allowed us to compare the drug effects on the FRET results of the *spd1* deletion and *spd1* mutants. None of the drug treatments changed the previously shown negative FRET in *spd2* deleted strains, as under no circumstances is the FRET signal positive. It concurs with the *spd1* deletion strain, and we can consider that Spd2 is necessary for a correct RNR conformation, enabling FRET to occur.

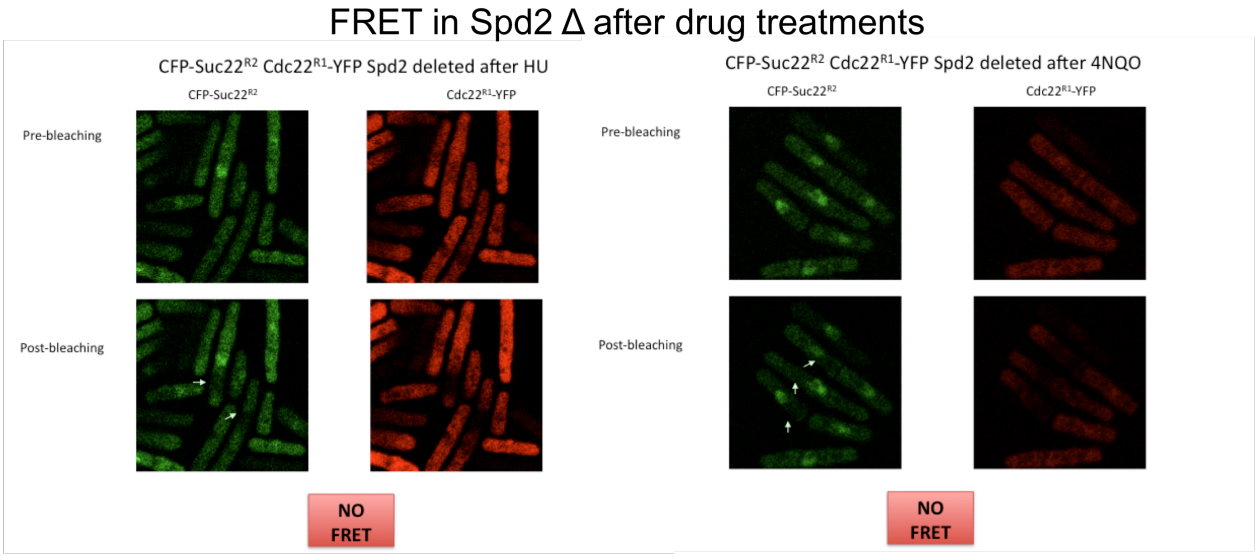

Figure V. 5 Images of the FRET experiment in Spd2 deleted strain after drug treatment
The decrease of fluorescence in the CFP channel is clear. Spd2 deletion abolishes FRET between the RNR subunits, and neither HU nor 4NQO modify this FRET result.

The FRET results have been measured, and are negative (Figure V.6).

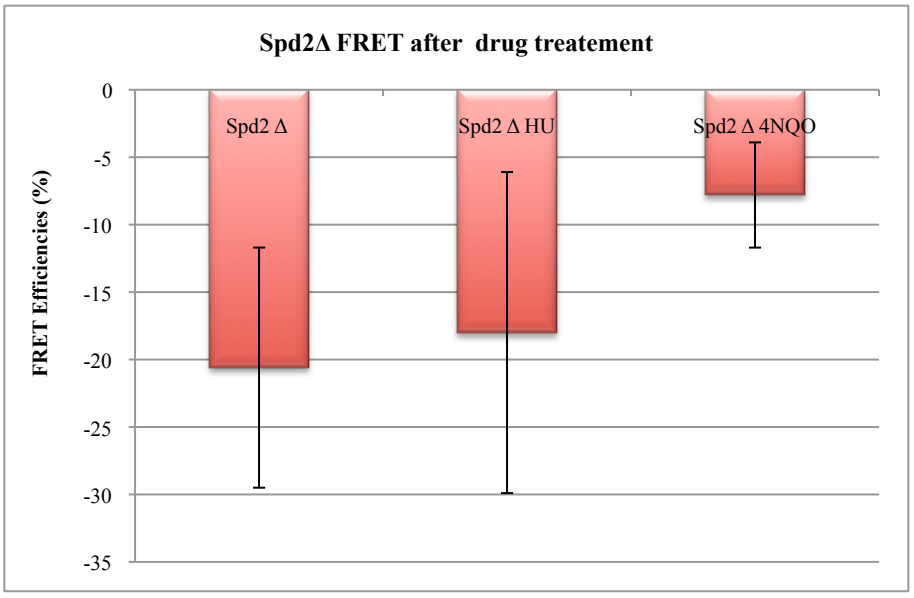

Figure V. 6 RNR FRET efficiencies in spd2 deleted strain after drug treatment
spd2 deletion leads to loss of the FRET signal between CFP-Suc22^{R2} and Cdc22^{R1}-YFP. Treatment with HU or 4NQO does not modify the FRET result, as the FRET remains negative.

IV. FRET experiments on *spd1 spd2* double delete strain

The next step was to have both RNR regulators deleted and observe the FRET results. One of the first observations in the CFP-Suc22^{R2} and Cdc22^{R1}-YFP *spd1* Δ *spd2* Δ strain is the clear loss of Suc22^{R2} nuclear localization. Thus the Spd1 nuclear importer role is abolished and gives the dominant phenotype of pan-cellular Suc22^{R2} (Figure V.7).

FRET experiments resulted in no energy transfer between CFP-Suc22^{R2} and Cdc22^{R1}-YFP, without treatment or with HU treatment (Figure V.8).

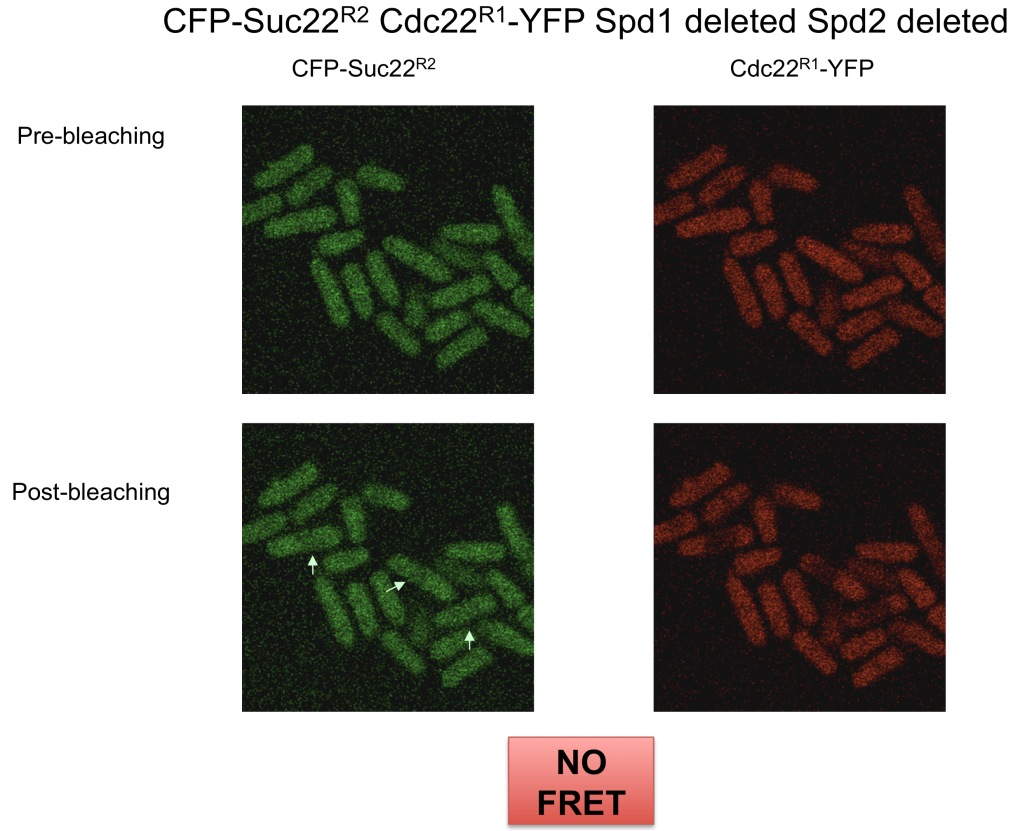

Figure V. 7 Images of the FRET experiment in spd1 Δ spd2 Δ strain

The double deleted strain shows a clear spd1Δ phenotype (loss of Suc22^{R2} nuclear localization). Additionally, the FRET signal is negative, visualized by the decrease in both the donor and acceptor's channels. Deletion of both RNR regulators therefore results in no FRET between CFP-Suc22^{R2} and Cdc22^{R1}-YFP.

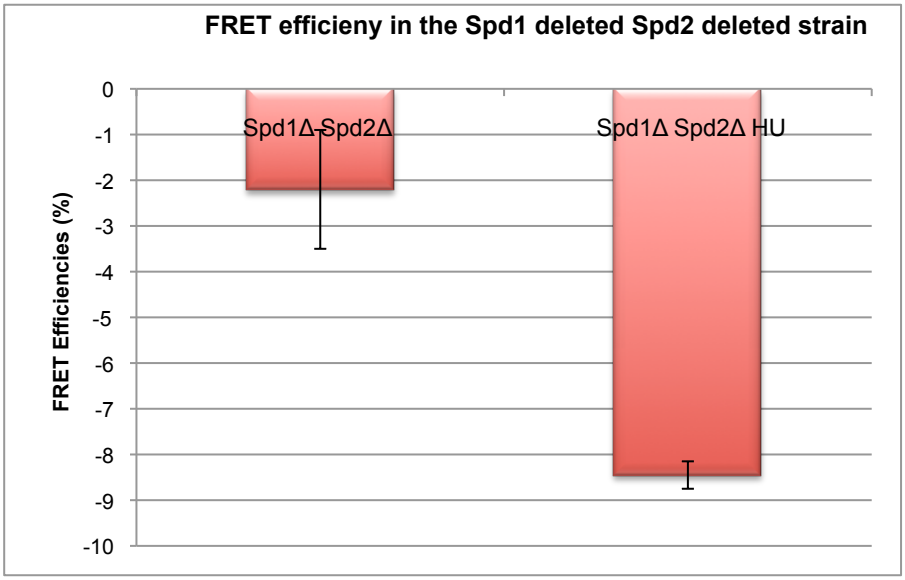

Figure V. 8 CFP-Suc22^{R2} and Cdc22^{R1}-YFP FRET efficiencies in spd1 Δ spd2 Δ strain

Deletion of both RNR regulators Spd1 and Spd2 results in loss of the FRET signal between CFP-Suc22^{R2} and Cdc22^{R1}-YFP. Treatment with HU does not modify the FRET result, as the FRET remains negative.

V. Conservation of the RNR regulators

The recent discovery of Spd2 shows that not all RNR regulators have been described yet, and that there might be more partner proteins involved in efficient RNR regulation than previously thought. Although Spd2 is not yet fully characterized, some early data shows that Spd2 is also involved in the inhibitory function of RNR, and that Spd2 is degraded after HU treatment in a Ddb1-dependent manner.

Despite the high similarity in sequence between Spd1 and Spd2, the two proteins seem to have different functions in the cell. It is therefore of interest to compare the proteins sequences for conservation as well as differences. In addition, the alignment with the *S. cerevisae* RNR regulators (Sml1, Dif1, Hug1) might give some further indications about the domains and their functions.

The HUG domain is conserved, and is between amino acid 32 to 62 according to the prediction. The second domain described and considered conserved is the R1 domain (a.a 91 to a.a 104). The HUG domain is considered as the R2 binding domain, while the R1 domain has been described as the domain for interaction with the large RNR subunit R1.

It is striking how some parts of the protein sequences are conserved, not only the HUG domain and the R1 domain, but also the domain 15-18 seems moderately conserved.

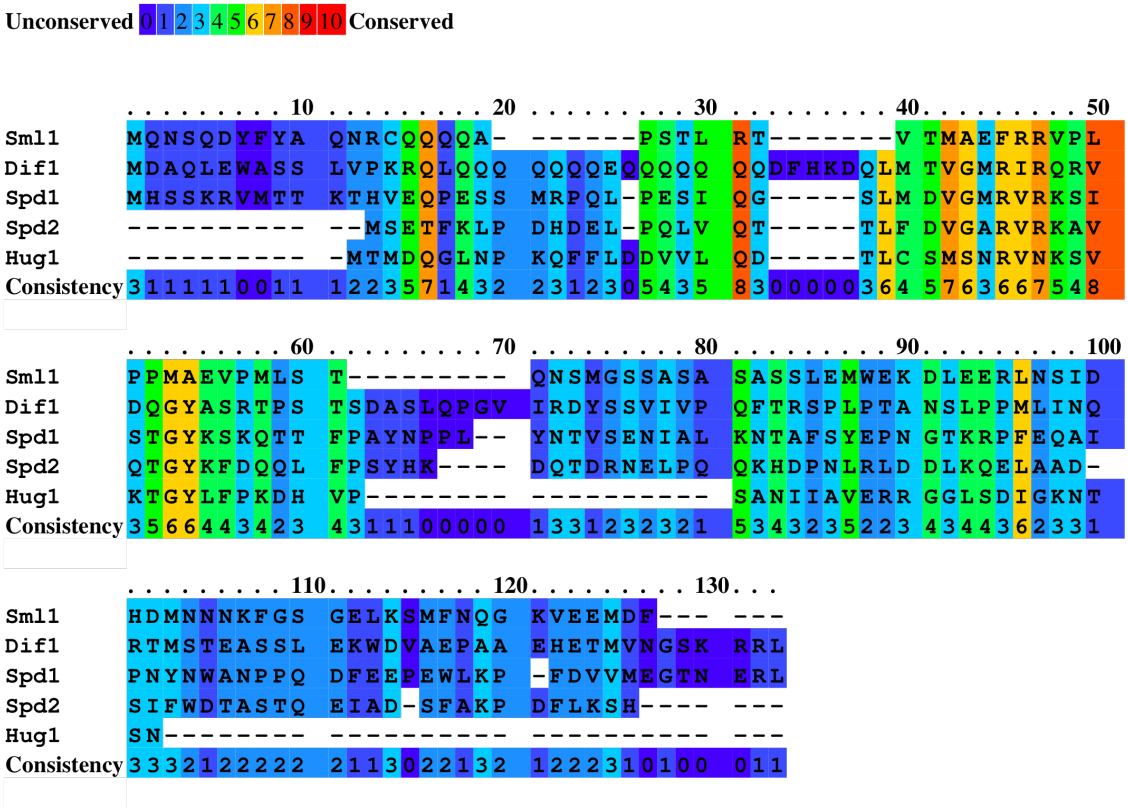

Figure V. 9 Amino acid alignment of RNR regulators from S. pombe and S. cerevisae

Comparison between the amino acid sequence alignment of the RNR regulators, in S. pombe and S. cerevisae. There is a strong conservation at the amino acid level, especially in the previously described conserved domains HUG and R1.

The conservation scoring is performed by PRALINE. The color assignments are in a color scheme indicating the amino acid conservation level, in addition the conservation consistency is annotated.

Comparing the structure between the RNR regulators was also done. Secondary structures of Sml1 and Dif1 shows more α-helices in the N-terminus, and are in general more structured proteins. A common feature for all the RNR regulators is the α-helix corresponding to the start of the HUG domain (~a.a 30 to 50). Also conserved between Sml1, Spd1 and Spd2 is a small α-helix prediction at the site of the R1 domain.

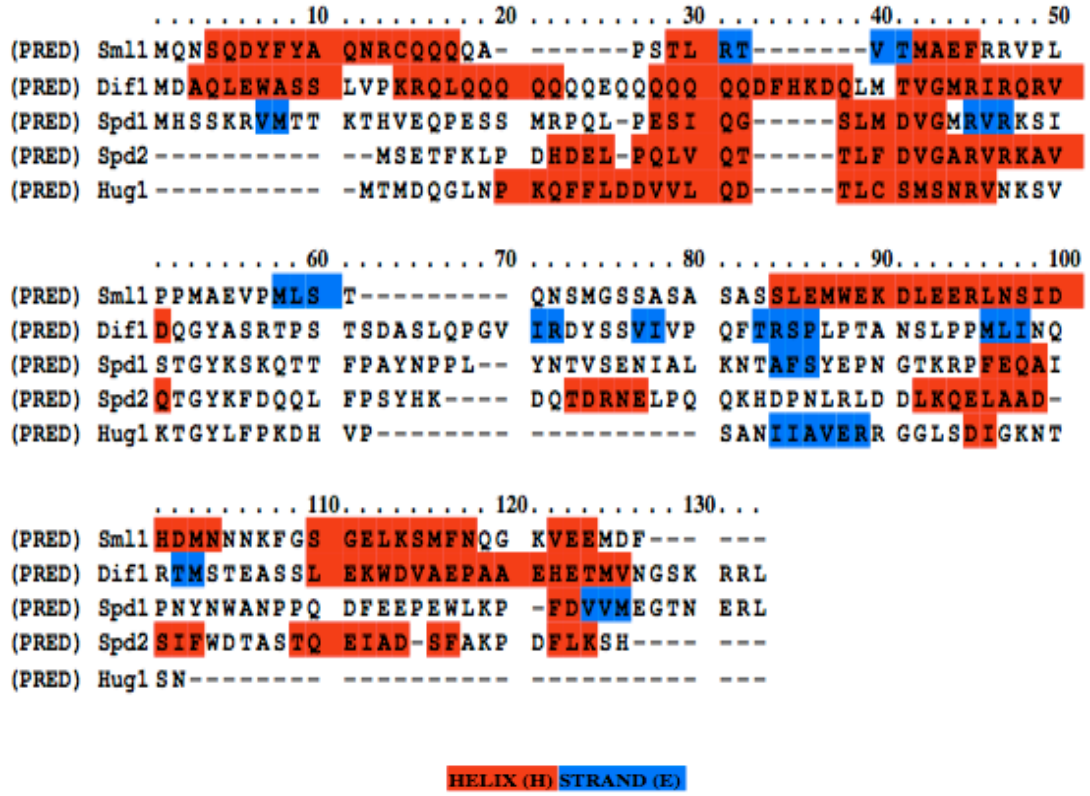

Figure V. 10 Prediction structures of RNR regulators from S. pombe and S. cerevisae
Comparison of predicted secondary structures of the RNR regulators in S. pombe and S. cerevisae. Most appear to have low amounts of predicted secondary structure. Some α-helices domains seem to be conserved between the five RNR regulators. (Done in PSIPRED)

Although Spd2 has not been extensively described yet, it has a role in RNR regulation, by affecting the structure and/or conformation of the RNR complex. How exactly Spd2 regulates RNR is not entirely clear at this time.

The conservation of some domains and structures in the RNR regulators through the species can allow us to compare the functions of these RNR regulators and understand how the RNR complex is regulated by a variety of small proteins.

CHAPTER VI Studying the RNR at the single molecule level

I. RNR structurally-induced regulation

To further investigate the Ribonucleotide Reductase complex, especially at the level of the stoichiometry and structural conformation, single molecules experiments were done.

Through the data collected in the previous three chapters, we can assume that there is indeed structural-dependent regulation of the RNR through Spd1 and Spd2, but also other effectors. We know that Spd1 and Spd2 are necessary for FRET to occur between the donor and the acceptor, because upon deletion of *spd1* and *spd2* no FRET is observed. During the two previous chapters of this thesis, we observed how the regulators influence the oligomerization or modify the conformation of the RNR complexes, allowing the tagged RNR to have a positive FRET signal or not. In addition, HU abolished the FRET, while 4NQO maintains the positive FRET signal (Fig. VI.1).

All these conditions can be repeated *in vitro*, keeping the components to a bare minimum and investigating the RNR regulation models *in vitro*. The aim is to be able to evaluate the number of each subunit, as well as observing conformational changes. Finally, repeating the FRET *in vitro* will allow us to understand our *in vivo* results, and push the interpretation further.

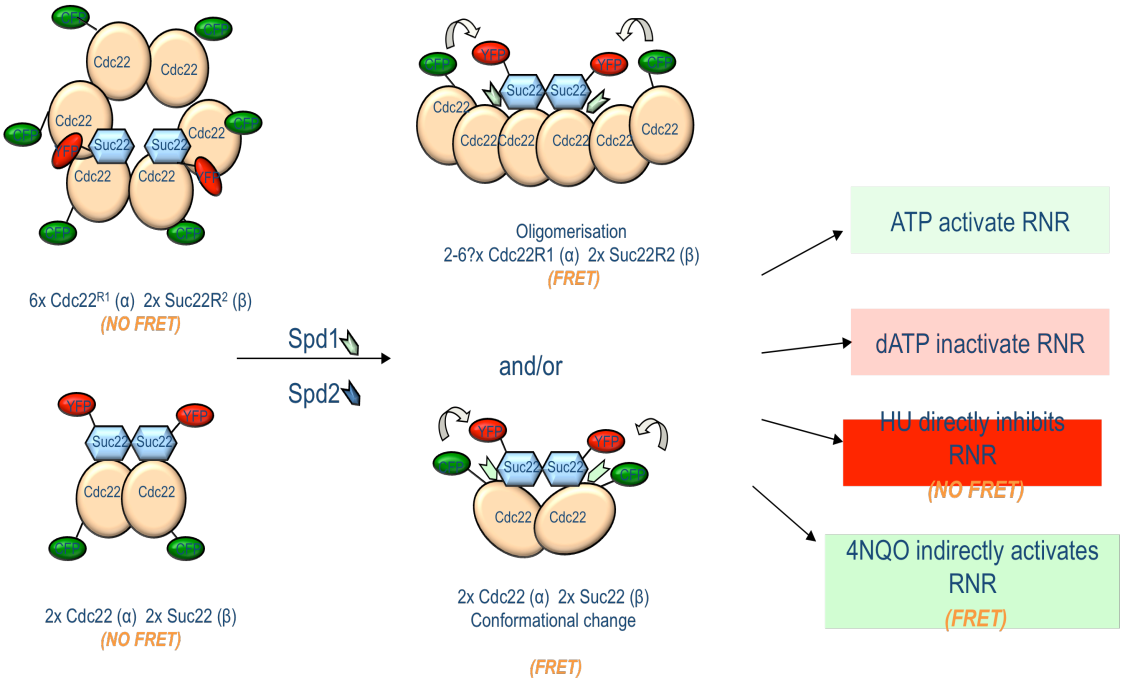

Figure VI. 1 Simplified model of the working model for structure-dependent RNR regulation

Schematic of the current model and possibilities for interpreting the FRET data in vivo. Spd1 and Spd2 are necessary for positive FRET to occur. The RNR complex could be in a $\alpha_2\beta_2$ or $\alpha_6\beta_2$ conformation, and the regulators Spd1 and Spd2 could modify the quaternary structure by oligomerization or conformational change. Also, ATP and dATP could have opposite effects. HU abolishes completely the FRET signal while 4NQO does maintain it and even recovers the FRET signal in Spd1 mutants.

II. Prediction structure of the small RNR subunit Suc22^{R2}

In order to better understand the RNR complex, investigating each subunit and their structure was done, as well as the predicted structure of the modified RNR for FRET. Using different *in silico* prediction softwares, the secondary structures composing XFP-Suc22^{R2} (XFP stands for any CFP, GFP, and YFP) as well as the tertiary structure (Fig. VI.2) could be observed. There are some very dense helical domains in Suc22^{R2}, as well as some flexible loops between those domains.

Figure VI. 2 Prediction structure of XFP-Suc22^{R2}

Using the softwares Phyre2, and I-TASSER the prediction structures were generated. The secondary structures clearly demonstrate the GFP-like fluorophore in N-terminus followed by the linker and the RNR subunit Suc22^{R2}. Suc22^{R2} is mainly composed of α-helices and when folded in its tertiary structure has a small size.

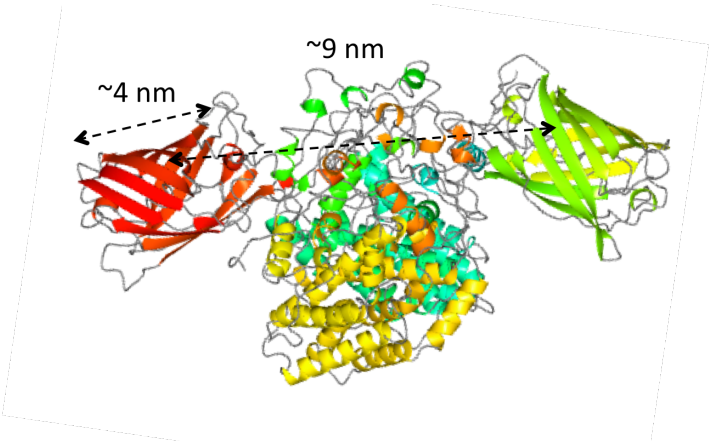

Figure VI. 3 Prediction structure of the CFP-Suc22^{R2} YFP-Suc22^{R2} dimer

Using the prediction structure of XFP-Suc22^{R2} as well as the established dimer structure of R2 in E. coli, we were able to superpose the structures and obtain the predicted dimer structure of Suc22^{R2} and assess the inter-fluorophore distance. Indeed, it seems that the distance between CFP and YFP in the Suc22^{R2} dimer is less than 10 nm, therefore FRET can occur.

The tertiary structure allows us to evaluate the size of the fusion protein, and remark how the fluorophore is almost as large as the Suc22^{R2} itself. Also, the flexible linker between "XFP" and Suc22^{R2} is in evidence and moreover is ideal for FRET to occur.

Having this predicted structure enabled us to evaluate the dimer conformation we should observe *in vivo*, and estimate the inter-fluorophore distance. Indeed, the distance between CFP and YFP appears to be less than 9 nm in the dimer conformation. The predicted structure has been aligned with the available R2 dimer of *E. coli*. Although it is only a prediction, this encouraging observation could corroborate with our *in vivo* homo-FRET data. In addition, the fluorescent proteins CFP and YFP have been cloned with a linker, allowing flexibility for closer juxtaposition and dipole alignment.

For the following single molecules studies, information about the studied proteins are important, as for some experiments i.e. FCS; weight and volume can be used to calculated theoretical values and compare it to the experimental data.

III. Prediction structure of the big RNR subunit Cdc22^{R1}

The same *in silico* methods have been used to obtain more information about the predicted structure of Cdc22^{R1}-XFP. Again, the secondary structure is very dense with α-helices and some flexible loops. The tertiary structure of Cdc22^{R1}-CFP Cdc22^{R1}-YFP shown in Figure VI.3 is a mere reconstruction of predicted structures, but allows us to have some views into the dimer. Unfortunately due to the large length of the protein, I was not able to obtain the full tertiary structure of the fusion protein through the size limitations of the prediction software. Nonetheless I could reconstitute a theoretical model by positioning the fluorescent proteins CFP and YFP at the C-terminus of the R1 dimer. The N-termini, where the ATP cones can be found, are clearly at the opposite ends of the subunit, as are the fluorophores. This can therefore explain the lack of homo-dimer FRET.

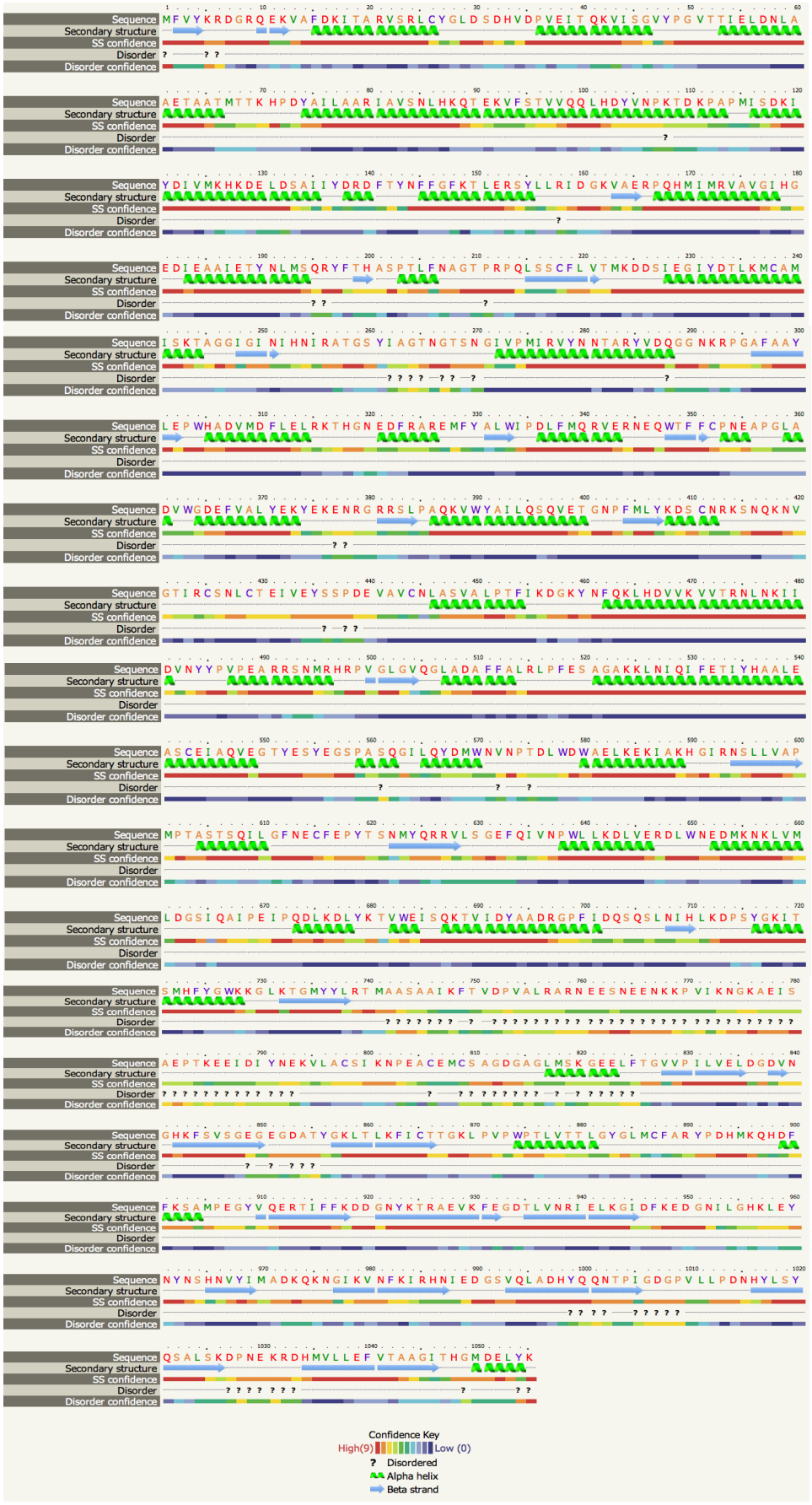
Sequence
Secondary structure
SS confidence
Disorder
Disorder confidence
Confidence Key
High(9) Low (0)
? Disordered
Alpha helix
Beta strand

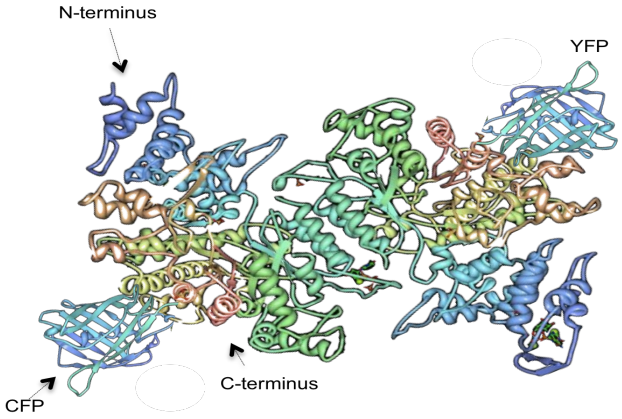

Figure VI. 4 Prediction structures of Cdc22^{R1}-XFP

Using the software "Phyre" the secondary structure predictions were determined. Cdc22^{R1} is a big protein constituted by many α-helices. In the N-terminus GFP is linked providing the Cdc22^{R1}-XFP fusion protein. No tertiary structure prediction was possible with Cdc22^{R1} but using the available R1 structures we could reconstitute what could possibly be the Cdc22^{R1}-CFP Cdc22^{R1}-YFP dimer.

IV. Fusion protein XFP-Suc22^{R2} expression and purification

To study the RNR through single molecules techniques *in vitro*, the fusion proteins had to be purified. After cloning CFP-Suc22^{R2} and YFP-Suc22^{R2} into pUC19, followed by cloning into the *E. coli* expression vector pET3a, expression of the fusion proteins were optimized by medium (TB), culture temperature and time of incubation. In addition, due to high protein degradation and cleavage of the fluorescent tag, significant amounts of proteinease inhibitors and efforts were done to avoid such degradation.

In first instance classical protein purification methods were approached (see chapter 2 material and methods): streptomycin sulfate precipitation, followed by 25%, 50% and 68% ammonium sulfate precipitation of the stable soluble fusion protein. But these methods were not optimal as the yield and specificities were too low (Fig VI.5 a.). In addition, the polishing steps of dialysis and size exclusion chromatography were unsuccessful due to the precipitation of the protein during dialysis and/or low levels of protein input. (Fig VI.5 b)

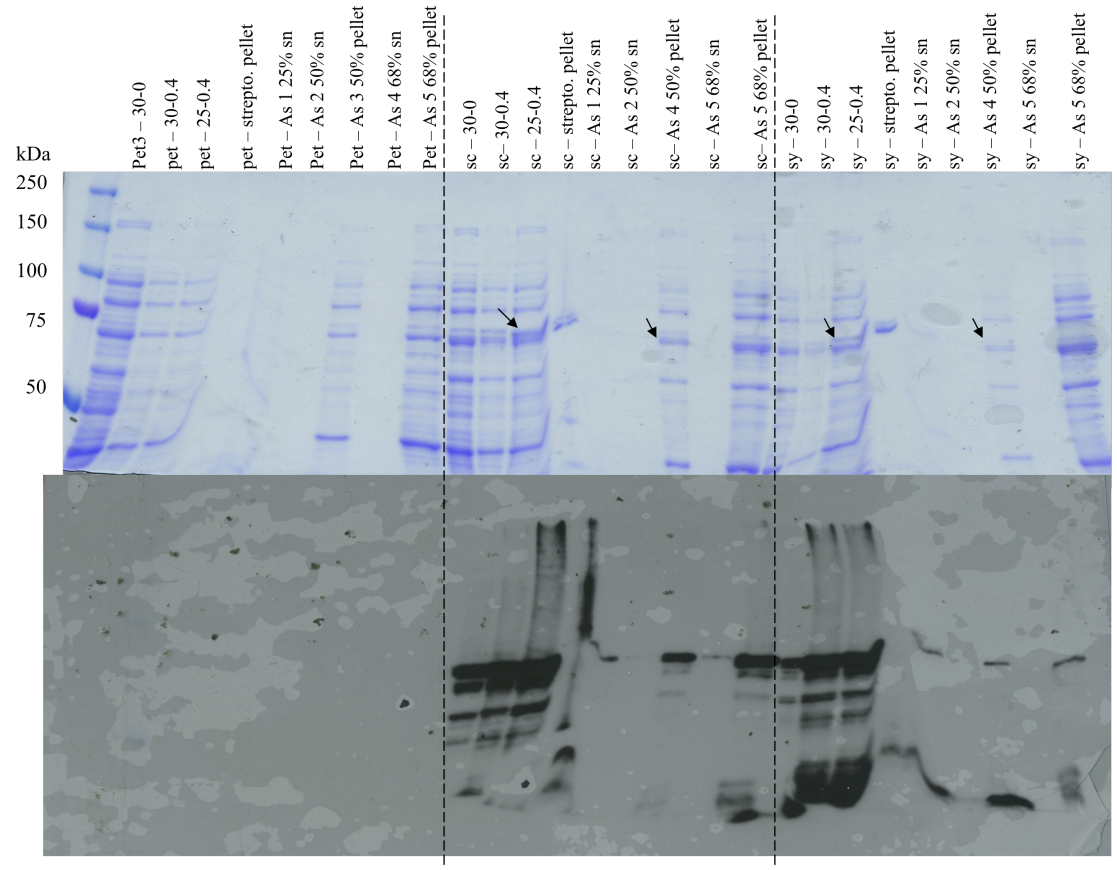

a.

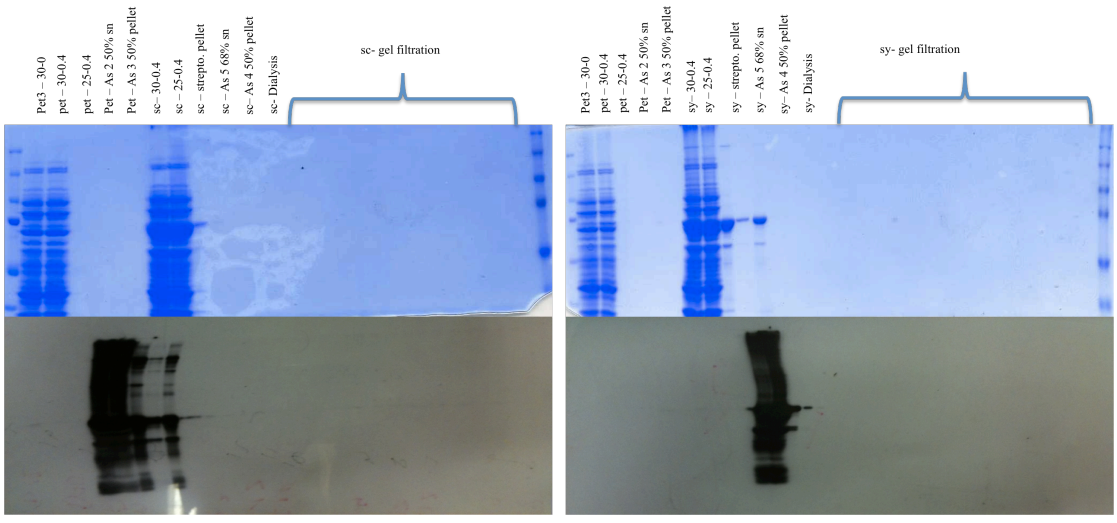

b.

Figure VI. 5 Classical protein purification of CFP-Suc22^{R2} and YFP-Suc22^{R2} from E. coli

Figure VI.5 represents the SDS-PAGE gel and immunostaining of protein purification of the recombinant proteins. Suc22^{R2} tagged with the fluorophores was cloned into pET3a, and expressed and induced by IPTG in TB medium at 30°C or 25°C.

In a., the empty vector was used as mock purification and control, and is annotated "pet3", CFP-Suc22^{R2} is annotated "sc": and YFP-Suc22^{R2} is noted as "sy". For these 3 purifications, a sample was taken from each expression test and step of purification:
30 - 0: sample of the culture in TB medium at 30°C at 0 mm IPTG
30 - 0.4: sample of the culture in TB medium at 30°C at 0.4 mm IPTG
25- 0.4: sample of the culture in TB medium at 25°C at 0.4 mm IPTG
Strepto. Pellet: sample of the streptomycin precipitation pellet
As 1: sample of the ammonium sulfate precipitation at 12% supernatant
As 2: sample of the ammonium sulfate precipitation at 50% supernatant
As 3: sample of the ammonium sulfate precipitation at 50% pellet
As 4: sample of the ammonium sulfate precipitation at 68% supernatant
As 5: sample of the ammonium sulfate precipitation at 68% pellet
Although the recombinant protein did precipitate at 50% of ammonium sulfate, the specificity and yield were not optimum.
The part b. illustrates one of the trials of dialysis on the partially purified protein samples. But the recombinant proteins did precipitate during dialysis, therefore yielding no signal on the gel filtration (Size Exclusion Chromatography).

Although cloning into a vector with a histidine affinity tag (pET28) was done, we wanted to limit the modifications on the protein, and unfortunately, even after cleavage of the histidine tag, some unwanted amino acids remain. We decided to avoid this, as we did not want to encounter false negative FRET results *in vitro*. Therefore the recombinant proteins needed to be exactly the same as the one *in vivo*. Thus we used the expression vector pET3a, as explained in material and methods.

Due to the unsuccessful classical protein purification, we decided to try immuno-precipitation (IP) using anti-GFP antibodies. Although at first it seemed to be an option, it became clear that most of the expressed recombinant proteins were lost during the washes. Various protocols were used (different concentrations of antibody -2 μg to 8 μg-) as well as two different sources of antibodies (mouse anti-GFP and rabbit anti-GFP). As seen in Figure VI.6, there seemed to be a problem to retain the CFP-Suc22^{R2} and YFP-Scu22^{R2} proteins. One of the reasons for this problem could be due the incorrect and inefficient binding of the antibodies to the dynabeads (Invitrogen).

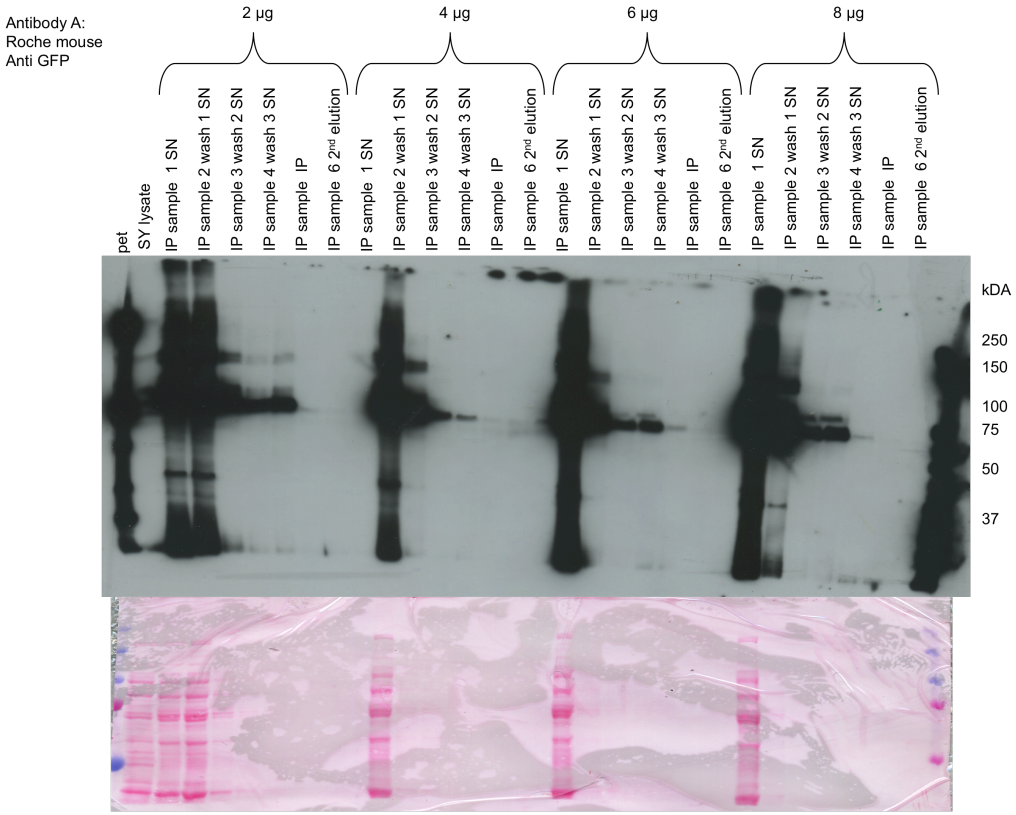
Antibody A:
Roche mouse
Anti GFP
2 µg
4 µg
6 µg
8 µg
pet
SY lysate
IP sample 1 SN
IP sample 2 wash 1 SN
IP sample 3 wash 2 SN
IP sample 4 wash 3 SN
IP sample IP
IP sample 6 2nd elution
kDA
250
150
100
75
50
37

a.

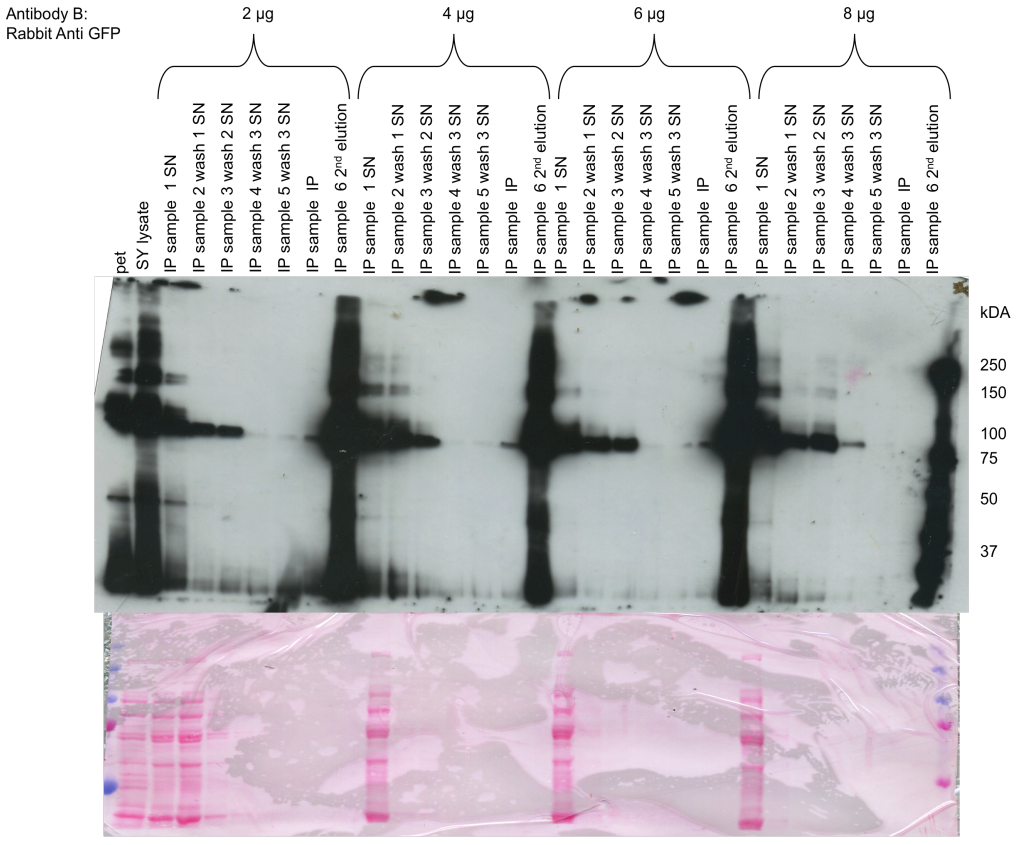
Antibody B:
Rabbit Anti GFP
2 µg
4 µg
6 µg
8 µg
pet
SY lysate
IP sample 1 SN
IP sample 2 wash 1 SN
IP sample 3 wash 2 SN
IP sample 4 wash 3 SN
IP sample 5 wash 3 SN
IP sample IP
IP sample 6 2nd elution
kDA
250
150
100
75
50
37

b.

Figure VI. 6 Immunoprecipitation with anti-GFP dynabeads of CFP-Suc22^{R2} and YFP-Suc22^{R2} from E. coli

These images represent the trails done at different antibody concentration, as well as different antibodies (In a. the mouse anti-GFP from Roche was used, and in b. the rabbit anti-GFP was used). The protein purification samples are shown by specific anti-GFP immunostaining after SDS-PAGE gel as well as staining of the membrane with ponceau red for total protein staining. In both gels, the samples loaded were:
Pet: empty vector
SY lysate: sample of the lysis after expression of YFP-Suc22^{R2} in E. coli
IP sample 1 SN: sample of the supernatant after the incubation
IP sample 2 wash 1 SN: sample of the supernatant after the first wash
IP sample 3 wash 2 SN: sample of the supernatant after the second wash
IP sample 4 wash 3 SN: sample of the supernatant after the third wash
IP sample 5 wash 2 SN: sample of the supernatant after the third wash
Sample IP: sample of the Immunoprecipitation
Sample 6 2nd elution: sample of a second elution of the immunoprecipitation

As the IP method seemed a good tool to increase the specificity, but due to technical problems, the dynabeads were not the most efficient method. Alternative protocols were tried, using beads already bound to anti-GFP. Three methods were tried on the recombinant proteins expressed in *E. coli*:

- GFP-TRAP agarose beads (Chromotek), this variant antibody has high affinity to GFP and is available bound to agarose beads
- GFP-TRAP magnetic beads, the same as above but bound to magnetic beads
- μMAC anti-GFP magnetic beads (Miltenyi) are classical magnetic beads but already bound with anti-GFP. In addition, the protocol uses efficient columns to allow a flow through of the lysate while retaining the magnetic beads. This system allows high throughput.

Figure VI.7 is an example of the trials done with the mock purification, the CFP-Suc22^{R2} and YFP-Suc22^{R2} proteins. This figure shows the end result of input, wash and IP done in parallel in the three systems to compare.

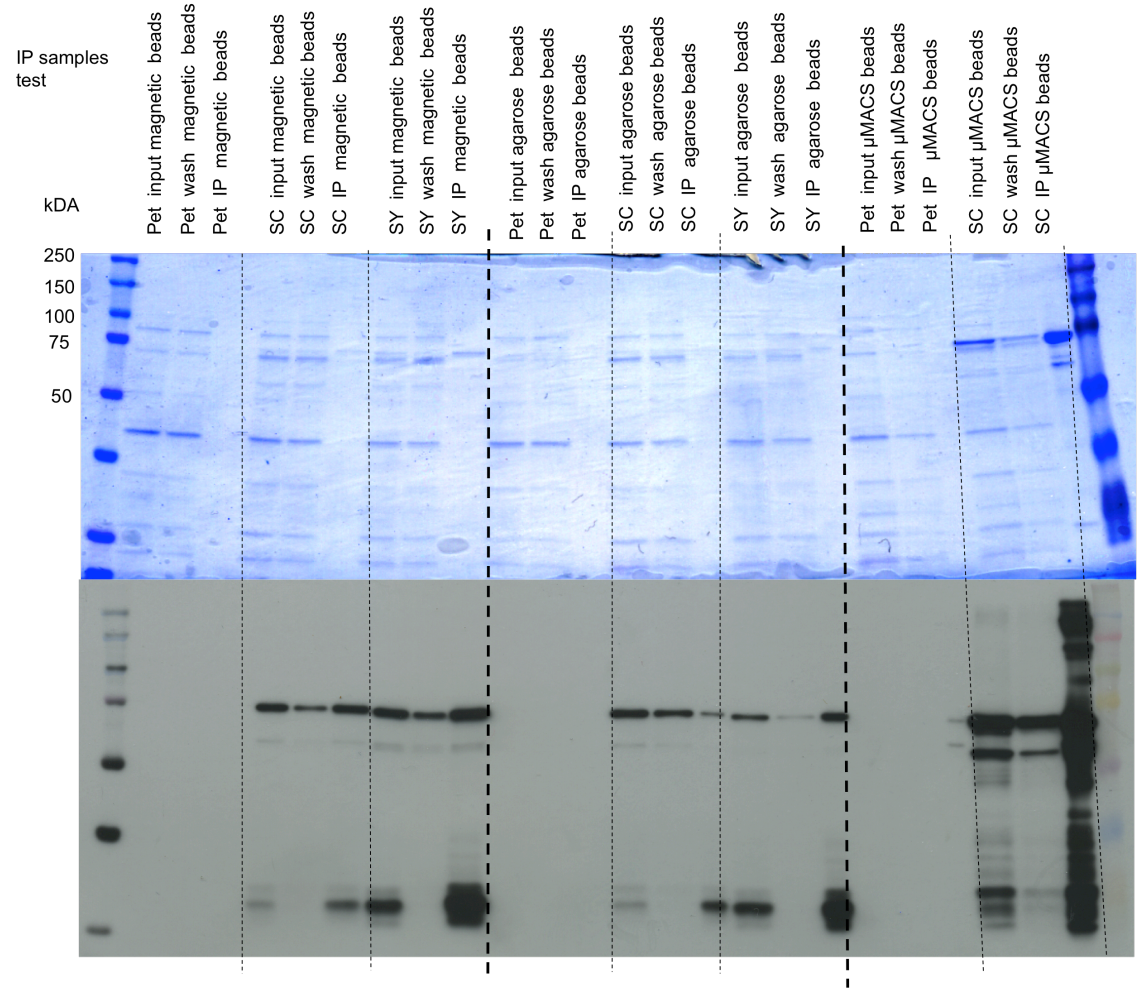

Figure VI. 7 Trials of three different IP methods with the CFP-Suc22^{R2} and YFP-Suc22^{R2} from E. coli

Three methods were tried the GFP-TRAP magnetic beads ("magnetic beads"), the GFP-TRAP agarose beads ("agarose beads") and the μMAC anti-GFP magnetic beads ("μMAC beads")
The empty vector was used as control negative vector for mock purification ("pet") while CFP-Suc22^{R2} ("SC") and YFP-Suc22^{R2} ("SY") were also used. The samples loaded represent the input, a sample from the wash (unbound) and the final elution.

Because of the very high yield and the available columns for high throughput the μMAC anti-GFP magnetic beads were used. After increasing the yield and modifying the protocol to obtain native eluted protein (Figure VI.8), this method was used routinely, procuring us with enough quantities of pure fusion proteins for the single molecule experiments (Figure VI.9).

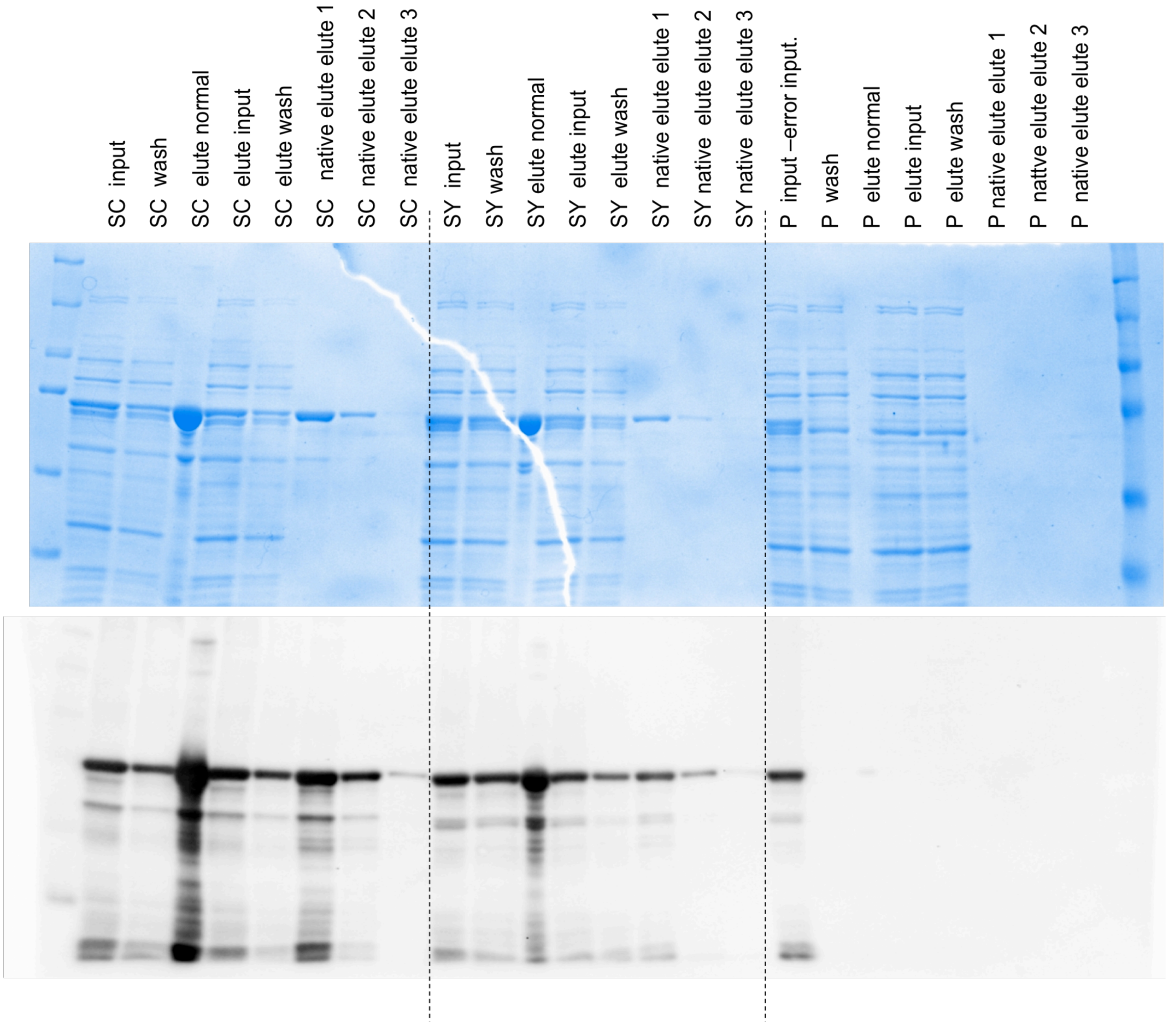

Figure VI. 8 Native elution of CFP-Suc22^{R2} and YFP-Suc22^{R2} purification from E. coli

The μMAC anti-GFP magnetic beads were used, but improvements had to be done to obtain the recombinant proteins pure and in a native state to be used for the single molecule experiments. This figure represents a trial comparing normal elution (boiling of the beads in sample buffer) and native elution. CFP-Suc22^{R2} was used ("SC"), YFP-Suc22^{R2} ("SY") and the empty vector ("P").

For each protein, the input was loaded ("input"), a sample of the supernatant after the wash ("wash") and a sample of the elution. In parallel, the same procedure was done loading the input, a sample of the wash and the native elutions 1 (first elution), 2 (2nd) and 3 (3rd).

The results are shown by commassie gel and by immunostaining with anti-GFP.

There was an error in the loading of the first lane of the empty vector "P".

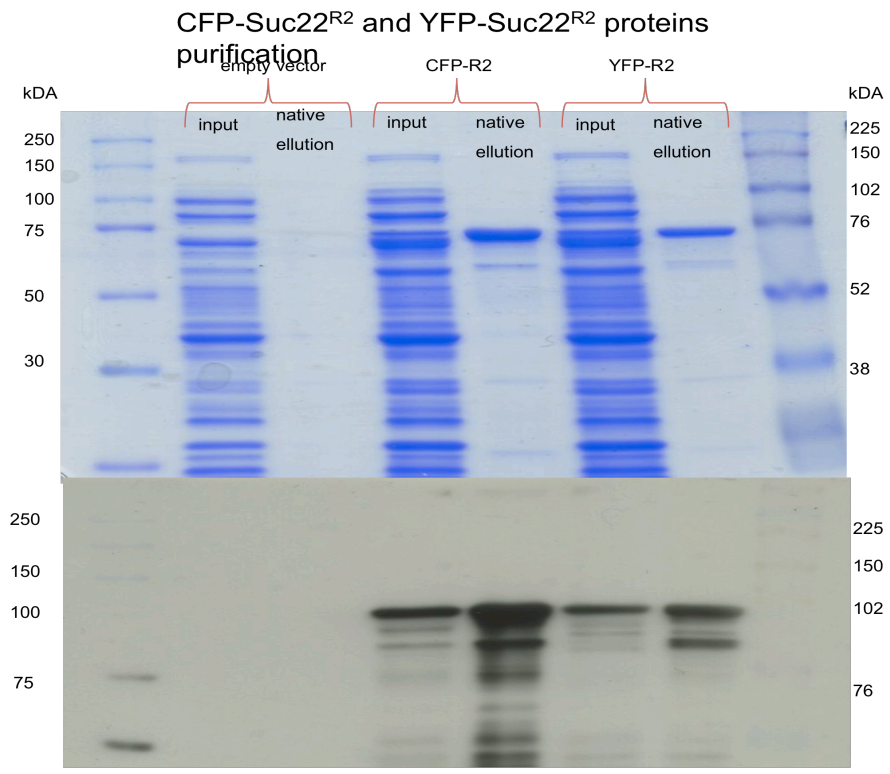

Figure VI. 9 Purified fusion protein CFP-Suc22^{R2} and YFP-Suc22^{R2} from E. coli

Suc22^{R2} tagged with the fluorophores was cloned into pET3a. Expression was induced by IPTG in TB medium at 30 °C. Both tagged Suc22^{R2} proteins (CFP and YFP) were purified with the most efficient method found, by microMAC anti-GFP magnetic beads columns and native elution by pH shift. The end result is shown on the commassie gel and western blot (anti-GFP antibody), and the proteins can be found around the expected size of 75 kDA. The lanes are: Empty vector input and native elution, CFP-Suc22^{R2}, followed by, CFP-Suc22^{R2} and YFP-Suc22^{R2} with similar input and native elution loading.

Those proteins were verified by mass spectrometry to confirm the purification of the proteins of interest as well as assessing the length of the protein purified. They are indeed the corresponding proteins of the small RNR subunit and are expressed in their full length (Figure VI.10)

CFP-Suc22^{R2}

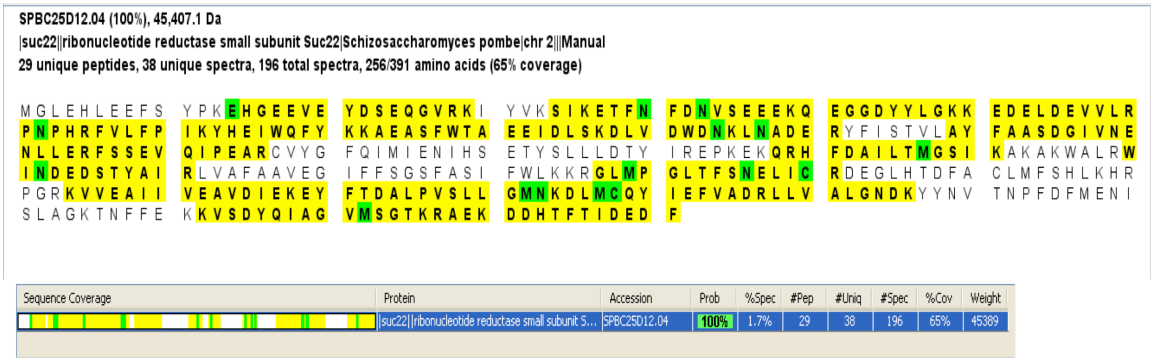

YFP-suc22^{R2}

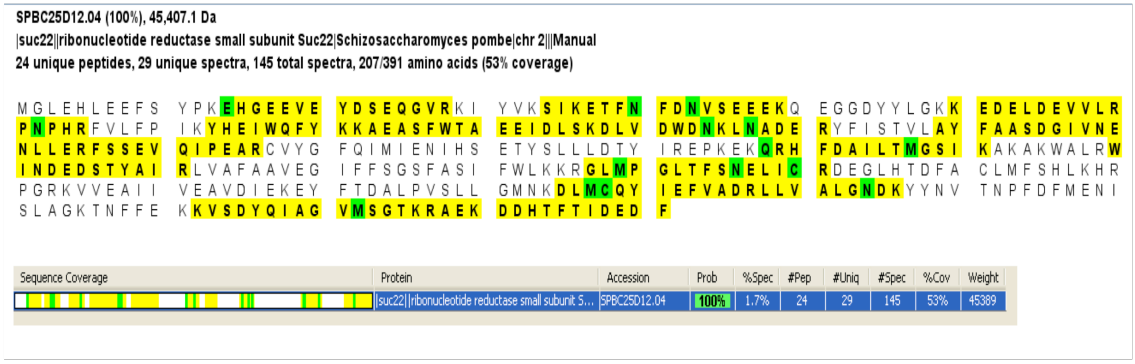

Figure VI. 10 Expression and Purification of E. coli expressed CFP-Suc22^{R2} and YFP-Suc22^{R2} proteins and verification by mass spectrometry (MS/MS)

These proteins were confirmed by mass spectrometry to be the correct protein expressed, but also confirming the full-length protein is expressed. (Mass spectrometry done in association with the proteomics department of the University of Sussex)

In addition, the purified recombinant proteins from *E. coli* were compared to the endogenous CFP-Suc22^{R2} and YFP-Suc22^{R2} (see Figure VI.11)

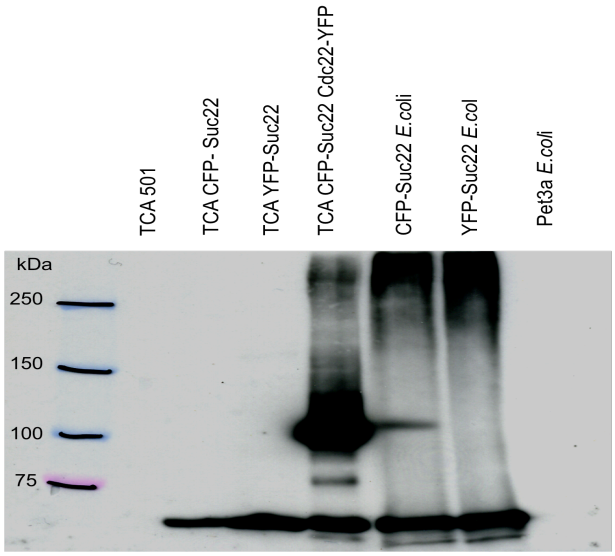

Figure VI. 11 Comparison of the purified CFP-Suc22^{R2} and YFP-Suc22^{R2} proteins from E. coli and endogenous proteins

This immunostaining using anti-GFP shows samples of TCA extracts (total protein extracts from yeast cells) of the strains 501 (wt, untagged RNR), TCA CFP-Suc22 (single tagged CFP-Suc22^{R2} strain), TCA YFP-Suc22 (single tagged YFP-Suc22^{R2} strain), TCA CFP-Suc22 Cdc22-YFP (double tagged CFP-Suc22^{R2} Cdc22^{R1}-YFP strain), CFP-Suc22 E. coli (purified CFP-Suc22^{R2} from E. coli), YFP-Suc22 E. coli (purified YFP-Suc22^{R2} from E. coli) and pET3a E. coli (mock purification).

V. Cdc22^{R1}-XFP Protein Expression and Purification

The fusion proteins Cdc22^{R1}-CFP and Cdc22^{R1}-YFP were expressed as well. The aim was to obtain the purified recombinant proteins for the *in vitro* experiments. The cloning of the fusion genes was slightly more complex due to the presence of an intron in the Cdc22^{R1} gene. Various methods of cloning were tried:

- Due to the presence of an intron, creation of a linker (including the first exon and the enzyme restriction sites) using the primers

pET3a_L_F TATGTTTGTATACAAAAGAGACGGACGTCGTAGGCGCGCCG

and

pET3a_L_R

GATCCGGCGCGCCTACGACGTCCGTCTCTTTTGTATACAAACA

- Cloning of linker as a NdeI/BamHI fragment into pET3a
- Amplifying the exon 2 and cloning as an AatII/AscI fragment

Technical problems with the linearization of pET3a were encountered, partly due to the redundancy of the AatII restriction enzyme site. Unfortunately, even after a PCR based mutagenesis of the site, a clear linearization of the fragment was not obtained. Finally, the cDNA of Cdc22^{R1} from Dr. Kostas Nestoras was used, enabling me to obtain the pET3a-Cdc22 no codon stop plasmid (using the InFusion method). The linker followed by the CFP as well as YFP genes were cloned into the C-terminus of Cdc22^{R1}, although with difficulties to find appropriate enzymes (as Cdc22^{R1} contains two BamH1 sites and pET3a had limited possibilities). Finally the cloning was done using NheI into another *E. coli* expression vector, pET21a.

The expression of the fusion proteins proved to be also tedious but there seems to be some expression (Fig. VI.12). The expression of Cdc22^{R1}-XFP has now to be improved (various temperatures, longer incubations), and most probably the same purification (anti-GFP magnetic beads columns) can be used.

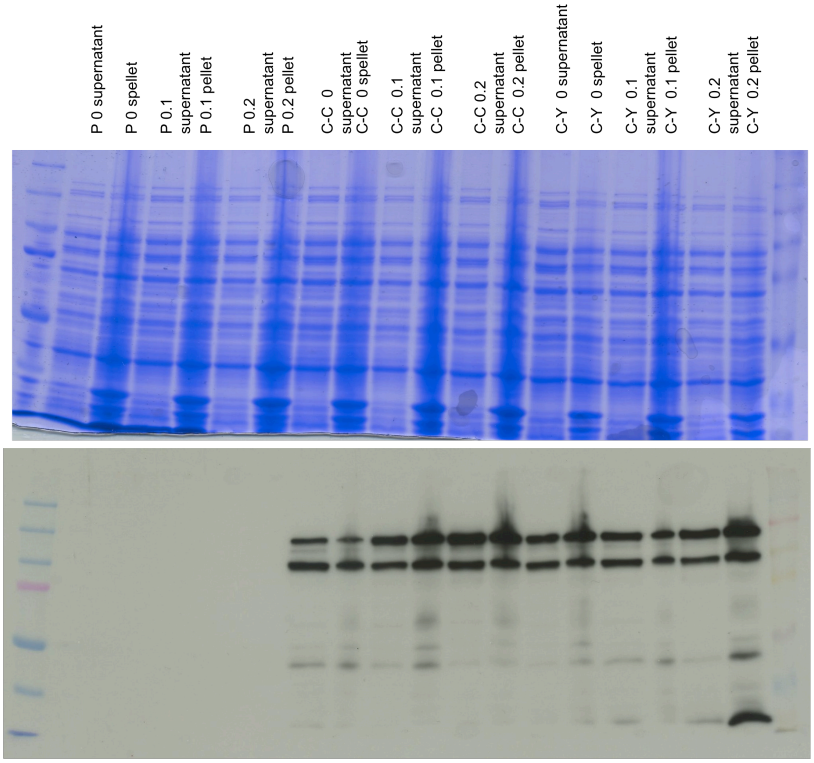

Figure VI. 12 Purification of E.coli expressed Cdc22^{R1}-CFP and Cdc22^{R1}-YFP proteins

Cdc22^{R1} tagged with the fluorophores was cloned into pET21a, and expressed in LB medium at 16 °C, followed by induction with IPTG and growth overnight. The lanes of the SDS-PAGE gel are empty vector pET21a without IPTG induction (P 0), and the supernatant as well as pellet

were loaded. Followed by the empty vector but at 0.1 mM IPTG (P 0.1) at 0.2 mM IPTG (P 0.2). The exact same protocol and loading was done for Cdc22-CFP (C-C 0 mM IPTG, C-C 0.1 mM IPTG and C-C 0.2 mM IPTG) as well as for Cdc22-YFP (C-Y 0 mM IPTG, C-Y 0.1 mM IPTG, C-Y 0.2 mM IPTG). Protein expression revealed by coomassie and western blot by anti-GFP antibody.

VI. RNR tagged proteins purified from *S. pombe*

The CFP and YFP tagged RNR proteins from *S. pombe* were also directly purified by anti-GFP immunoprecipitation (Dynabeads, Invitrogen), and although partially successful, the yield was quite low. (Figure VI.13)

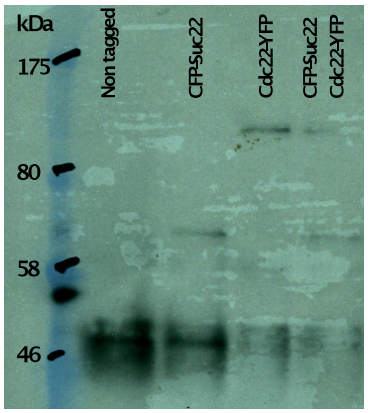

Figure VI. 13 Immunprecipitation of endogenous CFP-Suc22^{R2}, Cdc22^{R1}-YFP and CFP-Suc22^{R2} Cdc22^{R1}-YFP proteins

Using the classical IP procedure with Dynabeads and mouse anti-GFP on S. pombe cell lysates after grinding in liquid nitrogen, the endogenous RNR-tagged proteins were immunoprecipitated. The non-tagged control was loaded, followed by the IP sample from single tagged strain CFP-Suc22^{R2}, as well as Cdc22^{R1}-YFP. Finally, the double-tagged strain was loaded. The proteins are at the expected sizes of ~75 kDa for CFP-Suc22^{R2} and ~119 kDa for Cdc22^{R1}-YFP.

Therefore the three methods of IP used for the purification of over-expressed proteins in *E. coli* were also tried for the *S. pombe* cells. The μMAC anti-GFP showed too much non-specific binding; therefore the GFP-TRAP methods were used and compared to obtain the best conditions. (Figure VI.14)

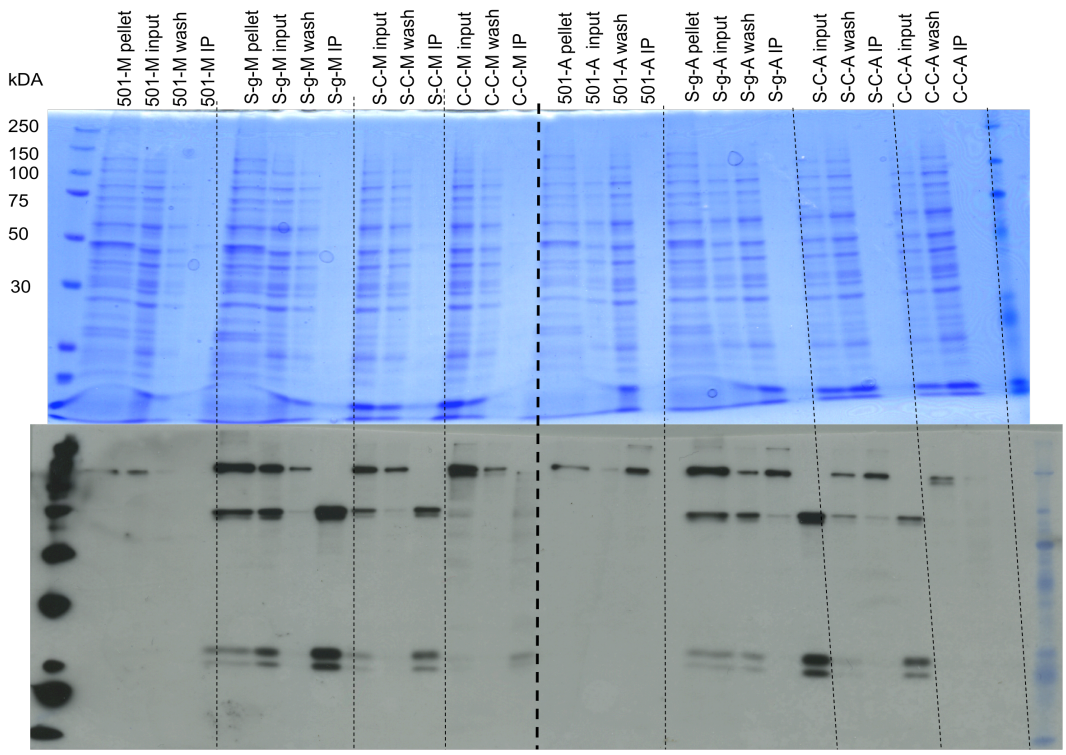

Figure VI. 14 Purification of endogenous XFP-Suc22^{R2} and Cdc22^{R1}-XFP proteins

Using the GFP-TRAP method, the RNR proteins were directly purified from the S. pombe strains. The strains used were 501: negative control as the RNR is not tagged, GFP-Suc22 ("S-g"), CFP-Suc22 ("S-C") and Cdc22-CFP (C-C). In parallel the GFP-TRAP bound to magnetic beads was tried ("M") and bound the agarose beads ("A"). Samples of the pellet ("pellet"), the input ("input") and the wash ("wash") were loaded. Also the final elution, thus the bound proteins were loaded ("IP")

Using the "GFP-trap" protocol vastly improved the yield and specificity of the purification of endogenous proteins. After ameliorating the conditions for native elution this method could be used on a range of strains. This procured us with enough quantities of pure fusion proteins for the single molecule experiments.

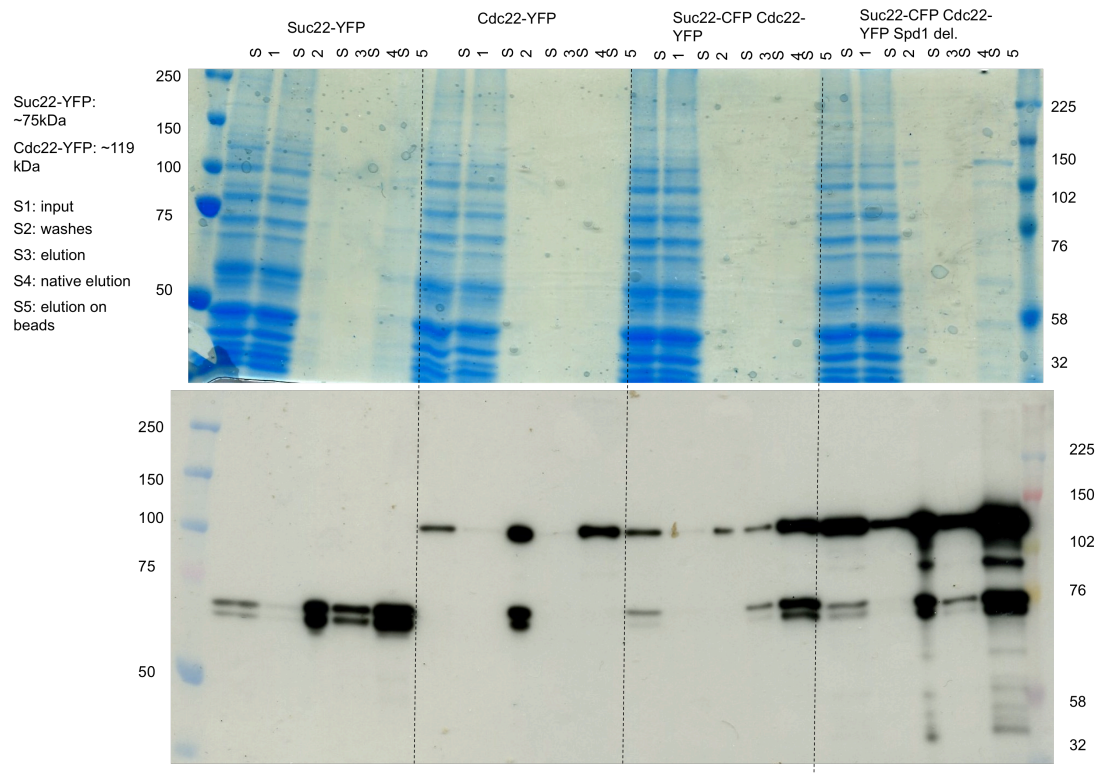

Figure VI. 15 Purification of endogenous XFP-Suc22^{R2} and Cdc22^{R1}-XFP proteins

Using a "GFP TRAP" method, the RNR proteins were directly purified from the S. pombe strains. Lysis of the cells followed by agarose beads bound to an anti-GFP variant. The 4 strains represented here are: single tagged Suc22^{R2}-YFP, single tagged Cdc22^{R1}-YFP, double tagged Suc22^{R2}-CFP Cdc22^{R1}-YFP and double tagged Suc22^{R2}-CFP Cdc22^{R1}-YFP spd1 Δ. For each strain the input, washes, and various elutions have been loaded. The purified proteins are revealed by SDS-PAGE after coomassie staining and western blot with the anti-GFP antibody.

VII. Photobleach step assay to determine stoichiometry using TIRFM (Total Internal Reflection Microscope)

One method we use to answer more precisely the oligomeric state of the purified proteins is the photobleaching step assay done on a total internal reflection microscope (TIRFM) (Reck-Peterson et al, 2010). After immobilizing the proteins on a slide using anti-GFP antibodies (Fig. VI.9 part a.), and washed with buffer and BSA, the purified proteins are being imaged and exposed until completely photobleached. Therefore the number of steps necessary to be fully photobleached can be observed, consequently revealing the number of fluorophores present (see Figure VI.16 part b.). If only one fluorophore is present, one step of photobleaching will be visible, but in the presence of two fluorophores there will be two steps of photobleaching and so on.

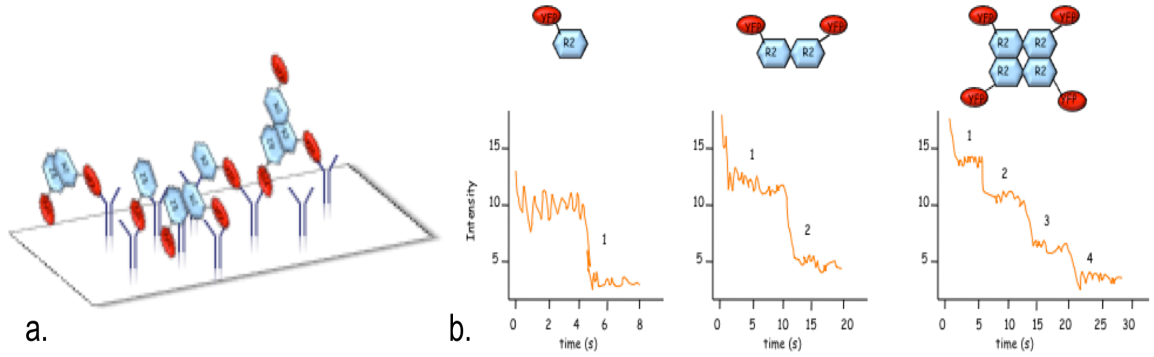

Figure VI. 16 Photobleach step assay set up on the TIRFM and principle
Schematic of the photobleach assay. In part a. the proteins of interest are tagged with fluorophores and will be immobilized by specific antibodies. Imaged on a TIRFM the proteins will be exposed until fully photobleached, and the number of steps a single molecule will take will be imaged and measured. Finally it will provide the number of proteins present.

The controls for the photobleach step assay were various: buffers and antibodies alone, but as well controls with purified eGFP proteins provided the calibration for the experiment. It also provided us with the expected result of a majority of single photobleach step population, meaning a preponderance of monomer population.

The photobleach step assay was used to reveal the stoichiometry of the purified XFP-Suc22^{R2}. Imaging the purified small subunit proteins supplied us with some information of the intensity of the fluorophores, which can be shown into a point spread function (PSF) with a scale for the intensity of the fluorescence (Figure VI.17 part a.). The assay revealed a majority of 1 step, although some 2 steps were observed as well (fig. VI.17 part b.). Purified XFP-Suc22^{R2} proteins have a mixed population: mostly monomers in addition of some dimers (Figure VI.17).

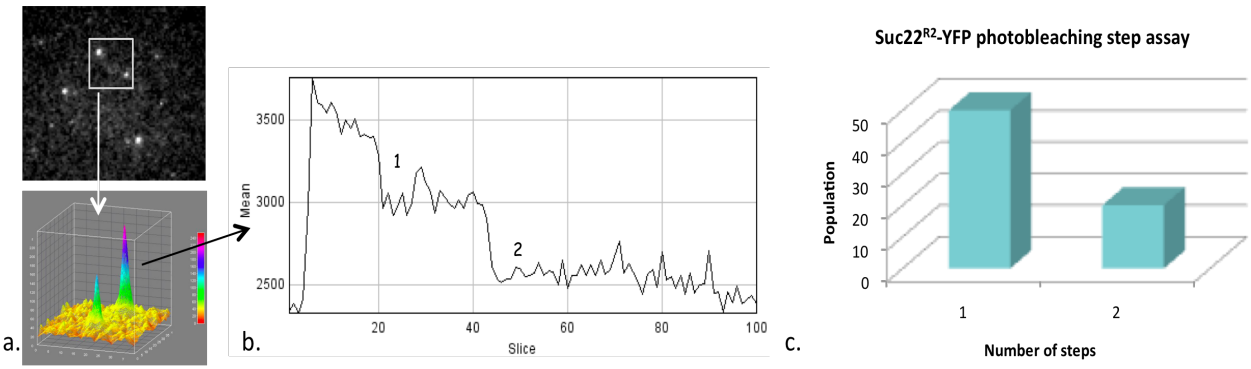

Figure VI. 17 Photobleaching step assay on XFP-Suc22^{R2} to determine the stoechiometry

The purified XFP-Suc22^{R2} proteins were first used on the Total Internal Reflection Microscope (TIRFM), and fixed on a slide before imaging. On the far left (a.) is an example of an obtained image, as well as the 3D point spread function reconstruction of a certain area. Next, each single molecule is photobleached and the bleaching profile of one single molecule will provide a number of steps, in this example two steps (b). This is done on a number of molecules. The result for YFP-Suc22^{R2} is a mixed population of monomer but as well some dimers (c). (Done in collaboration with Remi Boulineau)

VIII. Single molecule experiment using the FCS (Fluorescence Correlation Spectroscopy)

Another method used was Fluorescence correlation spectroscopy (FCS), which will ultimately provide us a characteristic diffusion time of the proteins dependent on their radius of gyration Rg (Fitzpatrick & Lillemeier, 2011; Price et al, 2011).

FCS is a method where in a small detection volume, diffusing fluorescent molecules are detected, and their signal intensities are measured during a certain time followed by correlation in order to have a diffusion time.

If the molecule aggregates, binds to other proteins or goes through large conformational changes, its diffusion time will increase and the correlated function will be shifted due to an increased molecular weight.

A fitting of the curve allows obtaining more information from the measurements, using the equation below:

$$y = y0 + \left(\frac{1}{N}\right) \times \left(\frac{1}{1+\frac{x}{d}}\right) \times (1 + \frac{A}{1-A})\exp\left(\frac{-x}{b}\right)$$

N is the number of molecules, d the diffusion time, A the intramolecular contribution and b the intramolecular time.

In first instance we verified the system with the purified GFP proteins, and could set up the calibration of the experiment references (done by Remi Boulineau). As FCS is very sensitive to autofluorescence, appropriate controls were done: the buffers alone, as well as mock protein purification from *E. coli* were used to assess the background. (Fig. VI.18)

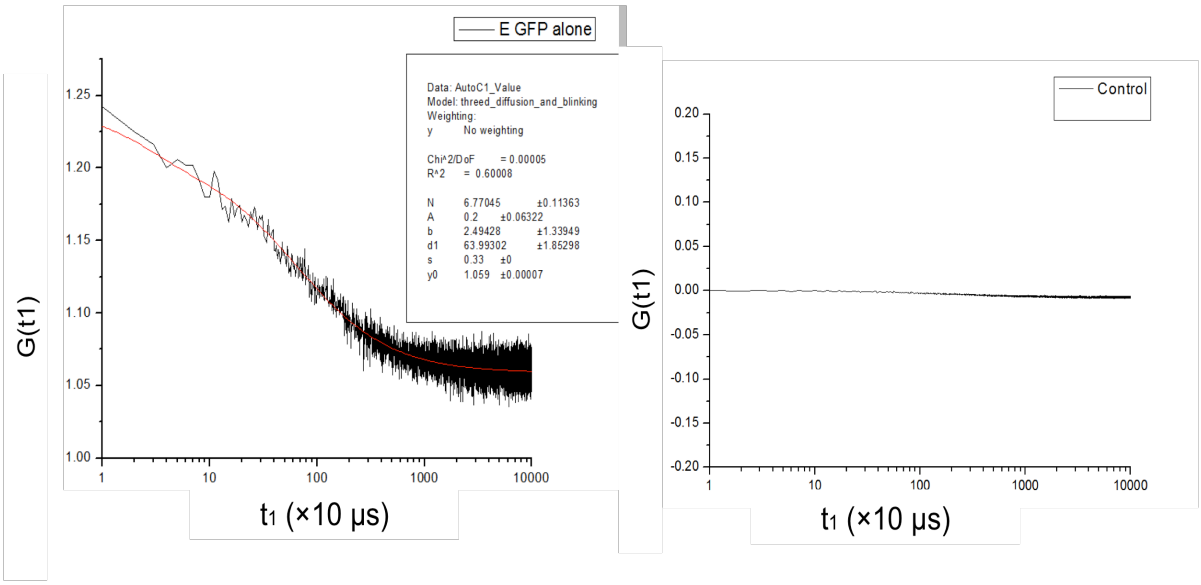

Figure VI. 18 Controls with GFP purified proteins and negative control with no correlation

The controls were done using purified GFP proteins (a), the buffers alone, as well as the mock purification from E. coli should give no correlation of the signal (b.), as this signal should be background. This figure is an example of a negative control ensuring that the signal observed is background, and random, thus no correlation is possible.

The specificity on the other hand was measured by measuring the CFP-Suc22^{R2} proteins on the YFP-Suc22^{R2} set up system, providing us with a strong negative control.

The purified YFP-Suc22^{R2} proteins were tested and diluted to low concentrations (~0.001mg/ml). The correlation of the signal from the single molecule fluorophores on the FCS was done by a software through ImageJ with our collaborators, consequently providing us with a diffusion time (Figure VI.19).

Next, additional controls were done to ensure that the signal was genuine and originated from the YFP-Suc22^{R2} fusion protein. The observed signal and assigned diffusion time were measured before and after treatments to the proteins. (Fig. VI.19) Denaturation of YFP-Suc22^{R2} by heating did result in the abolishment of the signal, and the remaining signal was background and random, thus not able to produce a correlation function. Same results were obtained after treatment of the proteins with the enzyme proteinase K in order to degrade the fusion proteins (Fig. VI.19).

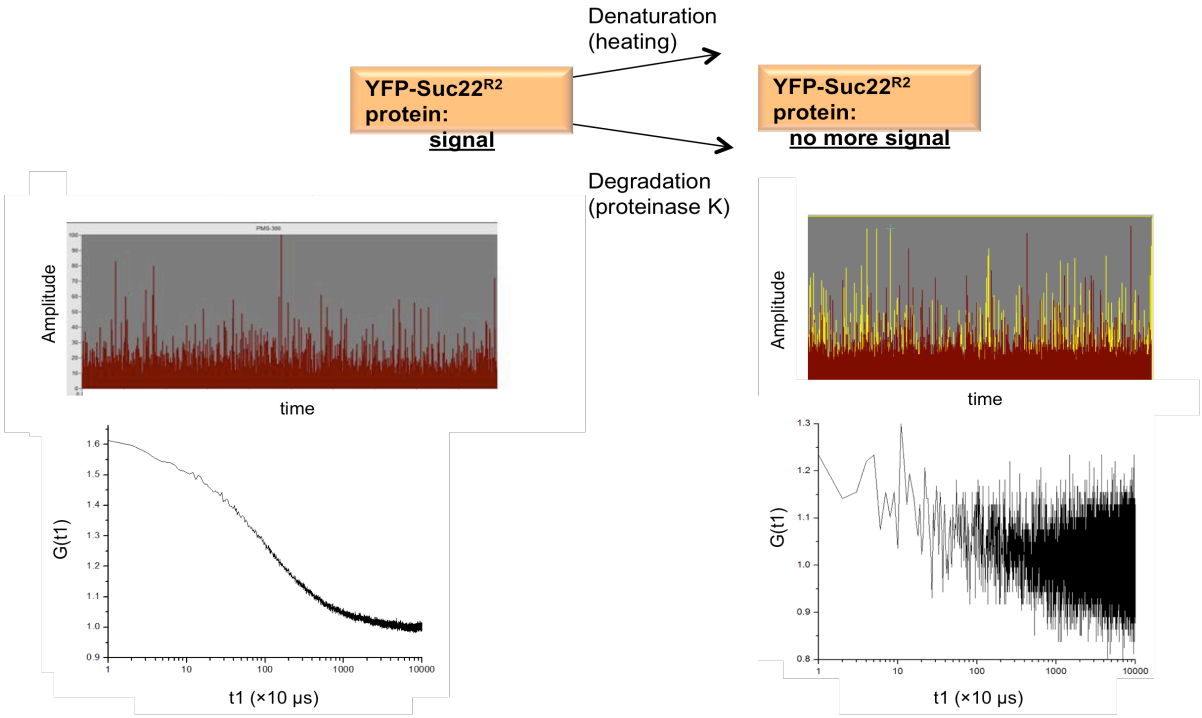

Figure VI. 19 Controls and verifications of the fluorescents single molecule on the Fluorescent Correlation Spectroscopy (FCS)

After obtaining the optimum conditions to measure the YFP-Suc22^{R2} protein at the single molecule level on the FCS, we verified if the signal was abolished after various controls. Indeed denaturation of YFP-Suc22^{R2} by heating, or degradation by enzyme treatment did reduce the signal and resulted in no real correlation function anymore, as it only the background was visible.

A recurring question was the stoichiometry of the purified YFP-Suc22^{R2}, therefore by using FCS we wanted to review this question as well as determine the effect of the mixed population of monomers and dimers observed by TIRFM.

The diffusion times of YFP-Suc22^{R2} in monomer or dimer can be calculated theoretically; in addition the correlation functions (Fig VI.20 a.) can also be simulated by which a diffusion time can also be obtained. The experimental diffusion time of YFP-Suc22^{R2} is 1.002 ms (Fig VI.20 b.). This can be compared to the theoretical calculations and simulations diffusion times, which are lower (Fig VI.20 c.). Thus the experimental YFP-Suc22^{R2} diffusion time does not entirely correspond to the expected diffusion times as a monomer or dimer. We can speculate that the mixture of population of monomeric and dimeric forms of YFP-Suc22^{R2} affects the results, as well as some cleaved YFP that could influence the measurements.

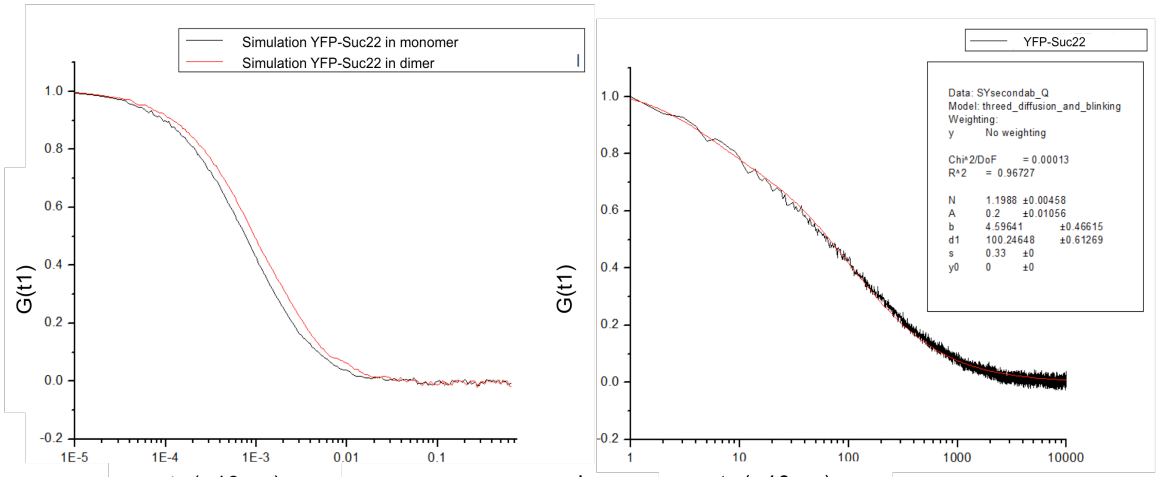

a. b.

	experimental	calculation	simulation
YFP-Suc22 monomer	1.002ms	0.795ms	0.73ms
YFP-Suc22 dimer	1.002ms	0.97ms	0.95ms

c.

Figure VI. 20 Comparison of the diffusion times of YFP-Suc22^{R2} with theoretical values

The diffusion times of YFP-Suc22^{R2} in monomeric form or dimeric form can be calculated, depending on the molecular weight of the complex. Simulations of the correlation function will also provide us diffusion times (a.). The experimental measurements (b.) on YFP-Suc22^{R2} give the genuine diffusion time of the purified proteins. But as the table of diffusion times shown in c., the experimental data does not match any theoretical value, nor for the monomeric diffusion times, nor dimeric ones. (Done in collaboration with Remi Boulineau)

IX. Protein binding measured by FCS

In order to prove the principle of this new method, but as well to set up the standards of the experiment, we proceeded to a protein binding experiment. To the optimum YFP-Suc22^{R2} concentration established beforehand, an increased amount of antibody anti-GFP was added. The increase of antibody concentration was concomitant with the shifting diffusion time, thus describing protein binding.

In addition, at the saturation conditions of anti-GFP bound to YFP-Suc22^{R2}, a secondary antibody to the anti-GFP was used. This resulted in additional protein binding and an even larger shift in the diffusion time (Fig. VI.21 a.). The data can then be fitted into a model, which can provide us with a ratio of bound/unbound proteins. (Fig. VI.21 b.)

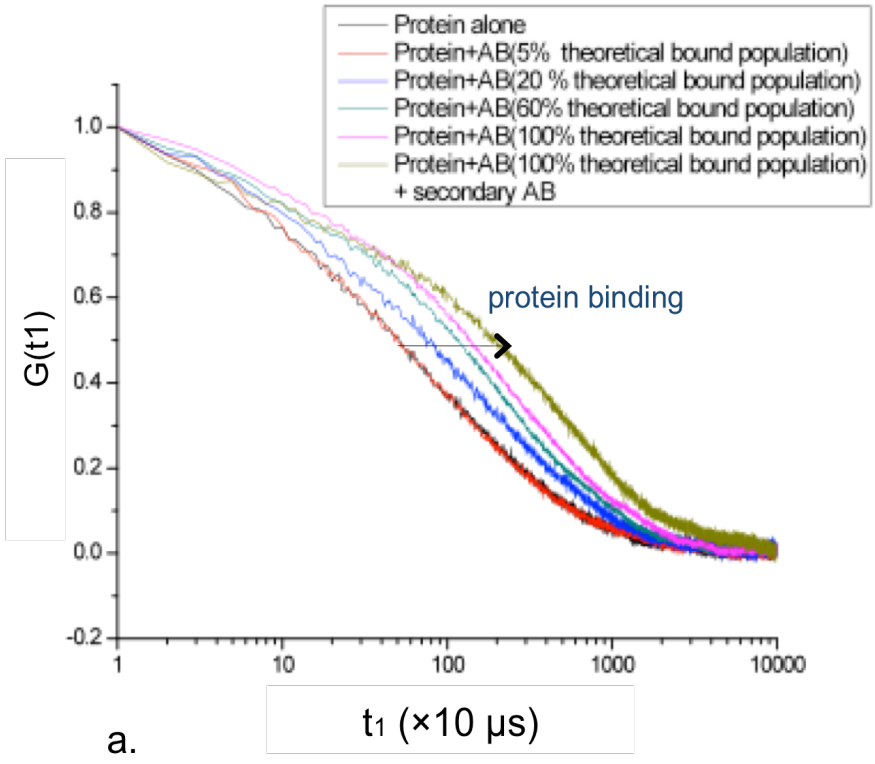

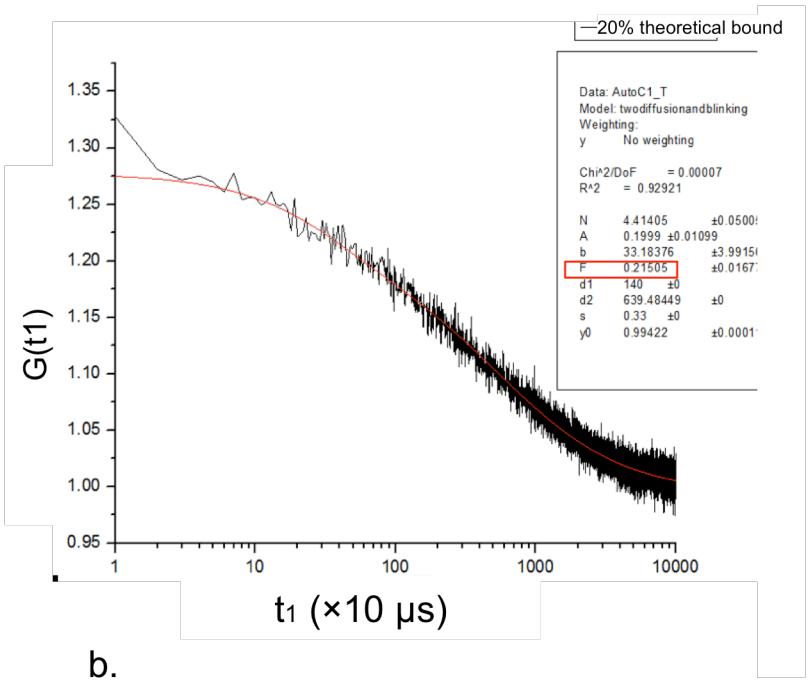

Figure VI. 21 Proof of principle of protein binding measured by FCS

Using the YFP-Suc22^{R2} in the optimum conditions as described earlier, an increased concentration of anti-GFP antibody was added. Indeed a shift in the correlation function is observed, meaning a higher diffusion time. At the saturation of YFP-Suc22^{R2} bound with anti-GFP, a secondary antibody binding to anti-GFP was added, shifting the diffusion time even

further. The correlation functions can than be fitted and provide the ratio (F) of bound/unbound population, for example here 21% of the population is bound, very close to the theoretical value of 20% bound.
(Done in collaboration with Remi Boulineau)

The endogenous RNR proteins from *S. pombe* were also purified and therefore used on the FCS. The diffusion times of YFP-Suc22^{R2} and Cdc22^{R1}-YFP were also measured. The protein binding experiments on the FCS were also done with the endogenous purified YFP-Suc22^{R2} proteins as well as Cdc22^{R1}-YFP, giving similar results i.e. upon binding with the anti-GFP antibodies, a shift in the diffusion time is observable therefore there is positive protein binding (Fig. VI.22). Finally the comparison of Cdc22^{R1}-YFP and YFP-Suc22^{R2} gave the expected result of a higher diffusion time for the bigger RNR subunit Cdc22^{R1} compared to the smaller subunit Suc22^{R2} (Fig VI.22 c).

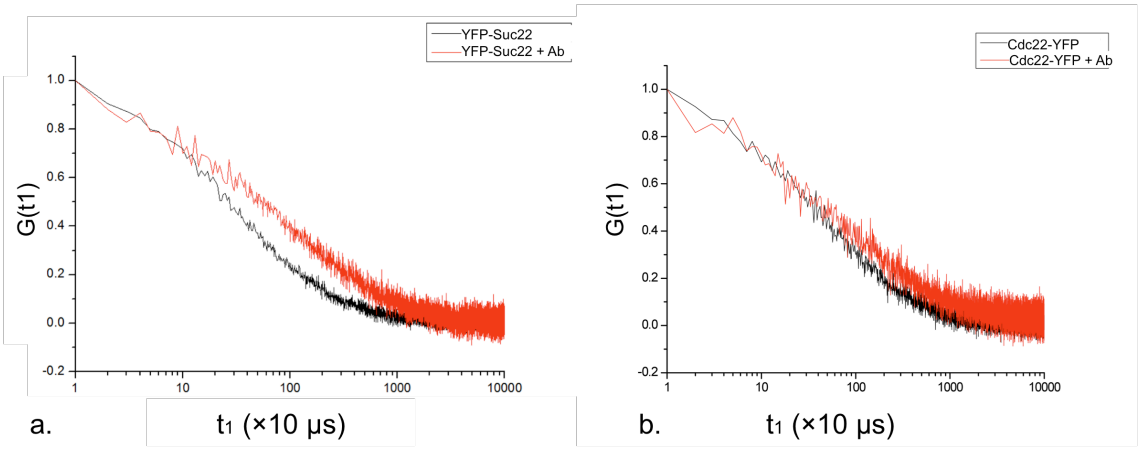

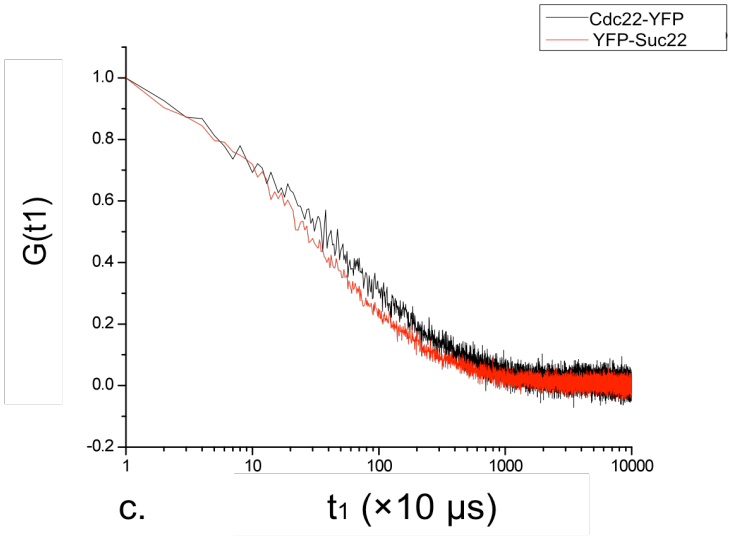

Figure VI. 22 Protein binding with the endogenous purified YFP-Suc22^{R2} and Cdc22^{R1}-YFP

The purified tagged RNR proteins from S. pombe YFP-Suc22^{R2} (a.) and Cdc22^{R1}-YFP (b.) were also used on the FCS and measured. The protein binding assay with the anti-GFP antibodies demonstrated a binding therefore a shift in the diffusion time for both RNR proteins (+Ab). In addition, the Cdc22^{R1}-YFP proteins show a higher diffusion time than the YFP-Suc22^{R2} proteins (c.).

(Done in collaboration with Remi Boulineau)

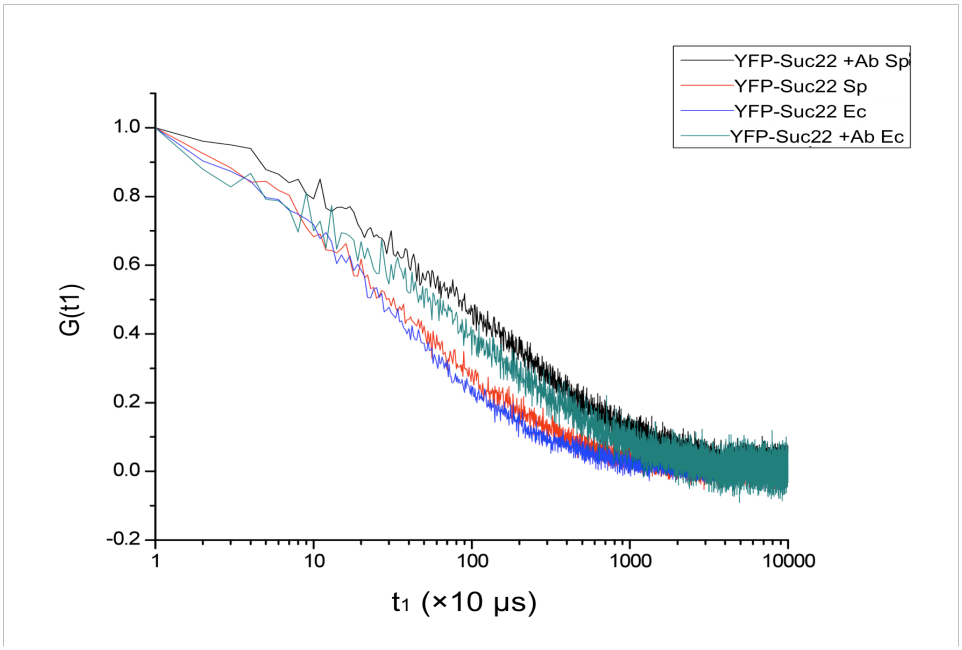

Figure VI. 23 Protein binding comparison with endogenous and E. coli expressed YFP-Suc22^{R2}

In this Figure the YFP-Suc22^{R2} from E. coli (Ec) is compared with the YFP-Suc22^{R2} from S. pombe (Sp), as well as their binding to the antibodies.

The diffusion times of YFP-Suc22^{R2} and Cdc22^{R1}-YFP were also measured. Interestingly enough, the diffusion time of YFP-Suc22^{R2} purified from *E. coli* (Ec, Figure VI.23) is slightly different than the YFP-Suc22^{R2} purified from *S. pombe* (Sp), the latter one having a smaller diffusion time. This could be explained by a different ratio of dimer/moner population, or an increase in cleaved proteins leading to a modification of the diffusion time by contamination of YFP. Other aspects should be considered, for example secondary modifications, different quaternary structure, or simply differences in the purification protocols.

Now that the system is set up and functioning, many experiments can be done, giving more insight of the RNR *in vitro* with regards to its stoichiometry and FRET capacities.

CHAPTER VII DISCUSSION: An insight into the complexity of the RNR Complex

RNR is a key enzyme for genome integrity, and the RNR complex is consistently tightly regulated. Parts of this regulation have been studied, for example the allosteric regulation by the effectors and the transcription control of the RNR proteins; but some aspects of the regulation of the RNR still remain unclear, especially the structure-mediated regulation. With recent publications supporting the structure-dependent regulation of RNR, the aim of this project was to investigate such a regulation *in vivo* in *S. pombe*.

Even though RNR has been studied for decades, the many layers of RNR regulation are still being revealed. The last years have seen numerous publications about the RNR structure in different species, with particular regard to the active form and the inactive form. Consequently, the mechanisms behind the "switching off" and "on" of the RNR are of interest, and observations suggest this might be linked to the quaternary structure of the complex .

In addition, the various functions of the RNR regulators (Spd1 and Spd2 in *S. pombe*) are not fully described yet. These were also investigated in this project. In particular the possible role of the regulators in the structure or conformation modification of the RNR have been studied.

My results have shed some more light on the *in vivo* complex dynamics of RNR, as well as further characterizing the architecture-related regulation of RNR.

I. Established FRET assay with Ribonucleotide Reductase

The FRET assay allowed us to investigate RNR *in vivo*, and we obtained positive FRET between the RNR subunits, as well as homo-FRET between the $Suc22^{R2}$ subunits.

This is consistent with the knowledge that the RNR subunits are able to interact, and form the RNR complex, which is essential for cell survival. A negative FRET readout for RNR in viable cells means a modification of the distance or

alignment of the fluorophores, indicating a stoichiometric and/or conformational change, rather than no protein interaction. However it has to be remembered that the readout of the FRET assay is indirect and we cannot distinguish the nature of the modification leading to the FRET result.

The RNR fluorescent-tagged strains allowed us to estimate the relative abundance of the big subunit $Cdc22^{R1}$, and the small subunit $Suc22^{R2}$ in both cellular compartments of S-phase cells and G2 phase cells. $Cdc22^{R1}$ is at least twice as abundant as $Suc22^{R2}$, and evenly distributed in the cells. $Suc22^{R2}$ levels and localization are more dynamic, with a predominantly nuclear localization in G2 cells. In S-phase cells the levels of $Suc22^{R2}$ are equally distributed in the two nuclei and a concomitant increase in the cytoplasm is observed. Thus the ratio of both RNR subunits and their quantification and localization shows that they are both present in the nucleus as well as in the cytoplasm during the whole cell cycle at similar protein levels.

The FRET assay between CFP-$Suc22^{R2}$ and $Cdc22^{R1}$-YFP (as well as YFP-$Suc22^{R2}$ and $Cdc22^{R1}$-CFP) was designed as a tool to investigate the *in vivo* formation of RNR complex in both cellular compartments and cell cycle stage specific cells.

The early observations of $Suc22^{R2}$ relocalization from the nucleus to the cytoplasm, leading to colocalization of both RNR subunits in the cytoplasm in S-phase, partially supported the hypothesis of active RNR complex formation in the cytoplasm during S-phase, when dNTPs are needed. Therefore, the expectation was a positive interaction mostly in the cytoplasm during S-phase, which is when the active heterocomplexes were predicted to form. However we could demonstrate an interaction between the subunits throughout the cell cycle in both cell compartments. Thus RNR heterocomplexes are formed in heterocomplexes at all times throughout the cell and $Suc22^{R2}$ and $Cdc22^{R1}$ are in close proximity as their fluorphores are not further apart than 10 nm.

In addition, the FRET experiment between $Suc22^{R2}$ homo-complexes proved to be a potential assay to assess the architecture of the complex, as the $Suc22^{R2}$ subunits are in a close dimer. In contrast, the $Cdc22^{R1}$ homo-complexes do not seem to be in a correct conformation to allow FRET, probably due to the fact that in the $Cdc22^{R1}$ dimer structure the C-termini ends are at opposite ends as well as in an uncertain oligomeric state.

II. Spd1 and Spd2 are required for structure-related RNR regulation

As Spd1 has been considered as an RNR inhibitor, upon Spd1 deletion it was anticipated that there would be an increase in active RNR complexes and therefore an increase in FRET positive RNR complexes. Surprisingly the FRET signal was lost and no energy transfer between CFP-Suc22^{R2} and Cdc22^{R1}-YFP (nor YFP-Suc22^{R2} and Cdc22^{R1}-CFP) was observed. Although no clear nuclear and cell cycle phase distinction is possible in those strains (due to complete lack of Suc22^{R2} nuclear localization), the negative FRET result was detected throughout the cells in a range of different sizes cells (i.e. different cell cycle stages). The positive FRET signal obtained between the homo-complexes Suc22^{R2} is lost after deletion of *spd1*.

Since that in *spd1* Δ strains RNR is active and providing even higher levels of dNTPS to the cells, this indicates that the FRET assay is measuring structural modifications and not a loss of RNR protein interactions. These are Spd1-dependent modifications in the association of Cdc22^{R1} and Suc22^{R2}, as well as the Suc22^{R2} dimer. This strongly suggests that Spd1 has a role in regulating the architecture of the RNR complexes. This additional level of RNR regulation controlled by Spd1 correlates with the inherent qualities, with regards to structural flexibility, of intrinsically disordered proteins (IDP or IUP -unstructured-), a group of proteins to which Spd1 belongs.

IDPs have been described in different cellular pathways, and their peculiar characteristics are thought to have biological roles with regards to protein interactions. They can be flexible linkers to recruit and connect partner proteins, as IDPs can freely rotate and move, thus modifying proteins conformations. Another feature of the IDPs is the “coupled binding and folding”: they can acquire a more structured state upon binding to their target proteins. These structural transitions are considered to be dynamic and have roles in regulating protein complexes with a variety of biological functions (Gunasekaran et al, 2003) (Galea et al, 2008b) .

Spd1 has the capacity to bind both subunits of RNR, hence as an IDP could mediate the conformation or stoichiometry of the RNR complex. However

size exclusion chromatography has indicated that no higher order structures are observed *in vivo* with or without Spd1 being present (Nestoras et al, 2010) .

It could be proposed that Spd1 mediates a conformational change in the RNR complex by forming an immature inactive RNR complex. These complexes could be in an optimal conformation (observed by a positive FRET signal) for activation once Spd1 is degraded. In the complete absence of Spd1 (*spd1* Δ), the cells lack the scaffolding role of Spd1 to build RNR into these complexes, thus FRET is never observed.

The novel *S. pombe* RNR regulator Spd2 also has a role in regulating RNR inhibition through a yet unknown mechanism. During this project it was shown that Spd2 has also a role in the architecture-dependent regulation of RNR. Spd2 is required for positive FRET of $Suc22^{R2}$ and $Cdc22^{R1}$. As Spd2 seems to be also an IDP, we can consider a similar RNR scaffolding role for this small protein.

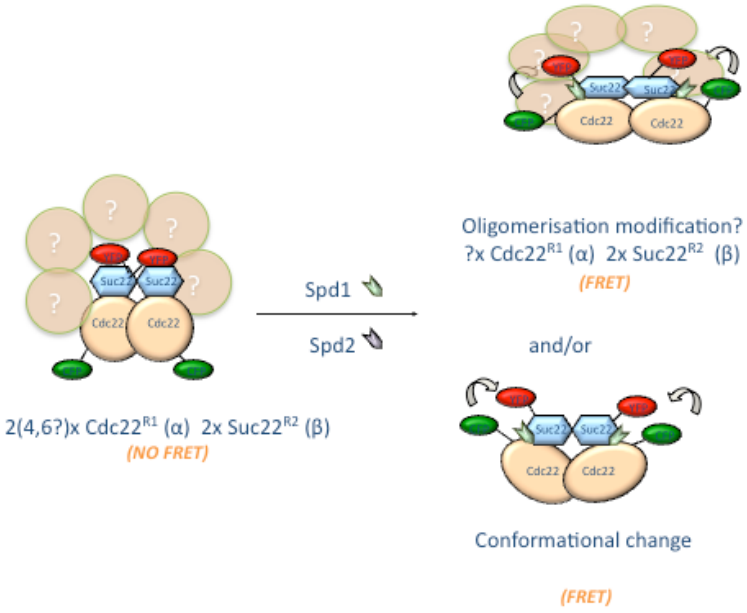

Figure VII. 1 Intermediate working model: Role of Spd1 and spd2 in architectural-dependent RNR regulation

This diagram represents an intermediate hypothesis of the role of Spd1 and Spd2 in the regulation of RNR activity through structural methods. The stoichiometry of the RNR in S. pombe in vivo is as yet unknown. It could be 2-6 big subunits $Cdc22^{R1}$ (α) and 2 small subunits $Suc22^{R2}$ (β). In presence of the RNR regulators, the RNR complexes adopt a different conformation, enabling FRET between the fluorophores. Before its degradation, the IDP Spd1 will have fulfilled its role of scaffold protein.

Further research is needed to understand the interplay between Spd1, Spd2, and the RNR. It is possible that Spd1 and Spd2 form a dimer, as in *S. cerevisae* Sml1 is a dynamic dimer (Andreson et al, 2010).

III. Spd1 domains and functions

Three possible *in vivo* functions of Spd1 can be postulated so far: regulation of $Suc22^{R2}$ nuclear import, role in RNR architecture and *in vivo* control of RNR activity. The restraint of RNR activity possibly correlates with the *in vitro* inhibition or the nuclear sequestration of $Suc22^{R2}$, or a combination of both.

To further investigate these potential functions and understand in more depth the role of Spd1 in regulating RNR, alanine-scanning mutagenesis of Spd1 has provided 41 mutants scanning the whole gene. These mutants were used in different assays to assess the effect the mutations had on the described functions of Spd1:

- Structure-dependent RNR regulation: FRET of CFP-$Suc22^{R2}$ $Cdc22^{R1}$-YFP
- Inhibition of RNR: *in vivo* rescue of $Rad3^{ts}$ *Csn1* Δ lethality or rescue of spore formation defect in *Ddb1* Δ
- Nuclear import: $Suc22^{R2}$ nuclear localization
- Spd1 mutants protein stability and degradation

Apart from the FRET data, the other assays were done by collaborators but will be included here for the full understanding of this project's results (Nestoras et al, 2010) .

The Spd1 mutants stability will first be reviewed (Fig VII.2 part e.). *In vitro* and *in vivo* degradation was studied in the 41 Spd1 mutants with the aim of finding a degron domain, as described in the *S. cerevisae*'s Sml1. Although *in vitro* degradation was indeed dependent on Cul4-Pcu4-Ddb1 and the signalosome (Liu et al, 2003) , no clear domain for degradation was identified.

In vivo degradation of the Spd1 mutants was assayed by treatment of the cells with HU, leading to Spd1 degradation by a Cul4-Ddb1 pathway. Spd1 protein levels before and after HU were observed by SDS-PAGE, and again no domain seemed necessary for Spd1 degradation. However, some of the mutations seemed to affect the initial protein levels, therefore their stability.

Next the nuclear localization of $Suc22^{R2}$ in the mutants are shown in Figure VII.2 part d. *spd1* mutants 2, 14 and 26 have completely lost their role of nuclear import, and have the same phenotype as the *spd1* Δ. Other mutants, for example *spd1* mutants 3, 11-16, 33; have an increase sensitivity to HU in terms of $Suc22^{R2}$ nuclear localization, as upon treatment with the drug the small subunit is completely pan-cellular (compared to *spd1*+ wt which retains 20% of $Suc22^{R2}$ in the nucleus). The region corresponding to the *spd1* mutants 10-19 (HUG domain) is proposed to bind to $Suc22^{R2}$ and promote nuclear import, by comparison to the role of the HUG domain in the orthologues Sml1, Dif1 and Hug1. In contrast, some *spd1* mutants (*spd1* mutants 21, 38-41) exhibit the opposite phenotype i.e. a strong $Suc22^{R2}$ nuclear localization after HU.

The results of the experiments measuring *in vivo* regulation of RNR inhibition by Spd1 are shown in fig. VII.2 part b and c. Two phenotypes were tested to evaluate Spd1-dependent restraint of RNR activity. The first one (part b.) uses the ability of *spd1* deletion to rescue the lethality of the double mutant strain $Rad3^{ts}$ *Csn1* Δ. The concomitant loss of the Rad3 checkpoint protein and the signalosome component Csn1 leads to cell death (Liu et al, 2003) because in those cells Spd1 is stable and RNR activity inhibited throughout the cell cycle including in S-Phase where dNTPs are necessary. The viability was assessed by survival of the strains at restrictive temperature.

The second *in vivo* experiment was the use of the *Ddb1* Δ spore formation defect, which is reverted by deletion of Spd1 (Holmberg et al, 2005) . Again, if Ddb1 is not present, Spd1 will not be degraded and meiosis will not be completed. This defect of meiosis progression (thus RNR inhibition) was measured by spore formation.

Both assays gave similar results, showing the Spd1 HUG domain (*spd1* mutants 9-19) was important for RNR inhibition. Other *spd1* mutants have a

spd1 Δ phenotype (loss of inhibition): *spd1* mutant 26 as well as *spd1* mutants 34 to 41 seem partially important for the inhibition role of Spd1.

Taking together the data so far, we can conclude that the role of Spd1 in RNR inhibition does not necessarily correlate with the role of nuclear import of $Suc22^{R2}$. A particular example to illustrate this is *spd1* mutant 2: the nuclear import role in this mutant is completely abolished whereas it has full capacity to inhibit the RNR. In contrast, *spd1* mutant 10 and 11 have a normal capacity to import $Suc22^{R2}$ into the nucleus but have lost the inhibition function.

The data suggest the importance of the HUG domain for $Suc22^{R2}$ localization and RNR inhibition. Mutations in the C-terminus of Spd1 (*spd1* mutants 34 to 41) also influences RNR inhibition, and was called the Spd1 domain (Nestoras et al, 2010) . In contrast, mutations in the R1 region (putative $R1^{Cdc22}$ interaction domain by similarity with the R1 domain of Sml1) do not affect either function.

Finally, the FRET results are represented in Figure VII.2, part a. Of the 41 *spd1* mutants, 29 *spd1* mutations did affect the ability of Spd1 to promote CFP-$Suc22^{R2}$ $Cdc22^{R1}$-YFP FRET. In most of the 12 *spd1* mutants with a positive FRET signal, the FRET efficiencies were comparable to the *spd1*+ wt. In addition, those FRET efficiencies have the same profile as the *spd1*+ wt i.e. FRET is observed in both compartments of S-phase cells and G2-phase cells. *spd1* mutants 8 and 36 have slightly lower FRET efficiencies.

The FRET results do not correlate with the other Spd1 roles: *spd1* mutants 4 and 5 have the same profiles (normal $Suc22^{R2}$ import and RNR inhibition) but have opposite FRET results. Similarly the *spd1* mutants 12 and 13, that lost the RNR inhibition but have a normal importer role, have opposite FRET results. The converse is also observed, as *spd1* mutants with different localization profiles (*spd1* mutant 1 and 2) also have different FRET results, and *spd1* mutants with similar $Suc22^{R2}$ localization but opposite RNR inhibition (*spd1* mutant 2 and *spd1* mutant 14) can have opposite FRET signals.

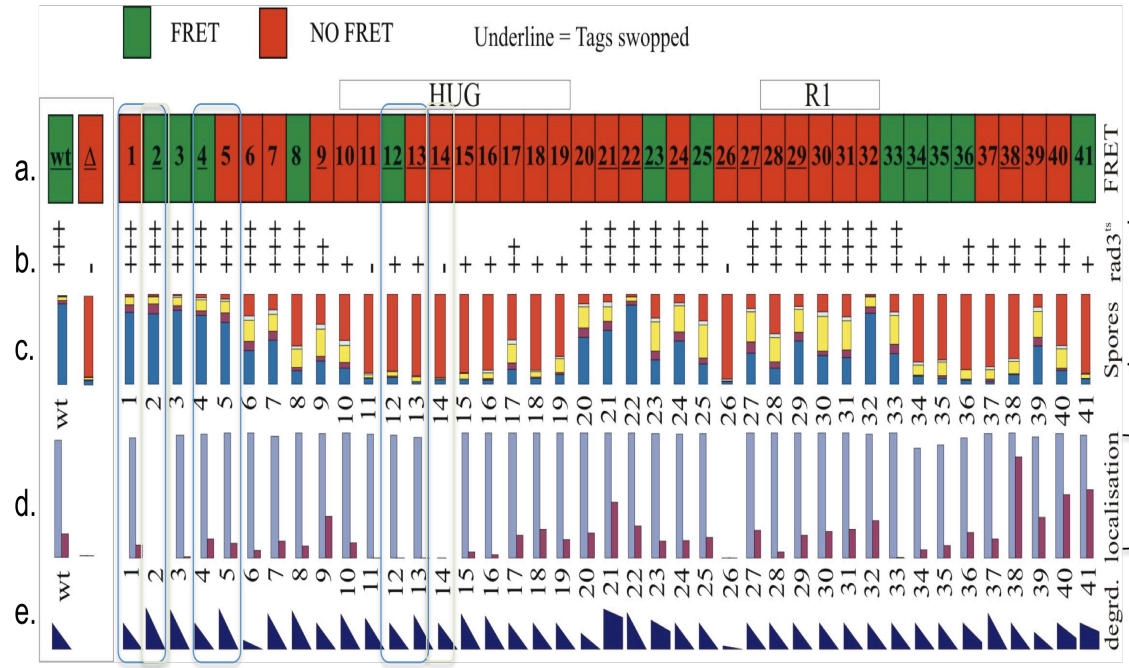

Figure VII. 2 Comparison of the FRET experiments with the other data of experiments conducted on the 41 spd1 mutants (Reproduced from Nestoras et al. 2010)

The spd1+ wt, spd1 Δ and the spd1+ mutants are compared in the different assays. The region corresponding to the HUG and RNR interaction domains are indicated above.

a. Ability to promote FRET between CFP-Suc22^{R2} and Cdc22^{R1}-YFP. Where the mutant number is underlined, FRET data has been verified by reversing the tags (i.e. YFP-Suc22^{R2} Cdc22^{R1}-CFP).

b. Inhibition of RNR in spd1 mutants strains, measured by the rescue of the synthetic lethality of the Rad3^{ts} Csn1Δ.

c. Inhibition of RNR in Spd1 mutants strains, measured by the rescue of the Ddb1Δ spores formation defect.

d. Spd1 nuclear import role assessed by nuclear accumulation of Suc22^{R2} (without HU -blue- and with HU –purple-).

e. Stability of the Spd1 mutants proteins estimated in vivo.

If one of the roles of Spd1 is to act as a scaffold for the RNR, this could occur in some of the *spd1* mutants background. The inherent structural flexibility of the IDP would be required rather than functional active domains. However comparing the FRET results with the secondary structure of Spd1, we can say that there is a slight tendency for the secondary structures in Spd1 to be important for the FRET of the RNR.

IV. RNR architecture after drugs or perturbed cell cycle

1. RNR inhibition: Hydroxyurea

HU is a free radical scavenger inhibiting the RNR activity, as the essential tyrosyl radical of $Suc22^{R2}$ is necessary for the enzyme's activity. In the presence of HU, the dNTPs levels drop drastically and cells transit to a slow replication mode (Poli et al, 2012). Also after addition of HU, $Suc22^{R2}$ relocalizes to the cytoplasm, due to checkpoint-dependent Spd1 degradation (Liu et al, 2003). The long-term transcriptional response of cells to HU and all the involved proteins is still under investigation (Dubacq et al, 2006) and we will only consider its role as a radical scavenger here. The consequence of the inactivation of the RNR will be a loss of the *de novo* synthesis of dNTPs, but a preservation of the pools present (Koc et al, 2004). Consequently replication initiation, rate, and length will be affected as they will all be reduced and slowed down (Davidson et al, 2012; Poli et al, 2012).

Upon treatment of the cells with HU, the FRET signal between CFP-$Suc22^{R2}$ and $Cdc22^{R1}$-YFP (and YFP-$Suc22^{R2}$ $Cdc22^{R1}$-CFP) is lost. The same results are achieved in the 12 *spd1* mutants that underwent FRET beforehand. The strains that did not FRET before still have a negative FRET signal.

The loss of the FRET signal is S-phase independent as demonstrated by the control with G2-phase blocked cells also loosing the FRET signal after addition of HU. Therefore, we can speculate that HU affects the RNR through modifying the structure or conformation of the $Suc22^{R2}$ $Cdc22^{R1}$ complex. As the free tyrosyl radical is embedded inside the small RNR subunit's structure, it could be that during the scavenging process, the RNR complex's structure is relaxed and/or the conformation modified. Another possibility is the modification of stoichiometry of the RNR complex as some partial higher order oligomerization of the RNR has occurred after HU treatment as observed by size exclusion chromatography. This observation was Spd1-independent. This suggests that there are various stiochiometry possibilities for the RNR complexes in *S. pombe*.

The FRET observed between the homo-dimers $Suc22^{R2}$ is also abolished after HU treatment. This could indicate that R2 becomes inactivated (apoR2) due to loss of the radical. This loss of radical could affect the structure of $Suc22^{R2}$ and have an effect on the general conformation of the complex, as it is known that the apoR2 has a different iron center organization to the active R2. It has been described that upon loss of the deeply embedded tyrosyl radical, the structure is modified with a slightly larger distance between the iron centers of each subunit. Although small, these differences in the inner structure of the R2 could be translated into the displacement of the fluorophores and loss of FRET.

Other reasons could explain the FRET signal abolishment, for example the energy transfer could be quenched. However, some publications have used HU and observed FRET on unrelated proteins: CFP-YFP FRET (Tian et al, 2007), GFP-RFP FRET (Morris et al, 2009) making us confident that this loss of FRET is due to biological reasons. In addition, when we added HU to a FRET positive DNA hairpin *in vitro*, preliminary results showed that the positive FRET signal remained.

2. RNR activation: 4NQO

The RNR complex is activated after DNA damage, and 4-NitroQuinoline 1-Oxide is an adequate drug to study DNA damage as it forms DNA base adducts through the 4NQO resulting metabolite 4-hydroxyaminoquinoline (Bailleul et al, 1981) (Thomas et al, 1991). DNA damage will trigger the cell cycle DNA damage checkpoint (Rad3 and Chk1-dependent) followed by an induction of the expression of the RNR genes leading to a 2 fold-increase in dNTPs in *S. pombe* (Hankansson et al, 2006b). Note that in *S. pombe* this increase in dNTPS levels is less than the increases observed in *E. coli*, *S. cerevisae* and mammals. The levels of dNTPs are higher following DNA damage than the increase of the dNTPs levels observed during the S-Phase of an unperturbed cell cycle (Chabes et al, 2003a).

Considering these observations, it is reasonable to assume that after addition of 4NQO, the RNR complexes will be active or even “hyper-active” (or “mature” complexes) to provide those higher levels of dNTPs locally for DNA repair. The

process of the dNTPs synthesis is not entirely clear, as questions remain on the nature of the dNTPs synthesis location and transport. Thus leading to the emergence of dNTPs channeling models. Channeling of dNTPs can be defined as direct transfer from one enzyme to the other, resulting in small sizes of dNTPs pools with a rapid turnover. The dNTPs compartmentalization and channeling hypothesizes have been discussed for many years (Mathews & Slabaugh, 1986) (Reichard, 1987), in addition recent research regarding dNTPs synthesis included as part of the DNA replication complex emphasizes this model (Poli et al, 2012) (Salguero et al, 2012).

Also involving RNR aggregation at a specific localization, recent studies have shown the recruitment and importance of RNR complex at the sites of DNA damage in form of foci (Niida et al, 2010a) (Moss et al, 2010) . In this context, it is interesting to remember the observation of the strong Suc22^{R2} nuclear localization after treatment of 4NQO. dNTPs levels are hard to measure *in vivo*, and the RNR proteins are abundant, thus limiting resources to investigate this hypothesis in a direct manner. However the above-mentioned research supports the suggestion that active RNR complexes can be in the nucleus of the cell.

The FRET results after DNA damage are interesting: the *spd1*+ wt CFP-Suc22^{R2} Cdc22^{R1}-YFP strain (as well with swapped tags) retain its positive FRET signal after treatment with 4NQO and in the *spd1* deleted strains, the FRET signal stays negative. However, all of the *spd1* mutants have a positive FRET signal after treatment with the DNA damaging agent, even the *spd1* mutants that did not have the capacity to FRET between the fluorophores beforehand now have the ability for positive FRET between CFP-Suc22^{R2} and Cdc22^{R1}-YFP. Like the *spd1*+ wt strain, the FRET efficiencies are positive throughout the cell and the cell cycle, although some *spd1* mutants have lower FRET efficiencies. The *spd1* mutants have different characteristics of RNR inhibition, RNR localization and Spd1 protein levels; but they have in common the ability to enable FRET after DNA damage.

From these observations, we can propose that upon DNA damage, there is a specific “mature/active” RNR structure in place, partially dependent on Spd1 (as the Spd1 deleted has no FRET signal). Spd1 could act as a scaffold (Gunasekaran et al, 2003), binding to both RNR subunit therefore inducing

modifications in the RNR complex, and even after degradation of Spd1 after DNA damage, the complex could be formed into the correct conformation allowing FRET. This mature/active complex could be through a modification of stoichiometry or a change in structural conformation.

We have seen how dNTPs are important for the DNA replication, in addition, the right balanced amount of the 4 dNTPs levels is important for limiting mutations (Kumar et al, 2010) . dNTPs levels are also important after DNA damage, to enable DNA repair, but also higher levels of dNTPs will allow DNA polymerases to bypass certain lesions (Sabouri et al, 2008). Some *spd1* mutants (i.e. *spd1* mutant 26) have very low protein expression, but it could be that very small amounts of the scaffold protein are enough. As mentioned earlier, the IDPs proteins have peculiar structural qualities, and we can speculate that upon DNA damage, the IDPs will conform their structure to form a scaffold for the RNR. It is also possible that some other proteins are involved.

Other interesting results were the homo-complexes FRET experiments, indicating that the small RNR subunits $Suc22^{R2}$ exhibits close interactions in normal cells and in cells after DNA damage. Although the FRET efficiency is not entirely quantifiable, the FRET efficiency of CFP-$Suc22^{R2}$ YFP-$Suc22^{R2}$ after 4NQO is reduced. This lower FRET efficiency could result from a fast turnover of new $Suc22^{R2}$ supply, or a modification in conformation, but $Suc22^{R2}$ remains in dimer after DNA damage.

An interesting observation about the ring structure of six big subunits $Cdc22^{R1}$ and a dimer of $Suc22^{R2}$ is the ratio of tyrosyl radicals available for the number of active sites: two to six. Thus this leads to the proposal of a dynamic turnover of $Suc22^{R2}$, providing new active tyrosyl radicals to the ring of $Cdc22^{R1}$.

It could be asked why the RNR complexes are not always in a “hyper-active” or “mature” form, but it has to be remembered that levels of dNTPs have to be kept to an optimum level to avoid an increase in the mutation rate.

3. Heat shock

Transcription of heat-shock proteins (HSPs) occurs in response to heat stress but also to other stresses (Gallo et al, 1991) . In non-stressed cells, HSPs function as chaperones, with roles varying to maintaining newly

synthesized protein in an unfolded state or assisting proteins to form higher order complexes. Upon heat shock, HSPs have various functions: sequestration of heat-damaged proteins (preventing protein aggregation) as well as regulating unfolded proteins (Morano et al, 2012) .

Heat shock has been described to affect the transcription of RNR: a larger *suc22+* transcript of 1.9kb is observed (Harris P, 1996). Compared to the smaller 1.4kb *suc22+* transcript, the larger transcript (1,9kb) has its initiation codon 550 bp upstream. The 1,9kb transcript is present at low levels during a normal cell cycle, but increased after heat shock in an Rad1-independent but Caf1-dependent manner (Harris P, 1996) (Takahashi et al, 2007).

After heat shock in the RNR –tagged strains, the FRET efficiency is maintained and even increased in the *spd1+* wt CFP-Suc22^{R2} Cdc22^{R1}-YFP. This increase in FRET could have several explanations: increase of FRET positive complexes in the population, or the fluorophores are in general closer together corresponding to a modification of the conformation of the RNR complex. Since, we are observing the interaction between tagged proteins, we are not detecting the hypothetical protein resulting of the larger *suc22+* transcript.

4. Live cell imaging observations

Finally, some very dynamic aggregations of RNR have been observed during live cell imaging. Although verifications have first to be made in order to confirm that those RNR foci are not laser-damage induced, some hypothesis can be made with regards to their origins. These could be the colocalization of the RNR with the replisome, or DNA repair factories. RNR could be recruited locally to the DNA to facilitate the replication and repair by providing dNTPs locally (Niida et al, 2010a). Other possibilities, which may be worth investigating, are colocalization with the spindle pole body, PML bodies or other vesicle-like formation in the cells.

The origins of these aggregates remains unexplained, but may be potentially interesting to have a clearer view of the dynamics and regulation of the enzyme.

V. RNR Oligomerization

Protein interactions are critical for many cellular processes in cells. Such interactions include the stable association of proteins within multi-subunit complexes and the transient association of regulatory proteins. Many of these multi-subunit complexes have been described in heterocomplexes, but also homocomplexes. Sometimes these quaternary structures are shaped in rings, for example: MCM complex , Cohesin , ORC complex, PCNA , Ku complexes, heat shock proteins… Many of these ring-structured complexes are linked to DNA-related mechanisms.

The simple colocalization of two proteins in the same subcellular compartment does not provide evidence that they interact; therefore to supply proof of protein-protein interaction we used FRET (Pietraszewska-Bogiel & Gadella, 2011). FRET is based on the ability of a donor fluorophore to transfer some of the energy from its excited state to a close acceptor fluorophore. Because FRET energy transfer is highly distance-dependent, detection of FRET requires the two fluorophores to be within 1-10nm, the distance typically found for directly interacting proteins.

Through our FRET data we have observed structural modifications of the RNR, which were dependent on Spd1 but also on the different drugs used. Conformational change is expected in the RNR as both subunits have various flexible domains and it has been suggested that different loops within the structure will allow conformational change (Larsson, 2004) (Xu et al, 2006) to adapt to the various effectors as well as substrates. Oligomerization has also been described in RNR complexes throughout different species (Hofer et al, 2012) . Considering the low sequence identity between those different species, the superposition of the obtained structures resulted in impressively high similarities. In addition, higher order complexes seem present throughout the different RNR species.

In vitro studies have been investigating in more detail the oligomeric formation of RNR. In mammals, $\alpha_2\beta_6$ (α_2: 2xR2 and β_6: 6xR1) is the major RNR form present, induced by ATP as well as dATP (Kashlan et al, 2001) (Rofougaran et al, 2006). The inhibited dATP RNR form has been demonstrated

to be in a ring-shaped homocomplex (Fairman, 2011) and similar observations were made for *S. cerevisae* by the same team (Fairman, 2011). The classical $\alpha_2\beta_2$ complexes seems to be only a minor form present. While it has been proposed that the RNR complex cycles from the active ATP-induced $\alpha_2\beta_6$ to the inactive dATP-induced $\alpha_2\beta_6$, the two forms seem to have different structures. Indeed, a point mutation disabling RNR to form dATP-dependent R1 hexamers could still form ATP-dependent hexamers (Fairman, 2011) (Hofer et al, 2011). This suggests a different structure for the active ATP-induced RNR form, although with similar stoichiometry.

In *E. coli*, similar larger complexes were depicted with the RNR varying from an active $\alpha_2\beta_2$ to an inactive $\alpha_4\beta_4$ (Rofougaran et al, 2008b). The inactive RNR form in *E. coli* has also been recently crystallized (Ando et al, 2011) and is also in a ring structure although a different ring: sequential small and big RNR dimers make the $\alpha_2\beta_2\alpha_2\beta_2$ ring.

In addition, other stoichiometries have been described, for example another inhibited RNR form was observed in a stable $\alpha_6\beta_6$ stiochiometry after addition of gemcitabine to the ATP induced α_6. Three β_2 were shown to bind to the α hexamer (Wang et al, 2009). Gemcitabine is a cytidine-based substrate analogue. The inhibition of RNR activity by gemcitabine is caused by the decay of the tyrosyl radical on the small subunit R2 and has been observed to alkylate the catalytic cysteine residues of the large subunit R1. A crystal structure of the gemcitabine bound-R1 in *S. cerevisiae* shows that the orientation of gemcitabine in the catalytic site is altered from the orientation of the natural cytidine-based substrate.

All these recent findings confirm the model of an $\alpha_n\beta_n$ regulation with various subunits “n”. The RNR activity regulation is linked to these various oligomeric conformations, by abolishing or facilitating the correct electron chain transport.

All these structures take into account the allosteric regulation of the RNR. As we wanted to investigate more precisely the stoichiometry of RNR with regards of the effects of Spd1 and Spd2, we decided to take the *S. pombe* RNR system *in vitro* to study the different RNR forms in a controlled environment, and observe the direct effect of Spd1 on the RNR complexes *in vitro*. This

would also allow us to estimate more precisely which RNR oligomeric or conformational forms have the ability to FRET or not. The aim was to correlate *in vivo* FRET data with the *in vitro* precision to allow us further interpretation of the *in vivo* data.

VI. Conclusion

The results of this project with other observations, allow us to propose a model with regards to the role of Spd1 and Spd2 in the structure-dependent regulation of RNR. Also, the mechanisms behind the activation and inactivation of RNR in vivo, independently of the regulators can be hypothesized.

We suggest that Spd1 mediates the formation of immature RNR complexes, and after Spd1 degradation those complexes are in the optimal conformation for catalytic activity. In *spd1* deleted cells, the absence of Spd1 would drive RNR to form an alternative architecture. These alternative RNR complexes are abundant and not inhibited by Spd1, thus the RNR activity is not limited by this variant architecture.

In support of this model, another IDP has been described with very similar roles: the p27 cyclin-dependent kinase inhibitor. It mediates the formation of immature inactive Cdk2-CycA complexes (Sherr & Roberts, 1999) (Borriello et al, 2007; Galea et al, 2008a) by binding to CyclinA and Cdk2, independently but simultaneously. The protein p27 has two distinct independent binding sites for CyclinA and Cdk2, and folds after binding, leaving only a flexible loop unbound. Interestingly, p27 binds Cdk2 inside a cleft, mimicking the method used by RNR and ATP, thus inhibiting Cdk2. These bindings involve drastic conformational changes regulating the complexes. After p27 degradation by phosphoprylation (Uranbileg et al, 2012), the complex is actived. This mechanism has since been described in other similar protein complexes (Sherr & Roberts, 1999) (Krukenberg et al, 2011) and suggested to strongly influence the cell cycle.

In the RNR complex, the R2 C-terminus is buried in a cleft of R1, and R2 C-terminal mimicking peptides interfere with this optimal conformation (Cohen, 1986) (Hamann et al, 1998). It has also been suggested that in *S. cereveisae*

(Zhao et al, 2000) Sml1 using its C-terminal binds this same R1 cleft, which is necessary for full RNR inhibition.

With regards to the drugs used, we can only speculate about the effect they have on the RNR complexes. HU is a radical scavenger and inactivates R2 thus the RNR activity. Considering the depth of the radical inside the R2, as well as the described different iron centre structure upon loss of the radical, we can expect a conformational change readable by loss of FRET. In addition, if we consider the ultimate effect of gemcitabine (loss of free radical) and the observed higher order complex associated with this RNR inactivation we can speculate that the same occurs in presence of HU. Partial higher-order complexes were observed after addition of HU to our strains.

The 4NQO result is less straightforward to interpret, but it seems to represent the active form of RNR. The complex in which RNR is formed after DNA damage is optimal for FRET to occur and seems dependent on Spd1. Maybe the inherent qualities of the IDP are required to configure the RNR in an optimum complex to provide high supplies of dNTPs.

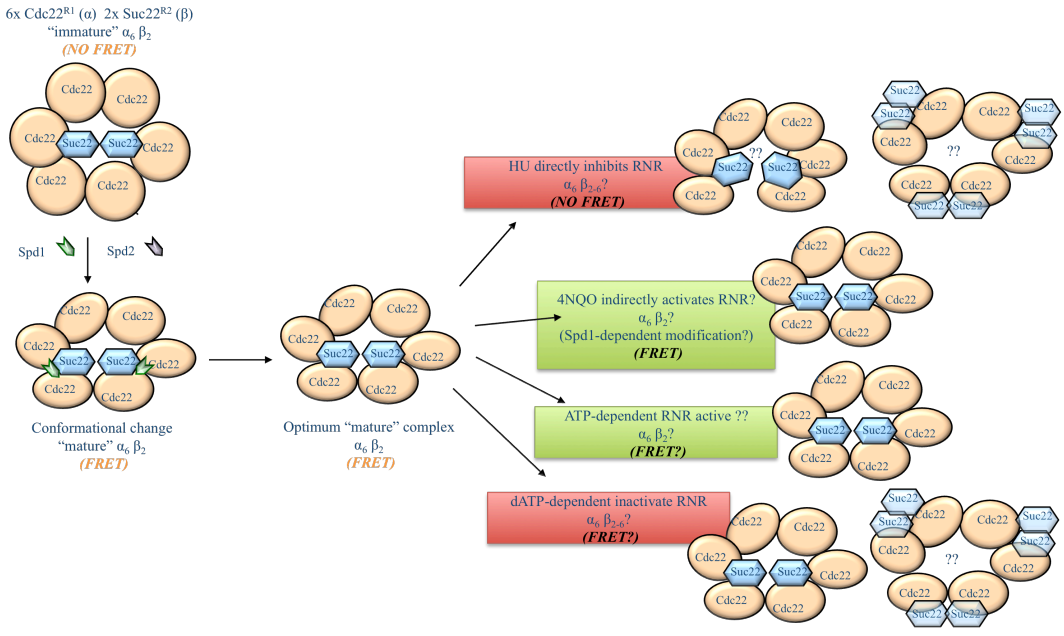

Figure VII. 3 Schematic model based on the hypothesis suggested during this project

Diagram representing the models for RNR regulation in S. pombe by structure-induced modifications. Without Spd1 the RNR complex is not in a specific conformation, but with the addition of Spd1 and Spd2, RNR is conformed to a more optimum conformation. After degradation of the RNR regulators proteins (Spd1 and Spd2), the RNR complex can still be

affected by other effectors. HU will inhibit the complex, resulting in a different conformation or oligomerization. DNA damage by 4NQO will keep the RNR complex in an optimum conformation for efficient dNTPs production. Activation of RNR activity by ATP will result in an efficient conformation for dNTPs production, and it has been described to be in a ring shaped of α_6 with a dimer of β_2 inside the structure. The inhibition of RNR by dATP will lead to a variant structure hexameric α_6, possibly $\alpha_6\beta_{2\text{-}6}$.

It is now accepted that the allosteric regulation of RNR happens through an $\alpha_n\beta_n$ mechanism, although this has been mostly studied *in vitro* and with dATP and ATP as effectors. Through this project we can say that the RNR regulators in *S. pombe* (Spd1 and Spd2) could also have structure-dependent regulatory functions.

Understanding the full details of RNR regulation is of great interest for basic research, but is also for the interest for drug developments. RNR inhibition is widely used and considered for treatments against viruses, cancer and other diseases (Cooperman, 2003) (Cerqueira et al, 2006) .

CHAPTER VIII Future directions

I. FRET assays *in vivo*

1. Complete the Spd2 FRET data

It would be interesting to obtain the *in vivo* FRET experiment with *spd1* Δ and *spd2* Δ after treatment with 4NQO to understand if Spd2 has a similar role to Spd1.
In addition, combining some *spd1* mutants with *spd2* Δ for FRET analysis without treatment, but especially after treatment with 4NQO.

2. Confirm the inactive RNR FRET data

As the FRET results after HU treatment was at first unexpected, additional experiments in conditions where RNR is inhibited would confirm this data. RNR inhibitors are various: nucleoside analogues, iron chelator or free-radical scavengers.

3. Confirm the active FRET (4NQO) data

Although 4NQO was a good tool to obtain active/"hyper-active" RNR complexes, it would be interesting to have a second experiment where upon DNA damage the FRET signal is positive in the spd1 wt strains as well as the *spd1* mutants.
Therefore, other damaging agents could be used: MMS and/or Bleomycine.
To ensure of the correct DNA damage occurrence as well as the DNA damage response pathways have been activated, controlling Chk1 phosphorylation would be an important control.

II. Single-molecule microscopy experiments

1. Further RNR purified proteins characterization

In first instance, Cdc22^{R1}-CFP and Cdc22^{R1}-YFP have to be purified from *E. coli* in order to characterize the proteins with regards to their diffusion time and stoichiometry for use in subsequent experiments.
Addition of dNTPS to the purified Cdc22^{R1} is an essential part for future directions, as the aim is to obtain an ATP-activated RNR as well as dATP-inhibited RNR.

2. Binding assays using RNR and the purified Spd1 proteins (wt and mutants)

This will enable us to observe a shift in the diffusion time, therefore a binding. Then the more precise measurements can be done using both tagged RNR subunits, adding or not the purified Spd1 proteins

- YFP-Suc22^{R2} with Cdc22^{R1}-CFP without Spd1 (and swapped tags)
- YFP-Suc22^{R2} with Cdc22^{R1}-CFP with Spd1 (and swapped tags)
- YFP-Suc22^{R2} with Cdc22^{R1}-CFP with the Spd1 mutants (and swapped tags)
- YFP-Suc22^{R2} with Cdc22^{R1}-CFP with Spd1 and Spd2 (and swapped tags)
- YFP-Suc22^{R2} with Cdc22^{R1}-CFP with Spd2 (and swapped tags)

In addition, the presence of the tyrosyl radical should be monitored to relate to the *in vivo* data.

3. *In vitro* FRET of the RNR

Finally, we could then proceed to the FRET measurement *in vitro* using the same samples as mentioned above. The FRET data *in vitro* should correspond to the *in vivo* data, and the advantage of a more controlled environment with a precise knowledge of the stoichiometry of each subunits will

help to interpret previous data. We should be able to draw a conclusion on the meaning of positive FRET signal and negative FRET signal in the context of the RNR proteins.

4. *S. pombe* purified proteins experiments

Further investigation could also be done with the endogenous purified RNR proteins. The purification process should be repeated in bigger volumes, and find methods to purify cross-linked RNR complexes after treatment of the cells with HU as well as 4NQO.

III. Additional key biochemistry experiments

1. Native PAGE gels of the purified proteins

This could be done to assess the stiochiometry of the purified RNR proteins, from *E. coli* as well as from *S. pombe*. Not only would these data indicate the state of the proteins, but it would confirm the photobleaching step assay done on the TIRFM.

2. Size exclusion chromatography (SEC) of RNR in *S. pombe* cells

Additional SEC data could be carried out in order to understand RNR regulation. After HU or 4NQO treatment to the cells, in the various RNR tagged strains: *spd1* Δ, *spd1* mutants, *spd2* Δ, and *spd1* Δ *spd2* Δ. This data could maybe help us correlate the FRET data with the oligomerization status of the RNR complexes.

IV. Additional Microscopy Experiments

1. $Suc22^{R2}$ dynamics and FRAP

As mentioned during this thesis, the small subunit $Suc22^{R2}$ has localization dynamics throughout the cell cycle, with mostly nuclear localization in G2 but partial cytoplasm relocalization during S-phase. Classical intensity measurements could be done on the long time-scale videos, but in addition, FRAP (Fluorescence Recovery After Photobleaching) could provide us information regarding the diffusion times of $Suc22^{R2}$ in various conditions and strains, but it could also supply protein binding data.

2. Determining the nature of the RNR foci

Confirming the laser power correlation with the number of foci followed by observing if the foci colocalize with various other cellular components could be of interest (PCNA tagged proteins to follow replication, DNA damage, using rad22 foci, degradation vesicles, spindle pole body (SPB) by using the marker Sad1 for example).

3. PALM

An important step for this project and future experiments is the use of PhotoActivable Light Microscopy (PALM). As mentioned in the introduction, this method will improve highly the resolution, achieving single molecule levels *in vitro*, along with other upcoming potentials.

CHAPTER IX Annexes and Publication

I. Annexe 1: FRET measurement by FACS

Alternative methods to measure FRET results in a faster and more automated way were of interest during this project. Therefore, the idea to use FACS for measuring the YFP fluorescence in a same amount of cells did seem testable, as in a FRET negative strain, there should be less YFP fluorescence. The method had been described before (Banning et al, 2010; You et al, 2006) thus the idea to try it with *S. pombe* cells.

In first instance, comparison between a FRET positive strain (CFP-Suc22^{R2} Cdc22^{R1}-YFP *spd1* wt) and a FRET negative strain (CFP-Suc22^{R2} Cdc22^{R1}-YFP *spd1* Δ) provided us with a specific result: distinct profile were observable as the FRET negative strain had less YFP fluorescence (shift of the measurements on the x axis: "FITC").

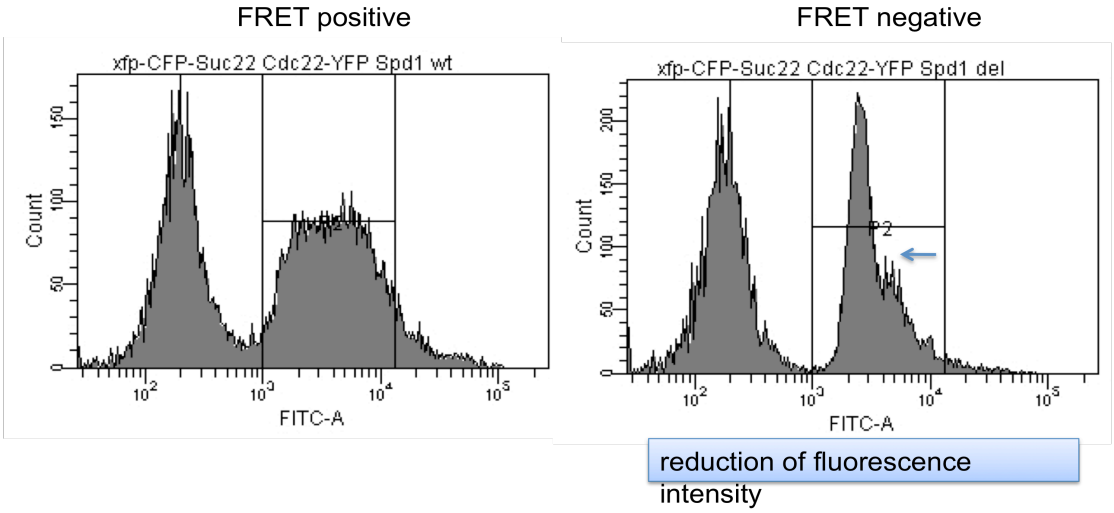

Figure IX. 1 FACS profiles of FRET positive and FRET negative strains

The FRET positive strain CFP-Suc22^{R2} Cdc22^{R1}-YFP Spd1 wt and the FRET negative strain CFP-Suc22^{R2} Cdc22^{R1}-YFP Spd1 Δ were compared after measurements on the FACS. Set quantities of unsynchronized cells were tested using s. pombe standards. The YFP fluorescence was measured using the FITC filters.

These results were encouraging therefore further controls were done to ensure the observable results were genuine. Non-tagged strains (501, 503) as well as single tagged strains: YFP-Suc22^{R2} and Cdc22^{R1}-YFP (positive YFP signal and "negative FRET" control), CFP-Suc22^{R2} and Cdc22^{R1}-CFP (negative YFP signal control) were used on the system. The FRET positive and FRET negative strains as well, enabling us to verify the controls and the repeatability of the system. All these controls were correct and reproducible.

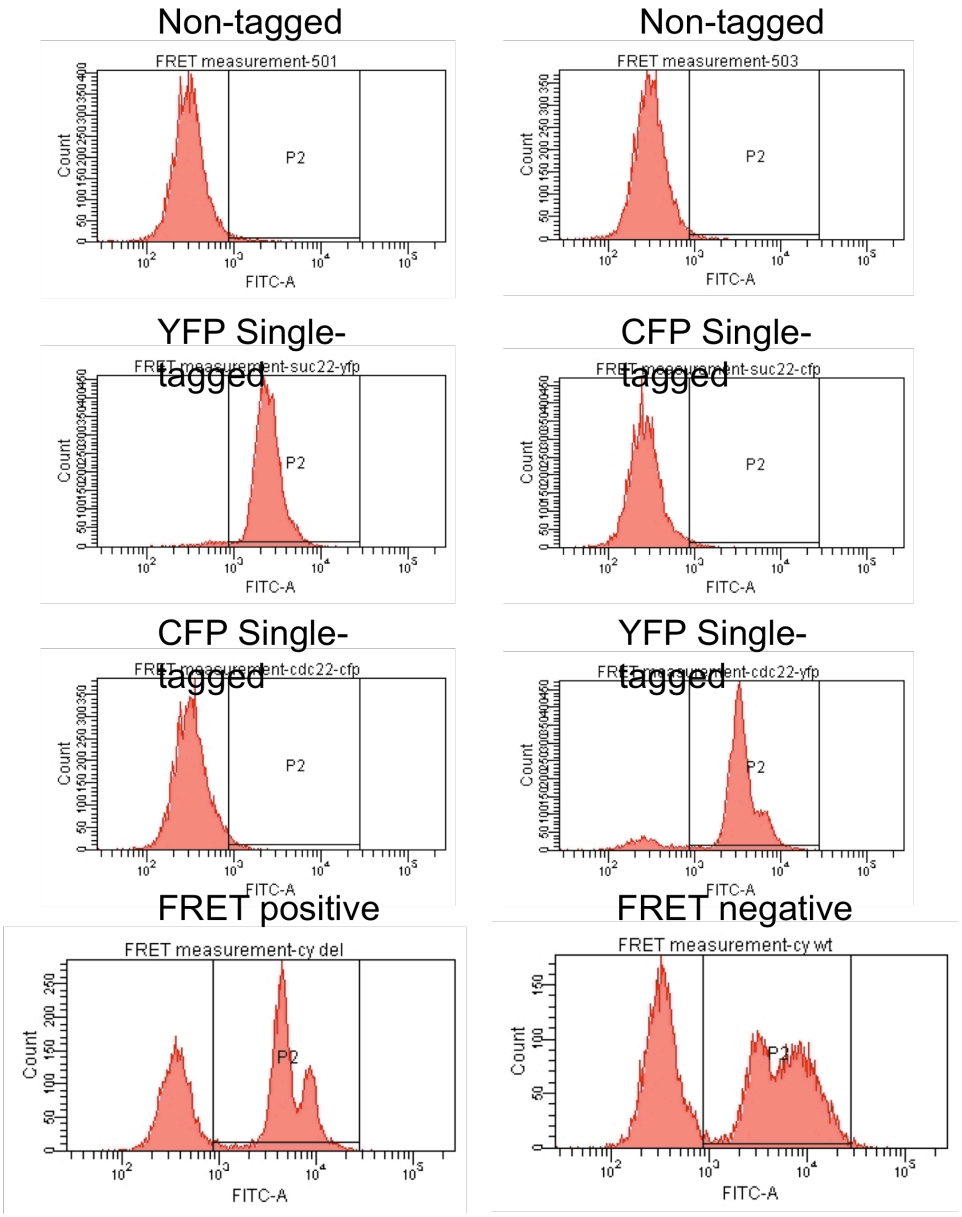

Figure IX. 2 FACS profiles of FRET controls

FACS measurements of the FRET was controlled using non-tagged strains (501 and 503) as well as single tagged strains (CFP/YFP-Suc22^{R2} and Cdc22^{R1}-CFP/YFP). The

FRET positive strain CFP-Suc22^{R2} Cdc22^{R1}-YFP Spd1 wt and the FRET negative strain CFP-Suc22^{R2} Cdc22^{R1}-YFP Spd1 Δ were also used. Set quantities of unsynchronized cells were tested using s. pombe standards. The YFP fluorescence was measured using the FITC filters.

Finally, various *spd1* mutants were measured on the FACS by a blind method to ensure a clear read-out would be possible. Unfortunately, the FACS profiles were not as straightforward as the FRET positive and FRET negative profiles, resulting in unsure interpretation. On the figure below, the FRET results as known by confocal measurements are annotated. Unfortunately it was not possible to distinct the results and correlate them to the know FRET results.

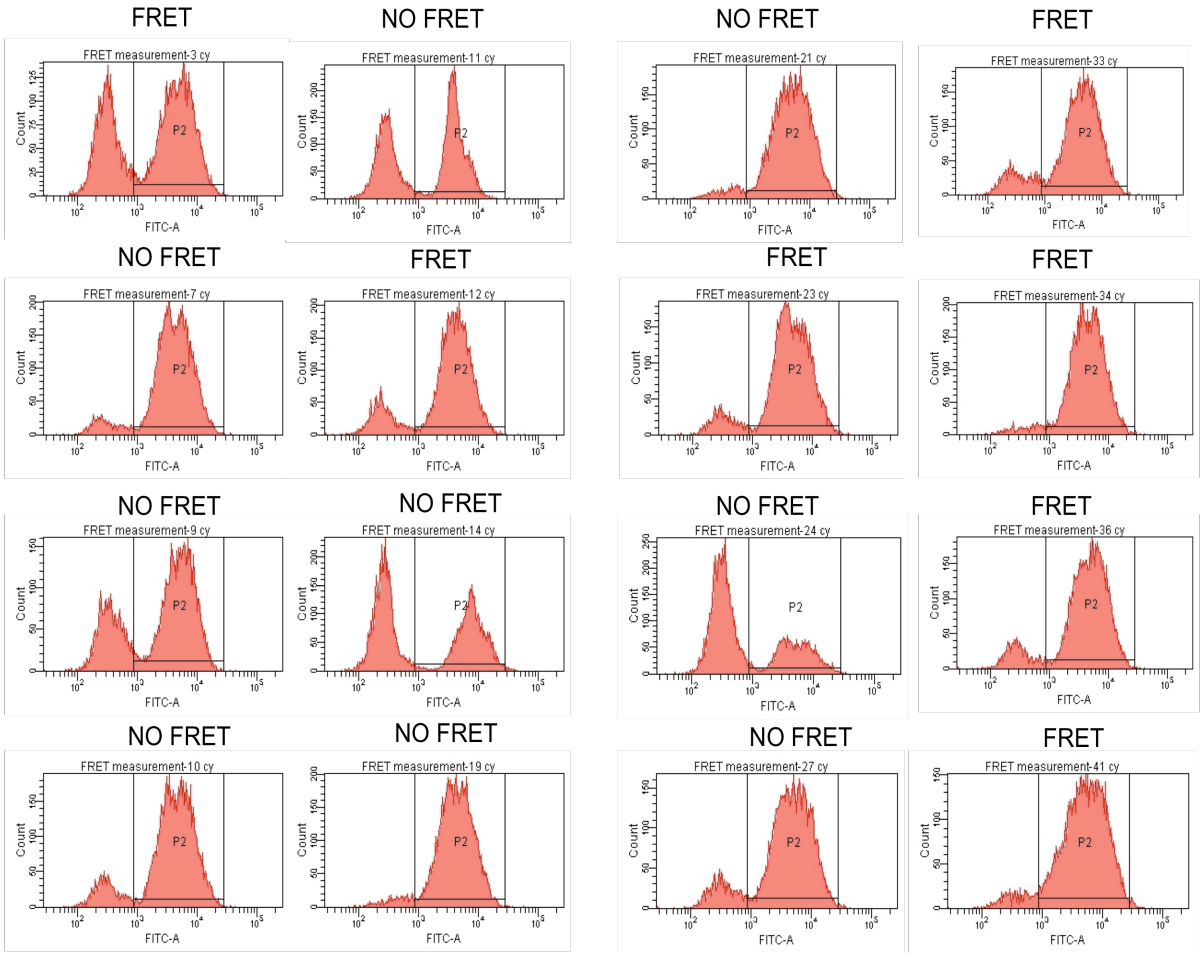

Figure IX. 3 FACS profiles of spd1 mutant strains

FACS measurements profiles of some spd1 mutant strains. The FRET status as measured by confocal is mentioned above. Set quantities of unsynchronized cells were tested using s. pombe standards. The YFP fluorescence was measured using the FITC filters.

II. Annexe 2: List of primers

Cloning:

pUC19-inserT-verif-F	5' GAAATACCGCACAGATGCGT 3'
pUC19-inserT-verif-R	5' GCTGGCACGACAGGTTTCCCG 3'
XFP-Suc22-F-1	5' GAATGGTATCAAAGTTAACTTCA 3'
XFP-Suc22-F-2	5' GCTCTGAAGTTCAGATCCCTG 3'
XFP-Suc22-R-1	5' CCTTAGGTTCACGAATGTATG 3'
XFP-Suc22-R-2	5' GACTTCAGCTCTGGTCTTGT 3'
Cdc22-XFP-F-1	5' GCCGGTACTCCTCGTCCCCAACT 3'
Cdc22-XFP-F-2	5' GCCGTAGCAATATGCGC 3'
Cdc22-XFP-F-3	5' GTCTTAAGACTGGAATGTACT 3'
Cdc22-XFP-R-1	5' GCCTTTCCATTCTTTATAACTG 3'
Cdc22-XFP-R-2	5' GCATCGGCAAGACCTTGAACA 3'
Cdc22-XFP-R-3	5' GTCGTCTTTCATCGTAACGAGG 3'
T7-Check-f	5' AATTAATACGACTCACTATAGGG 3'
T7-Check-r	5' TGCTAGTTATTGCTCAGCGG 3'
yfp-A-peT3A-F	5'AAGGAGATATACATATGTCTAAAGGTGAAGAATTATTCA 3'
yfp-A-peT3A-R	5' GTCATGCTAGCCATATGTTATTTGTACAATTCATCCATACC3'
Cdc22-CDNA-infusion-F	5' AAGGAGATATACATATGTTTGTATACAAAAGAGACGGACGTC 3'
Cdc22-CDNA-infusion-R	5' GACGGAGCTCGAATTCGGCTGAGCACATTTCGCAAGC 3'
New-P-Cdc22-F	5' AAGGAGATATACATATGTTTGTATACAAAAGAGACGGACGTC 3'
New-P-Cdc22-R	5' GTCATGCTAGCCATATGGGCTGAGCACATTTCGCAAGC 3'

New-l-xfp-F	5' AGCCCATATGGCTAGCGGTTTAATGTCTAAAGGTGAAGAATTATTC 3'
New-l-xfp-R	5' CACCAGTCATGCTAGCTTATTTGTACAATTCATCCATACCATGG 3'
InFusion-l-x-F-fin	5' GCTCAGCCGAATTCGAGCTCGGTTTAATGTCTAAAGGTGAAGAATT 3'
InFusion-l-x-R-fin	5' TGCTCGAGTGCGGCCGCTTATTTGTACAATTCATCCATACCATGG 3'
pET3a_L_F	5'TATGTTTGTATACAAAAGAGACGGACGTCGTAGGCGCGCCG 3'
pET3a_L_R	5'GATCCGGCGCGCCTACGACGTCCGTCTCTTTTGTATACAAACA 3'
cdc22EX2_F	5'GACGGACGTCAAGAGAAAGTGG 3'
XFP_R	5'AAGTGGCGCGCCTTATTTGTACAATT 3'
suc22XFP_pET_F	5'GGGGAAGCTTCATATGTCTAAAGGTGAAGAATTATTCACTGGT 3'
suc22_pET_R	5'GGGGGATCCCTAAAAGTCCTCATCGATTGTAAATGTATGATC 3'

Strains Checking

Cdc22-Check-F	5’ TTATTGAGATGAACTATTACTC 3’
Cdc22-Check-R	5’ AAACATTAAAAGAAACAATAAAATGT 3’
Cdc22 Check-2 F	5' CCGGTTTCCACTCTTAGCTT 3'
Cdc22 Check-2 R	5' CCATTCTGAGCCTGCTCACT 3'
Suc22-Chk-F	5' CAA GAG ATA ATC GCG GTG GAA GA 3'
Suc22-Chk-R	5' GCA AAA GTG AGT AGG TCT CAG AG 3'
Spd1-Chk2-F	5' GATCCGTGTTCGATAGGCAT 3'
Spd1-Chk2-R	5' GAGAGACAAATGCCCAAAAG 3'
Spd2-Check- F	5’ CATTGAAAATTAAAAGATTGCTC 3’

Spd2-Check-R1	5'CAGGCTTGGCAAAAGAATC3'
Spd2-Check-R2	5' GAGTAATAGTTCATCTCAATAA 3'
Spd2-Check2-F	5' GTAATTGCTAGCATTTGTGATTCACC 3'
Spd2-Check2-R2	5' CCAATAGTATCGAAAGCTTTATCTTGC 3'
Ura4-R2	5' CCAACCAGCTTCTCTATATCTCTTG 3'
XFP reverse	5' TGTGGTCTCTCTTTTCGTTTGGA 3'

Strains Construction and other primers:

n-Term spd1 F	5'AAACGTCACAAAGCCGAGTAGCAAACGCTCCCACAACCAAACACTACACAAAGGTTCGTCGACAATTTATTTTGGAAAAAATGTCTAAAGGTGAAGAATT 3'
n-Term spd1 R	5'GCTTTCGGGAAGCTGAGGACGCATTGAAGACTCAGGCTGCTCAACATGAGTCTTTGTGGTCATAACTCGCTTGCTGCTGTGCATACCACCCCCGCGCCC 3'
n-Term cdc22 F	5' AGCGTGACGCGTCTGAACGCGTTTTTCATTTACTATAAATATTCCCGGTATTTACCACCTTACAAACTAGAACAAACACGATGTCTAAAGGTGAAGAATT 3'
n-Term cdc22 R	5' AAACGGCAACGTTGTAACAAAATTTCTACTAATCTTCTAACTGTATTTTATTTCCTGTTTCATACCTCTTTTGTATACAAACATACCACCCCCGCCGC C 3'
mEOS2-subClone-Cdc22-F	5' AAAA TTA ATT AA CATGAGTGCGATTAAGCCAGACAT 3'
mEOS2-subClone-Cdc22-R	5' AAAAGGCGCGCCTTATCGTCTGGCATTGTCAGGC 3'
mEOS2-subClone-suC22-F	5' AAAAGGATCCATGAGTGCGATTAAGCCAGACAT 3'
mEOS2-subClone-suC22-R	5' AAAAGTCGACTCGTCTGGCATTGTCAGGCAAT 3'
pFA6A-verif-F	5' TTATGTATCATACACATACGATTTAG 3'
pFA6A-verif-R	5' GAGCCGTAATTTTTGCTTCGC 3'

pGEM-verif-F	5' CGTTGTAAAACGACGGCCAGT 3'
pGEM-verif-R	5' CAGCTATGACCATGATTACGCC 3'
GFP-F	5' TAAAGGTGAAGAATTATTCACTGGTG 3'
GFP-R	5' TATTTGTACAATTCATCCATACCATGG 3'
CFP-F	5' CTTTGACTTGGGGTGTTCAATG 3'
CFP-R	5' CGAAAGGGCAGATTGTGTGG 3'
YFP-F	5' GGCCAACACTTGTCACTACTTTC 3'
YFP-R	5' GATCTTTCGAAAGGGCAGATTGATAG 3'

III. Annex 3: Publication

Regulation of ribonucleotide reductase by Spd1 involves multiple mechanisms

Konstantinos Nestoras, Asma Hadi Mohammed, Ann-Sofie Schreurs, et al.

Genes Dev. 2010 24: 1145-1159
Access the most recent version at doi:10.1101/gad.561910

Regulation of ribonucleotide reductase by Spd1 involves multiple mechanisms

Konstantinos Nestoras,[1] Asma Hadi Mohammed,[2,6] Ann-Sofie Schreurs,[1,6] Oliver Fleck,[3] Adam T. Watson,[1] Marius Poitelea,[1] Charlotte O'Shea,[4] Charly Chahwan,[5] Christian Holmberg,[3] Birthe B. Kragelund,[4] Olaf Nielsen,[3] Mark Osborne,[2] Antony M. Carr,[1,7] and Cong Liu[1]

[1]Genome Damage and Stability Centre, School of Life Sciences, University of Sussex, Brighton BN1 9RQ, United Kingdom; [2]Department of Chemistry, School of Life Sciences, University of Sussex, Brighton BN1 9RJ, United Kingdom; [3]Department of Biology, University of Copenhagen, DK-2200 Copenhagen, Denmark; [4]Structural Biology and NMR Laboratory, Department of Biology, University of Copenhagen, DK-2200 Copenhagen, Denmark; [5]Department of Molecular Genetics, University of Toronto, Toronto, Ontario M5S 1A8, Canada

The correct levels of deoxyribonucleotide triphosphates and their relative abundance are important to maintain genomic integrity. Ribonucleotide reductase (RNR) regulation is complex and multifaceted. RNR is regulated allosterically by two nucleotide-binding sites, by transcriptional control, and by small inhibitory proteins that associate with the R1 catalytic subunit. In addition, the subcellular localization of the R2 subunit is regulated through the cell cycle and in response to DNA damage. We show that the fission yeast small RNR inhibitor Spd1 is intrinsically disordered and regulates R2 nuclear import, as predicted by its relationship to *Saccharomyces cerevisiae* Dif1. We demonstrate that Spd1 can interact with both R1 and R2, and show that the major restraint of RNR in vivo by Spd1 is unrelated to R2 subcellular localization. Finally, we identify a new behavior for RNR complexes that potentially provides yet another mechanism to regulate dNTP synthesis via modulation of RNR complex architecture.

[*Keywords*: Ribonucleotide reductase; intrinsically disordered proteins; nuclear import; Cullin 4]

Received October 9, 2009; revised version accepted April 7, 2010.

Faithful DNA replication, a prerequisite for maintaining genome integrity, requires the maintenance of the correct concentration and the relative ratios of dNTPs (Chabes et al. 2003; Holmberg et al. 2005). dNTPs are formed by ribonucleotide reductase (RNR), which converts ribonucleoside diphosphates into their deoxy forms. Eukaryotes use type Ia RNR complexes comprised of multimers of two subunits: the large (R1) catalytic subunit, and the small (R2) diferric-tyrosyl radical-generating subunit (Stubbe 2003; Nordlund and Reichard 2006). Distinctive for type Ia RNR complexes are two allosteric nucleotide-binding sites on R1 (Reichard 2002; Nordlund and Reichard 2006). The N-terminal "overall activity" site is an ATP cone domain that binds either ATP (stimulatory) or dATP (inhibitory). The specificity site can bind ATP, dATP, dTTP, or dGTP and selects the substrate to be reduced, thus maintaining the appropriate dNTP ratios (Nordlund and Reichard 2006).

RNR is also regulated by a number of further mechanisms. In all eukaryotes studied, RNR protein levels are regulated via transcription. This is particularly obvious in response to genotoxic stress, when DNA repair synthesis requires dNTPs to be present outside of S phase. Work in the budding yeast *Saccharomyces cerevisiae* identified a further layer of control via the binding of a small RNR inhibitor protein, Sml1, to the R1 subunit (Zhao et al. 1998, 2000; Chabes et al. 1999). Sml1 is degraded as cells enter S phase and in response to genotoxic stress outside of S phase (Zhao et al. 2001). Work in the fission yeast *Schizosaccharomyces pombe* (Liu et al. 2003) demonstrated that the R2 subunit is localized primarily to the nucleus in non-S-phase cells, and is relocalized to the cytoplasm in response either to S-phase entry or following DNA damage checkpoint activation. Because the majority of the R1 subunit is constitutively cytoplasmic, this relocalization was proposed to promote RNR complex formation and dNTP synthesis. R2 nuclear localization depends on a small RNR regulator, Spd1. In *S. cerevisiae*, an Spd1-related protein, Dif1, was subsequently shown to promote R2 nuclear import (Lee et al. 2008; Wu and Huang 2008). In cooperation with a nuclear anchor, Wtm1 (Lee and Elledge 2006), Dif1-dependent import results in R2 nuclear accumulation. R2 nuclear accumulation is regulated by S-phase-dependent or genotoxic stress-dependent Dif1 degradation. The reduced

[6]**These authors contributed equally to this work.**
[7]**Corresponding author.**
E-MAIL a.m.carr@sussex.ac.uk; FAX: 44-1273-678121.
Article is online at http://www.genesdev.org/cgi/doi/10.1101/gad.561910.

Dif1 level decreases nuclear import while nuclear export remains active, promoting a net increase in cytoplasmic R2 (Lee et al. 2008).

S. cerevisiae Sml1 and Dif1 proteins share a domain, the SML box (Fig. 1A; Lee et al. 2008). Synteny analysis suggests that the *SML1* and *DIF1* genes are derived from the same ancestral locus, diverging when *S. cerevisiae* underwent genome duplication during its evolution. The *SML1* locus subsequently underwent a further direct duplication event so that a related gene, *HUG1*, is immediately adjacent (Lee et al. 2008). Hug1 and Dif1 also share a sequence motif, the HUG box, that is not apparent in Sml1. Hug1 function is not well defined; its transcript is induced by DNA damage, and it has been proposed to regulate RNR feedback inhibition (Basrai et al. 1999; Benton et al. 2006).

Spd1 in *S. pombe* and Dif1 in *S. cerevisiae* regulate R2 nuclear localization. The HUG domain is conserved between Spd1 and Dif1. Dif1 binds R2 via the HUG domain (Lee et al. 2008) to facilitate R2 nuclear import, suggesting that Spd1 may share this function. Spd1 also shares a region of sequence similarity with Sml1, equating to the last half of the suggested Sml1 RNR1-binding domain (Zhao et al. 2000; Lee et al. 2008). This region resides downstream from the C-terminal α-helix region of Sml1, a region with a clear role in RNR1 inhibition (Zhao et al. 2000). Conservation of an R1 interface, albeit limited, would be consistent with the direct association between Spd1 and $Cdc22^{R1}$ reported to mediate vitro biochemical inhibition of RNR (Hakansson et al. 2006). The sequence conservation between Spd1, Dif1, Sml1, and Hug1 indicates that Spd1 may be the sole *S. pombe* ortholog of the ancestral gene (summarized in Fig. 1).

Here we provide evidence that Spd1 is an intrinsically disordered protein (IDP) that acts as an import factor for the RNR R2 subunit. Using FRET analysis, we demonstrate that Spd1 controls RNR complex architecture. However, this does not correlate to the formation of active complexes. We suggest it reflects an additional level of RNR regulation beyond formation of canonical RNR tetramers of 2xR1 and 2xR2 subunits ($\alpha_2\beta_2$ tetramer). By structure–function analysis, we separate three roles for Spd1: We identify a mutant defective specifically for $Suc22^{R2}$ nuclear import (*spd1-M2*), mutants specifically defective in their ability to restrain RNR function in vivo (i.e., *spd1-M12* and *spd-M35*), and mutants that have specifically lost the ability to promote FRET (i.e., *spd1-M1* and *spd1-M6*). Thus, each of these three roles can be separated from each other, underlining the segmental distribution of function typical of IDPs. Contrary to expectation, we show that the ability of Spd1 to restrain RNR activity in vivo (and thus interfere with S phase) is

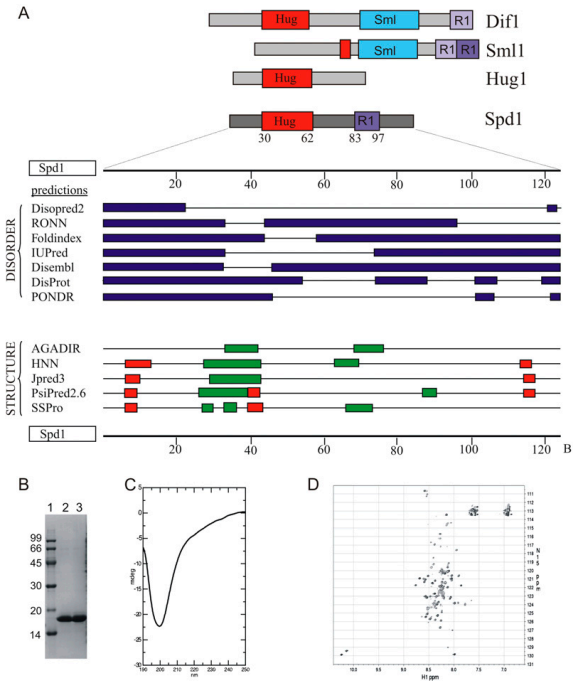

Figure 1. Spd1 is an intrinsically unfolded protein. (*A*, *top*) Cartoon representation of relationship to *S. cerevisiae* Dif1, Sml1, and Hug1 (data adapted from Lee et al. 2008). (*Bottom*) Disorder and structure predictions from the indicated software. (Red boxes) Coil; (green boxes) helix. (*B*) Spd1 was purified to homogeneity and showed a lower electrophoretic mobility than expected (18 kDa vs. 14 kDa). Lane *2* (fraction 6) and lane *3* (fractions 7 and 8) of the MonoQ purification after buffer change to PBS (pH 7.4). (Lane *1*) Low-molecular-weight markers; molecular weight is indicated in kilodaltons. (*C*) A far-UV CD spectrum of Spd1 recorded from 250 to 190 nm on 10 μM Spd1 and 10 mM NaH_2PO_4 (pH 7.4). A large negative ellipticity with a maximum at 199 nm suggests an unfolded protein with little or no secondary structure. (*D*) An $^{15}N,^{1}H$-HSQC NMR spectrum of 1.0 mM ^{15}N-Spd1 and 10 mM NaH_2PO_4 (pH 7.4) recorded at 10°C. Very little dispersion of signals is seen, as well as variable peak intensities.

not a consequence of its ability to sequester Suc22^{R2} in the nucleus. The restraint of RNR activity in vivo likely reflects the in vitro inhibition of RNR by Spd1 identified by biochemical analysis, although this remains to be established formally.

Results

Spd1 is an IDP

Sml1 is a member of a group of proteins that are intrinsically disordered (Danielsson et al. 2008). An IDP lacks a well-structured three-dimensional fold (Tompa 2002). However, nuclear magnetic resonance (NMR) studies show that IDPs can adopt transient structure in solution, and that some IDPs fold onto their interaction partner when they associate. This process, coupled folding and binding, can result in protein–protein interactions with relatively low affinity but high specificity (Sugase et al. 2007). The Spd1 sequence has the typical characteristics of an IDP: a high content of charged residues (23%), and a low aliphatic index (52.85; for reference, myoglobin = 95.1). Structural prediction programs such as DrDOS (Ishida and Kinoshita 2007) predict a high probability of disorder, with minor regions that can potentially form intermittent secondary structures. Most consistent are the two helical regions between residues 27–44 and 66–76, plus the possibility of shorter, extended structures between 6–10 and 115–120 (Fig. 1A).

To investigate the disorder characteristics by spectroscopy, recombinant Spd1 was purified to >98% homogeneity (Fig. 1B). Electrophoretic mobility corresponded to ~18 kDa, higher than the expected 14.2 kDa. This is a general attribute of IDPs (Tompa 2002). A far-UV CD spectrum showed no distinct signs of pronounced secondary structure elements, with very little negative ellipticity in the 210- to 220-nm range (Fig. 1C). Instead, a large negative signal with maximum at 199 nm was evident, highly indicative of an unfolded protein. An $^{15}N,^{1}H$- HSQC NMR spectrum recorded at 10°C showed a very narrow distribution of signals in the ^{1}H dimension, also typical of unfolded proteins (Fig. 1D). Importantly, a distribution of both high and low intensities of the NMR signals was observed, which suggests some residues of Spd1 are in intermediate exchange on the NMR time scale, possibly due to sampling of several conformations. Thus, Spd1 possesses all of the hallmarks of an IDP: low electrophoretic mobility, a lack of secondary structure in far-UV CD, and a collapsed NMR spectrum corresponding to an unfolded protein. Similar results have been established previously for Sml1 (Danielsson et al. 2008).

Spd1 regulates R2 nuclear import, but does not act as a nuclear anchor

In *S. cerevisiae*, two distinct mechanisms contribute to nuclear accumulation of R2: Dif1-dependent nuclear import, and R2 retention by the Wtm1 nuclear anchor. To establish if Spd1 shares the nuclear import function, we examined if Suc22^{R2} accumulates in the nucleus in *spd1-d* cells by blocking nuclear export with leptomycin B (LMB), which inhibits Crm1-dependent nuclear export of Suc22^{R2} (Liu et al. 2003). Suc22^{R2} did not accumulate in the nucleus in response to LMB treatment (Fig. 2A), indicating that Suc22^{R2} is no longer transported into the nucleus in the absence of Spd1 and thus cannot accumulate there when export is blocked.

Despite considerable effort, we did not identify a homolog or ortholog of the Wtm1 nuclear anchor mechanism in *S. pombe*. In addition, *spd1* deletion results in complete Suc22^{R2} delocalization from the nucleus. In *S. cerevisiae*, Dif1 deletion only partially disrupts R2 nuclear accumulation. The remaining accumulation is Wtm1-dependent (Lee and Elledge 2006). This suggests there is no nuclear anchor for Suc22^{R2} in *S. pombe*, but it remains formally possible that Spd1 both contributes to Suc22^{R2} nuclear import and acts as a canonical Suc22^{R2} nuclear anchor. If so, forced Spd1 localization to the nucleolus would be predicted to result in concomitant nucleolar Suc22^{R2}. We thus modified the *spd1*$^{+}$ locus to express a C-terminal fusion of 13-Myc epitopes followed by the Fib1 fibrillarin-like protein that is known to localize to the nucleolus (Gallagher et al. 1993). The fusion protein (Fig. 2B) expressed by the *spd1* promoter retained function, as judged by the correct profile and dynamics of Suc22^{R2} localization (Fig. 2C; data not shown). In a GFP-Suc22^{R2} background, we observed that Spd1-13Myc-Fib1 localized to the nucleolus, but Suc22^{R2} was not enriched in the nucleolus when compared with *spd1*$^{+}$ controls (Fig. 2C). Thus, Spd1 shares a nuclear import function with Dif1, but does not contribute to nuclear retention via a nuclear anchor function.

Spd1 is required for FRET between Cdc22^{R1} and Suc22^{R2}

The increased colocalization of R1 and R2 subunits in the cytoplasm during S phase and in response to genotoxic stress is proposed to allow active RNR complexes to form when dNTPs are required (Liu et al. 2003, 2005; Holmberg et al. 2005; Zhang et al. 2006; Wu and Huang 2008). To explore this possibility, we established a FRET assay (Fig. 3A,B) to examine the Cdc22^{R1}/Suc22^{R2} interaction. First, we used the fluorescent protein tags to estimate the relative abundance of Cdc22^{R1} and Suc22^{R2} in both the nuclear and cytoplasmic compartments in G2- and S-phase cells. The relative fluorescence between Cdc22^{R1} and Suc22^{R2} is 3:1 (data not shown). In G2 phase, Suc22^{R2} fluorescence was approximately threefold more intense in the nucleus than the cytoplasm, with ~74% of the signal residing in the nucleus (Fig. 3C). In S phase, nuclear Suc22^{R2} fluorescence is partitioned between two nuclei and comprises ~26.5% of the GFP-Suc22^{R2} signal. Individually, each nucleus shows a significant loss of intensity compared with G2 phase. We also see a corresponding gain in intensity (from 26% to 63.5%) in the cytoplasm (Fig. 3C).

In *spd1*$^{+}$ cells, FRET could be detected in the cytoplasm and the nucleus of cells in both G2 and S phase

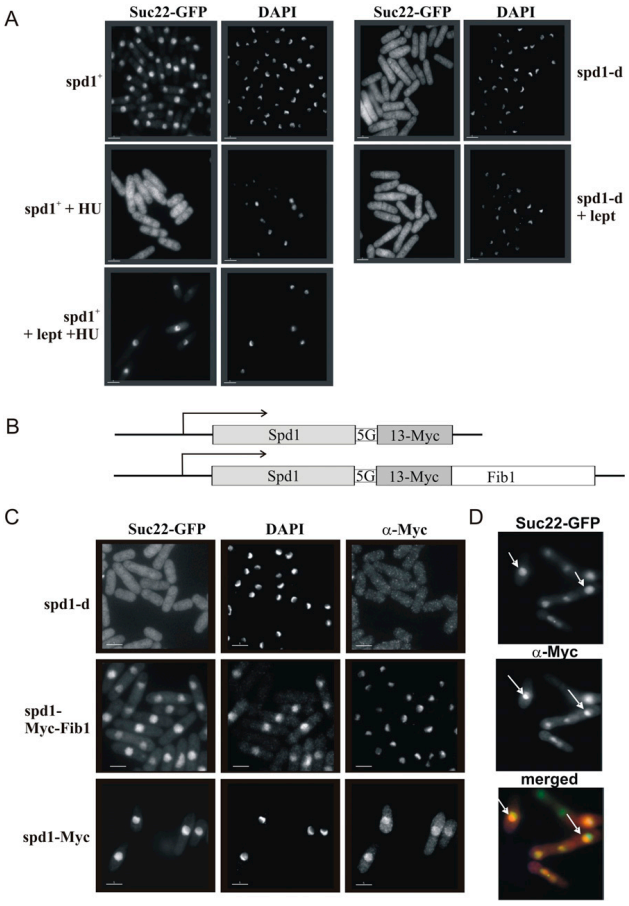

Figure 2. Spd1 regulates $Suc22^{R2}$ nuclear import. (*A*) *spd1*$^+$ *CFP-suc22* and *spd1-d CFP-suc22* cultures were treated with HU (20 mM) to arrest cells in S phase and/or leptomycin (100 ng/mL) to block nuclear export. After 2 h, cells were formaldehyde-fixed, and GFP was visualized by epifluorescence and DNA was visualized by DAPI staining. In *spd1*$^+$ cells treated with HU, $Suc22^{R2}$ becomes pan-cellular. (*Bottom left*) Concomitant treatment with leptomycin prevents nuclear export and $Suc22^{R2}$ redistribution. (*Bottom right*) In the absence of Spd1, GFP-Suc22 is distributed throughout the cell and does not accumulate in the nucleus when nuclear export is blocked. (*B*) Cartoon representation of the *spd1-Myc* and *spd1-Myc-Fib1* constructs integrated at the *spd1* locus under control of the *spd1* promoter. A 5× glycine linker (5G) separates Spd1 from the tags. (*C*) GFP-Suc22 (epifluorescence), DAPI-stained DNA, and the Myc epitope (indirect immunofluorescence) visualized in fixed cells following logarithmic growth. (*D*) Merged images of Myc and GFP-Suc22 localization from the *spd1-Myc-Fib1* culture. White arrows indicate example Myc staining nucleoli. Bars, 5 μm.

(Fig. 3D). In this case, FRET was used simply as an indicator of the R1–R2 interaction and not as a quantitative measure of association number or structural proximity. Surprisingly, in *spd1-d* cells, we did not detect FRET in the cytoplasm or nucleus of either S-phase or G2 cells (Fig. 3E). Treating *spd1*$^+$ cells with hydroxyurea (HU), an agent that inhibits RNR and synchronizes cells in S phase, resulted in the FRET signal disappearing (Fig. 3E). However, FRET was similarly lost when *cdc25-22* cells synchronized in G2 were held in G2 and treated with HU (data not shown), indicating an S-phase-independent effect of HU. Taken together, these data indicate that Spd1 affects the association of $Cdc22^{R1}$/$Suc22^{R2}$ subunits, but that this does not correlate with apparent activation of RNR.

Alanine scanning mutagenesis of Spd1

From the available data, we can postulate three possible in vivo functions for Spd1: regulation of $Suc22^{R2}$ nuclear import, an influence on RNR complex architecture that equates to our FRET analysis, and, finally, an in vivo restraint of RNR activity that correlates with an increased dNTP concentration in the absence of Spd1 in *csn1-d* and *ddb1-d* cells (Holmberg et al. 2005) and is possibly equivalent to either the inhibition observed in vitro (Hakansson et al. 2006), the nuclear sequestration of $Suc22^{R2}$, or a combination of both. To understand how these potential functions relate to each other, and to shed light on the mechanism by which Spd1 inhibits RNR, we created 41 independent *spd1* mutants in which each

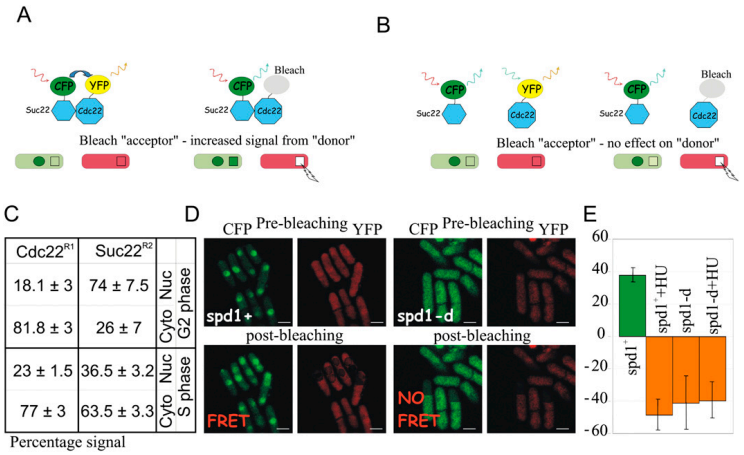

Figure 3. Spd1 is required for FRET between Cdc22^{R1} and Suc22^{R2}. (*A*) Cartoon representation of FRET between CFP- and YFP-tagged RNR subunits. Bleaching the YFP acceptor results in an increased emission signal from the CFP donor. The green circle represents the nucleus (Suc22^{R2} accumulates in the nucleus). Squares represent the bleached area; in this instance, a region of cytoplasm. (*B*) Equivalent cartoon showing result when fluorophores are not sufficiently aligned for FRET. Notice that, instead of an increase in the signal from the donor (i.e., evidence of FRET), a moderate decrease is seen (as opposed to no change) due to some overlap in the absorption spectra for CFP and YFP. (*C*) Percentage of nuclear and cytoplasmic fluorescent intensity of Cdc22-CFP and CFP-Suc22 in single tagged cells visualized under the same microscope slide. (*D*) Representative images from *spd1*$^{+}$ and *spd1-d* cultures without treatment with HU. (*E*) Quantification of combined nuclear and cytoplasmic FRET signal. Error bars, SD from mean. Negative FRET (formally no-FRET) results from nominal photobleaching of the donor along with the acceptor.

sequential group of three residues were substituted for alanine (Fig. 4A), and examined their influence on Spd1 degradation and Spd1-dependent phenotypes.

Analysis of Spd1 degradation in vitro and in vivo

We established an in vitro assay for Spd1 degradation by incubating ^{35}S methionine-labeled Spd1 in whole-cell extract. Degradation kinetics were monitored by SDS-PAGE and autoradiography (Fig. 4B). Degradation was dependent on the Cullin 4 E3 ubiquitin ligase Pcu4–Ddb1^{Cdt2} and the signalosome, as predicted (Liu et al. 2003). Each individual mutant protein (Fig. 4C) was ^{35}S methionine-labeled and incubated with degradation-competent extract, and the percentage of protein remaining after 10 and 20 min was quantified. The results did not identify a domain responsible for degradation, but did reveal a single stable mutant, Spd1-M14. Deconvolution of this mutant into the three individual alanine substitutions revealed that a single lysine residue (K42) was required for efficient degradation (Fig. 4D).

We were surprised not to define a degron domain, and were also wary of the observation that a single lysine is required: Usually, disrupting a single lysine residue in vivo results in adjacent lysines acting as alternative ubiquitin acceptor sites. We thus integrated each mutant into the *spd1* locus, where they are expressed under control of the *spd1* promoter. To assay degradation, each strain was grown to logarithmic phase and treated with 20 mM HU. This induces the Cdt2 targeting subunit of Cul4–Ddb1^{Cdt2} ubiquitin ligase and promotes Spd1 degradation (Liu et al. 2005). Samples for Western blot analysis were prepared immediately before HU addition and at 1, 2, and 4 h. Again we did not define a specific domain controlling Spd1 degradation (Fig. 4E). The Spd1-M14 and Spd1-K42A mutant proteins identified in the in vitro studies also showed no evidence of stability (Fig. 4E; data not shown). There were several additional observations. First, a double mutant encompassing the two checkpoint kinase consensus sites, Spd1-M(3 + 18), was not stabilized (Fig. 4F). Second, the initial protein levels of many mutants varied significantly. This is a reproducible observation seen with two independent α-Spd1 antibodies, and likely reflects that triple alanine substitution in an IDP is expected to affect intrinsic stability. Third, only two mutant proteins, Spd1-M21 and Spd1-M23, were significantly stabilized.

Separation of Suc22^{R2} localization and RNR inhibitory regulation

We crossed each *spd1* mutant into the *GFP-suc22* background and observed Suc22^{R2} localization by direct fluorescence in untreated cells and cells exposed to 20 mM HU for 4 h (Fig. 5). In *spd1*$^{+}$ cells, Suc22^{R2} was largely nuclear (most asynchronous *S. pombe* cells are in G2).

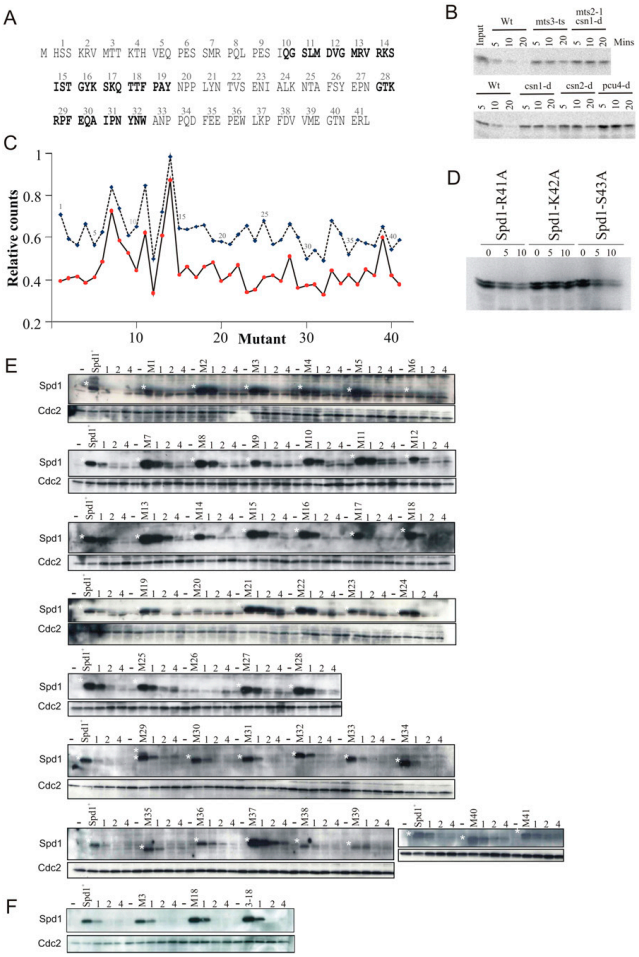

Figure 4. Stability of Spd1 mutant proteins. (*A*) The 41 mutants of *spd1* created. These are designated as *spd1-M1*, *spd1-M2*, etc. Each mutant results in the three indicated amino acids being changed to alanine. Bold indicates conserved HUG and R1 domains (see Fig. 1A). (*B*) In vitro degradation of ^{35}S-labeled Spd1. In vitro translated Spd1 is incubated for the indicated number of minutes with whole-cell extract derived from either wild type (Wt) or the indicated mutants. *mts3-ts* and *mts2-1* are mutations in genes encoding subunits of the proteasome and show compromised degradation in this assay. As is seen in vivo, Spd1 degradation is dependent on the signalosome subunits Csn1 and Csn2, and on the Cullin 4 homolog Pcu4. (*C*) Quantification of in vitro degradation assay for the individual mutants. (Blue symbols and dashed line) 10-min incubation; (red symbols and solid line) 20-min incubation. (*D*) The three amino acids mutated in *spd1-M14* were changed individually to alanine and tested for stability in wild-type cell extract. Both bands are Spd1-specific. (*E*) In vivo stability of Spd1 mutant proteins. Each mutant was integrated separately at the *spd1* genomic locus under control of the *spd1* promoter. Logarithmically growing cells were incubated with HU (20 mM) for 1, 2, and 4 h; extract was prepared and subjected to SDS-PAGE; and Spd1 was detected by Western analysis with polyclonal α-Spd1 antisera. A white star marks the Spd1-specific bands. Before each mutant, a control lane contains extract from *spd1-d* cells. Blots were probed in parallel for Cdc2 as a loading control. (*F*) Identical analysis of *spd1-M3*, *spd1-M18*, and the combined *spd1-M3-18* mutations that cover the two conserved Cds1^{Chk2} kinase consensus sites.

Following HU treatment (cells arrested in S phase; Spd1-degraded), ~20% of cells retained weak nuclear GFP fluorescence, and Suc22^{R2} became pan-cellular in the remaining ~80%. *spd1-m2*, *spd1-m14*, and *spd1-m26* were fully defective for Suc22^{R2} nuclear accumulation. A small but notable effect on nuclear accumulation was observed for *spd1-m34*, *spd1-m35*, and *spd1-m36*. Four mutants—*spd1-m11*, *spd1-m12*, *spd1-m13*, and *spd1-m33*—showed more dramatic loss of Suc22^{R2} nuclear accumulation upon HU treatment compared with *spd1*$^{+}$ cells. Finally, four mutants—*spd1-m21*, *spd1m-38*, *spd1-m40*, and *spd1-m41*—displayed robust Suc22^{R2} nuclear accumulation poorly reversed by HU treatment. No mutant showed a complete inability to delocalize Suc22^{R2} to the cytoplasm (the phenotype seen when Spd1 is completely stable; i.e., in *pcu4-d*, *cdt2-d*, and *csn1-d* mutants). Notably, the region that corresponds to the conserved HUG domain (*spd1-m10* through *spd1-m20*) was particularly sensitive to mutation in the assay for nuclear localization. In Dif1, this domain is proposed to bind the R2 subunit and promote its nuclear import.

If the mechanisms by which Spd1 restrains RNR function in vivo depend on its ability to localize Suc22^{R2} in the nucleus, then RNR activation would be at least partially dependent on the loss of nuclear Suc22^{R2} accumulation in S phase, and *spd1* mutants unable to accumulate

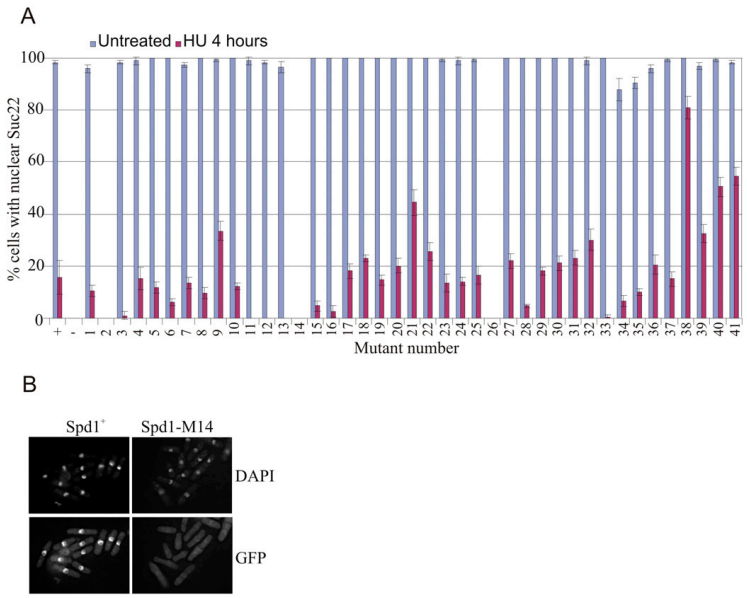

Figure 5. Subcellular localization of Suc22^{R2} in the individual *spd1* mutants. (*A*) GFP-Suc22 was visualized by epifluorescence in fixed untreated cells and cells treated for 4 h with HU (20 mM) before fixation to arrest S phase. Controls were *spd1*$^{+}$ (+) and *spd1-d* (−). These are shown on the *left*. The majority of *spd1*$^{+}$ cells show nuclear GFP-Suc22. Following incubation in HU, no evidence of nuclear accumulation of GFP-Suc22 is seen in >80% of cells, the signal being pan-cellular. In the absence of Spd1, nuclear accumulation is not seen in either untreated or treated cells. (*B*) A representative image: *spd1-M14* behaves like a null mutant of *spd1* in this assay. GFP-Suc22 was visualized in *spd1-M14* cells without HU treatment. DNA was visualized by DAPI staining. Error bars, SD from mean.

Suc22^{R2} in the nucleus should phenocopy the *spd1-d* null. We thus tested two robust phenotypes for Spd1-dependent restraint of RNR activity. The first is the ability of *spd1*-null mutants to suppress the synthetic inviability associated with concomitant loss of the *csn1* signalosome component and the *rad3* checkpoint gene (Liu et al. 2003). Essentially, in *csn1-d* mutants, Spd1 is stable, and thus RNR activity is restrained in S phase—a situation reminiscent of the inviability of *MEC1* deletion and the ability of *SML1* deletion to suppress this (Zhao et al. 1998). Mutants in the HUG domain—plus *spd1-m26*, *spd1-M34*, *spd1-M35*, and *spd1-M41*—rescued *rad3-d csn1-d* synthetic lethality with significant efficiency, in many cases approaching that of the *spd1-d* null (Fig. 6A).

The second assay we chose is the ability of *spd1* deletion to rescue the spore formation defect evident in the *ddb1-d* background (Liu et al. 2003; Holmberg et al. 2005). Ddb1 is a component of the Pcu4–Ddb1^{Cdt2} ubiquitin ligase required for Spd1 degradation, so Spd1 restrains RNR activity in S phase and lowers dNTP pools in *ddb1-d* mutants, and thus they cannot progress through meiosis and form spores. This phenotype and the low dNTP pools are reversed by deleting *spd1*. We combined each of the 41 *spd1* mutants with *h*^{90} *ddb1-d* and scored the percentage of asci with either zero, one, two, three, or four spores (Fig. 6B). Spore formation was restored (>70% four-spored asci, close to that of *ddb1-d spd1-d* double-null cells: >90%) in mutants *spd1-m11* through *spd1-m16*, *spd1-m18*, *spd1-m19*, *spd1-m26*, *spd1-m34* through *spd1-m38*, and *spd1-m41*.

Both of these assays are robust and semiquantitative (Liu et al. 2003; Holmberg et al. 2005). Taking them together, we conclude that the defect in Suc22^{R2} nuclear import does not correlate with the biological evidence for restraint of RNR activity. Of particular interest are mutants *spd1-m2* (import-defective, no defect in restraining RNR) and *spd1-m10* plus *spd1-m11* (little or no import defect, but significantly unable to restrain RNR activity). The broader trends in the data make clear that HUG domain mutations (*spd1-m10* through *spd1-m20*) influence both import and restraint. Mutations in the C-terminal region (*spd1-m34* through *spd1-m41*) also influence both import and restraint, and likely define a new segment of Spd1. We suggest this is named the Spd1 domain, in keeping with the nomenclature of Lee et al. (2008). Finally, mutations within the putative R1-binding region (of which only three residues are identical between Sml1 and Spd1) do not appear to dramatically influence

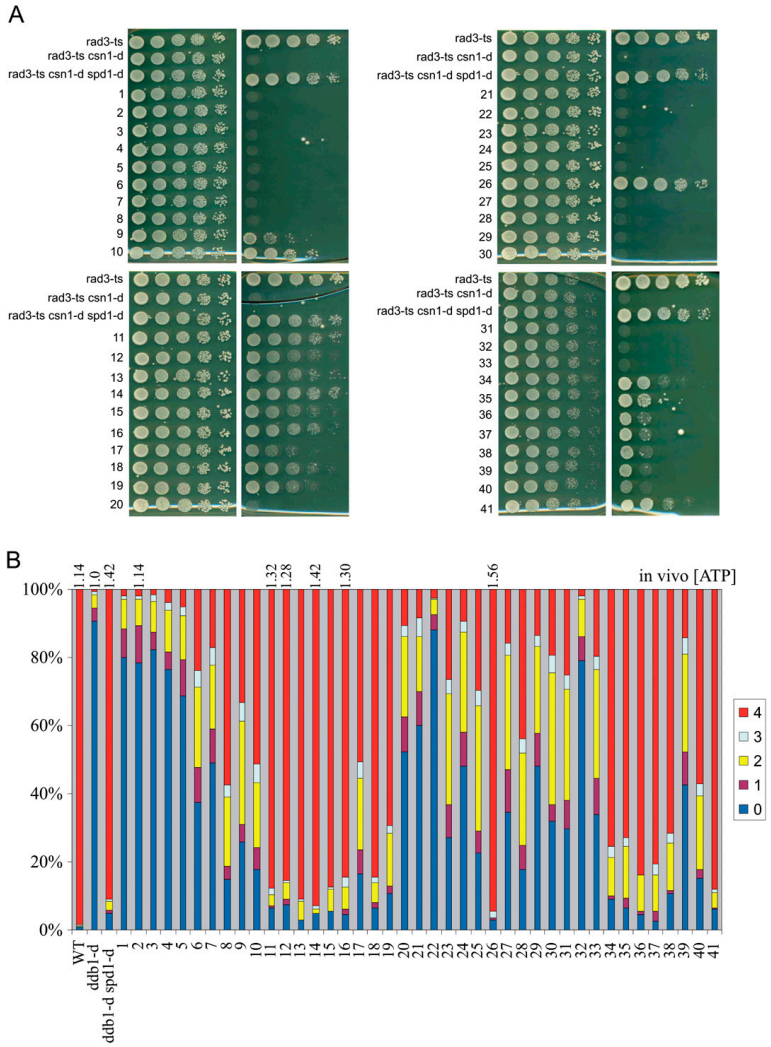

Figure 6. Ability of individual *spd1* mutants to restrain RNR function in vivo. Two in vivo assays for RNR function are shown. (*A*) The ability of *spd1* mutants to rescue the synthetic lethality of a *rad3-ts csn1-d* double mutant at 34°C. A dilution series for each mutant was spotted, and plates were incubated at 34°C (partial loss of checkpoint). Viability is a semiquantitative measure of the loss of the in vivo inhibitory function of Spd1 (Liu et al. 2003). (*B*) The ability of *spd1* mutants to rescue the spore formation defect of homothalic/h^{90} *ddb1-d* mutants. The number of spores formed gives a semiquantitative measure of the loss of the in vivo inhibitory function (Holmberg et al. 2005). The in vivo dATP concentration relative to *ddb1-d* cells were measured in selected mutants and are given *above*. Loss of inhibitory function correlates with increased dNTP pools. Wild-type (Wt) *ddb1-d* and *ddb1-d spd1-d* controls are shown on the *left*.

either import or restraint of RNR activity (*spd1-m28* through *spd1-m32*).

The ability to promote R1–R2 FRET does not correlate with RNR inhibition or nuclear import

Each of the 41 *spd1* mutants was crossed into the *cdc22^{R1}-CFP YFP-Suc22^{R2}* strain and tested for their ability to promote Cdc22^{R1}–Suc22^{R2} FRET. Only 12 of the 41 mutants could promote R1–R2 FRET (Fig. 7A). In most of these 12 cases, the FRET signal was comparable with that seen in *spd1*$^+$ cells, and was seen in G2 and S phase in both the nuclear and the cytoplasmic compartments (Fig. 7B). The ability to promote R1–R2 FRET did not correlate with either the Suc22^{R2} nuclear import function of Spd1 or its ability to restrain RNR activity. For example, *spd1-M2* keeps the R1–R2 FRET signal but lacks the R2 nuclear localization function. Mutant *spd1-M12* similarly promotes R1–R2 FRET but has lost the ability to restrain RNR activity. Mutants demonstrating the converse are also apparent; i.e., *spd1-M1* kept both the Suc22^{R2} nuclear import function and the ability to restrain RNR activity, but has lost the ability to promote FRET.

Spd1 can interact with both Cdc22^{R1} and Suc22^{R2}

Active RNR in vitro consists of an $\alpha_2\beta_2$ tetramer consisting of 2xR1 and 2xR2 subunits (Nordlund and Reichard 2006). Since RNR is active in *spd1-d* cells, R1–R2 FRET cannot simply reflect active tetramers. Furthermore, R1–R2 FRET does not decrease when cells enter S phase, so it is unlikely that the FRET signal reflects inactive R1–R2 complexes. Both *Escherichia coli* (Rofougaran et al. 2008) and mouse (Rofougaran et al. 2006) R1 subunits can be induced to form hexamers (α_6) in vitro by either dATP or ATP binding. These subsequently form $\alpha_6\beta_2$ octamers by association with a 2xR2 dimer (β_2). $\alpha_6\beta_2$ complexes have been suggested to represent the primary active RNR form because sufficient ATP is available in cells to occupy the majority of activity sites, and a correlation has been observed between α_6 hexamer formation and ATP activation (Rofougaran et al. 2008). We used size fractionation to establish whether the presence of Spd1 correlated with the presence of higher-order RNR complexes (Fig. 8A). No evidence for multimer formation was observed in either exponential *spd1*$^+$ or *spd1-d* cells. Limited higher-mass complexes were observed following HU treatment, but these were not *spd1*-dependent. Thus, we believe it unlikely that R1–R2 FRET reflects different higher-order complex formation.

Despite extensive efforts, we were not able to identify conditions where Spd1 can be coprecipitated with Cdc22^{R1} or Suc22^{R2} from cell extracts. IDPs can bind multiple substrates with high specificity but low affinity, which is consistent with the low-affinity Spd1–Cdc22^{R2} interaction

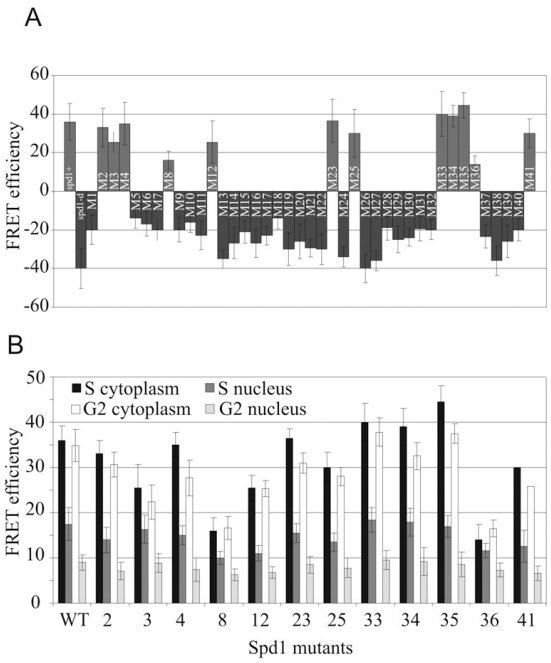

Figure 7. Ability of the individual *spd1* mutants to promote Cdc22^{R1}-Suc22^{R2} FRET. Each of the 41 individual mutants was crossed to the *cdc22-YFP CFP-suc22* background and tested for FRET signal. (*A*) Summary of FRET intensities. FRET was examined in both the nucleus and the cytoplasm of both mononuclear (G2) and septating binucleate (S-phase) cells. (*Left*) Controls are *spd1*$^+$ and *spd1-d*. (*B*) The data for each circumstance for the mutants able to promote FRET. Error bars, SD from mean.

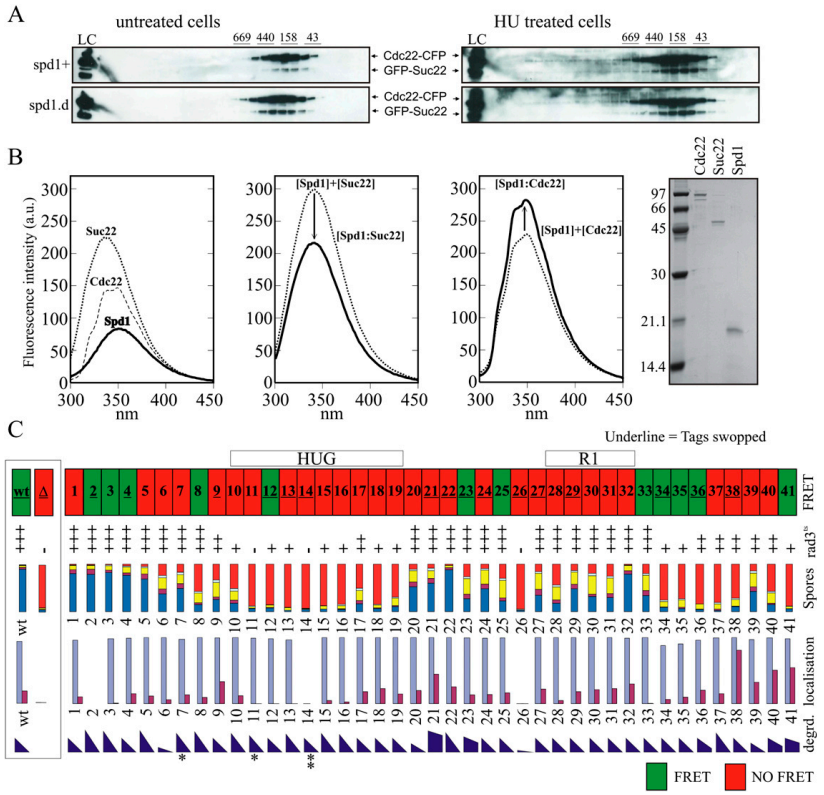

Figure 8. Spd1 interacts with both Cdc22^{R1} and Suc22^{R2}. (*A*) Gel filtration of extracts prepared from *cdc22-CFP GFP-suc22* double-tagged *spd1*$^{+}$ and *spd1-d* cells after cross-linking with (*right*) and without (*left*) 4-h HU treatment. The $\alpha_2\beta_2$ complex is predicted to be 274.6 kDa. Size markers are given *above*. (*B*) Fluorescence quenching assay for interaction between individual RNR subunits and Spd1. (Far *left*) Fluorescence emission spectra of individual proteins. (*Middle left*) Suc22^{R2} + Spd1. Predicted additive fluorescence emission (thin line) and experimental results (thick line) differ, demonstrating an interaction. (*Middle right*) Equivalent assay for Cdc22^{R1} + Spd1. (Far *right*) Aliquots of purified proteins assessed by SDS-PAGE. (*C*) Summary of data. (From the *top*) Ability to promote FRET. The region corresponding to the HUG and RNR interaction domains (see Fig. 1) are indicated. Where the mutant number is underlined, FRET data have been verified by reversing the tags (i.e., *cdc22-CFP YFP-suc22*). The ability of *spd1* mutant cells to grow at 34°C in the *rad3-ts csn1-d* mutant background. Growth is scored semiquantitatively from the data in Figure 6A and several repeats. Spore viability data are reproduced from Figure 6B. Nuclear accumulation of Suc22^{R2} is reproduced from Figure 5A. The degradation of Spd1 in vivo is semiquantitatively estimated (by eye) from the data in Figure 4E and several repeats for all mutants. Asterisks indicate those mutants with partial (*) or complete (**) resistance to the in vitro degradation assay.

reported (Hakansson et al. 2006). We thus used fluorescence quenching to establish if Spd1 could bind either R1 or R2 subunits (Fig. 8B). Recombinant Spd1 can interact with both Cdc22^{R1} and Suc22^{R2} in vitro, as predicted by Hakansson et al. (2006) and supported by our identification of a role for Spd1 in Suc22^{R2} nuclear import.

Discussion

RNR dysregulation results in inappropriate total dNTP levels and/or unbalanced dNTP ratios, which are changes detrimental to genome stability (Chabes et al. 2003). RNR subunit availability is regulated in most organisms via transcriptional control (Elledge et al. 1993; Nordlund and Reichard 2006). In the fission yeast, *cdc22*^{R1} and *suc22*^{R2} are induced transcriptionally at the transition between G1 and S phase by the Cdc10, Res1, and Res2-containing transcription factor MBF (Fernandez Sarabia et al. 1993). In addition, DNA structure checkpoint activation results in inhibition of the Nrm1 MBF corepressor and subsequent MBF-dependent transcription (de Bruin et al. 2006). However, in cycling cells, the levels of Cdc22^{R1}

and Suc22^{R2} protein do not change dramatically during the cell cycle or after checkpoint activation (Watson et al. 2004). Most likely, transcriptional regulation ensures that cells entering the cell cycle from stationary phase, or those damaged during stationary phase, have a supply of RNR subunits. A significant proportion of RNR regulation in cycling cells thus occurs post-translationally.

The in vivo inhibitory function(s) of Spd1

In *S. cerevisiae*, the Sml1 inhibitor binds to the R1 subunit (Zhao et al. 2000; Zhang et al. 2007) and prevents dNTP synthesis by inserting its C-terminal aromatic residue into a cleft usually occupied by the C-terminal residue of R2. Each S phase, Mec1 kinase activates the downstream Dun1 kinase to promote Sml1 degradation (Zhao and Rothstein 2002), likely by phosphorylating serine residues within the Sml1 phospho-degron (SML box) (see Fig. 1). When Mec1 is absent, Sml1 is not degraded, and dNTP synthesis is inhibited during S phase. Since *mec1* mutants are also checkpoint-defective, *MEC1* is an essential gene: A combination of low dNTP pools and a checkpoint defect results in cell death. Concomitant deletion of *SML1* and *MEC1* restores cell viability because S phase is no longer inhibited and the checkpoint thus is not required (Zhao et al. 2001).

Like *S. cerevisiae* Sml1, *S. pombe* Spd1 inhibits RNR in vitro (Hakansson et al. 2006) and restrains RNR activity in vivo when present in S phase (Liu et al. 2003). Importantly, restraint of RNR activity did not correlate with Suc22^{R2} relocalization. Both of the previously characterized biological assays for in vivo RNR activity gave consistent results and identified several mutants that clearly separate the nuclear import role of Spd1 from its ability to restrain RNR activity in vivo. Specifically, *spd1-M12* is unable to restrain RNR activity but is competent for Suc22^{R2} nuclear import, while mutant *spd1-M2* keeps the ability to restrain RNR activity but is, as far as the assay allows us to judge, fully defective for the nuclear import function. The complementary specific loss of function between these two mutants strongly suggests that the major regulatory role of Spd1 on RNR activity is not directly dependent on subcellular distribution of RNR subunits. Most likely, the restraint of RNR activity in vivo correlates with the in vitro inhibition via binding to Cdc22^{R1} (Hakansson et al. 2006).

We can identify two specific regions of Spd1 that, when mutated, result in decreased restraint of RNR. These two regions are the HUG domain and an additional region, the Spd1 domain, defined by mutants *spd1-M34* through *spd1-M41*. The HUG domain is required for both the nuclear import function and the ability to restrain RNR activity in vivo. This raises the possibility that Spd1 interacts with both R1 and R2 subunits in *S. pombe* minimally through its HUG domain. We demonstrated that Spd1 can indeed bind both Cdc22^{R1} and Suc22^{R2} in vitro, but defining the mechanism of association awaits further biophysical characterization, as the dual specificity of Spd1 likely reflect the potential for low-affinity interactions between IDPs and several substrates.

Spd1 functions to promote nuclear import but is not a nuclear anchor

To establish if Spd1 shares the Dif1 function in nuclear import, we explored whether blocking nuclear export in *spd1*-deleted cells resulted in nuclear Suc22^{R2} accumulation: The absence of nuclear export will result in Suc22^{R2} nuclear accumulation if import is active. In LMB-treated *spd1-d* cells, Suc22^{R2} did not accumulate in the nucleus, demonstrating that Spd1 is required for active Suc22^{R2} nuclear import. A cluster of the mutants analyzed (*spd1-M11* through *spd1-M16*) were either partially or completely defective for Suc22^{R2} import (data summarized in Fig. 8C). This cluster largely encompasses the conserved HUG domain, suggesting that, like for Dif1, the HUG domain is important for nuclear import and likely defines an R2 interaction surface, a prediction consistent with our identification of a direct association between Suc22^{R2} and Spd1 in vitro. Two additional mutants, *spd1-M2* and *spd1-M26*, also lost Suc22^{R2} nuclear accumulation function.

In *S. cerevisiae*, loss of active import (*DIF1* deletion) results in decreased but not absent R2 nuclear accumulation because the Wtm1-dependent nuclear anchor retains R2 subunits (Lee and Elledge 2006). Loss of both Dif1 (active import) and Wtm1 (anchoring) is required for complete loss of R2 nuclear accumulation. In *S. pombe*, loss of Spd1 alone results in complete loss of Suc22^{R2} nuclear accumulation. Either there is no R2 nuclear anchor in *S. pombe*, or Spd1 itself fulfils both import and anchoring roles. However, when Spd1 is localized artificially to the nucleolus, we did not detect additional Suc22^{R2} in the nucleolus, implying that there is no nuclear anchor for Suc22^{R2}.

Alanine scanning mutagenesis did not define a degron domain

In *S. cerevisiae*, the SML box of the Sml1 and Dif1 proteins is thought to define a phospho-degron targeted by Mec1^{ATR}-dependent Dun1 kinase activity. In *S. pombe*, Spd1 degradation is independent of Rad3^{ATR} and the downstream kinase Cds1^{Chk2} during S phase. While Spd1 degradation becomes dependent on both kinases in response to checkpoint activation, this dependency is known, at least in part, to reflect the checkpoint dependence of *cdt2* transcript induction. *cdt2* encodes the adaptor for the ubiquitin ligase Pcu4–Ddb1^{Cdt2} that targets Spd1 for degradation. We did not define a distinct domain required for Spd1 degradation. This is consistent with the lack of evidence for regulation of Spd1 degradation by phosphorylation (Liu et al. 2005). Furthermore, no single serine or threonine mutation prevented degradation. There are no consensus Rad3^{ATR} sites on Spd1, but two potential Cds1^{Chk2} sites are evident. Mutating both of these sites individually (*spd1-M3* and *spd1-M18*) or together (*spd1-M3–18*) did not affect Spd1 stability.

Four mutants—*spd1-M21*, *spd1-M23*, *spd1-M40*, and *spd1-M41*—were partially resistant to degradation. Cells expressing these partially stable proteins were less

responsive to loss of nuclear accumulation of $Suc22^{R2}$ following HU, but none were synthetically lethal with *rad3-ts* (data not shown). This indicates that, unlike indirect stabilization of Spd1 via deletion of E3 ligase components, these mutant proteins did not keep their ability to fully restrain RNR activity. Intriguingly, the in vitro degradation assay identified a single lysine required for $Cul4–Ddb1^{Cdt2}$ and signalosome-dependent E3 ubiquitin ligase degradation of Spd1. However, mutating this residue made no difference to in vivo Spd1 stability. One possibility is that K42 is the sole Ub acceptor in vitro, but is likely substituted by other lysines in vivo.

A novel Spd1-dependent level of RNR regulation?

Since we and others have speculated previously that active RNR complexes are formed in the cytoplasm after colocalization of $Cdc22^{R1}$ and $Suc22^{R2}$ following Spd1 degradation, we established a FRET assay to examine R1–R2 association in different cellular compartments. Our assumption was that 2xR1–2xR2 tetramer formation ($\alpha_2\beta_2$ complex) would be enhanced in the cytoplasm following Spd1 degradation. While we could clearly visualize FRET between Cdc22-YFP and CFP-Suc22 (and similarly when the tags were reversed) (data not shown), R1–R2 FRET was not enhanced upon loss of Spd1, but was instead completely Spd1-dependent and did not correlate with RNR activity: It was neither increased nor decreased in the cytoplasm of S-phase cells compared with G2 cells. R1–R2 FRET also disappeared when $spd1^+$ cells were treated with HU. However, $spd1^+$ cells held in G2 and treated with HU lost the FRET signal within 30 min (data not shown), despite not progressing into S phase, indicating that HU, a free-radical scavenger, may independently quench the FRET signal.

Of the 41 *spd1* mutants tested for R1–R2 FRET, 12 were positive. While there was some variation in the intensity of the FRET signal in these mutants, this was modest, relatively evenly distributed between the nuclear and cytoplasmic compartments, and not specifically different for either G2- or S-phase cells. Interestingly, the distribution of the mutants able to FRET did not correlate with either the nuclear import role or the in vivo restraint of RNR activity. For example, *spd1-M2* cells were FRET-competent and had lost nuclear import completely, while *spd1-M12* cells were FRET-competent but were unable to restrain RNR activity.

What does the FRET signal represent? In vitro, active RNR complexes consist of 2xR1 and 2xR2 subunits ($\alpha_2\beta_2$). Both ATP (activating) and dATP (inhibitory) binding to the allosteric overall activity site stimulate $\alpha_2\beta_2$ formation, despite their opposite effects on activation. Our gel filtration data indicate the presence of R1–R2 complexes at the size expected for $\alpha_2\beta_2$ complexes and show that these were not dependent on $spd1^+$. Combined with the observation that Spd1 loss leads to RNR activation, we can conclude that the presence of active $\alpha_2\beta_2$ tetramers cannot be the cause of the FRET signal. Recent work using both *E. coli* (Rofougaran et al. 2008) and mouse (Rofougaran et al. 2006) RNR proteins has suggested that both dATP and ATP induce the formation of R1 hexamers (α_6) that can form an $\alpha_6\beta_2$ octamer by association with a dimer (β_2) of R2 subunits. However, by gel filtration analysis, we did not observe evidence for Spd1-dependent higher-order RNR complexes. A subfraction of $Cdc22^{R1}$ and $Suc22^{R2}$ were seen to migrate at higher molecular weight, but this occurred after treatment with HU and was independent of *spd1* status.

Our data suggest that Spd1-dependent FRET between R1 and R2 subunits reflects a changed conformation of the RNR $\alpha_2\beta_2$ complex. We hypothesize that Spd1 mediates formation of immature inactive RNR complexes. In these inactive complexes, the fluorophores are appropriately aligned to allow FRET between $Cdc22^{R1}$ and $Suc22^{R1}$, reflecting an optimal complex architecture for subsequent activation when Spd1 is degraded. In support of this proposal, the p27 cyclin-dependent kinase inhibitor is an IDP that mediates formation of immature inactive Cdk2–CycA complexes (Russo et al. 1996). p27 folds onto the Cdk2 and CycA subunits, both individually and at the same time. Intriguingly, p27 directly inhibits Cdk2 by altering the conformation of the catalytic cleft and inserting a tyrosine residue as an ATP-mimicking residue. In this context, we note that, in active $\alpha_2\beta_2$ tetramers, the R2 C-terminal residue is buried in a deep cleft of R1, and that interference with optimal RNR complex architecture has been observed using R2 C-terminal-mimicking peptides (Cohen et al. 1986). It has also been suggested that the C-terminal Phe of Sml1 (F104), which is mandatory for full inhibition in *S. cerevisiae* (Zhao et al. 2000), may also insert into the same deep cleft of R1 that is the binding pocket for the C-terminal aromatic residue of the R2 subunit. The change in fluorescence emission also supports the involvement of tyrosines and/or tryptophans in the interactions.

Once Spd1-dependent inactive complexes are formed, we propose that Spd1 degradation would leave them in the optimal conformation for catalytic activity by removing the direct inhibition and allowing activation via ATP binding to the allosteric "overall activity" site. To explain why *spd1-d* cells never exhibit FRET but maintain RNR in an active form, we postulate that, in the absence of Spd1, RNR complexes do still form, but with an alternative suboptimal architecture. The fact that these are abundant and not inhibited by Spd1 compensates for the loss of the Spd1-dependent forms.

Conclusion

We showed that Spd1 acts as an import factor for $Suc22^{R2}$, as predicted from its relationship to Dif1 in *S. cerevisiae*. Since it also functions to restrain RNR activity in vivo, we asked if these two phenomena were related. Contrary to our expectation, the assays measuring restraint of RNR activity in vivo did not correlate with $Suc22^{R2}$ import, demonstrating that the major function of Spd1 in regulating dNTP synthesis is unrelated to its role in nuclear sequestration of $Suc22^{R2}$. We also established a FRET assay that revealed a novel aspect of RNR behavior that has the potential to provide yet another mechanism to

regulate RNR, possibly through alterations of tetramer architecture. The precise role for this new effect of Spd1 on RNR and how it relates to the regulation of RNR awaits further analysis. The segmental distribution of Spd1 functionality uncovered here is reminiscent of the hallmarks of IDPs, including the association with multiple partners. Thus, the IDP nature of Spd1 likely explains how this small protein is able to regulate R1–R2 complexes in multiple ways.

Materials and methods

Cloning, expression, stability, purification, and interactions of recombinant proteins

The *spd1*, *suc22*, and *cdc22* ORFs were PCR-amplified, cloned into appropriate vectors, and verified by sequencing. Individual *spd1* mutations were constructed using oligonucleotide-directed mutagenesis, and each was verified by sequencing. Coupled in vitro transcription–translation (Promega) was performed using the manufacturer's instructions to produce ^{35}S-labeled protein. Cell extracts were prepared by resuspending cell pellets in an equal volume of HB buffer (25 mM Tris-HCl at pH 7.5, 15 mM EGTA, 15 mM $MgCl_2$ 0.1% NP-40, 1 mM DTT, 0.1 mM NaF) and grinding by mortar and pestle under liquid nitrogen, and were clarified by 10-min centrifugation in a microfuge at 4°C. In vitro degradation reactions were started by adding ^{35}S-labeled protein and were stopped after 10- or 20-min incubation at room temperature by adding SDS sample buffer. Labeled protein was visualized by SDS-PAGE and was quantified using a Storm PhosphorImager. Expression and purification of Cdc22 and Suc22 was as reported previously (Hakansson et al. 2006). For expression of recombinant protein *spd1*$^+$, ORF was ligated into pET11a and expressed in BL21(DE3) (0.1 M IPTG). For production of ^{15}N-labeled protein, cells were grown in 1 L LB media (100 μg/mL ampicillin) to OD_{600} 0.7–0.8, harvested by centrifugation (25 min at 2000*g*), resuspended in M9 media (100 μg/mL ampicillin) with $(^{15}NH_4)_2SO_4$ (1.5 g/L) as the sole nitrogen source, and grown for 1 h before induction. Induction was for 3 h at 37°C. Induced cells were harvested (15 min at 5000*g*); resuspended in 25 mL of 1× PBS (140 mM NaCl, 2.7 mM KCl, 10 mM Na_2HPO_4, 1.8 mM KH_2PO_4), 25% (w/v) sucrose, 5 mM EDTA, and 1% (w/v) Triton X-100; and sonicated three times with intermediate washes in the same buffer. Spd1 was found in the pellets, and this was dissolved in 50 mL of 20 mM Tris (pH 8), 4.5 M urea, and 0.1% (v/v) Triton X-100, and spun 15 min at 20,000*g*. Supernatant was applied to a Mono Q column equilibrated in buffer A (20 mM Tris at pH 8, 4.5 M urea, 0.1% [v/v] Triton X-100) and eluted in a linear gradient of buffer B (20 mM Tris at pH 8, 4.5 M urea, 0.1% [v/v] Triton X-100, 1 M NaCl). The relevant fractions were identified and dialyzed extensively against 1× PBS (pH 7.4) using a cut-off of 3000 g/mol. Protein was concentrated and stored at −20°C until further use. Gel filtration was performed by loading 2 mg total cross-linked protein on a Superose 6 column following extraction of proteins by grinding in liquid nitrogen. Cells were first incubated with 2 mM homobifunctional cross-linker SDP (Thermo Scientific) for 30 min. Log-phase cells were either treated or not with 20 mM HU for 4 h. Interactions between Cdc22 or Suc22 with Spd1 were assayed by fluorescence quenching spectroscopy using a Perkin-Elmer LS50B and 1 μM protein concentrations alone or in mixture in 10 mM sodium phosphate (pH 7.4). Excitation was at 280 nm at room temperature, averaging five scans and subtracting buffer backgrounds. Theoretical emission spectra for the case of noninteracting proteins were generated by addition of spectra recorded on individual proteins. To assay dATP concentration, small molecule extracts were prepared from 50-mL cultures growing in minimal medium and harvested at 5.0×10^6 cells per milliliter on a 0.45-μm filter, washed once in ice cold water, and resuspended in ice-cold 500-μL 20%TCA/15 mM $MgCl_2$. After three freeze–thaw cycles and final centrifugation, the supernatant was ether-extracted seven times to remove TCA. ATP was measured indirectly using a luciferase-based ATP determination kit from Biaffin GmbH and Co., KG, according to instructions. dATP was determined by a primer extension assay on a dA-specific template as described in Roy et al. (1999). Extended products were quantified on a Storm PhosphorImager.

Spectroscopy

A sample of 10 μM Spd1 was prepared in 10 mM NaH_2PO_4 adjusted to pH 7.4 using NaOH. A far-UV CD spectrum was recorded at room temperature on a Jasco 810 spectropolarimeter using a light path length of 1 mm. A total of five scans were accumulated from 250 to 190 nm, and buffer background was subtracted. Scanning speed was 20 nm/min, and data pitch was 0.1 nm. The resulting spectrum was smoothed using an FFT filter supplied by the Jasco software. A ^{15}N,^{1}H-HSQC NMR spectrum was recorded at 10°C on a Varian INOVA 750-MHz (^{1}H) spectrometer with 48 transients in the direct dimension and 400 increments in t1. The spectrum was transformed and visualized using NMRPipe (Delaglio et al. 1995). The NMR sample was 1 mM ^{15}N-Spd1 and 10 mM NaH_2PO_4 (pH 7.4) in 300 μL, which was centrifuged for 5 min at 5000*g* and transferred to a 5-mm Shigemi NMR tube.

Cell biology and genetics

Yeast strains were constructed using standard methods. *spd1* mutants and genomic tagged constructs were created by PCR-amplifying the desired ORF using primers with ~80-base-pair (bp) homology with the sequences flanking the genomic ORF. The resulting fragment was purified and transformed into an *spd1::ura4* strain where *ura4*$^+$ had replaced the *spd1* ORF. Replacements were selected by growth on 5-FOA, tested by PCR, and verified as correct by sequencing. To assay spore formation, strains were incubated on malt extract agar plates and incubated for 3 d at 25°C, and 200 U were assessed for zygotes/asci with zero to four spores. dATP measurements were performed on purified nucleotides by assessing ability to support primer extension against dNTP standard controls. The dATP level is calculated relative to ATP in the extract; i.e., the primer extension assay was performed on extract volume equal to 75 nmol ATP, as determined by a luciferase-based assay.

For epifluorescence and indirect immunofluorescence, cells were grown in log culture at 30°C (unless otherwise specified) in supplemented yeast extract (YE) media with or without drug as specified. For FRET analysis, cells were harvested, washed with PBS, and air dried on the slide; a drop of mounting medium (50% glycerol, 50% water) and a cover slip were added; and fluorescent proteins were visualized using a laser scanning confocal microscope (LSM 510, Zeiss). Photobleaching of the acceptor was performed by scanning the 514-nm Argon laser across a specific region of interest (ROI) within a cell (cytoplasm or nucleus). Images were processed in ImageJ (NIH). To calculate FRET, images were normalized and intensities were measured for the ROI. IDA indicates intensity of the donor in the presence of acceptor (prebleach), ID indicates intensity of the donor in the absence of acceptor (post-bleach), and IAUTO indicates background intensity (autofluorescence of an untagged control). The

FRET efficiency is expressed as a percentage: $1 - [(IDA - IAUTO.)/(ID - IAUTO.)] \times 100$. We also verified FRET efficiencies using a dedicated ImageJ macro. Levels of complexed and dissociated R1–R2 were unresolved in the present assay: Donor intensities were not corrected for noninteracting R1–R2, rendering FRET efficiencies as a marker of subunit association a quantitative measure of R1–R2 complex concentration or donor–acceptor proximity. Concomitant photobleaching of donor with the acceptor is similarly not accounted for, resulting in negative FRET efficiencies in the absence of R1–R2 interaction and a lower estimate of FRET in cases of positive association.

Acknowledgments

We thank Signe Agernæs Sjørup for assistance with RNR and Spd1 purification. K.N. was supported by CRUK grant C5514/A10722 and MRC grant G0600233. A.-S.S. was supported by EU grant PIOTNGA 215148. C.H. and O.N. acknowledge support from The Danish Cancer Society.

References

Basrai MA, Velculescu VE, Kinzler KW, Hieter P. 1999. NORF5/HUG1 is a component of the MEC1-mediated checkpoint response to DNA damage and replication arrest in *Saccharomyces cerevisiae*. *Mol Cell Biol* **19:** 7041–7049.

Benton MG, Somasundaram S, Glasner JD, Palecek SP. 2006. Analyzing the dose-dependence of the *Saccharomyces cerevisiae* global transcriptional response to methyl methanesulfonate and ionizing radiation. *BMC Genomics* **7:** 305. doi: 10.1186/1471-2164-7-305.

Chabes A, Domkin V, Thelander L. 1999. Yeast Sml1, a protein inhibitor of ribonucleotide reductase. *J Biol Chem* **274:** 36679–36683.

Chabes A, Georgieva B, Domkin V, Zhao X, Rothstein R, Thelander L. 2003. Survival of DNA damage in yeast directly depends on increased dNTP levels allowed by relaxed feedback inhibition of ribonucleotide reductase. *Cell* **112:** 391–401.

Cohen EA, Gaudreau P, Brazeau P, Langelier Y. 1986. Specific inhibition of herpesvirus ribonucleotide reductase by a nonapeptide derived from the carboxy terminus of subunit 2. *Nature* **321:** 441–443.

Danielsson J, Liljedahl L, Barany-Wallje E, Sonderby P, Kristensen LH, Martinez-Yamout MA, Dyson HJ, Wright PE, Poulsen FM, Maler L, et al. 2008. The intrinsically disordered RNR inhibitor Sml1 is a dynamic dimer. *Biochemistry* **47:** 13428–13437.

de Bruin RA, Kalashnikova TI, Chahwan C, McDonald WH, Wohlschlegel J, Yates J 3rd, Russell P, Wittenberg C. 2006. Constraining G1-specific transcription to late G1 phase: The MBF-associated corepressor Nrm1 acts via negative feedback. *Mol Cell* **23:** 483–496.

Delaglio F, Grzesiek S, Vuister GW, Zhu G, Pfeifer J, Bax A. 1995. NMRPipe: A multidimensional spectral processing system based on UNIX pipes. *J Biol NMR* **6:** 277–293.

Elledge SJ, Zhou Z, Allen JB, Navas TA. 1993. DNA damage and cell cycle regulation of ribonucleotide reductase. *Bioessays* **15:** 333–339.

Fernandez Sarabia MJ, McInerny C, Harris P, Gordon C, Fantes P. 1993. The cell cycle genes $cdc22^+$ and $suc22^+$ of the fission yeast *Schizosaccharomyces pombe* encode the large and small subunits of ribonucleotide reductase. *Mol Gen Genet* **238:** 241–251.

Gallagher IM, Alfa CE, Hyams JS. 1993. p63cdc13, a B-type cyclin, is associated with both the nucleolar and chromatin domains of the fission yeast nucleus. *Mol Biol Cell* **4:** 1087–1096.

Hakansson P, Dahl L, Chilkova O, Domkin V, Thelander L. 2006. The *Schizosaccharomyces pom*be replication inhibitor Spd1 regulates ribonucleotide reductase activity and dNTPs by binding to the large Cdc22 subunit. *J Biol Chem* **281:** 1778–1783.

Holmberg C, Fleck O, Hansen HA, Liu C, Slaaby R, Carr AM, Nielsen O. 2005. Ddb1 controls genome stability and meiosis in fission yeast. *Genes Dev* **19:** 853–862.

Ishida T, Kinoshita K. 2007. PrDOS: Prediction of disordered protein regions from amino acid sequence. *Nucleic Acids Res* **35:** W460–W464. doi: 10.1093/nar/gkm363.

Lee YD, Elledge SJ. 2006. Control of ribonucleotide reductase localization through an anchoring mechanism involving Wtm1. *Genes Dev* **20:** 334–344.

Lee YD, Wang J, Stubbe J, Elledge SJ. 2008. Dif1 is a DNA-damage-regulated facilitator of nuclear import for ribonucleotide reductase. *Mol Cell* **32:** 70–80.

Liu C, Powell KA, Mundt K, Wu L, Carr AM, Caspari T. 2003. Cop9/signalosome subunits and Pcu4 regulate ribonucleotide reductase by both checkpoint-dependent and -independent mechanisms. *Genes Dev* **17:** 1130–1140.

Liu C, Poitelea M, Watson A, Yoshida SH, Shimoda C, Holmberg C, Nielsen O, Carr AM. 2005. Transactivation of *Schizosaccharomyces pombe* $cdt2^+$ stimulates a Pcu4–Ddb1–CSN ubiquitin ligase. *EMBO J* **24:** 3940–3951.

Nordlund P, Reichard P. 2006. Ribonucleotide reductases. *Annu Rev Biochem* **75:** 681–706.

Reichard P. 2002. Ribonucleotide reductases: The evolution of allosteric regulation. *Arch Biochem Biophys* **397:** 149–155.

Rofougaran R, Vodnala M, Hofer A. 2006. Enzymatically active mammalian ribonucleotide reductase exists primarily as an $\alpha 6\beta 2$ octamer. *J Biol Chem* **281:** 27705–27711.

Rofougaran R, Crona M, Vodnala M, Sjoberg BM, Hofer A. 2008. Oligomerization status directs overall activity regulation of the *Escherichia coli* class Ia ribonucleotide reductase. *J Biol Chem* **283:** 35310–35318.

Roy B, Beuneu C, Roux P, Buc H, Lemaire G, Lepoivre M. 1999. Simultaneous determination of pyrimidine or purine deoxyribonucleoside triphosphates using a polymerase assay. *Anal Biochem* **269:** 403–409.

Russo AA, Jeffrey PD, Patten AK, Massague J, Pavletich NP. 1996. Crystal structure of the p27Kip1 cyclin-dependent-kinase inhibitor bound to the cyclin A–Cdk2 complex. *Nature* **382:** 325–331.

Stubbe J. 2003. Radicals with a controlled lifestyle. *Chem Commun* 2511–2513.

Sugase K, Dyson HJ, Wright PE. 2007. Mechanism of coupled folding and binding of an intrinsically disordered protein. *Nature* **447:** 1021–1025.

Tompa P. 2002. Intrinsically unstructured proteins. *Trends Biochem Sci* **27:** 527–533.

Watson A, Mata J, Bahler J, Carr A, Humphrey T. 2004. Global gene expression responses of fission yeast to ionizing radiation. *Mol Biol Cell* **15:** 851–860.

Wu X, Huang M. 2008. Dif1 controls subcellular localization of ribonucleotide reductase by mediating nuclear import of the R2 subunit. *Mol Cell Biol* **28:** 7156–7167.

Zhang Z, An X, Yang K, Perlstein DL, Hicks L, Kelleher N, Stubbe J, Huang M. 2006. Nuclear localization of the *Saccharomyces cerevisiae* ribonucleotide reductase small subunit requires a karyopherin and a WD40 repeat protein. *Proc Natl Acad Sci* **103:** 1422–1427.

Zhang Z, Yang K, Chen CC, Feser J, Huang M. 2007. Role of the C terminus of the ribonucleotide reductase large subunit in

enzyme regeneration and its inhibition by Sml1. *Proc Natl Acad Sci* **104:** 2217–2222.

Zhao X, Rothstein R. 2002. The Dun1 checkpoint kinase phosphorylates and regulates the ribonucleotide reductase inhibitor Sml1. *Proc Natl Acad Sci* **99:** 3746–3751.

Zhao X, Muller EG, Rothstein R. 1998. A suppressor of two essential checkpoint genes identifies a novel protein that negatively affects dNTP pools. *Mol Cell* **2:** 329–340.

Zhao X, Georgieva B, Chabes A, Domkin V, Ippel JH, Schleucher J, Wijmenga S, Thelander L, Rothstein R. 2000. Mutational and structural analyses of the ribonucleotide reductase inhibitor Sml1 define its Rnr1 interaction domain whose inactivation allows suppression of mec1 and rad53 lethality. *Mol Cell Biol* **20:** 9076–9083.

Zhao X, Chabes A, Domkin V, Thelander L, Rothstein R. 2001. The ribonucleotide reductase inhibitor Sml1 is a new target of the Mec1/Rad53 kinase cascade during growth and in response to DNA damage. *EMBO J* **20:** 3544–3553.

CHAPTER X References

Aberg A, Nordlund P, Eklund H (1993) Unusual clustering of carboxyl side chains in the core of iron-free ribonucleotide reductase. *Nature* **361**

Al-Soufi W, Reija B, Felekyan S, Seidel CAM, Novo M (2008) Dynamics of Supramolecular Association Monitored by Fluorescence Correlation Spectroscopy. *ChemPhysChem* **9:** 1819-1827

Ando N, Brignole EJ, Zimanyi CM, Funk MA, Yokoyama K, Asturias FJ, Stubbe J, Drennan CL (2011) Structural interconversions modulate activity of Escherichia coli ribonucleotide reductase. *Proceedings of the National Academy of Sciences* **108:** 21046-21051

Andreson BL, Gupta A, Georgieva BP, Rothstein R (2010) The ribonucleotide reductase inhibitor, Sml1, is sequentially phosphorylated, ubiquitylated and degraded in response to DNA damage. *Nucleic Acids Research* **38:** 6490-6501

Axelrod D (2001) Total Internal Reflection Fluorescence Microscopy in Cell Biology. *Traffic* **2:** 764-774

Aylon Y, Kupiec M (2004) New insights into the mechanism of homologous recombination in yeast. *Mutation Research/Reviews in Mutation Research* **566:** 231-248

Bähler J, Wu J-Q, Longtine MS, Shah NG, McKenzie Iii A, Steever AB, Wach A, Philippsen P, Pringle JR (1998) Heterologous modules for efficient and versatile PCR-based gene targeting in Schizosaccharomyces pombe. *Yeast* **14:** 943-951

Bailleul B, Gali√®gue S, Loucheux-Lefebvre M-H (1981) Adducts from the Reaction of O,O,Ä≤-Diacetyl or O-Acetyl Derivatives of the Carcinogen 4-Hydroxyaminoquinoline 1-Oxide with Purine Nucleosides. *Cancer Research* **41:** 4559-4565

Banning C, Votteler Jr, Hoffmann D, Koppensteiner H, Warmer M, Reimer R, Kirchhoff F, Schubert U, Hauber J, Schindler M (2010) A Flow Cytometry-Based FRET Assay to Identify and Analyse Protein-Protein Interactions in Living Cells. *PLoS ONE* **5:** e9344

Baroni E, Viscardi V, Cartagena-Lirola H, Lucchini G, Longhese MP (2004) The Functions of Budding Yeast Sae2 in the DNA Damage Response Require Mec1- and Tel1-Dependent Phosphorylation. *Molecular and Cellular Biology* **24:** 4151-4165

Benton M, Somasundaram S, Glasner J, Palecek S (2006) Analyzing the dose-dependence of the Saccharomyces cerevisiae global transcriptional response to methyl methanesulfonate and ionizing radiation. *BMC Genomics* **7:** 305

Bondar T, Ponomarev A, Raychaudhuri P (2004) Ddb1 Is Required for the Proteolysis of the Schizosaccharomyces pombe Replication Inhibitor Spd1 during S Phase and after DNA Damage. *Journal of Biological Chemistry* **279:** 9937-9943

Borgne A, Nurse P (2000) The Spd1p S phase inhibitor can activate the DNA replication checkpoint pathway in fission yeast. *J Cell Sci* **113:** 4341-4350

Borriello A, Cucciolla V, Oliva A, Zappia V, Ragione FD (2007) p27Kip1 Metabolism: A Fascinating Labyrinth. *Cell Cycle* **6:** 1053-1061

Brown NC, Eliasson R, Reichard P, Thelander L (1968) Nonheme iron as a cofactor in ribonucleotide reductase from. *Biochemical and Biophysical Research Communications* **30:** 522-527

Caldecott KW (2008) Single-strand break repair and genetic disease. *Nature review genetics* **9:** 619-631

Carr A (1994) Cell cycle co-ordination after too much rum. *Bioessays* **16:** 309-312

Carr AM (1998) Analysis of fission yeast DNA structure checkpoints:1996 Fleming Lecture. *Microbiology* **144:** 5-11

Carracedo A, Ito K, Pandolfi PP (2011) The nuclear bodies inside out: PML conquers the cytoplasm. *Current Opinion in Cell Biology* **23:** 360-366

Caspari T, Dahlen M, Kanter-Smoler G, Lindsay HD, Hofmann K, Papadimitriou K, Sunnerhagen P, Carr AM (2000) Characterization of Schizosaccharomyces pombeHus1: a PCNA-Related Protein That Associates with Rad1 and Rad9. *Molecular and Cellular Biology* **20:** 1254-1262

Caspari T, Murray JM, Carr AM (2002) Cdc2,Äìcyclin B kinase activity links Crb2 and Rqh1,Äìtopoisomerase III. *Genes & Development* **16:** 1195-1208

Caspari TCA (1999) DNA structure checkpoint pathways in Schizosaccharomyces pombe. *Biochimie* **81:** 173-181

Cerqueira NMFSA, Fernandes PA, Ramos MJ (2006) Enzyme Ribonucleotide Reductase:,Äâ Unraveling an Enigmatic Paradigm of Enzyme Inhibition by Furanone Derivatives. *The Journal of Physical Chemistry B* **110:** 21272-21281

Chabes A, Georgieva B, Domkin V, Zhao X, Rothstein R, Thelander L (2003a) Survival of DNA Damage in Yeast Directly Depends on Increased dNTP Levels Allowed by Relaxed Feedback Inhibition of Ribonucleotide Reductase. *Cell* **112:** 391-401

Chabes A, Georgieva B, Domkin V, Zhao X, Rothstein R, Thelander L (2003b) Survival of DNA damage in yeast directly depends on increased dNTP levels allowed by relaxed feedback inhibition of ribonucleotide reductase. *Cell* **112:** 391-401

Chabes A, Stillman B (2007) Constitutively High dNTP Concentration Inhibits Cell Cycle Progression and the DNA Damage Checkpoint in Yeast Saccharomyces cerevisiae. *Proceedings of the National Academy of Sciences of the United States of America* **104:** 1183-1188

Chabes A, Thelander L (2003) DNA Building Blocks at the Foundation of Better Survival. *Cell Cycle* **2:** 171-172

Chalfie M, Tu Y, Euskirchen G, Ward W, Prasher D (1994) Green fluorescent protein as a marker for gene expression. *Science* **263:** 802-805

Christensen PU, Bentley NJ, Martinho RG, Nielsen O, Carr AM (2000) Mik1 levels accumulate in S phase and may mediate an intrinsic link between S phase and mitosis. *Proceedings of the National Academy of Sciences* **97:** 2579-2584

Clerici M, Mantiero D, Guerini I, Lucchini G, Longhese MP (2008) The Yku70-Yku80 complex contributes to regulate double-strand break processing and checkpoint activation during the cell cycle. *EMBO J* **9**

Clerici M, Mantiero D, Lucchini G, Longhese MP (2006) The Saccharomyces cerevisiae Sae2 protein negatively regulates DNA damage checkpoint signalling. *EMBO report* **7**

Cody CP, DC, Westler, WM; Prendergast, FG; Ward, WW (1993) Chemical structure of the hexapeptide chromophore of the Aequorea green-fluorescent protein. *Biochemistry* **32:** 1212-1218

Cohen EAG, P.; Brazeau, P.;Langelier, Y. (1986) Specific inhibition of herpesvirus ribonucleotide reductase by a nonapeptide derived from the carboxy terminus of subunit 2. *Nature* **321:** 441

Cooperman BS (2003) Oligopeptide inhibition of class I ribonucleotide reductases. *Peptide Science* **71:** 117-131

Cotruvo JA, Stubbe J (2011) Class I Ribonucleotide Reductases: Metallocofactor Assembly and Repair In Vitro and In Vivo. *Annual Review of Biochemistry* **80:** 733-767

Daley JM, Palmbos PL, Wu D, Wilson TE (2005) NONHOMOLOGOUS END JOINING IN YEAST. *Annual review of genetics* **39:** 431-451

Davidson MB, Katou Y, Keszthelyi A, Sing TL, Xia T, Ou J, Vaisica JA, Thevakumaran N, Marjavaara L, Myers CL, Chabes A, Shirahige K, Brown GW (2012) Endogenous DNA replication stress results in expansion of dNTP pools and a mutator phenotype. *EMBO J* **advance online publication**

Diffley JF (1996) Once and only once upon a time: specifying and regulating origins of DNA replication in eukaryotic cells. *Genes & Development* **10:** 2819-2830

Diffley JFX (2011) Quality control in the initiation of eukaryotic DNA replication. *Philosophical Transactions of the Royal Society B: Biological Sciences* **366:** 3545-3553

Dronkert MLG, de Wit J, Boeve M, Vasconcelos ML, van Steeg H, Tan TLR, Hoeijmakers JHJ, Kanaar R (2000) Disruption of Mouse SNM1 Causes Increased Sensitivity to the DNA Interstrand Cross-Linking Agent Mitomycin C. *Molecular and cellular biology* **20:** 4553-4561

Dubacq C, Chevalier A, Courbeyrette R, Petat C, Gidrol X, Mann C (2006) Role of the iron mobilization and oxidative stress regulons in the genomic response of yeast to hydroxyurea. *Molecular Genetics and Genomics* **275:** 114-124

Durkacz B CA, Nurse P (1986) Transcription of the cdc2 cell cycle control gene of the fission yeast Schizosaccharomyces pombe. *EMBO J* **5:** 369-373

Eklund H, Uhlin U, F√§rneg√•rdh M, Logan DT, Nordlund Pr (2001) Structure and function of the radical enzyme ribonucleotide reductase. *Progress in Biophysics and Molecular Biology* **77:** 177-268

Eklund UUH (1994) Structure of ribonucleotide reductase protein R1. *Nature* **370:** 533 - 539

Elford HL (1968) Effect of hydroxyurea on ribonucleotide reductase. *Biochemical and Biophysical Research Communications* **33:** 129-135

Elledge SJ, Zhou Z, Allen JB (1992) Ribonucleotide reductase: regulation, regulation, regulation. *Trends in Biochemical Sciences* **17:** 119-123

Enoch T, Carr AM, Nurse P (1992) Fission yeast genes involved in coupling mitosis to completion of DNA replication. *Genes & Development* **6:** 2035-2046

Eriksson MU, U; Ramaswamy, S; Ekberg, M; Regnstrom, K; Sjoberg, BM; Eklund, H (1997) Binding of allosteric effectors to ribonucleotide reductase protein R1: reduction of active-site cysteines promotes substrate binding. *Structure* **5**

Evans T, Rosenthal ET, Youngblom J, Distel D, Hunt T (1983) Cyclin: A protein specified by maternal mRNA in sea urchin eggs that is destroyed at each cleavage division. *Cell* **33:** 389-396

Fairman JWW, Sanath Ranjan; Ahmad, Md Faiz; Xu, Hai; Nakano, Ryo; Jha, Shalini; Prendergast, Jay; Welin, R Martin; Flodin, Susanne; Roos, Annette; Nordlund, Par; Li, Zongli; Walz, Thomas; Dealwis, Chris Godfrey (2011) Structural basis for allosteric regulation of human ribonucleotide reductase by nucleotide-induced oligomerization. *Nature Structural Molecular Biology* **18:** 316-322

Fantes CBGaPA (1986) The cdc22 gene of Schizosaccharomyces pombe encodes a cell cycle-regulated transcript. *EMBO J* 2981–2985

Fernandez Sarabia MJ MC, Harris P, Gordon C, Fantes P. (1993) The cell cycle genes cdc22+ and suc22+ of the fission yeast Schizosaccharomyces pombe encode the large and small subunits of ribonucleotide reductase. *Mol Gen Genet* **238(1-2):** 241-251.

Fernandez-Sarabia MJ, Fantes PA (1990) Ribonucleotide reductase and its regulation during the cell cycle. *Trends in Genetics* **6:** 275-275

Fitzpatrick JAJ, Lillemeier BF (2011) Fluorescence correlation spectroscopy: linking molecular dynamics to biological function in vitro and in situ. *Current Opinion in Structural Biology* **21:** 650-660

Furuya K, Carr AM (2003) DNA checkpoints in fission yeast. *Journal of Cell Science* **116:** 3847-3848

Galea CA, Nourse A, Wang Y, Sivakolundu SG, Heller WT, Kriwacki RW (2008a) Role of Intrinsic Flexibility in Signal Transduction Mediated by the Cell Cycle Regulator, p27Kip1. *Journal of Molecular Biology* **376:** 827-838

Galea CA, Wang Y, Sivakolundu SG, Kriwacki RW (2008b) Regulation of Cell Division by Intrinsically Unstructured Proteins: Intrinsic Flexibility, Modularity, and Signaling Conduits‚Ä†. *Biochemistry* **47:** 7598-7609

Gallo GJ, Schuetz TJ, Kingston RE (1991) Regulation of heat shock factor in Schizosaccharomyces pombe more closely resembles regulation in mammals than in Saccharomyces cerevisiae. *Molecular and Cellular Biology* **11:** 281-288

Giepmans BNG, Adams SR, Ellisman MH, Tsien RY (2006) The Fluorescent Toolbox for Assessing Protein Location and Function. *Science* **312:** 217-224

Guittet O, Hankansson P, Voevodskaya N, Fridd S, GrÃ¤slund A, Arakawa H, Nakamura Y, Thelander L (2001) Mammalian p53R2 Protein Forms an Active Ribonucleotide Reductasein Vitro with the R1 Protein, Which Is Expressed Both in Resting Cells in Response to DNA Damage and in Proliferating Cells. *Journal of Biological Chemistry* **276:** 40647-40651

Gunasekaran K, Tsai C-J, Kumar S, Zanuy D, Nussinov R (2003) Extended disordered proteins: targeting function with less scaffold. *Trends in Biochemical Sciences* **28:** 81-85

Hadjantonakis A-K, Nagy A (2001) The color of mice: in the light of GFP-variant reporters. *Histochemistry and Cell Biology* **115:** 49-58

Hamann CS, Lentainge S, Li LS, Salem JS, Yang FD, Cooperman BS (1998) Chimeric small subunit inhibitors of mammalian ribonucleotide reductase: a dual function for the R2 C-terminus? *Protein Engineering* **11:** 219-224

Hamelin R, Chalastanis A, Colas C, El Bchiri J, Mercier D, Schreurs AS, Simon V, Svrcek M, Zaanan A, Borie C, Buhard O, Capel E, Zouali H, Praz F, Muleris M, Flejou

JF, Duval A (2008) [Clinical and molecular consequences of microsatellite instability in human cancers]. *Bulletin du cancer* **95:** 121-132

Hammel M, Yu Y, Mahaney BL, Cai B, Ye R, Phipps BM, Rambo RP, Hura GL, Pelikan M, So S, Abolfath RM, Chen DJ, Lees-Miller SP, Tainer JA (2010) Ku and DNA-dependent Protein Kinase Dynamic Conformations and Assembly Regulate DNA Binding and the Initial Non-homologous End Joining Complex. *Journal of Biological Chemistry* **285:** 1414-1423

Han W-G, Noodleman L (2011) DFT Calculations for Intermediate and Active States of the Diiron Center with a Tryptophan or Tyrosine Radical in Escherichia coli Ribonucleotide Reductase. *Inorganic Chemistry* **50:** 2302-2320

Hankansson P, Dahl L, Chilkova O, Domkin V, Thelander L (2006a) The Schizosaccharomyces pombe Replication Inhibitor Spd1 Regulates Ribonucleotide Reductase Activity and dNTPs by Binding to the Large Cdc22 Subunit. *Journal of Biological Chemistry* **281:** 1778-1783

Hankansson P, Hofer A, Thelander L (2006b) Regulation of Mammalian Ribonucleotide Reduction and dNTP Pools after DNA Damage and in Resting Cells. *Journal of Biological Chemistry* **281:** 7834-7841

Harris P KP, McInerny CJ, Fantes PA. (1996) Cell cycle, DNA damage and heat shock regulate suc22+ expression in fission yeast. *Mol Gen Genet* **252:** 284-291.

Helleday T, Lo J, van Gent DC, Engelward BP (2007) DNA double-strand break repair: From mechanistic understanding to cancer treatment. *DNA Repair* **6:** 923-935

Heyduk T (2002) Measuring protein conformational changes by FRET/LRET. *Current Opinion in Biotechnology* **13:** 292-296

Hillisch A, Lorenz M, Diekmann S (2001) Recent advances in FRET: distance determination in protein-DNA complexes. *Current Opinion in Structural Biology* **11:** 201-207

Hinz JM (2010) Role of homologous recombination in DNA interstrand crosslink repair. *Environmental and Molecular Mutagenesis* **51:** 582-603

Ho CK, Mazón G, Lam AF, Symington LS (2010) Mus81 and Yen1 Promote Reciprocal Exchange during Mitotic Recombination to Maintain Genome Integrity in Budding Yeast. *Molecular Cell* **40:** 988-1000

Hofer A, Crona M, Logan DT, Sj√∂berg B-M (2011) DNA building blocks: keeping control of manufacture. *Critical Reviews in Biochemistry and Molecular Biology* **47:** 50-63

Hofer A, Crona M, Logan DT, Sj√∂berg B-M (2012) DNA building blocks: keeping control of manufacture. *Critical Reviews in Biochemistry and Molecular Biology* **47:** 50-63

Holloman WK (2011) Unraveling the mechanism of BRCA2 in homologous recombination. *Nat Struct Mol Biol* **18:** 748-754

Holmberg C, Fleck O, Hansen HA, Liu C, Slaaby R, Carr AM, Nielsen O (2005) Ddb1 controls genome stability and meiosis in fission yeast. *Genes & Development* **19:** 853-862

Huang M, Elledge SJ (1997) Identification of RNR4, encoding a second essential small subunit of ribonucleotide reductase in Saccharomyces cerevisiae. *Mol Cell Biol* **17:** 6105-6113

Hunt T (1991) Cell cycle gets more cyclins. *Nature* **350**

Jun S-H, Kim TG, Ban C (2006) DNA mismatch repair system. *FEBS Journal* **273:** 1609-1619

Kashlan OB, Scott CP, Lear JD, Cooperman BS (2001) A Comprehensive Model for the Allosteric Regulation of Mammalian Ribonucleotide Reductase. Functional Consequences of ATP- and dATP-Induced Oligomerization of the Large Subunitâ€ *Biochemistry* **41:** 462-474

Kass EM, Jasin M (2010) Collaboration and competition between DNA double-strand break repair pathways. *FEBS Letters* **584:** 3703-3708

Koc A, Wheeler LJ, Mathews CK, Merrill GF (2004) Hydroxyurea Arrests DNA Replication by a Mechanism That Preserves Basal dNTP Pools. *Journal of Biological Chemistry* **279:** 223-230

Kolberg M, Strand KR, Graff Pl, Kristoffer Andersson K (2004) Structure, function, and mechanism of ribonucleotide reductases. *Biochimica et Biophysica Acta (BBA) - Proteins & Proteomics* **1699:** 1-34

Kolin D, Wiseman P (2007) Advances in Image Correlation Spectroscopy: Measuring Number Densities, Aggregation States, and Dynamics of Fluorescently labeled Macromolecules in Cells. *Cell Biochemistry and Biophysics* **49:** 141-164

Krogh BO, Symington LS (2004) RECOMBINATION PROTEINS IN YEAST. *Annual Review of Genetics* **38:** 233-271

Krukenberg KA, Street TO, Lavery LA, Agard DA (2011) Conformational dynamics of the molecular chaperone Hsp90. *Quarterly Reviews of Biophysics* **44:** 229-255

Kumar D, Viberg J, Nilsson AK, Chabes A (2010) Highly mutagenic and severely imbalanced dNTP pools can escape detection by the S-phase checkpoint. *Nucl Acids Res***:** gkq128

Labib K, Moreno S, Nurse P (1995) Interaction of cdc2 and rum1 regulates Start and S-phase in fission yeast. *Journal of Cell Science* **108:** 3285-3294

Lambert S, Carr AM (2005) Checkpoint responses to replication fork barriers. *Biochimie* **87:** 591-602

Langerak P, Russell P (2011) Regulatory networks integrating cell cycle control with DNA damage checkpoints and double-strand break repair. *Philosophical Transactions of the Royal Society B: Biological Sciences* **366:** 3562-3571

Larsson A, Karlsson M, Sahlin M, SjÃ¶berg BM (1988) Radical formation in the dimeric small subunit of ribonucleotide reductase requires only one tyrosine 122. *Journal of Biological Chemistry* **263:** 17780-17784

Larsson K-MJ, Albert; Eliasson, Rolf; Reichard, Peter; Logan, Derek T; Nordlund, Par (2004) Structural mechanism of allosteric substrate specificity regulation in a ribonucleotide reductase. *Nature* **11:** 11

Lee YD, Elledge SJ (2006) Control of ribonucleotide reductase localization through an anchoring mechanism involving Wtm1. *Genes & Development* **20:** 334-344

Lee YD, Wang J, Stubbe J, Elledge SJ (2008) Dif1 Is a DNA-Damage-Regulated Facilitator of Nuclear Import for Ribonucleotide Reductase. *Molecular Cell* **32:** 70-80

Lehmann AR (2003) DNA repair-deficient diseases, xeroderma pigmentosum, Cockayne syndrome and trichothiodystrophy. *Biochimie* **85:** 1101-1111

Lehmann AR (2011) DNA polymerases and repair synthesis in NER in human cells. *DNA Repair* **10:** 730-733

Leupold U (1949) Die Vererbung von Homothallie und Heterothallie bei Schizosaccharomyces Pombe.

Lieber MR (2010) NHEJ and its backup pathways in chromosomal translocations. *Nat Struct Mol Biol* **17:** 393-395

Lieber MR, Ma Y, Pannicke U, Schwarz K (2003) Mechanism and regulation of human non-homologous DNA end-joining. *Nat Rev Mol Cell Biol* **4:** 712-720

Lindsay HD, Griffiths DJF, Edwards RJ, Christensen PU, Murray JM, Osman F, Walworth N, Carr AM (1998) S-phase-specific activation of Cds1 kinase defines a subpathway of the checkpoint response in Schizosaccharomyces,Äâpombe. *Genes & Development* **12:** 382-395

Liu C, Poitelea M, Watson A, Yoshida S-h, Shimoda C, Holmberg C, Nielsen O, Carr AM (2005) Transactivation of Schizosaccharomyces pombe cdt2+ stimulates a Pcu4-Ddb1-CSN ubiquitin ligase. *EMBO J* **24:** 3940-3951

Liu C, Powell KA, Mundt K, Wu L, Carr AM, Caspari T (2003) Cop9/signalosome subunits and Pcu4 regulate ribonucleotide reductase by both checkpoint-dependent and -independent mechanisms. *Genes & Development* **17:** 1130-1140

Livet JW, Tamily A. ;Kang, Hyuno; Draft, Ryan W. ; Lu, Ju ; Bennis, Robyn A. ; Sanes, Joshua R. ; Lichtman, Jeff W. (2007) Transgenic strategies for combinatorial expression of fluorescent proteins in the nervous system. *Nature* **450:** 56-62

Logan DT SX, Aberg A, Regnström K, Hajdu J, Eklund H, Nordlund P. (1996) Crystal structure of reduced protein R2 of ribonucleotide reductase: the structural basis for oxygen activation at a dinuclear iron site. *Structure* **4**

Longhese MP, Clerici M, Lucchini G (2003) The S-phase checkpoint and its regulation in Saccharomyces cerevisiae. *Mutation Research/Fundamental and Molecular Mechanisms of Mutagenesis* **532:** 41-58

Longhese MP, Foiani, Marco, Muzi-Falconi, Marco, Lucchini, Giovanna, Plevani, Paolo (1998) DNA damage checkpoint in budding yeast. *EMBO J* **17:** 5525-5528

Longhese MP, Mantiero D, Clerici M (2006) The cellular response to chromosome breakage. *Molecular Microbiology* **60:** 1099-1108

Mantiero D, Clerici M, Lucchini G, Longhese MP (2007) Dual role for Saccharomyces cerevisiae Tel1 in the checkpoint response to double-strand breaks. *EMBO J* **8**

Maqbool Z, Kersey PJ, Fantes PA, McInerny CJ (2003) MCB-mediated regulation of cell cycle-specific <i>cdc22</i> ⁺ transcription in fission yeast. *Molecular Genetics and Genomics* **269:** 765-775

Marc T, Morad Z, Jean-Claude M, Marie-Jo M, Maïté C-M (2006) Sensitivity of CFP/YFP and GFP/mCherry pairs to donor photobleaching on FRET determination by fluorescence lifetime imaging microscopy in living cells. *Microscopy Research and Technique* **69:** 933-939

Marti TM, Kunz C, Fleck O (2002) DNA mismatch repair and mutation avoidance pathways. *Journal of Cellular Physiology* **191:** 28-41

Martín M, Terradas M, Tusell L, Genescà A ATM and DNA-PKcs make a complementary couple in DNA double strand break repair. *Mutation Research/Reviews in Mutation Research*

Martín M, Terradas M, Tusell L, Genescà A (2012) ATM and DNA-PKcs make a complementary couple in DNA double strand break repair. *Mutation Research/Reviews in Mutation Research*

Mathews CK, Slabaugh MB (1986) Eukaryotic DNA metabolism: Are deoxyribonucleotides channeled to replication sites? *Experimental Cell Research* **162:** 285-295

McEachern MJ, Krauskopf A, Blackburn EH (2000) TELOMERES AND THEIR CONTROL. *Annual review of genetics* **34:** 331-358

Mitchison JM (1957) The growth of single cells. i. schizosaccharomyces pombe. . *Experimental Cell Research* **13:** 244-262

Morano KA, Grant CM, Moye-Rowley WS (2012) The Response to Heat Shock and Oxidative Stress in Saccharomyces cerevisiae. *Genetics* **190:** 1157-1195

Morgan DO (1995) Principles of CDK regulation. *Nature* **374:** 131-134

Morris JR, Boutell C, Keppler M, Densham R, Weekes D, Alamshah A, Butler L, Galanty Y, Pangon L, Kiuchi T, Ng T, Solomon E (2009) The SUMO modification pathway is involved in the BRCA1 response to genotoxic stress. *Nature* **462**

Moss J, Tinline-Purvis H, Walker CA, Folkes LK, Stratford MR, Hayles J, Hoe K-L, Kim D-U, Park H-O, Kearsey SE, Fleck O, Holmberg C, Nielsen O, Humphrey TC (2010) Break-induced ATR and Ddb1–Cul4Cdt2 ubiquitin ligase-dependent nucleotide synthesis promotes homologous recombination repair in fission yeast. *Genes & Development* **24:** 2705-2716

Nestoras K, Schreurs A-S, Mohammed AH, Fleck O, Watson AT, Poitelea M, O'Shea C, Chahwan C, Holmberg C, Kragelund BB, Nielsen O, Osborne M, Carr AM, Liu C (2010) Regulation of ribonucleotide reductase by Spd1 involves multiple mechanisms. *Genes & Development* **24:** 1145-1159

Nielsen O (2003) COP9 Signalosome: A Provider of DNA Building Blocks. *Current Biology* **13:** R565-R567

Niida H, Katsuno Y, Sengoku M, Shimada M, Yukawa M, Ikura M, Ikura T, Kohno K, Shima H, Suzuki H, Tashiro S, Nakanishi M (2010a) Essential role of Tip60-dependent recruitment of ribonucleotide reductase at DNA damage sites in DNA repair during G1 phase. *Genes & Development* **24:** 333-338

Niida H, Shimada M, Murakami H, Nakanishi M (2010b) Mechanisms of dNTP supply that play an essential role in maintaining genome integrity in eukaryotic cells. *Cancer Science* **101:** 2505-2509

Norbury C, Nurse P (1992) Animal cell cycles and their control. *Annual review of biochemistry* **61:** 441-470

Nordlund P, Eklund H (1993) Structure and Function of the Escherichia coli Ribonucleotide Reductase Protein R2. *Journal of Molecular Biology* **232:** 123-164

Nordlund Pr, Reichard P (2006) Ribonucleotide Reductases. *Annual Review of Biochemistry* **75:** 681-706

Nouspikel T (2009) DNA Repair in Mammalian Cells. *Cellular and Molecular Life Sciences* **66:** 963-967

Nowotschin S, Eakin GS, Hadjantonakis A-K (2009) Dual transgene strategy for live visualization of chromatin and plasma membrane dynamics in murine embryonic stem cells and embryonic tissues. *genesis* **47:** 330-336

Nurse P (1992) Ciba Medal Lecture. Eukaryotic cell-cycle control. *Biochemical Society transactions* **20:** 239-242

Nurse P, Thuriaux P (1980) REGULATORY GENES CONTROLLING MITOSIS IN THE FISSION YEAST SCHIZOSACCHAROMYCES POMBE. *Genetics* **96:** 627-637

Nurse P TP, Nasmyth K. (1976) Genetic control of the cell division cycle in the fission yeast Schizosaccharomyces pombe. *Mol Gen Genet* **146:** 167-178.

O'Connell MJ, Walworth NC, Carr AM (2000) The G2-phase DNA-damage checkpoint. *Trends in Cell Biology* **10:** 296-303

Ohta T, Sato K, Wu W (2011) The BRCA1 ubiquitin ligase and homologous recombination repair. *FEBS Letters* **585:** 2836-2844

Ormo M, Cubitt AB, Kallio K, Gross LA, Tsien RY, Remington SJ (1996) Crystal Structure of the Aequorea victoria Green Fluorescent Protein. *Science* **273:** 1392-1395

Ormo M, Regnstrom K, Wang Z, Que L, Sahlin M, Sjoberg B-M (1995) Residues Important for Radical Stability in Ribonucleotide Reductase from Escherichia coli. *Journal of Biological Chemistry* **270:** 6570-6576

Osamu S, Frank HJ, Yo S (1962) Extraction, Purification and Properties of Aequorin, a Bioluminescent Protein from the Luminous Hydromedusan, <I>Aequorea</I>. *Journal of Cellular and Comparative Physiology* **59:** 223-239

Paciotti V, Clerici M, Scotti M, Lucchini G, Longhese MP (2001) Characterization of mec1Kinase-Deficient Mutants and of New Hypomorphic mec1Alleles Impairing Subsets of the DNA Damage Response Pathway. *Molecular and Cellular Biology* **21:** 3913-3925

Patterson G, Davidson M, Manley S, Lippincott-Schwartz J (2010) Superresolution Imaging using Single-Molecule Localization. *Annual Review of Physical Chemistry* **61:** 345-367

Periasamy A, Day RN (1998) Chapter 18: Visualizing Protein Interactions in Living Cells Using Digitized GFP Imaging and FRET Microscopy. In *Methods in Cell Biology*, Kevin FS, Steve AK (eds), Vol. Volume 58, pp 293-314. Academic Press

Phadnis N, Hyppa RW, Smith GR (2011) New and old ways to control meiotic recombination. *Trends in Genetics* **27:** 411-421

Pietraszewska-Bogiel A, Gadella TWJ (2011) FRET microscopy: from principle to routine technology in cell biology. *Journal of Microscopy* **241:** 111-118

Poli J, Tsaponina O, Crabbe L, Keszthelyi A, Pantesco V, Chabes A, Lengronne A, Pasero P (2012) dNTP pools determine fork progression and origin usage under replication stress. *EMBO J* **31:** 883-894

Pollok BA, Heim R (1999) Using GFP in FRET-based applications. *Trends in Cell Biology* **9:** 57-60

Prasher DC, Eckenrode VK, Ward WW, Prendergast FG, Cormier MJ (1992) Primary structure of the Aequorea victoria green-fluorescent protein. *Gene* **111:** 229-233

Price ES, Aleksiejew M, Johnson CK (2011) FRET-FCS Detection of Intralobe Dynamics in Calmodulin. *The Journal of Physical Chemistry B* **115:** 9320-9326

Raji H, Hartsuiker E (2006) Double-strand break repair and homologous recombination in Schizosaccharomyces pombe. *Yeast* **23:** 963-976

Reck-Peterson SL, Derr ND, Stuurman N (2010) Imaging Single Molecules Using Total Internal Reflection Fluorescence Microscopy (TIRFM). *Cold Spring Harbor Protocols* **2010:** pdb.top73

Reece SY, Hodgkiss JM, Stubbe J, Nocera DG (2006) Proton-coupled electron transfer: the mechanistic underpinning for radical transport and catalysis in biology. *Philosophical Transactions of the Royal Society B: Biological Sciences* **361:** 1351-1364

Reichard P (1987) Regulation of deoxyribotide synthesis. *Biochemistry* **26:** 3245-3248

Reichard P, Baldesten A, Rutberg L (1961) Formation of Deoxycytidine Phosphates from Cytidine Phosphates in Extracts from Escherichia coli. *Journal of Biological Chemistry* **236:** 1150-1157

Reichard P, Estborn B (1951) UTILIZATION OF DESOXYRIBOSIDES IN THE SYNTHESIS OF POLYNUCLEOTIDES. *Journal of Biological Chemistry* **188:** 839-846

Robertson A, Klungland A, Rognes T, Leiros I (2009) DNA Repair in Mammalian Cells. *Cellular and Molecular Life Sciences* **66:** 981-993

Rofougaran R, Crona M, Vodnala M, Sj√∂berg B-M, Hofer A (2008a) Oligomerization Status Directs Overall Activity Regulation of the Escherichia coli Class Ia Ribonucleotide Reductase. *Journal of Biological Chemistry* **283:** 35310-35318

Rofougaran R, Crona M, Vodnala M, SjÃ¶berg B-M, Hofer A (2008b) Oligomerization Status Directs Overall Activity Regulation of the Escherichia coli Class Ia Ribonucleotide Reductase. *Journal of Biological Chemistry* **283:** 35310-35318

Rofougaran R, Vodnala M, Hofer A (2006) Enzymatically Active Mammalian Ribonucleotide Reductase Exists Primarily as an alpha6beta2 Octamer. *Journal of Biological Chemistry* **281:** 27705-27711

Sabouri N, Viberg Jr, Goyal DK, Johansson E, Chabes A (2008) Evidence for lesion bypass by yeast replicative DNA polymerases during DNA damage. *Nucleic Acids Research* **36:** 5660-5667

Salguero I, Guarino E, Shepherd Marianne EA, Deegan Tom D, Havens Courtney G, MacNeill Stuart A, Walter Johannes C, Kearsey Stephen E (2012) Ribonucleotide Reductase Activity Is Coupled to DNA Synthesis via Proliferating Cell Nuclear Antigen. *Current biology : CB*

Sazer S, Sherwood SW (1990) Mitochondrial growth and DNA synthesis occur in the absence of nuclear DNA replication in fission yeast. *Journal of Cell Science* **97:** 509-516

Schmolze DB, Standley C, Fogarty KE, Fischer AH (2011) Advances in Microscopy Techniques. *Archives of Pathology & Laboratory Medicine* **135:** 255-263

Seward HE, Bagshaw CR (2009) The photochemistry of fluorescent proteins: implications for their biological applications. *Chemical Society Reviews* **38:** 2842-2851

Sherr CJ, Roberts JM (1999) CDK inhibitors: positive and negative regulators of G1-phase progression. *Genes & Development* **13:** 1501-1512

Smith P, Zhou B, Ho N, Yuan Y-C, Su L, Tsai S-C, Yen Y (2009) 2.6 Å X-ray Crystal Structure of Human p53R2, a p53-Inducible Ribonucleotide Reductase. *Biochemistry* **48:** 11134-11141

Stillman B (2008) DNA Polymerases at the Replication Fork in¬†Eukaryotes. *Molecular Cell* **30:** 259-260

Stubbe J (1998) Ribonucleotide reductases in the twenty-first century. *Proceedings of the National Academy of Sciences of the United States of America* **95:** 2723-2724

Stubbe J, Cotruvo Jr JA (2011) Control of metallation and active cofactor assembly in the class Ia and Ib ribonucleotide reductases: diiron or dimanganese? *Current Opinion in Chemical Biology* **15:** 284-290

Sugase K, Dyson HJ, Wright PE (2007) Mechanism of coupled folding and binding of an intrinsically disordered protein. *Nature* **447:** 1021-1025

Sveiczer A, Novak B, Mitchison JM (1996) The size control of fission yeast revisited. *Journal of Cell Science* **109:** 2947-2957

Sveiczer A, Novak B, Mitchison JM (1999) Mitotic control in the absence of cdc25 mitotic inducer in fission yeast. *Journal of Cell Science* **112:** 1085-1092

Szostak JW, Orr-Weaver TL, Rothstein RJ, Stahl FW (1983) The double-strand-break repair model for recombination. *Cell* **33:** 25-35

Tadross MR, Park SA, Veeramani B, Yue DT (2009) Robust approaches to quantitative ratiometric FRET imaging of CFP/YFP fluorophores under confocal microscopy. *Journal of Microscopy* **233:** 192-204

Takahashi S, Kontani K, Araki Y, Katada T (2007) Caf1 regulates translocation of ribonucleotide reductase by releasing nucleoplasmic Spd1-Suc22 assembly. *Nucl Acids Res* **35:** 1187-1197

Tanaka H, Arakawa H, Yamaguchi T, Shiraishi K, Fukuda S, Matsui K, Takei Y, Nakamura Y (2000) A ribonucleotide reductase gene involved in a p53-dependent cell-cycle checkpoint for DNA damage. *Nature* **404:** 42-49

Thelander L, Reichard P (1979) Reduction of Ribonucleotides. *Annual Review of Biochemistry* **48:** 133-158

Thomas DC, Husain I, Chaney SG, Panigrahi GB, Walker IG (1991) Sequence effect on incision by (A)BC excinuclease of 4NQO adducts and UV photoproducts. *Nucleic Acids Research* **19:** 365-370

Tian H, Ip L, Luo H, Chang DC, Luo KQ (2007) A high throughput drug screen based on fluorescence resonance energy transfer (FRET) for anticancer activity of compounds from herbal medicine. *British Journal of Pharmacology* **150:** 321-334

Truong K, Ikura M (2001) The use of FRET imaging microscopy to detect protein-protein interactions and protein conformational changes in vivo. *Current Opinion in Structural Biology* **11:** 573-578

Tsien RY (1998) THE GREEN FLUORESCENT PROTEIN. *Annual Review of Biochemistry* **67:** 509-544

Ulrich HD (2011) Timing and spacing of ubiquitin-dependent DNA damage bypass. *FEBS Letters* **585:** 2861-2867

Uranbileg B, Yamamoto H, Park J-h, Mohanty AR, Arakawa-Takeuchi S, Jinno S, Okayama H (2012) Cdc6 Protein Activates p27KIP1-bound Cdk2 Protein Only after the Bound p27 Protein Undergoes C-terminal Phosphorylation. *Journal of Biological Chemistry* **287:** 6275-6283

Wallrabe H, Periasamy A (2005) Imaging protein molecules using FRET and FLIM microscopy. *Current Opinion in Biotechnology* **16:** 19-27

Wang J, Lohman GJS, Stubbe J (2009) Mechanism of Inactivation of Human Ribonucleotide Reductase with p53R2 by Gemcitabine 5‚Ä≤-Diphosphate. *Biochemistry* **48:** 11612-11621

Wang L, Chen T, Qu J, Wei X (2010) Photobleaching-Based Quantitative Analysis of Fluorescence Resonance Energy Transfer inside Single Living Cell. *Journal of Fluorescence* **20:** 27-35

Wang X, Liu X, Xue L, Zhang K, Kuo M-L, Hu S, Zhou B, Ann D, Zhang S, Yen Y (2011) Ribonucleotide reductase subunit p53R2 regulates mitochondria homeostasis and function in KB and PC-3 cancer cells. *Biochemical and Biophysical Research Communications* **410:** 102-107

Wang Y, Shyy JY-J, Chien S (2008) Fluorescence Proteins, Live-Cell Imaging, and Mechanobiology: Seeing Is Believing. *Annual Review of Biomedical Engineering* **10:** 1-38

Wei N, Deng XW (2003) THE COP9 SIGNALOSOME. *Annual Review of Cell and Developmental Biology* **19:** 261-286

Werler PJ HE, Carr AM. (2003) A simple Cre-loxP method for chromosomal N-terminal tagging of essential and non-essential Schizosaccharomyces pombe genes. *Gene* **304:** 133-141

Williams GJ, Lees-Miller SP, Tainer JA (2010) Mre11–Rad50–Nbs1 conformations and the control of sensing, signaling, and effector responses at DNA double-strand breaks. *DNA Repair* **9:** 1299-1306

Wilson TE, Grawunder U, Lieber MR (1997) Yeast DNA ligase IV mediates non-homologous DNA end joining. *Nature* **388:** 495-498

Wood V, Gwilliam R, Rajandream MA, Lyne M, Lyne R, Stewart A, Sgouros J, Peat N, Hayles J, Baker S, Basham D, Bowman S, Brooks K, Brown D, Brown S, Chillingworth T, Churcher C, Collins M, Connor R, Cronin A, Davis P, Feltwell T, Fraser A, Gentles S, Goble A, Hamlin N, Harris D, Hidalgo J, Hodgson G, Holroyd S, Hornsby T, Howarth S, Huckle EJ, Hunt S, Jagels K, James K, Jones L, Jones M, Leather S, McDonald S, McLean J, Mooney P, Moule S, Mungall K, Murphy L, Niblett D, Odell C, Oliver K, O'Neil S, Pearson D, Quail MA, Rabbinowitsch E, Rutherford K, Rutter S, Saunders D, Seeger K, Sharp S, Skelton J, Simmonds M, Squares R, Squares S, Stevens K, Taylor K, Taylor RG, Tivey A, Walsh S, Warren T, Whitehead S, Woodward J, Volckaert G, Aert R, Robben J, Grymonprez B, Weltjens I, Vanstreels E, Rieger M, Schafer M, Muller-Auer S, Gabel C, Fuchs M, Fritzc C, Holzer E, Moestl D, Hilbert H, Borzym K, Langer I, Beck A, Lehrach H, Reinhardt R, Pohl TM, Eger P, Zimmermann W, Wedler H, Wambutt R, Purnelle B, Goffeau A, Cadieu E, Dreano S, Gloux S, Lelaure V, Mottier S, Galibert F, Aves SJ, Xiang Z, Hunt C, Moore K, Hurst SM, Lucas M, Rochet M, Gaillardin C, Tallada VA, Garzon A, Thode G, Daga RR, Cruzado L, Jimenez J, Sanchez M, del Rey F, Benito J, Dominguez A, Revuelta JL, Moreno S, Armstrong J, Forsburg SL, Cerrutti L, Lowe T, McCombie WR, Paulsen I, Potashkin J, Shpakovski GV, Ussery D, Barrell BG, Nurse P (2002) The genome sequence of Schizosaccharomyces pombe. *Nature* **415:** 871-880

Woollard A BG, Nurse P (1996) A novel S phase inhibitor in fission yeast. *EMBO J* **15:** 4603-4612

Wu L, Hickson ID (2006) DNA Helicases Required for Homologous Recombination and Repair of Damaged Replication Forks. *Annual review of genetics* **40:** 279-306

Xu H, Faber C, Uchiki T, Racca J, Dealwis C (2006) Structures of eukaryotic ribonucleotide reductase I define gemcitabine diphosphate binding and subunit assembly. *Proceedings of the National Academy of Sciences of the United States of America* **103:** 4028-4033

You X, Nguyen AW, Jabaiah A, Sheff MA, Thorn KS, Daugherty PS (2006) Intracellular protein interaction mapping with FRET hybrids. *Proceedings of the National Academy of Sciences* **103:** 18458-18463

Youds JL, Boulton SJ (2011) The choice in meiosis – defining the factors that influence crossover or non-crossover formation. *Journal of Cell Science* **124:** 501-513

Zhang Y, Liu L, Wu X, An X, Stubbe J, Huang M (2011) Investigation of in Vivo Diferric Tyrosyl Radical Formation in Saccharomyces cerevisiae Rnr2 Protein. *Journal of Biological Chemistry* **286:** 41499-41509

Zhang Z, Yang K, Chen C-C, Feser J, Huang M (2007) Role of the C terminus of the ribonucleotide reductase large subunit in enzyme regeneration and its inhibition by Sml1. *Proceedings of the National Academy of Sciences* **104:** 2217-2222

Zhao X, Georgieva B, Chabes A, Domkin V, Ippel JH, Schleucher J, Wijmenga S, Thelander L, Rothstein R (2000) Mutational and Structural Analyses of the Ribonucleotide Reductase Inhibitor Sml1 Define Its Rnr1 Interaction Domain Whose Inactivation Allows Suppression of mec1 and rad53 Lethality. *Mol Cell Biol* **20:** 9076-9083

Zhou B, Liu X, Mo X, Xue L, Darwish D, Qiu W, Shih J, Hwu EB, Luh F, Yen Y (2003) The Human Ribonucleotide Reductase Subunit hRRM2 Complements p53R2 in Response to UV-Induced DNA Repair in Cells with Mutant p53. *Cancer Research* **63:** 6583-6594

Zhou Z, Elledge SJ (1992) Isolation of crt Mutants Constitutive for Transcription of the DNA Damage Inducible Gene RNR3 in Saccharomyces cerevisiae. *Genetics* **131:** 851-866